

Martin-Luther-Universität Halle-Wittenberg

Institut für Physik

der Naturwissenschaftlichen Fakultät II

Fachgruppe Quantentheorie des Festkörpers

Von-Seckendorff-Platz 1, 06120 Halle (Saale), Germany



Dissertation

zur Erlangung des akademischen Grades

doctor rerum naturalium (Dr. rer. nat.)

Magnetization dynamics and magnetic ground state properties from first principles

vorgelegt von

DIPL. PHYS. DANNY THONIG

geboren am 06.05.1986 in Bad Frankenhausen

Halle (Saale), den 05. November 2013

Erstgutachter: PD Dr. rer. nat. habil. Jürgen Henk
Zweitgutachter: Prof. Dr. rer. nat. habil. Steffen Trimper
Drittgutachter: Prof. Dr. rer. nat. habil. Olle Eriksson

Tag der Abgabe: 05.11.2013

Tag der öffentlichen Verteidigung: 06.05.2014

Vorsitzender der Promotionskommission: Prof. Dr. Jörg Schilling

„Very often such a simplified model throws more light on the real workings of nature than any number of “ab initio” calculations of individual situations, which even where correct often contain so much detail as to conceal rather than reveal reality. It can be a disadvantage rather than an advantage to be able to compute or to measure too accurately, since often what one measures or computes is irrelevant in terms of mechanism. After all, the perfect computation simply reproduces Nature, does not explain her.“

P.W. Anderson, Nobel Lecture, 1977

Contents

List of figures	iii
List of abbreviations	v
1 Introduction	1
2 Atomistic magnetization dynamics	7
2.1 Magnetism and magnetic interaction	7
2.2 Landau-Lifshitz-Gilbert equation	11
2.3 Extended Landau-Lifshitz-Gilbert equation—nutaton and retardation	16
3 Electronic structure and magnetic properties	23
3.1 Density functional theory	24
3.2 Multiple-scattering theory	27
3.3 Magnetic properties within multiple-scattering theory	32
3.4 Tight-binding model	34
3.5 Anisotropic magnetic exchange within crystals with low symmetry	38
3.6 Disordered local moment theory	44
3.7 Gilbert damping tensor	51
4 Selected Results	57
4.1 Magnetic systems at elevated temperatures by non-relativistic disordered local moment theory	60
4.2 Non-collinear spin structures in ultrathin (111)-films	67
4.3 Gilbert damping tensor within the breathing Fermi surface model: anisotropy and non-locality	72
4.4 Nutation in magnetic nanostructures	88
5 Conclusion and Outlook	93
A Heisenberg-type disordered local moment theory: Distribution function	i
B Anisotropic exchange and free-energy derivatives	iii
C Overview of treated models	v
Bibliography	vii

List of Figures

Chapter 1 — Section 1.0

1.0.1 Storage density developments in the last 50 years	1
1.0.2 Magnetic reversal trajectories	2
1.0.3 Magnetic effects on different time- and length-scales	3

Chapter 2 — Section 2.1

2.1.1 Types of magnetic order	9
---	---

Chapter 2 — Section 2.2

2.2.1 Thermodynamic reservoirs	12
2.2.2 Scheme of the evolution $\partial m/\partial t$	15

Chapter 2 — Section 2.3

2.3.1 Set of magnetic moments treated by Boltzmann probability distribution function	17
2.3.2 Magnetic moment evolution $\partial m/\partial t$ influenced by its mass	19
2.3.3 Nutation at the edge atom in 2ML thick Co nanoislands on Cu(111)	20

Chapter 3 — Section 3.2

3.2.1 Wigner-Seitz construction and muffin-tin assumption	28
3.2.2 Scattering process between two sites considering the magnetization density	31

Chapter 3 — Section 3.3

3.3.1 Magnetic exchange parameter versus distance r	34
---	----

Chapter 3 — Section 3.4

3.4.1 Band splitting of N degenerate states	35
3.4.2 Periodic crystal potential and orbital overlap	36
3.4.3 Non-spinpolarized bandstructure calculated with the tight-binding and the KKR method	38
3.5.1 Lattice symmetries contributing to the Dzyaloshinskii-Moriya interaction	40

Chapter 3 — Section 3.5

3.5.2 Dzyaloshinskii-Moriya interaction in perovskites and spin glasses	41
3.5.3 Dzyaloshinskii-Moriya vectors for various surfaces	42

Chapter 3 — Section 3.6

3.6.1 Coherent potential approximation for a binary alloy $A_{1-x}B_x$	45
3.6.2 Von Mises-Fisher distribution for different width κ	47
3.6.3 DOS and principle model in Ising-type and Heisenberg-type DLM	49
Chapter 3 — Section 3.7	
3.7.1 Breathing Fermi-Surface model	53
3.7.2 Inter- and intra-band transition in the Kamberský model	55
Chapter 4 — Section 4.2	
4.2.1 Magnetization curve for 1 ML Fe on Pt(111)	67
Chapter C — Section C.0	
C.1 Topics and method overview	v

List of abbreviations

γ	Gyromagnetic ratio $\gamma = e g_e/2m_e = g\mu_B/\hbar = 1.761 \cdot 10^{11} \text{ 1/Ts}$
μ_0	Vacuum permeability $\mu_0 = 4\pi \cdot 10^{-7} \text{ N/A}^2$
μ_B	Bohr magneton $\mu_B = 5.788 \cdot 10^{-5} \text{ eV/T}$
\mathbf{k}_F	Fermi momentum
E_F	Fermi energy
h, \hbar	Planck constant $h = 6.626 \cdot 10^{-34} \text{ Js}$, $\hbar = \frac{h}{2\pi}$
(L)DOS	(Local) density of states
(rel)DLM	(relativistic) disordered local moment theory
(ST-)FMR	Spin-torque ferromagnetic resonance
BZ	Brillouin zone
CPA	Coherent potential approximation
DFT	Density functional theory
DM	Dzyaloshinskii-Moriya interaction
GGA	Generalized gradient approximation
KKR	Korringa-Kohn-Rostoker method
L(S)DA	Local (spin) density approximation
LL	Landau-Lifshitz equation
LLG	Landau-Lifshitz-Gilbert equation
LLMS	Landau-Lifshitz-Miyazaki-Seki equation
MC	Monte Carlo
ML	Monolayer
MOKE	Magneto-optical Kerr effect
MT	Muffin-tin
SPEELS	Spin-polarized electron energy loss spectroscopy
STM	Scanning tunneling microscope
SW	Stoner-Wohlfarth model
TB	Tight-binding
TDDFT	Time-dependent density functional theory
XMCD	X-ray magnetic circular dichroism

Introduction

Since the beginning of the twentieth century computers become more powerful. Inevitably this calls for higher data storage densities and faster storage velocities (figure 1.0.1). Starting from the oldest (1725) known form of a data storage device, punch cards, magnetic tapes up to floppy disks, efforts pursuing better information storage and retrieval performances enhanced continuously. But this enhancement reached a dead-end during the beginning of the 1980's.

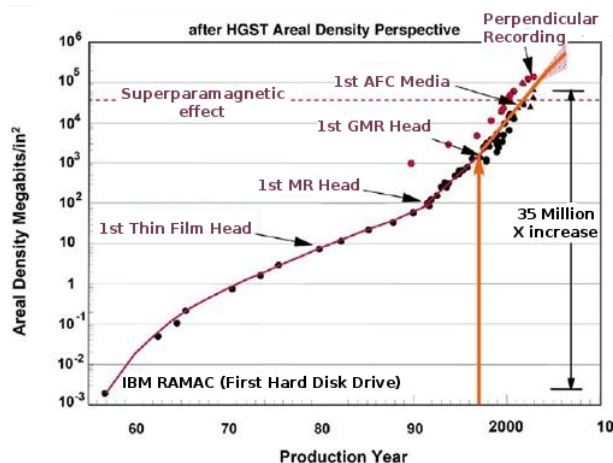


Figure 1.0.1.: Storage density developments in the last 50 years¹. Since the GMR effect systematically adopt into magnetic storage applications, the density increases exponentially. Nevertheless, the density is restricted by a thermal limit in ferromagnetic nanosystems (superparamagnetic limit). Temperature destabilizes the ordered magnetic structure in such a way, that the magnetic order stays in time, whereas simultaneously the collinear state responds coherently to the thermal fluctuations. The limit is affected by the anisotropy of the magnetic material that reduces the coupling to the thermal bath. An increase of the anisotropy in attempts to overcome the superparamagnetic limit was successfully pursued over the last decade, e.g. via developments of antiferromagnetically coupled (AFC) media.

The giant magnetoresistance (GMR) effect, discovered by Peter Grünberg and Albert Fert (Nobel Prize in Physics 2007), increased the data storage density per year dramatically [131, 269] (figure 1.0.1, marked with ‘1st GMR Head’). Devices based on this mechanism

¹Taken from <http://www.hs-weingarten.de/modet/referate/Datenspeicher.htm>

utilize the enhanced electric resistivity from an antiferromagnetic alignment of two magnetic layers to store information, as opposed to a ferromagnetic orientation lowers the resistivity. Both the macroscopic dimensions of the magnetic layers (micrometer length scale) and the large relaxation time of switching the magnetic moment (nanoseconds up to microseconds, figure 1.0.2 a) limit in practice the application of GMR-based technologies. This has been one of the reasons behind stagnation in hard-disk developments; so the industry switched towards solid state-based alternatives. In the latter, the elementary logic elements is a transistor, offers a faster writing and reading (by a factor of 10).

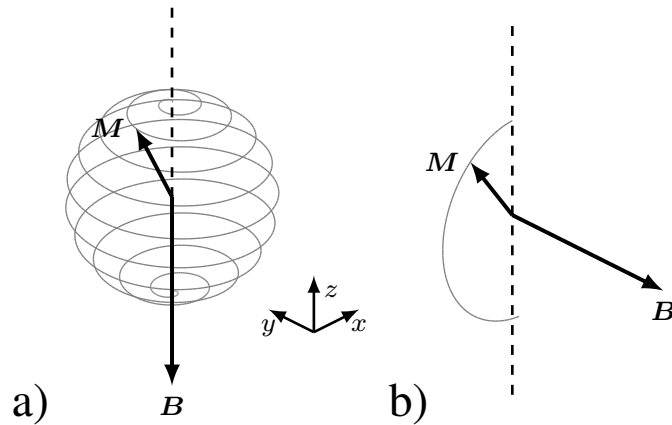


Figure 1.0.2.: *Magnetic reversal trajectories under influence of an external magnetic field B , as relevant to magnetic storage applications. a) An nearly anti-parallel alignment of the field B to the magnetization M lets the magnetic moment slowly precess in the direction of the field. This type of switching is slow and in the range of nanoseconds up to microseconds. b) A perpendicular alignment of the field B and the magnetization M twists the magnetic moment much faster than in a). The switched state is achievable on a picosecond time scale.*

In order to reflate ‘magnetic’ devices towards smaller time- and length-scales for instance, new ways were discovered in the last decade [124]. Khajetoorians et al. [151], e.g., showed a way to write information on nanoislands, that are connected by magnetic chains. Skyrmion lattices with nanometer length scale [227] or bistabilized magnetic atom arrays [180] were also proposed for storage applications. These arrays are predicted to push the data capability up to 400 TB. From a very fundamental viewpoint and for all these potential applications, the question about how to achieve efficient magnetic reversal (magnetic ‘writing’) arises. Therefore, an external magnetic field B can be applied antiparallel (figure 1.0.2 a) or perpendicular (figure 1.0.2 b) to the average magnetization M . More precisely, in the first case the magnetic damping dominates the relaxation time (ns up to μ s), where in the second case the precession around the field forces the switching to ≈ 100 ps (Larmor frequency). Apart from that, rapid switching can be also achieved by applying an external electric field to materials with strongly coupled multiferroic properties [251].

Reduction of time and length scale is accompanied also with so far neglected couplings between nanoscopic degrees of freedom (figure 1.0.3). Magnetism is affected by various properties of the crystal, such as the electron ground state, spin-orbit coupling or the crystal

²Referred to <http://www.psi.ch/swissfel/time-and-length-scales-in-magnetism.htm>

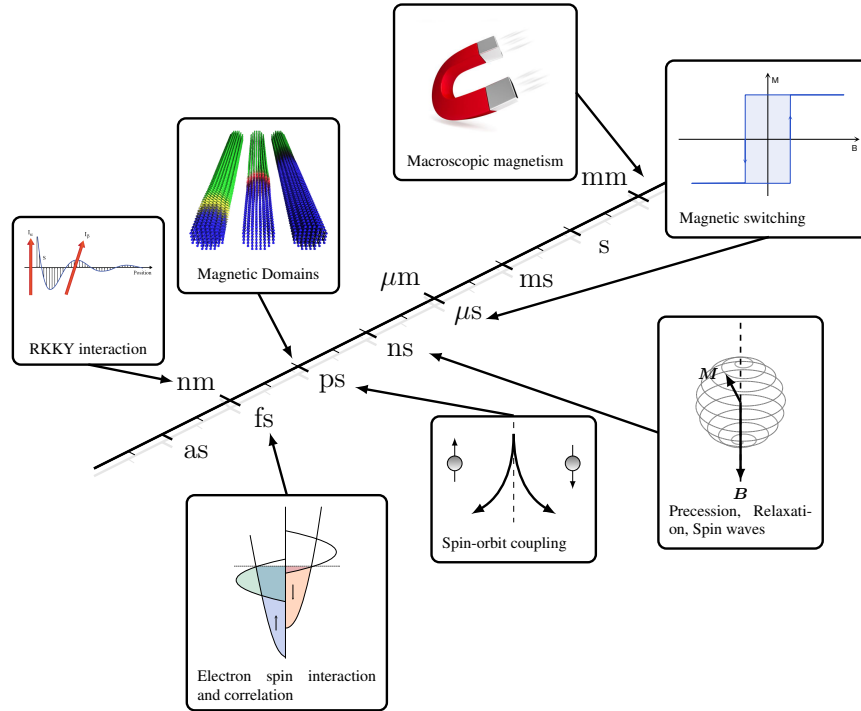


Figure 1.0.3.: Magnetic effects on different time- and length-scales². This thesis focuses on a nanometer and (sub-)picosecond time scale, where retardation effects due to different time scales of reservoirs that act on magnetism become important (electron correlation and spin-orbit coupling). The retardation is determined by the adiabatic limit. This limit, where the magnetic moment is considered as constant in the electronic system, is the limiting factor in diverse theoretical modeling and exists on a femtosecond up to picosecond time scale.

dimension. Hence, developing new data storage devices relying on magnetism on atomistic length scales requires a detailed characterization of *i*) the magnetic ground state and *ii*) the atomistic dynamics.

Various models exist to describe magnetism on a mesoscopic level [108, 212, 292]. One of the most applied models is the Stoner-Wohlfarth macrospin (SW) theory [16, 215, 238, 259, 263]. In this approach the atomic magnetic moments are regarded without interaction and merged into a so-called macrospin. Since the SW model accounts for magnetic anisotropy and the influence of an external magnetic field, it is able to simulate magnetic hysteresis. But due to the macrospin assumption, this theory will be not applicable to magnetic phenomena on small length scales, such as magnetic nanodomains, Skyrmions [14, 25], or in the superparamagnetic limit [33] (figure 1.0.1). Furthermore, it does not include any dynamics, switching times or reversal mechanisms. Hence, a more fundamental theory is required, going beyond the Stoner-Wohlfarth *ansatz*.

Heisenberg's model from 1928 [127] predicts for instance an exchange coupling mechanism with strength J between two atomic magnetic moments. This quantum-mechanical coupling improves the above picture, which provides access to an atomistic modeling of magnetism, and dictates, among other things, the dynamics of atomic magnetic moments, shown by Landau, Lifshitz and Gilbert [109, 166]. Here, the evolution of the magnetic

moment is the superposition of a precession around and a damping in the direction of the Heisenberg exchange field. This model has been successfully deployed on magnetic multilayers [245], nanometer domain walls [56], and magnetically doped semiconductors [128].

The electronic structure is fundamental for magnetic properties of a material, since magnetism stems from the spin and orbital angular momentum of the quantum-mechanically treated electrons. This corroborates, in a naive picture of separated reservoirs for various atomic degrees of freedom (electron, spin, and lattice reservoir), strong correlations between the reservoirs. The latter is neglected in all earlier listed studies on nm-magnetism and, thus, it leads in general to discrepancy between theory and experiment, especially in postulating the phase transition temperature, the magnetic ground state or magnetic switching. This calls for an extended methodology on simulating magnetism on short time- and length-scales. Hence, one aim of this thesis will be to consider the exchange between the reservoirs in the magnetic ground state and the magnetization dynamics, especially on a ps-time and nm-length scale. Therefore, first, the role of the magnetic moment on the electronic structure is examined in detail. Second, the contribution coming from the lattice reservoir is then studied, looking in particular at the lack of inversion symmetry in the crystal. Both ingredients have a bearing on the thermal equilibrium of the magnetic material.

Since each of these reservoirs acts in principle on different time scales, retardation in time and space can appear. The first originates in the delay that the electrons need to become correlated and ‘form’ magnetism, which regards the mass of magnetic moments. Non-local anisotropic energy dissipation, however, provokes additionally some retardation in space. Hence, a second aim is to consider retardation in time and in space near the adiabatic limit.

This thesis is composed of the following parts. The reader is first introduced to the conventional concepts of magnetism and the dynamics of magnetic materials (section 2.1 and 2.2). Thereby, magnetism on an ultrashort time scale will be discussed, examining model extensions far from the Heisenberg and the Landau-Lifshitz-Gilbert *ansatz* (section 2.3). Since the electronic structure is fundamental for magnetism, the second part contains the basic principle for electronic structure calculations. Thus, the thesis introduces the concept of density functional theory (DFT) (section 3.1) and focuses on band-structure methods of choice, the Korringa-Kohn-Rostoker Green function method (section 3.2) and the tight-binding method (section 3.4). Based on this foundations, magnetic properties can be calculated. In particular, the connection between magnetic order and crystal symmetry, especially at surfaces, gives rise to an extended Heisenberg model, motivated by Dzyaloshinskii and Moriya (section 3.5). The disordered local moment theory (DLM) is then used to discuss the impact of the magnetic ‘noise’ on the electron ground state (section 3.6). In section 3.7 the mechanism of damping in magnetic materials will then be described within two approaches: *i*) linear response theory and *ii*) the Kamberský breathing Fermi surface model.

In the last part (chapter 4), four publications have been chosen to present the results on an extended model, that accounts for the connection between spin-, electron and lattice-reservoir on ultrashort scales. Meanwhile, the application takes place on various magnetic materials including ‘basic’ Stoner magnets. The first paper discusses the temperature-dependent magnetic properties at elevated temperatures, based on the disordered local moment theory. The second publication considers non-collinear spin structures on ultrathin magnetic films grown on substrates with strong spin-orbit coupling. The third pa-

per deals with the magnetic damping effects in bulk and low-dimensional systems. The last publication proceeds with the dynamics on ultrashort times scales; more precisely, with nutation in magnetic systems. A summary and an outlook will conclude this thesis.

Atomistic magnetization dynamics

An equation of motion is required in order to simulate atomistic magnetization on ultrashort time scales and connect magnetism with other atomic degrees of freedom. On the one hand, the quantum-mechanical equation of motion for the spin operator \hat{S} can be solved, whereas, on the other hand, the semi-classical *ansatz* of the Landau-Lifshitz-Gilbert equation for a continuous macroscopic magnetic moment \mathbf{M} provides an approximation that reproduces experimental measurements quit well on the micrometer length scale [8, 130, 176].

The simplest continuation, creating an atomistic equation of motion, is to transform the mesoscopic dynamic equation of the continuous quantity $\mathbf{M}(\mathbf{r})$ into a discrete set of atomic moments \mathbf{m}_i . Various nanoscale exchange mechanisms will dictate the magnetic ground state. However, the transformation from a mesoscopic to a nanoscopic length scale holds only when the electron-spin exchange mechanism is assumed as adiabatic, which is always valid in the mesoscopic scale, as well if the Ehrenfest theorem holds [283]. More precisely, quantum mechanical and classical equations of motion agree if the Hamiltonian is linear in \mathbf{m}_i . Hence, the question arises of how the nanoscopic classical Landau-Lifshitz-Gilbert equation extends near the adiabatic and quantum mechanical limit.

This chapter is arranged as follows: first, a brief overview of magnetism and the concept of magnetic exchange will be given (section 2.1). Section 2.2 focuses on the derivation of the classical equation of motion for \mathbf{m}_i from the quantum mechanical one. Following Gilbert idea, the dissipation loss reflected by a damping term in the dynamic equation will be discussed. Section 2.3 proceeds with various models going beyond Gilbert's assumption and approaching the adiabatic and quantum mechanic limit.

2.1 Magnetism and magnetic interaction

There exist various ways in the literature to introduce the topic of magnetism. Starting from the classical point of view using Maxwell's equation [212], a magnetic contribution \mathbf{j}_m to the current at an atom appears, which is the result of the motion of electrons in their stationary orbitals. This defines the magnetic moment \mathbf{m}_i at the local position \mathbf{R}_i :

$$\mathbf{m}_i = \frac{1}{2} \int (\mathbf{r} - \mathbf{R}_i) \times \mathbf{j}_m^{(i)} d\mathbf{r}. \quad (2.1.1)$$

Supposing the electrons affect only the magnetic moment, one obtains the relation between the magnetic moment and the total angular momentum \mathbf{L} of the electron: $\mathbf{m} = -e/2m\mathbf{L} = -\gamma\mathbf{L}$, where the absolute value of γ is the gyromagnetic ratio. According to Maxwell's laws, the magnetic moment responds to an external magnetic field \mathbf{B} within 'linear' materials [108] via

$$\mathbf{m} = \chi\mathbf{B}. \quad (2.1.2)$$

Thereby, the response function or susceptibility χ contains all necessary information. Simultaneously, the external magnetic field couples to the moment: $\mathbf{m} = -\partial E_{\text{mag}}/\partial\mathbf{B}$ [60], giving a magnetic energy E_{mag} :

$$E_{\text{mag}} = -\int_0^{\mathbf{B}} \mathbf{m} \, d\mathbf{B}' = -\frac{1}{2}\mathbf{m} \cdot \mathbf{B}. \quad (2.1.3)$$

The magnetization \mathbf{M} is defined as the macroscopic average of all magnetic moments ($\mathbf{M} = \langle \mathbf{m} \rangle$) [108], which is eventually measured in experiment.

From a quantum-mechanical point of view [212], the Schrödinger equation has to be solved

$$\left(\hat{H} - E_{\text{mag}}\right) |\psi\rangle = 0, \quad (2.1.4)$$

where \hat{H} is a hermitian many-body Hamiltonian, related to the magnetic-moment operator $\hat{m} = -\partial\hat{H}/\partial\mathbf{B}$, in accordance to the classical theory (2.1.3). The total magnetic moment, however, is composed of a magnetic moment \mathbf{m}_{ind} , induced by an external magnetic field, and $-\gamma(\mathbf{L} + 2\mathbf{S})$, where \mathbf{L} is the total orbital angular momentum and \mathbf{S} is the spin momentum. So, magnetism stems from the orbital momentum and the spin of the electron. This is valid only, if one considers localized electrons in a homogeneous external magnetic field and neglects the spin-orbit coupling (SOC) [212].

One of the main problem in modern theories of magnetism is to extract the magnetic current in a correlated many-body system, which will be introduced later in this thesis using density functional and multiple-scattering theory. Here, one distinguishes between two limits *i) strongly localized moments* and *ii) itinerant magnetism* [212]. Magnetism in metals (band magnetism), e.g. in Fe, Co, Ni, is of delocalized nature and comes from a preferred spin orientation of the electrons due to the exchange splitting between the spin-up and the spin-down channels. This can be described within the Hubbard model [135, 201]. Localized magnetism exists in materials doped with magnetic impurities (Kondo effect), and is a feature that emerges from different 'groups' of electrons within an effective interaction model (e.g. s-d or s-f model [137]).

Concerning the susceptibility χ , one classifies the magnetic phenomena in three classes:

Paramagnetism Paramagnetic materials carry a permanent magnetic moment, which tends to reorient itself parallel to an external magnetic field; it is featured with positive susceptibility χ_{para} . Sensitivity to thermal excitations, however, prevent complete reorientation along the external field. Since the atomic magnets are randomly orientated at elevated temperatures, the magnetization disappears (figure 2.1.1 a).

Diamagnetism Almost all organic substances, superconductors below their critical temperature, and some metals like Bi, Zn or Hg, exhibit an induced magnetic dipole due to an external field. According to Lenz's law, this orients itself antiparallel to the field and is, thus, associated with a negative response: $\chi_{\text{dia}} < 0$. All materials show diamagnetic properties, but often these are too small compared to other magnetic effects.

Collective Magnetism Quantum-mechanical effects, such as the exchange field and the crystal field [273], force permanent magnetic moments into collective magnetism. Below a certain temperature T_c , this type of magnetism appears as a spontaneous macroscopic magnetization even without external stimuli. The exchange field provides short range order and allows domain wall formations or spin waves. Under collective magnetism one can distinguish four sub-classes of ground state ordering: *i*) ferromagnetism (FM), *ii*) antiferromagnetism (AFM), *iii*) ferrimagnetism (FiM), and *iv*) non-collinear magnetism (NCM) (figure 2.1.1). Non-collinear magnetism is featured by non-parallel, disordered magnetic moments and occurs beside the paramagnetic limit. There exist three mechanisms forcing non-collinearity: competing exchange mechanisms, geometric frustration, and direct anisotropic exchange from spin-orbit coupling. Spin vortices, a special example of non-collinearity, also known as Skyrmions, can e.g. appear at surfaces. Such structures are alike in terms of their topology and are, due to topological protection mechanisms, stable and robust. In contrast to magnetically ordered structures, such as ferromagnets, a local order parameter cannot be defined.

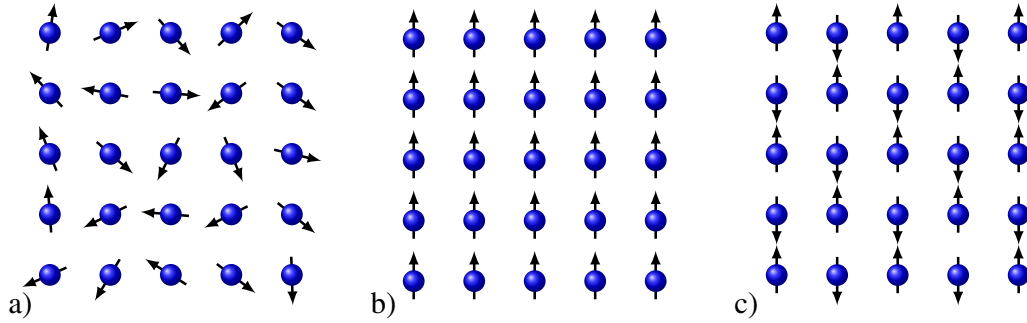


Figure 2.1.1.: Different types of magnetic order: a) paramagnetic state, b) ferromagnetic state and c) antiferromagnetic state. Atomic magnetic moments are marked by the black arrows, crystal sites are illustrated by the blue spheres.

Since this thesis discusses in particular collective magnetism effects, an in-depth focus on magnetic formation mechanisms is required. Collective magnetism emerges via a second-order phase transition: below the critical temperature T_c there exists a spontaneous ordering towards reduced symmetry, since the magnetic moments break the symmetry of the crystal lattice. Above T_c this ordering vanishes, the symmetry increases and the system behaves as a paramagnet. The dipole-dipole interaction could predict a T_c of around 1.16 K [212], for too small in comparison to the typical experimental value of $\propto 1000$ K [48] in Fe, Co and Ni. Hence, the dipole-dipole interaction cannot be the driving mechanism of magnetism. The actual mechanism was discovered in 1926 by Dirac and Heisenberg [71, 126]: the exchange interaction, resulting in an effective operator

$$\hat{H}_{ex} = - \sum_{ij} J_{ij} \mathbf{m}_i \cdot \mathbf{m}_j, \quad (2.1.5)$$

where the J_{ij} are the exchange integrals. The spin-spin coupling $\mathbf{m}_i \cdot \mathbf{m}_j$ between site i and j simulates the exchange matrix elements of the Coulomb interaction. In this thesis the magnetic moments \mathbf{m}_i are considered as classical localized magnetic moments ($|\mathbf{m}_i| = m_s$).

The Weiss model [108], developed by the French physicist Pierre-Ernest Weiss in 1906 [280], was the first phenomenological theory of ferromagnetism, devised to account for magnetic phase transitions. It assumes an exchange field B_{ex} based on the Heisenberg model and proportional to the magnetization ($\mathbf{M} = \lambda \mathbf{B}_{ex}$). The proportionality factor λ puts the action of the Weiss field on par with the external magnetic field. It expresses the phase-transition temperature according to the Curie law $\lambda_c/T_c = 1$. However, this model makes no statement about the source of the exchange field, which is of pure quantum-mechanical origin and a direct consequence of the Pauli's exclusion-principle [189].

In band magnetism, many electrons can flip without gaining too much single-particle kinetic energy, if there is a distinct peak in the density of states $n(\varepsilon_F)$ at the Fermi energy (Stoner-criterion) $U n(\varepsilon_F) > 1$ [7, 108, 257, 258], where U is the exchange splitting in the density of states. Heitler and London show in their model [108, 292] the character of the magnetic exchange: if the wavefunctions of the participating electrons overlap, then ferromagnetism should occur. Contrary to this, insulators or transition metal oxides, e.g. MnO [6, 169], show a magnetic order, inspite of a direct overlap between the manganese orbitals due to the large spacing. This type of magnetism is driven by a number of indirect exchange mechanisms, like Rudermann-Kittel-Kasuya-Yosida (RKKY) interaction [148, 236, 291], super exchange (Goodenough-Kanamori-Anderson (GKA)-rules) [3, 115, 147] and double exchange [107, 298], and leads to an effective Heisenberg-type Hamiltonian (2.1.5).

The Heisenberg Hamiltonian is to this day, the most intensely investigated and also best understood model of magnetism. In contrast to experimental predictions [4, 132, 256, 287, 288], Heisenberg magnetism is isotropic in space ($J_{ij} = J_{ji}, J_{ii} = 0$) and does not account for any 'crystal anisotropy'. Physical properties in crystals are, however, typically anisotropic due to the crystal field. This splits degenerate electronic levels and fixes the orbital momentum \mathbf{L} in space relative to the solid orientation. Consequently, the crystal field and the spin-orbit coupling reorient the magnetic moment direction. The magnetization will favor alignment with the largest component in the orbital momentum \mathbf{L} minimizing spin-orbit energy as given by the crystal symmetry. This type of anisotropy is known as magnetocrystalline anisotropy \hat{H}_{mca} .

Similar to the Heisenberg exchange energy and due to the broken time reversal symmetry, the energy has to be invariant under inversion of the magnetic moments direction [212]. Thus,

$$\hat{H}_{mca} = \mathbf{K}_0 + \mathbf{m}\mathbf{K}_1\mathbf{m} + \mathbf{m}\mathbf{m}\mathbf{K}_2\mathbf{m}\mathbf{m} + \dots, \quad (2.1.6)$$

where \mathbf{K}_0 , \mathbf{K}_1 and \mathbf{K}_2 are the anisotropy tensors of zero, first and second order, respectively. Considering only diagonal elements, one obtains the uniaxial form of the anisotropy. The anisotropic properties of magnetic system, which are treated in this thesis, are in general of uniaxial nature up to the first order aligned in z direction.

In addition to the magnetocrystalline anisotropy, there exist also *i*) shape anisotropy, *ii*)

induced magnetic anisotropy (e.g. by an external magnetic field) and *iii*) stress anisotropy. The first is reflected by the dipole-dipole interaction. Magnetic moments are dipoles that are not dividable into monopoles (although magnetic monopoles separated by a Dirac string [72, 139] can exist). As such, they interact with each other via the dipole-dipole interaction

$$\hat{H}_{dd} = - \sum_{ij} \mathbf{m}_i \mathbf{Q}_{ij} \mathbf{m}_j, \quad \text{with } Q_{ij}^{\mu\nu} = \frac{\mu_0}{8\pi} \frac{3r_{ij}^\mu r_{ij}^\nu - r_{ij}^2 \delta_{\mu\nu}}{r_{ij}^5}, \quad (2.1.7)$$

where $\mathbf{r}_{ij} = \mathbf{r}_i - \mathbf{r}_j$ is the distance between two dipoles, $\delta_{\mu\nu}$ is the Kronecker delta ($\mu, \nu = x, y, z$), μ_0 is the vacuum permeability. As distinct from the exchange interaction, this is a weak, but long-range coupling mechanism and takes into account shape effects of low dimensional clusters, such as nanoislands, nanotubes, or in spin ice.

The isotropic character of the Heisenberg model can also be broken by an external magnetic field \mathbf{B}_{ext} , leading to the Zeeman term

$$\hat{H}_{ext} = -\gamma \mathbf{B}_{ext} \sum_i \mathbf{m}_i, \quad (2.1.8)$$

that couples the average magnetic moment $\mathbf{M} = \sum_i \mathbf{m}_i$ to the external magnetic field.

In this thesis the stress anisotropy will be neglected, but it can be considered by the distance-dependence of the exchange parameters. Finally, the total Hamilton operator, which forms the basis for all simulations in this thesis, reads

$$\hat{H} = \hat{H}_{ex} + \hat{H}_{mca} + \hat{H}_{dd} + \hat{H}_{ext}. \quad (2.1.9)$$

As already mention, the dipole-dipole interaction \hat{H}_{dd} account only for the shape of magnetic nanostructures, such as in 2ML Co islands on Cu(111) [32]. Since the magnetic coupling constants J_{ij} are in the range of meV, the magnetic exchange energy \hat{H}_{ex} is the dominant term in equation (2.1.9). Compared to this, energies in the range of $\approx 10 - 100 \mu\text{eV}$ are attributed to the magnetocrystalline anisotropy, which is in the same order as the external magnetic field energy \hat{H}_{ext} .

The effective field $\mathbf{B} = -\partial\hat{H}/\partial\mathbf{m}$ of the energy contributions (2.1.9) drives the dynamics of magnetic moments (precession and damping), since it defines e.g. spin-wave modes or controls, for instance, the magnetic relaxation times. A detailed derivation of this field can be found in Ref. [32, 245].

2.2 Landau-Lifshitz-Gilbert equation

Let us focus now on excitations of non-equilibrium magnetic states. Considering initially a ferromagnetic spin chain, reversal of one atomic moment or a single spin flip enhance the energy above the ground state energy. This costs $\Delta E = 4JS^2$, where J is the coupling strength between neighboring moments. Excitations lower in energy, which are spatially extended over the entire chain, correspond to spin waves (magnons). These waves propagate through the spin lattice with a certain lifetime τ and $\mathbf{k} \cdot \mathbf{r} \ll 1$, where \mathbf{k} is the propagation vector. More precisely, τ and the propagation are adjusted by various nanoscopic degrees of freedom, which can be accounted for in an appropriate magnetization dynamics model.

Such an equation of motion, e.g. for magnons in magnetic chains, was first formulated by Landau and Lifshitz [41, 166]. In general, the quantum-mechanical equation of motion for the spin operator $\hat{\mathbf{S}}$ [128, 245] reads

$$\frac{\partial \hat{\mathbf{S}}}{\partial t} = -\frac{i}{\hbar} [\hat{\mathbf{S}}, \hat{H}_{KS}], \quad (2.2.1)$$

where \hat{H}_{KS} is the Kohn-Sham Hamilton operator. Having the separation *ansatz* (shown in section 3.1, equation (3.1.11)) at hand, the Kohn-Sham Hamiltonian is expressed as

$$\hat{H}_{KS} = \hat{H} + \mu_B \hat{\boldsymbol{\sigma}} \cdot \hat{\mathbf{B}}. \quad (2.2.2)$$

With this Hamiltonian, equation (2.2.1) can be simplified by the commutation rules of the Pauli matrices $\hat{\boldsymbol{\sigma}}$ [32, 245]

$$\frac{\partial}{\partial t} \hat{\mathbf{S}} = -\gamma \hat{\mathbf{S}} \times \hat{\mathbf{B}} - \nabla \cdot \hat{\mathbf{j}}, \quad (2.2.3)$$

which has the form of a continuity equation. Without spin-orbit coupling, $\hat{\mathbf{S}}$ commutes with \hat{H} , with the exception of the kinetic energy. Hence, the current operator $\hat{\mathbf{j}}$ has to be taken into account. However, $\nabla \cdot \hat{\mathbf{j}}$ vanishes in the *atomic moment approximation* [245], which postulates negligible instabilities of the atomic moment length. This holds only, when the Kohn-Sham system is equilibrated, measured in terms of the electron relaxation time τ_e . The latter is typically smaller than the magnetic relaxation τ_s (*adiabatic approach*) (figure 2.2.1) and can be estimated by $\tau_e < 1$ ps and $\tau_s \approx 1$ ps, respectively [256]. The interaction $J_{es} \approx \hbar/\tau_{es}$ between both reservoirs, however, exhibits $\tau_{es} \approx 10 - 100$ fs [245]. Magnetization dynamics on time scales close to τ_{es} , which will be focused on in this thesis, requires methodological extensions, since it has to consider the coupling between different microscopic degrees of freedom (figure 2.2.1).

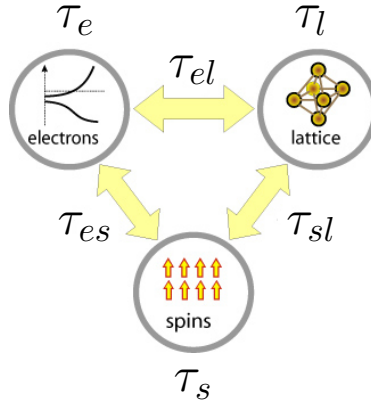


Figure 2.2.1.: Thermodynamic reservoirs (electrons, spin, lattice) [155]. All three degrees of freedom interact with each other with the strength $J \approx \hbar\tau_{\mu\nu}^{-1}$ and relax into the ground state within a typical relaxation time (τ_e , τ_l , τ_s). Hence, the electronic and the lattice reservoirs can in principle affect the dynamics of a magnetic material, especially on ultrashort time scales.

Considering the Ehrenfest theorem, one can transform the continuity equation for the spin operator $\hat{\mathbf{S}}$ (2.2.3) into the spin density representation \mathbf{m}_i [32, 245]. This holds

$$\frac{\partial}{\partial t} \mathbf{m}_i = -\gamma \mathbf{m}_i \times \mathbf{B}. \quad (2.2.4)$$

Here, i is the atomic index, labeling the dynamics of an atomistic magnetic moment as an adiabatic, non-dissipative precession around the effective field \mathbf{B} .

A quantum-mechanical derivation of the equation of motion is also given by Wieser [282, 283] who considers the quantum-mechanical time evolution $\hat{U}(t + \delta t, t)$ of the state $|\psi(t)\rangle$:

$$|\psi(t + \Delta t)\rangle = \hat{U}(t + \Delta t, t) |\psi(t)\rangle. \quad (2.2.5)$$

Assuming that the time steps Δt are small, Wieser derived the quantum-mechanical counterpart of the Landau-Lifshitz-Gilbert equation

$$i\hbar \frac{d}{dt} |\psi(t)\rangle = \left(\hat{H} - i\alpha \left[\hat{\Gamma} - \langle \hat{\Gamma} \rangle \right] \right) |\psi(t)\rangle. \quad (2.2.6)$$

Here, the term $i\alpha \left[\hat{\Gamma} - \langle \hat{\Gamma} \rangle \right]$ correlates to energy dissipation, if $\hat{\Gamma} = \hat{H}$. He concludes that a discrepancy between classical and quantum-mechanical model exists, if the magnetic Hamiltonian is not linear with respect to the magnetic moment.

The precession of the magnetic moment (2.2.4) is dynamically reversible. However, in out-of-equilibrium magnetic systems [154, 155] remagnetization was observed, where the rate is determined by damping mechanisms; the dynamics becomes irreversible. This is, so far, not included in equation (2.2.4). “Damping involved loss of energy from the macroscopic motion of the local magnetization field by transfer of energy to microscopic thermal motion.” (Gilbert [109]), such as spin waves, phonons, eddy currents, and lattice defects. In 1935 Landau and Lifshitz introduced a phenomenological damping term [166] and extended the effective precession-causing field \mathbf{B} by a dissipation part $\mathbf{B}^{diss} = \alpha_{LL} \mathbf{m} \times \mathbf{B}$. This dissipation field is, however, only valid for small damping parameters, since no physical solution can be achieved for $\alpha_{LL} \rightarrow \infty$. To account for the limit of high damping [186], Gilbert redefines the phenomenological damping term [109] in terms of a viscose damping mechanism that is proportional to the velocity of the magnetic moment $\mathbf{B}^{diss} = \alpha \partial \mathbf{m} / \partial t$. In addition, this type of damping conserves the length of the magnetic moment. The Gilbert damping constant α comprises all damping mechanisms, extrinsic and intrinsic, as well as direct (induced by the spin-orbit coupling) and indirect processes, and introduces an effective energy transfer. The intrinsic damping is experimentally the smallest observable magnetic damping that do not depend for instance on the stacking number of the crystal, whereas the extrinsic damping is mediated by e.g. structural changes, defects or the size of the system. However, both contributions—intrinsic and extrinsic—are controversially discussed in literature [10, 149, 249]. Different other proposals concerning the nature of the dissipation field \mathbf{B}^{diss} exist, e.g. the Bloch-Bloembergen equation [23, 24] or the Landau-Lifshitz-Bloch equation [50, 104, 105, 278], both not conserving the moment length.

The Gilbert damping for equation (2.2.4) is derived using the Euler-Lagrange formalism, where the Lagrangian \mathcal{L} is a functional of the magnetic moments \mathbf{m} and the magnetic velocity $\mathbf{u} = \dot{\mathbf{m}} = \frac{\partial}{\partial t} \mathbf{m}$. It comprises a kinetic energy $\mathcal{T}[\mathbf{m}, \dot{\mathbf{m}}]$ as well as a potential energy $\mathcal{U}[\mathbf{m}]$ part, whereas $\mathbf{B} = -\frac{\partial \mathcal{U}}{\partial \mathbf{m}}$, and an additional Rayleigh dissipation functional \mathcal{R} [191, 268]. Thus,

$$\frac{d}{dt} \frac{\partial \mathcal{L}(\mathbf{m}, \dot{\mathbf{m}})}{\partial \dot{\mathbf{m}}} - \frac{\partial \mathcal{L}(\mathbf{m}, \dot{\mathbf{m}})}{\partial \mathbf{m}} + \frac{\partial \mathcal{R}(\dot{\mathbf{m}})}{\partial \dot{\mathbf{m}}} = 0, \quad (2.2.7)$$

where

$$\mathcal{R} = \frac{1}{2} \sum_i \sum_j \dot{\mathbf{m}}_i \eta_{ij} \dot{\mathbf{m}}_j. \quad (2.2.8)$$

Here, the tensor $\boldsymbol{\eta}$ quantifies the non-local damping throughout the sample. This form considers non-uniform damping mechanisms like rapid spin reorientation, defects and impurities. Since most experiments predict a uniform, isotropic dissipation transfer [103, 217], the rate $\boldsymbol{\eta}$ simplifies to

$$\boldsymbol{\eta}_{ij} = -\frac{\alpha}{\gamma m_s} \mathbf{E} \delta_{ij}, \quad (2.2.9)$$

where \mathbf{E} is the unit matrix and $m_s = |\mathbf{m}|$ is the moment length. With $\frac{\partial \mathcal{U}[\mathbf{m}]}{\partial \dot{\mathbf{m}}} = 0$ and $\frac{\partial \mathcal{R}[\dot{\mathbf{m}}]}{\partial \dot{\mathbf{m}}} = -\mathbf{B}_{\text{diss}} = -\frac{\alpha}{\gamma m_s} \dot{\mathbf{m}}$, one notices a reduction of the effective field \mathbf{B} by the ‘damping field’ \mathbf{B}_{diss} and thus, a modification of the torque in field direction:

$$\frac{d}{dt} \frac{\partial \mathcal{T}(\mathbf{m}, \dot{\mathbf{m}})}{\partial \dot{\mathbf{m}}} - \frac{\partial \mathcal{T}(\mathbf{m}, \dot{\mathbf{m}})}{\partial \mathbf{m}} + \left(\mathbf{B} - \frac{\alpha}{\gamma m_s} \dot{\mathbf{m}} \right) = 0. \quad (2.2.10)$$

Consequently, the equation of motion for an atomistic magnetic moment (Landau-Lifshitz-Gilbert equation) ends up with

$$\frac{\partial}{\partial t} \mathbf{m}_i = \mathbf{m}_i \times \left(-\gamma \mathbf{B} + \frac{\alpha}{m_s} \frac{\partial \mathbf{m}_i}{\partial t} \right). \quad (2.2.11)$$

As will be shown later in this thesis (chapter 3.7), the energy transfer rate α is strongly influenced by the spin-orbit coupling. This spin-orbit contribution, however, differs from those pointed out by Skubic et al. [245] in the continuity equation (2.2.3).

The magnetic damping can be experimentally observed by means of (spin-torque) ferromagnetic resonance measurements ((ST)-FMR) [103, 217]. Magnetic properties, such as g -factor, magnetic anisotropy and interlayer magnetic coupling [125] are obtained by estimating the resonance field H_R of the FMR spectra. The width of the resonance peak ΔH_R is depicted as the superposition of three contributions: the line width due to intrinsic damping, the distribution of the signal magnitude and the direction of the effective demagnetization field. The first contribution correlates linearly to the damping constant α [198]. The resonance field is used to analyze also magnetic inhomogeneities in thin films [198, 217]. A second experimental method is the heterodyne magneto-optical microwave microscope (H-MOMM)¹ [55]. Here, beat-frequency microwaves are generated, which produce spin waves in the magnetic system. Using the magneto-optical Kerr effect (MOKE) in the experimental set-up, the excited magnetic order (magnon) and its dissipative behavior are observable, in particular the inhomogeneous damping in nanomagnets.

Equation (2.2.11) contains energy and angular momentum dissipation, mimicked by the damping contribution and the magnetic Hamiltonian, respectively. However, the coupling to the thermal bath is so far neglected. Three reservoirs [2, 154] characterized by the spin temperature T_s , the electron temperature T_e as well as the lattice temperature T_l , affect in principle the dynamics of atomistic magnetic moments (figure 2.2.1). In the following, only the spin temperature will be considered. The role of the spin temperature on the electronic ground state will be illustrated in section 3.6. Nevertheless, the coupling between all three temperatures can be depicted with the three temperature model [54, 67, 211].

In the presence of thermal spin agitation at finite temperature, introduced by Brown [40], each atomic moment is impacted by a small field $\mathbf{h}(t)$, where its statistical average is zero.

¹<http://www.nist.gov/pml/electromagnetics/magnetics/nanomagnet-spin-damping.cfm>

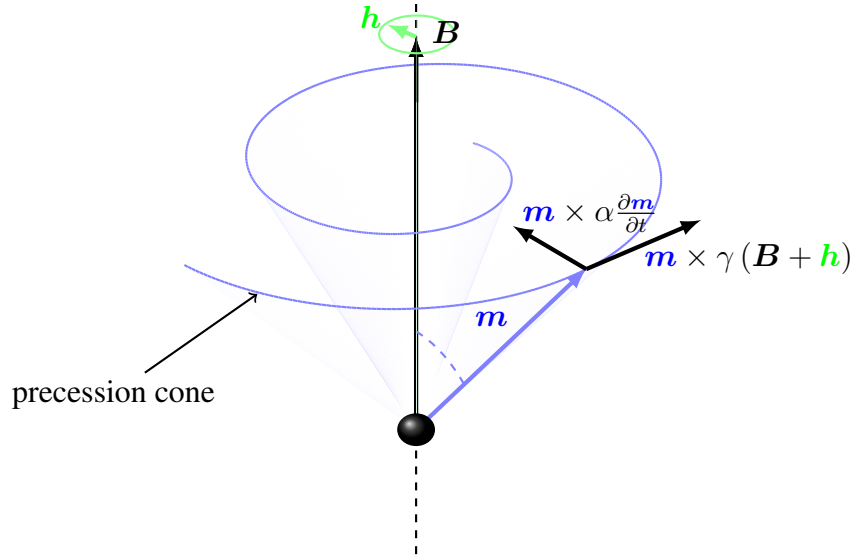


Figure 2.2.2.: Scheme of the evolution $\partial\mathbf{m}/\partial t$. The magnetic moment precesses (blue cone and lines) around the field \mathbf{B} (black arrow) and dissipates in the direction of the field. The temperature, caused by an additional white noise field \mathbf{h} (green cone and arrow), deflects the effective field from its present equilibrium position.

Hence, the temperature in equation (2.2.11) is approximated by a Brownian motion [39, 81] and obeys Langevin dynamics [32]. The random field $\mathbf{h}(t)$ complies with the following properties [40]:

- i)* the process $\mathbf{h}(t)$ is stationary;
- ii)* $\mathbf{h}(t)$ is Gauss-distributed;
- iii)* $\mathbf{h}_i(t)$ and $\mathbf{h}_j(t + \tau)$ are correlated in shorter time interval τ than the changes of \mathbf{m} according to (2.2.11): $\langle \mathbf{h}_i(t) \mathbf{h}_j(t + \tau) \rangle_{\text{av}} = D_{ij} \delta(\tau)$, where D_{ij} is the distribution width;
- iv)* \mathbf{h} is independent of \mathbf{m} and isotropic: $D_{ij} = D \delta_{ij}$.

These properties mimic white noise, simulated as Gauss-distributed random numbers [37]. The distribution width D of the Gauss peak is obtained by solving the Fokker-Planck equation [100], deduced from the corresponding Langevin equation [32] and based on the Stratonovich analysis [216]. Since the equilibrium distribution in the Fokker-Planck equation follows a Boltzmann distribution, the fluctuation strength D reads [32, 245]

$$D = \alpha \frac{k_B T_s}{\gamma m_s}. \quad (2.2.12)$$

k_B is the Boltzmann factor and γ the gyromagnetic ratio. The thermal fluctuation strength and the dissipation are correlated to each other. This is the main statement of the fluctuation-dissipation theorem [52, 214]: The macroscopic quantity α is coupled with the microscopic value D .

For this thesis, the atomistic assumption of the Landau-Lifshitz-Gilbert equation was first utilized to study the superparamagnetic effect and the validity of the Stoner-Wohlfarth

model in 2ML Co islands on Cu(111), published in [32] (not shown in this thesis). The main emphasis was to reproduce the experiment, predicting ferromagnetic behavior only above a critical island size. Below this critical size the islands are superparamagnetic. Magnetization dynamics of various other surfaces, for instance Fe/Pt(111) or Fe/Cu(001), were also studied in terms of long-range magnetic excitations (not shown in this thesis). Based on these works, the completeness of the simulation model became arguable: For instance anisotropic exchange effects or the dissipation-fluctuation theorem at surfaces were not or not exactly accounted for. Due to the adiabatic and the quantum-mechanical limit, the LLG equation exhibited also a restricted validity at short time scales. These mismatches required an methodological extension of the atomistic magnetization dynamics on nm-length- and fs-time scale.

2.3 Extended Landau-Lifshitz-Gilbert equation—nutaton and retardation

In the previous section 2.2, two crucial assumptions were made that are only valid at longer time scales (typical ns -time scale):

- i)* A uniform, uniaxial distribution of energy loss and angular momentum transfer due to damping;
- ii)* Validity of a macroscopic ansatz on ultra-short time scales ($t < \tau$, where τ is the response time of the system).

Let us assume, that the magnetization \mathbf{m} has a mass \mathbf{m} , which was already predicted by Döring et al. [73] for domain walls and experimentally verified in Josephson junction [101, 102]. This mass is not related to the inertia of the matter, but to the inertia of the magnetic moment [57] due to ‘formation’ of magnetism. The existence of a mass has two consequences:

- The magnetization dynamics follow Newton’s second axiom: $\mathbf{B} = \mathbf{m}\partial\mathbf{u}/\partial t$;
- The kinetic energy of the magnetic moment is proportional to $\mathbf{m}\mathbf{u}^2/2$, where $\mathbf{u} = \partial\mathbf{m}/\partial t$ is the velocity of the magnetic moment.

Both hypotheses implicate inertia of magnetic moment. If there is no magnetic center of mass, a complex magnetic inertia tensor $\boldsymbol{\iota}$ exists instead. The kinetic energy is then given by $\mathbf{L}^2/2\boldsymbol{\iota}$, where \mathbf{L} is the angular momentum of the magnetic cluster. Hence, the dynamics of atomistic magnetic moments becomes equivalent to the dynamics of a gyroscope. Perturbing a gyroscope results in a precession around the gravity field. Such a displacement occurs always perpendicular to the force. Due to the mass and the resulting inertia, the precession axis does not coincide with the angular momentum axis. The superposition of the precession around the gravity field and around the angular momentum axis causes a cycloidal trajectory (illustrated in figure 2.3.2). This effect is called nutation and it is small compared to the precession.

Cornei et al. [57, 58] used mesoscopic non-equilibrium thermodynamics [69, 161] to study the inertia in magnetization dynamics of macroscopic magnetic moments, that will be shortly illustrated in the following. Let’s assume a set of magnetic moments $\{\mathbf{m}, d\mathbf{m}\} = m_s \{\mathbf{e}, d\mathbf{e}\}$

with the velocity $\{\mathbf{u}, d\mathbf{u}\}$. In the Boltzmann formalism [53, 285, 299], one can establish the conservation law for the distribution function $f(\mathbf{e}, \mathbf{u}, t)$ (see figure 2.3.1)

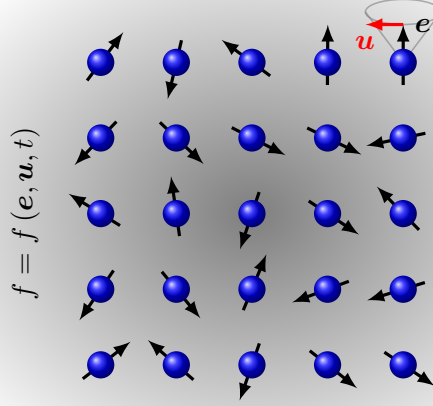


Figure 2.3.1.: Out-of-equilibrium magnetic system treated by the Boltzmann probability distribution function. The distribution function f considers a many-body magnetic diluted ‘gas’, where each individual carries a normalized magnetic moment \mathbf{e} (black arrows) and the magnetic velocity \mathbf{u} (red arrow).

$$\frac{\partial f}{\partial t} + \frac{\mathbf{u}}{m_s} \frac{\partial f}{\partial \mathbf{e}} + \frac{\mathbf{B}}{m} \frac{\partial f}{\partial \mathbf{u}} = \left(\frac{\partial f}{\partial t} \right)_c = \left(\frac{\partial \mathbf{I}}{\partial \mathbf{u}} \right). \quad (2.3.1)$$

The Boltzmann equation deals with the dynamics of the distribution function in time. The second term on the left-hand side is due to the precession and damping of the magnetic moment, whereas the third addendum illustrates the mass of the magnetic moment according to Newton’s second axiom. The term on the right-hand side is the collision term and describes the variation of the distribution function due to exchange of the angular momentum as a function of the thermal bath, that leads to an additional flux \mathbf{I} in the Boltzmann equation (2.3.1). The evolution of the particle density $n(\mathbf{e})$ and the conservation law of the average magnetic moment $n\dot{\mathbf{M}}$ is expressed as

$$\frac{\partial n(\mathbf{e})}{\partial t} = \int \frac{\partial f}{\partial t} d\mathbf{u} = \frac{1}{m_s} \frac{\partial (n\dot{\mathbf{M}})}{\partial \mathbf{e}}, \quad \frac{\partial (n\dot{\mathbf{M}})}{\partial t} = \int \frac{\partial f}{\partial t} \mathbf{u} d\mathbf{u}. \quad (2.3.2)$$

The derivative of the distribution function in equation (2.3.2) can be replaced by the Boltzmann equation (2.3.1). This gives the dynamics of the average velocity [57, 58]

$$n \frac{\partial \dot{\mathbf{M}}}{\partial t} = -\frac{1}{m m_s} \frac{\partial \mathbf{P}}{\partial \mathbf{e}} - n \frac{1}{m} \mathbf{B} + \int \mathbf{I} d\mathbf{u}. \quad (2.3.3)$$

$\mathbf{P} = \int m f (\mathbf{u} - \dot{\mathbf{M}})^2 d\mathbf{u}$ relates to the pressure of the diluted magnetic particle ‘gas’ [57, 58]. The second term illustrates the proportionality between the average velocity and field \mathbf{B} , where the third and the first one mimic the interaction with the thermal bath via a

dissipation field and the magnetic pressure. Since the thermal flux is equal to the Gilbert damping [109], \mathbf{I} is replaced by $\mathbf{I} = \alpha/\gamma m_s m \mathbf{f}\mathbf{u}$. Thus, the viscose damping $n\dot{\mathbf{M}} = \int \mathbf{f}\mathbf{u}d\mathbf{u}$ appears in equation (2.3.3). Hence, the Boltzmann equation relates to the effective field in the Landau-Lifshitz-Gilbert equation (2.2.11)

$$m \frac{\partial \dot{\mathbf{M}}}{\partial t} = -\mathbf{B} + \frac{\alpha}{\gamma m_s} \dot{\mathbf{M}} - \frac{1}{n m_s} \frac{\partial \mathbf{P}}{\partial \mathbf{e}}. \quad (2.3.4)$$

Without pressure gradient, equation (2.3.4) is the same as equation (2.2.10) in Gilbert's Lagrange formalism, assuming the kinetic energy \mathcal{T} is $m\dot{\mathbf{M}}^2/2$.

The angular momentum is always transferred perpendicular to the average magnetic moment \mathbf{M} and the velocity $\partial \mathbf{M}/\partial t$. In his assumption (2.2.9) Gilbert accounts only for the magnetic inertia tensor components that move in the direction of the magnetization vector. However, having the full inertia tensor at hand, the ensemble from the spatial inertial system transforms to the body-fixed inertial system¹. This acts as an additional contribution to the equation (2.3.4) that balances the effective and interaction field: the centrifugal field $-m\boldsymbol{\Omega} \times \frac{\partial \mathbf{M}}{\partial t}$ and the Euler field $-m \frac{\partial \boldsymbol{\Omega}}{\partial t} \times \mathbf{M}$, where $\boldsymbol{\Omega}$ is the angular velocity of the rotating average magnetic moment \mathbf{M} . With the tensor representation of the double cross product [57] and $\partial \mathbf{M}/\partial t = \boldsymbol{\Omega} \times \mathbf{M}$, equation (2.3.4) holds

$$\boldsymbol{\iota} \frac{\partial \boldsymbol{\Omega}}{\partial t} + \boldsymbol{\Omega} \times \boldsymbol{\iota} \boldsymbol{\Omega} = \mathbf{M} \times \left(-\mathbf{B} + \frac{\alpha}{\gamma m_s} \dot{\mathbf{M}} - \frac{1}{n m_s} \frac{\partial \mathbf{P}}{\partial \mathbf{e}} \right). \quad (2.3.5)$$

Regarding the classical relation between the angular velocity and the angular momentum $\mathbf{L} = \boldsymbol{\iota} \boldsymbol{\Omega} = m \mathbf{M} \times (\boldsymbol{\Omega} \times \mathbf{M})$, where $\boldsymbol{\iota} = m m_s^2 (\mathbf{E} - \mathbf{e} \otimes \mathbf{e})$ and \mathbf{E} is the unit tensor, the angular momentum conservation law obeys

$$\frac{\partial \mathbf{L}}{\partial t} + \boldsymbol{\Omega} \times \mathbf{L} = \mathbf{M} \times \left(-\mathbf{B} + \frac{\alpha}{\gamma m_s} \dot{\mathbf{M}} - \frac{1}{n m_s} \frac{\partial \mathbf{P}}{\partial \mathbf{e}} \right). \quad (2.3.6)$$

The moment of inertia tensor with a 'body-like' magnetic mass, where the symmetry axis and the center of mass is given by the magnetization orientation \mathbf{e} ,

$$\boldsymbol{\iota} = \begin{pmatrix} \iota_1 & 0 & 0 \\ 0 & \iota_1 & 0 \\ 0 & 0 & \iota_3 \end{pmatrix}, \quad (2.3.7)$$

simplifies equation (2.3.6) to

$$\begin{aligned} \dot{\Omega}_1 + \Omega_2 \Omega_3 \left(\frac{\iota_3}{\iota_1} - 1 \right) &= \frac{m_s}{\iota_1} B_2 + \tau_1^{-1} \Omega_1 - \left[\frac{1}{n \iota_1} \frac{\partial \mathbf{P}}{\partial \mathbf{e}} \right]_1, \\ \dot{\Omega}_2 + \Omega_1 \Omega_3 \left(1 - \frac{\iota_3}{\iota_1} \right) &= -\frac{m_s}{\iota_1} B_1 + \tau_1^{-1} \Omega_2 - \left[\frac{1}{n \iota_1} \frac{\partial \mathbf{P}}{\partial \mathbf{e}} \right]_2, \\ \iota_3 \dot{\Omega}_3 &= \tau_3^{-1} \Omega_3 = 0. \end{aligned} \quad (2.3.8)$$

The third equation is zero, since the applied torque is perpendicular to the magnetization. Therefore, the relaxation times $\tau_i = \iota_i \gamma / m_s \alpha$ are proportional to the ratio of the moment of inertia and the Gilbert damping. The relaxation time τ_1 indicates two limiting cases: $t \gg \tau_1$ and $t \approx \tau_1$. In the first case, $\dot{\boldsymbol{\Omega}}$ is negligible with respect to $\tau_1^{-1} \boldsymbol{\Omega}$ and equation (2.3.6) represents the Landau-Lifshitz-Gilbert equation (2.2.9). In the second case, the inertia term

¹www.mathpages.com/home/kmath633/kmath633.htm

$\dot{\Omega}$ is significant. Expressing the left-hand side of equation (2.3.6) in terms of \mathbf{M} via the gyromagnetic ratio $\mathbf{L} = \mathbf{M}/\gamma$ and $\partial\mathbf{M}/\partial t = \boldsymbol{\Omega} \times \mathbf{M}$

$$\boldsymbol{\Omega} \times \mathbf{L} = \frac{1}{\gamma} \frac{\partial \mathbf{M}}{\partial t}, \quad (2.3.9)$$

$$\iota \frac{\partial \boldsymbol{\Omega}}{\partial t} = \iota \frac{\partial}{\partial t} \left(\mathbf{M} \times \frac{\partial \mathbf{M}}{\partial t} \right) = \iota \mathbf{M} \times \frac{\partial^2 \mathbf{M}}{\partial t^2}, \quad (2.3.10)$$

yields the generalized Landau-Lifshitz-Gilbert equation for the atomic moment:

$$\frac{\partial \mathbf{m}_i}{\partial t} = \mathbf{m}_i \times \left(-\gamma \mathbf{B} + \frac{\alpha}{m_s} \frac{\partial \mathbf{m}_i}{\partial t} + \gamma \frac{\iota}{m_s} \frac{\partial^2 \mathbf{m}_i}{\partial t^2} \right). \quad (2.3.11)$$

Due to the inertia, a previous magnetic state at time t' operates on the current state at time t , creating a retardation in time. More precisely, in non-coherent states, where the magnetic velocity varies significantly, the third term on the right-hand side contributes to the dynamics. This is due to the angular momentum transfer caused by the Heisenberg model. Since $\mathbf{M} = \sum_i \mathbf{m}_i$, nutation should also become visible in the total magnetization \mathbf{M} if all moments nutate coherently by applying large external fields.

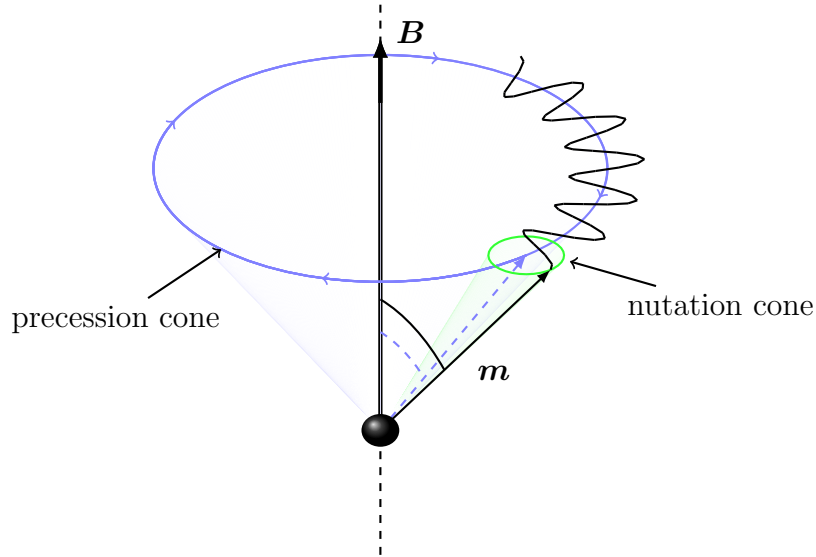


Figure 2.3.2.: Magnetic moment evolution $\partial\mathbf{m}/\partial t$ influenced by its mass. The inert reaction of the magnetic moment due to small perturbations, e.g. from an external magnetic field, consequences an additional precession around the angular-momentum axis (green cone). The superposition of the precession around the effective field \mathbf{B} (black arrow) and the precession caused by the inertia results in a cycloidal trajectory (black oscillating lines).

The extended equation of motion (2.3.11) neglects the exchange with the thermal bath. Brown's *ansatz* (white noise), where $D \propto \delta(t - t')$, states that an event at time t simultaneously entails a response at $t' = t$. Retardation due to the formation of magnetism originating from electron-electron interaction and response in nutation are neglected. If a discretization of time intervals is adopted, the probability distribution density P in the Fokker-Planck equation depends only on the very previous time step; the process has no memory and follows

the Markov theory [213]. However, according to the quantum-mechanical Nyquist formula [111, 152], the noise is regarded as white up to a frequency of $k_B T/h$, which is about 10^{13} s^{-1} ($\tau_c = 1 \text{ ps}$) at room temperature. The resonant Lamor frequency $\omega = \gamma B$ is equivalent to a field of 100 T.

Thermally excited magnetization evolution, where the relaxation times are smaller than the aforementioned Nyquist correlation time, such as in demagnetization [154, 155] or nutation, is not feasible within the Brownian *ansatz*; the magnetization has memory. Hence, the third property of the noise field $\mathbf{h}(t)$ (see section 2.2) is lost and an exponentially correlated noise should be assumed (colored noise: the power depends on the frequency)

$$\langle \mathbf{h}_i(t) \mathbf{h}_j(t') \rangle_{\text{av}} = \frac{D}{\tau_c} \exp\left(-\frac{|t-t'|}{\tau_c}\right), \quad (2.3.12)$$

where $\langle \dots \rangle_{\text{av}}$ denotes ensemble average.

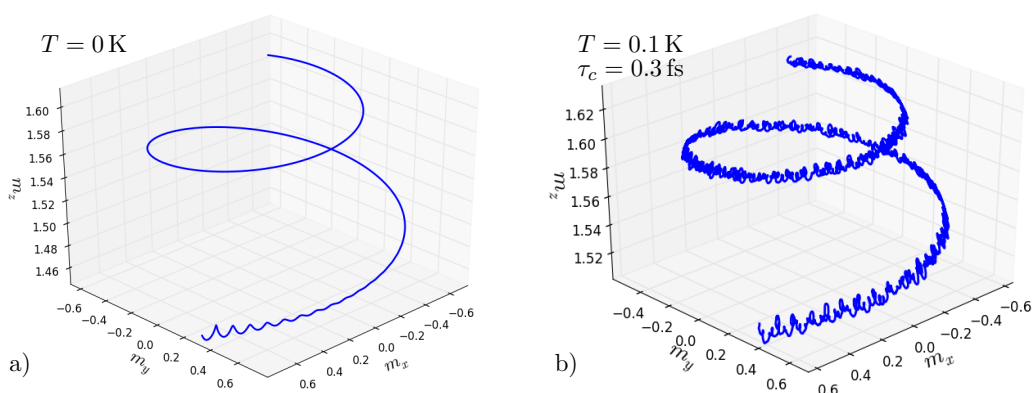


Figure 2.3.3.: Nutation occurs at the edge atom in 2ML thick Co nanoislands on Cu(111) [33]. a) At zero temperature a cycloidal trajectory appears, damped on a time scale of 500 fs. b) Temperature, simulated by a colored noise field \mathbf{h} , maintains the nutation ($T = 0.1 \text{ K}$), when the correlation time τ_c is smaller than the magnetic exchange parameter ($\tau_J \approx 100 \text{ fs}$).

Let us assume a separation of the thermal bath and the evolution of the magnetic moments. In the first step, the thermal field \mathbf{h} acts as random fluctuations of the effective field \mathbf{B} (figure 2.2.2), where the magnetic moments are constant at that precise time. Thereby, the fluctuation magnitude D of the thermal field is related to the relaxation time τ_c , indicating the retardation induced by other atomic degrees of freedom. Thus, the evolution of the thermal bath can be expressed in terms of Langevin equation [61, 167]:

$$\frac{d}{dt} \mathbf{h} = -\frac{1}{\tau_c} \mathbf{h} + \mathbf{R}. \quad (2.3.13)$$

\mathbf{R} exhibits white-noise properties with the fluctuation strength $D = 2\chi k_B T / \tau_c$ and $\chi = \langle h^2 \rangle_{\text{av}} / k_B T$. χ is the response of the local thermal field to the current orientation of the magnetic moments. The fluctuation-dissipation theorem for \mathbf{h} can be deployed, assuming a Boltzmann-distribution P [245] in the thermally equilibrated Fokker-Planck equation [32].

In the second step, the magnetic moment fluctuation has to be taken into account, using the exchange energy between the magnetic moment and the total effective field. The magnetic energy (2.1.3) is extended by the contribution, which is required to produce the thermal field $1/2k_B T$

$$U(\mathbf{m}, \mathbf{h}) = \frac{1}{2\chi} \mathbf{h}^2 - (\mathbf{B} + \mathbf{h}) \cdot \mathbf{m}. \quad (2.3.14)$$

Miyazaki and Seki [197] claim equal contributions of the moment \mathbf{m} and the thermal field \mathbf{h} . Finally, the Fokker-Planck equation with and without connection between the thermal bath and the magnetic moment gives

$$\frac{d}{dt} \mathbf{h} = -\frac{1}{\tau_c} (\mathbf{h} - \chi \mathbf{m}) + \mathbf{R}, \quad (2.3.15)$$

$$\frac{\partial}{\partial t} \mathbf{m} = -\gamma \mathbf{m} \times (\mathbf{B} + \mathbf{h}). \quad (2.3.16)$$

In case of the correlation time being smaller than the system response ($\tau_c \rightarrow 0$), Miyazaki and Seki [197] proved that equation (2.3.16) is identical to the Landau-Lifshitz equation. Furthermore, the Landau-Lifshitz-Miyazaki-Seki equation accounts for time retardation, especially for nutation, in the thermal field via τ_c . This manifests that the time scale of the different reservoirs has to be regarded in atomic magnetization dynamics.

The role of colored noise was also analytically investigated by T. Bose et al. [31]. They postulated physical solutions in selected areas of the phase space, controlled by the Gilbert damping parameter α , the dissipation strength D as well as the dephasing time τ_c in equation (2.3.13). Thus, the stability of the solution as well as the range in the phase space can be enhanced using an applied external magnetic field. They motivate an additional damping mechanism, which is only due to the stochastic nature of the equation of motion. More precisely, this stochastic damping annihilates the pure deterministic damping α for a critical correlation time τ_c^* . The second derivative of the magnetic moment in equation (2.3.11) can be considered in general terms to give retardation in magnetization dynamics. LLG dynamics is accompanied by a simultaneous variation due to the cause: a perturbation at t entails instantaneously a response at $t' = t$. But in principle a certain amount of time must pass, before the action follows from the cause. For this reason, Bose et al. introduces the retarded dynamics equation

$$\frac{\partial m_i}{\partial t} = \int_0^t dt' \sum_j \Upsilon_{ij}(t-t') \left\{ \mathbf{m}_j(t') \times \left[-\gamma \mathbf{B}_j(t') + \alpha \frac{\partial \mathbf{m}_j(t')}{\partial t'} \right] \right\}, \quad (2.3.17)$$

with the retardation function Υ . Both retardation in time and in space were accounted for and result in microscopic dephasing of the magnetic moments that is macroscopically detectable as an additional damping mechanism. In particular, the Heisenberg coupling and the coupling coming from the retardation are opposed operations. Later on in this thesis a non-local damping will be introduced, producing also retardation effects and reduced relaxation times.

Time correlation in magnetic relaxation, especially nutation, is hard to observe experimentally. A local, ultrashort measuring method will be required. The scanning-tunneling microscope (STM) offers spatial resolutions on a nm-length scale [19, 20] and the possibility of applying strong external magnetic field up to 10 T [98, 209]. However, due to the scanning process a femto-second resolution is not achievable. Pump-probe techniques [153], in

contrast, provide a femtosecond time-resolution [162]. Combining both could be in principle used to measure such phenomena. Even so, observing magnetic correlation in time will remain an experimental challenge.

Magnetic nanodomains e.g. in Co islands on Cu(111) indicate the existence of non-coherent magnetic states, that are significant for nutation. Hence, I analyzed the role of time retardation and nutation in low-dimensional magnetic systems at zero and finite temperatures. The results were published in [35]. Here, the non-equilibrium thermodynamics and the Landau-Lifshitz-Miyazaki-Seki equation were applied to the microscopic magnetization dynamic, in contrast to the mesoscopic *ansatz* in literature [57]. I summarized with the importance of nutation on a fs-time scale and for rim atoms in nanostructures. Thus, magnetic retardation must be account for near the adiabatic limit.

Since nutation correlates to the angular momentum transfer, the question to the isotropy of this transfer and, in addition, the energy dissipation occur. Moreover, the non-statistical impact of other microscopic degrees of freedom are neglected so far. Hence, an extended methodological model will be required.

Electronic structure and magnetic properties

Magnetism is a correlation effect of electrons in solid state matter. Hence, the characterization of magnetic materials are accompanied by investigations of the ground state of the many-body electron system. The Holy Grail of condensed matter physics is the solution of the eigenvalue problem of the Hamiltonian \hat{H} for the electrons-ions system

$$\hat{H} = \hat{T}_n + \hat{T}_e + \hat{V}_{nn} + \hat{V}_{ee} + \hat{V}_{ne} + \hat{V}_{ext}. \quad (3.0.1)$$

\hat{T}_n and \hat{T}_e represent the kinetic energy of the nuclei and the electrons, respectively. \hat{V}_{nn} , \hat{V}_{ee} and \hat{V}_{ne} are the repulsive nuclei interaction, the electron interaction (Coulomb interaction) and the attractive nucleus-electron interaction, respectively [233]; so one has to deal with the coupled Schrödinger (or Dirac) equations about 10^{26} particles.

The complexity of the many-body problem is reduced, when the electron-nucleus coupling is weak, so that the electrons are decoupled from the nuclei and move in an effective nuclei potential (Born and Oppenheimer 1927 [29]). In 1965 Hohenberg, Kohn and Sham proposed a way to describe the many-body problem in which the total energy is considered as a functional of the charge density. The physical problem loses intricacy and reduces to an effective one-electron problem [133, 160]. This quantum-mechanical approach, called density functional theory (DFT) [158], solves the many-body electron system exactly in the limit of a completely known exchange-correlation functional.

The first section 3.1 introduces the basic concepts of density functional theory. The numerical implementation of the density functional theory relies on different methods such as pseudopotential plane wave or multiple-scattering methods. The latter, known as Korringa-Kohn-Rostoker (KKR) method (section 3.2), is used in this thesis to obtain the electronic structure for systems of interest. Information about spin and orbital momentum of the electron, electron correlations and, consequently, magnetism are expressed in a Green function formalism, which will be discussed in sections 3.2 and 3.3. Within the limit of strongly localized electrons with a small orbital overlap, the tight-binding method (section 3.4) can also be used to extract magnetic properties.

The role of nanoscopic degrees of freedom on magnetism and the electronic structure will be also discussed further: the lack of inversion symmetry in the crystal lattice entails spin-dependent electronic scattering, induced by spin-orbit coupling, which manifests itself non-collinear magnetism (section 3.5). The magnetic exchange can also be sensitive to the coupling with a thermal bath. Hence, magnetic disorder within the coherent potential approximation (CPA), introduced in section 3.6, reflects the magnetic thermal noise in the electron

system. Another distinctive property of the magnetization dynamics is the relaxation rate α . The intrinsic magnetic damping is determined by perturbation of the electronic ground state due to rotation of the magnetic moment, as it will be discussed in the torque-torque correlation and the breathing Fermi-surface model (section 3.7).

3.1 Density functional theory

Density functional theory is one of the most successful applied theories for the study of electronic structure¹, in particular for atoms, molecules or crystals. It has its conceptual roots in the Thomas-Fermi model [90, 265]. 1998 Walter Kohn was awarded the Nobel prize in chemistry for predicting a great variety of molecular properties with DFT: molecular structures, vibrational frequencies, ionization energies, electric and magnetic properties, etc.

Density functional theory deals with the many-body Hamiltonian of an electronic system in the Born-Oppenheimer approximation [29], which is composed of the kinetic energy \hat{T} , the electron-electron interaction \hat{W} , determined by the Coulomb energy and the effective ‘underlying’ potential \hat{V} , which originates from the interaction with the nuclei and dictates how the electrons propagate:

$$\hat{H} = \hat{T} + \hat{V} + \hat{W}. \quad (3.1.1)$$

In a system of N coupled electronic wavefunctions $\psi_\sigma = \psi_\sigma(\mathbf{r}_1, \mathbf{r}_2, \dots, \mathbf{r}_N)$ with spin σ , the spin-resolved electron density

$$n_\sigma(\mathbf{r}) = \int |\psi_\sigma(\mathbf{r}, \mathbf{r}_2, \dots, \mathbf{r}_N)|^2 d\mathbf{r}_2 d\mathbf{r}_3 \dots d\mathbf{r}_N \quad (3.1.2)$$

contributes to the total electron density n and the magnetization density m

$$\begin{aligned} n(\mathbf{r}) &= n_\uparrow(\mathbf{r}) + n_\downarrow(\mathbf{r}) \\ m(\mathbf{r}) &= n_\uparrow(\mathbf{r}) - n_\downarrow(\mathbf{r}) \quad \text{or} \quad m(\mathbf{r}) = \frac{e\hbar}{2m} \psi^+(\mathbf{r}) \hat{\beta} \sigma \psi(\mathbf{r}). \end{aligned} \quad (3.1.3)$$

Here, $\hat{\beta}$ comes from the Dirac equation and is traceless. The variation principle [207] yields the ground state energy as expectation value of the Hamiltonian \hat{H} for the ground state wavefunction $|\psi\rangle$ of the total system,

$$E[\psi] = \frac{\langle \psi | \hat{H} | \psi \rangle}{\langle \psi | \psi \rangle}, \quad (3.1.4)$$

and implicates the ground state energy $E_0 = \lim_{\psi \rightarrow N} E[\psi]$ as a functional of the number of electrons and the nuclear ‘external’ potential \hat{V} .

Hohenberg and Kohn showed in 1965 [133] that the expectation value of any ground state observables depends only on the electronic density. In particular, the density functional theory is based on the two Hohenberg-Kohn theorems:

¹From the Nobel prize lecture of Walter Kohn “Electronic structure of matter - wave functions and density functionals”, 1999

The first H–K theorem states the ground state properties of a many-electron system are uniquely determined by the ground state electronic density. The ground state energy E_0 can be expressed in terms of the electron density as

$$E[n_\sigma] = T[n_\sigma] + U[n_\sigma] + W[n_\sigma]. \quad (3.1.5)$$

The second H–K theorem states that the exact ground state density $n_\sigma^0(\mathbf{r})$ minimizes the energy functional $E[n_\sigma]$, such that for any given n_σ , $E[n_\sigma^0] \leq E[n_\sigma]$.

These theorems give no explicit form for the functionals in (3.1.1), which was, however, first realized by Kohn and Sham [160]. They made the following assumption: the energy can be expressed in a non-interacting electron system by an effective one-particle potential corresponding to the same electron density

$$E[n_\sigma] = T[n_\sigma] + V[n_\sigma] + E_H[n_\sigma] + E_{xc}[n_\sigma], \quad (3.1.6)$$

with the Hartree energy $E_H[n_\sigma] = 1/2 \int n_\sigma(\mathbf{r})n_\sigma(\mathbf{r}')/|\mathbf{r}-\mathbf{r}'| \, d\mathbf{r}d\mathbf{r}'$ [7, 66] and the exchange-correlation energy $E_{xc}[n_\sigma]$. According to the second Hohenberg-Kohn theorem, the variation of equation (3.1.6) leads to the Kohn-Sham equation

$$\underbrace{\left(-\frac{\hbar^2}{2m} \nabla^2 + v(\mathbf{r}) + u_H(\mathbf{r}) + u_{xc}(\mathbf{r}) \right)}_{\hat{H}_{KS}} \phi_{i,\sigma}(\mathbf{r}) = \varepsilon_{i,\sigma} \phi_{i,\sigma}(\mathbf{r}), \quad (3.1.7)$$

with the Hartree potential

$$u_H(\mathbf{r}) = \int \frac{n_\sigma(\mathbf{r}')}{|\mathbf{r}-\mathbf{r}'|} \, d\mathbf{r}', \quad (3.1.8)$$

and the exchange-correlation potential

$$u_{xc}(\mathbf{r}) = \frac{\delta E_{xc}[n_\sigma]}{\delta n_\sigma}. \quad (3.1.9)$$

Here, $\phi_{i,\sigma}(\mathbf{r})$ is the non-interacting one-electron wave function with spin σ . This simplifies the initial many-body electron problem with 10^{26} degrees of freedom to a single inhomogeneous differential equation.

In order to include spin-orbit effects, a relativistic generalization of the density functional theory will be required. N interacting electrons propagate in a external four-potential $V^\mu = (V, \mathbf{A})$, where \mathbf{A} is the vector potential implicated by the presence of a magnetic field. Thus, the ground state energy is a functional of the four-component current $J^\mu = (n, \mathbf{j})$ [235]

$$E[J^\mu(\mathbf{r})] = T[J^\mu(\mathbf{r})] + W[J^\mu(\mathbf{r})] + \int [n(\mathbf{r})V(\mathbf{r}) - m(\mathbf{r})B(\mathbf{r})] \, d\mathbf{r}, \quad (3.1.10)$$

with the magnetization density $m(\mathbf{r})$ (equation (3.1.3)). One can find a similar expression as in the non-relativistic case, namely the Dirac-Kohn-Sham equation [235]

$$\left(c\hat{\alpha}\hat{\mathbf{p}} + \hat{\beta}mc^2 + v_{eff}(\mathbf{r}) - \mathbf{m}(\mathbf{r}) \cdot \mathbf{B}_{eff}(\mathbf{r}) \right) \psi_i = \varepsilon_i \psi_i. \quad (3.1.11)$$

The effective potential constitutes the external potential, the Hartree contribution, as well as the exchange-correlation term,

$$v_{eff}(\mathbf{r}) = V(\mathbf{r}) + \int \frac{n_\sigma(\mathbf{r}')}{|\mathbf{r} - \mathbf{r}'|} d\mathbf{r}' + \frac{\delta E_{xc}[n_\sigma(\mathbf{r}), \mathbf{m}(\mathbf{r})]}{\delta n_\sigma(\mathbf{r})}. \quad (3.1.12)$$

In addition, the effective field is composed of the external field and the variation of the exchange-correlation field with respect to the magnetization density:

$$\mathbf{B}_{eff}(\mathbf{r}) = \mathbf{B}_{ext}(\mathbf{r}) + \frac{\delta E_{xc}[n_\sigma(\mathbf{r}), \mathbf{m}(\mathbf{r})]}{\delta \mathbf{m}(\mathbf{r})}. \quad (3.1.13)$$

Since the exact form of the exchange-correlation potential is not known, approximations are necessary. But in principle, if the exchange-correlation functional is known, the solution of the Kohn-Sham equation would be exact within the Born-Oppenheimer approximation. Let $\varepsilon_{xc}^{unif}(n_\sigma(\mathbf{r}))$ be the exchange-correlation energy density of the homogeneous electron gas for the charge density $n_\sigma(\mathbf{r})$. The *local (spin) density approximation* (L(S)DA)[160] states that, if the charge density $n_\sigma(\mathbf{r})$ is slowly varying in space, the exchange correlation energy is the same as

$$E_{xc}^{LDA}[n_\uparrow, n_\downarrow] = \int \varepsilon_{xc}^{unif}(n_\uparrow(\mathbf{r}), n_\downarrow(\mathbf{r})) n(\mathbf{r}) d\mathbf{r}, \quad (3.1.14)$$

as first suggested by Kohn and Sham [160]. However, this approach tends to underestimate atomic ground state and ionization energies, while overestimating binding energies. The exchange and the correlation part are linearly decomposed, where analytical forms of correlation energy E_c are given by e.g. Vosko-Wilk-Nusair [277], Perdew-Zunger [226], Cole-Perdew [64] or Perdew-Wang [223–225].

If the criterium of a homogeneous charge density is not guaranteed, the gradient of the density has to be accounted for. Thus, the integrand f in the *generalized gradient approximation* (GGA), that replaces $n\varepsilon_{xc}$ in the LSDA, is a functional of the first derivative of the density and the density itself:

$$E_{xc}^{GGA}[n_\uparrow, n_\downarrow] = \int f[n_\uparrow, n_\downarrow, \nabla n_\uparrow, \nabla n_\downarrow] d\mathbf{r}. \quad (3.1.15)$$

When comparing both exchange-correlation functionals, the GGA tends to improve energies, ionization energies, geometrical energy differences, expands and softens chemical bonds. It is remarkably successful for small molecules, but fails for delocalized electrons in the uniform gas when $f(n_\uparrow, n_\downarrow, 0, 0) \neq n\varepsilon_{xc}^{unif}$ and, thus, in metals. An analytical form for this exchange-correlation function is expressed e.g. by Perdew-Burke-Ernzerhof [222]. Meta-GGA methods contain the derivative of the local density up to the second order [264]. Further advanced approaches for calculating the self-energy of the many-body electron system, such as L(S)DA+U [5], self-interaction correction (SIC) [182, 226] and the self-energy correction (GW) [11, 106, 119–121], have also been applied to first-principles calculations. These functionals improve the band gaps in insulators [221] or rare earth metals [68], in better accordance with experiments.

The Kohn-Sham problem focuses mainly on the equilibrium (or stationary) state of the electronic system. Non-equilibrium considerations as well as external excitations, such as femtosecond laser pulses, are not included in DFT. The dynamics of a many-body problem, caused by a time-dependent potential, is instead described within the time-dependent density functional theory (TDDFT) [187], founded on the Runge-Gross theorem [237]. This is

the equivalent of the Hohenberg-Kohn theorem of DFT and postulates a unique mapping between the time-dependent external potential and the time-dependent electronic density of the system. The energy minimization principle does not apply, since it does not exist for excited states [117]. The time-dependent density $n(\mathbf{r}, t)$ can be obtained by fictitious systems of non-interacting electrons in the Kohn-Sham system, where the electrons ‘feel’ an effective time-dependent Kohn-Sham potential [117]. If the external perturbation is small, then the time dependence will be regarded within a linear-response perturbation theory [117], which can be applied for magnon-lifetime and complex magnetization-dynamics studies [44–46]. Accounting for TDDFT in magnetization dynamics simulation provides a more fundamental approximation of nano-reservoirs (electron, spin, phonon) and their connection. But this will be studied in the future.

Within the density functional theory, magnetic information can only be extracted by analyzing the total energy. Here, the magnetic exchange parameter J can be gained from the total energy variation with respect to rotation of atomic spins. Especially in metal oxides, this procedure underestimates the induced moment in the oxygen [239, 240]. This misfit calls for methods giving direct access to the magnetic moment and the exchange interaction but still base on DFT, e.g. the Green function technique.

3.2 Multiple-scattering theory

The band structure of a material offers valuable clues to its electric and magnetic properties. In the framework of a single-electron picture, different theories have been developed to calculate the dispersion relation $\varepsilon_{\mathbf{k},n}$, characterized by the band index n and the wave vector \mathbf{k} . The gradient of the dispersion is mainly determined from the crystal potential and the electron-electron interaction. There exist two different limiting cases: the potential of the cores is negligibly small compared to the kinetic energy of the electrons (nearly-free electron model) [7, 156] and are, thus, simulated as a perturbation in the free-electron motion. This model holds for valence states, but not for core states. In contrast, the potentials can be considered as strong (tight-binding model; see section 3.4). This *ansatz* is valid for core states and fails for partially filled d - or f -shells. Electron-electron interaction is not considered in the tight-binding as well as in the nearly-free electron model. This calls for a method that acts between these two limits, giving furthermore direct access to magnetic properties.

The periodicity of a crystal ‘boils down’ the single-electronic problem for the whole bulk to just one reduced region: the Schrödinger (or Dirac) equation (3.2.1) has to be solved only within the Wigner-Seitz cell, around the site \mathbf{R}_n (figure 3.2.1). Using subsequently the translation symmetry based on Bloch’s theorem, [7, 22, 156] one obtains the solution for the entire crystal. More precisely, the Bloch theorem states that the eigenstates of a periodic system may be written as product of a phase factor and a lattice periodic Bloch function. Assuming a spherically symmetric potential within the Wigner-Seitz cell (atomic sphere approximation [ASA]; figure 3.2.1 red spheres), the solution of the Schrödinger equation for the many-body electron Hamiltonian in the Born-Oppenheimer approximation

$$\hat{H}\psi_{\mathbf{k},n} = \varepsilon_{\mathbf{k},n}\psi_{\mathbf{k},n} \quad (3.2.1)$$

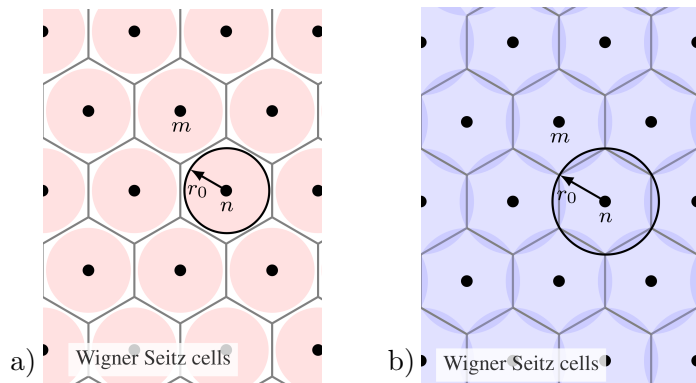


Figure 3.2.1.: Wigner-Seitz construction of the lattice (gray honeycomb structure) and muffin-tin approximation. The potential of the crystal will be approximated as non-overlapping spherical potentials (red circles in a). The radius of the spheres is the muffin-tin radius r_0 , where the potential will be approximated as constant at the interstitial region between the spheres. If the radius is larger than the Wigner Seitz radius, the spheres overlap (blue spheres in b). The nucleation center is labeled by n and m .

yields in spherical harmonics basis $Y_{lm}(\check{\mathbf{r}})$ for fixed n, \mathbf{k} ,

$$\psi(\mathbf{r}) = \sum_{lm} A_{lm} R_l(r) Y_{lm}(\check{\mathbf{r}}). \quad (3.2.2)$$

Here, A_{lm} are constants and $R_l(r)$ is a radial-only wave function; l and m are the orbital and magnetic quantum numbers. In order to avoid unsolvable boundary condition [108] between the Wigner-Seitz cells, the crystal potential is represented as a muffin-tin potential [246, 275], where the radius r_{MT}^i of the potential is determined through non-overlapping spheres (figure 3.2.1 a). Within this approximation, the effective potential of the whole lattice is then a superposition of radial potentials, each measured from a particular ionic position \mathbf{R}_i ,

$$V^{\text{eff}}(\mathbf{r}) = \sum_i V_i(\mathbf{r} - \mathbf{R}_i) \quad \text{with} \quad V_i(\mathbf{r}) = \begin{cases} V(r) & r \leq r_{MT}^i \\ 0 & r > r_{MT}^i \end{cases}. \quad (3.2.3)$$

However, spheres with the Wigner-Seitz radius r_{WS}^i , where typically $r_{MT}^i < r_{WS}^i$, are needed to account for the full cell volume and lead to some overlap in the interstitial region (figure 3.2.1 b), tending to give a better representation of the full potential. Hence, *ab initio* methods are set out to obtain the expansion coefficients A_{lm} .

Korringa [163] and independently Kohn and Rostoker [159] have introduced a method [141, 199, 242] that extracts the coefficients A_{lm} and the dispersion relation $\varepsilon_{\mathbf{k},n}$ by rewriting the Schrödinger equation (3.2.1) as an integral equation based on the Green function technique and as a functional of the state (3.2.2). The concept of the Greenian is a useful and general technique, named after the British mathematical physicist George Green [66, 244]. Green function is the pulse response of an inhomogeneous differential equation

$$\mathcal{L}(\mathbf{r}) u(\mathbf{r}) = f(\mathbf{r}). \quad (3.2.4)$$

where \mathcal{L} is a linear differential operator. Via the superposition principle, the convolution of the Green function with an arbitrary function $f(\mathbf{r})$ is the solution of the inho-

mogeneous differential equation for $u(\mathbf{r})$. The Greenian refers to various types of correlation functions, indicating that Green functions are always symmetric in space arguments.

By definition, the Greenian \hat{G} of equation (3.2.1) is specified as

$$\left(z\hat{E} - \hat{H}\right) \hat{G}(z) = \hat{E} \quad \text{or} \quad \hat{G}(z) = \left(z\hat{E} - \hat{H}\right)^{-1}. \quad (3.2.5)$$

$z = \varepsilon + i\Gamma$ is a complex energy, \hat{E} is the unit operator, and \hat{H} is the Kohn-Sham Hamiltonian \hat{H}_{KS} defined in equation (3.1.7). The Green function contains essentially all of the physical information [79, 112, 113, 293], e.g. the trace of the imaginary part of \hat{G} is related to the density of states. Furthermore, the Green function is linked to the wave propagation according to the Lippmann-Schwinger equation [293]

$$\psi_{\mathbf{k}}(\mathbf{r}) = \int G(\mathbf{r}, \mathbf{r}', z) V(\mathbf{r}') \psi_{\mathbf{k}}(\mathbf{r}') \, d\mathbf{r}'. \quad (3.2.6)$$

$V(\mathbf{r})$ is the potential in the Hamilton operator \hat{H} . One has in principle to distinguish between retarded ($\Gamma \rightarrow 0^+$; \hat{G}^+) and advanced ($\Gamma \rightarrow 0^-$; \hat{G}^-) propagation [293]. The propagator \hat{G} is also conveyed by the Lehmann spectral representation that gives a general expression for the two-point function [143, 170]

$$\hat{G}(z) = \sum_{\nu} \frac{|\psi_{\nu}\rangle \langle \psi_{\nu}|}{z - \varepsilon_{\nu}}. \quad (3.2.7)$$

Here, the poles are the eigenvalues ε_{ν} of the Hamilton operator \hat{H} in equation (3.2.5). This representation is based on some quantum field axioms *i*) invariance under inhomogeneous Lorentz group, *ii*) local commutativity, *iii*) positive definiteness of the norm in the Hilbert space [181].

Suppose the solution of equation (3.2.5) for a reference system \hat{H}_0 is \hat{G}_0 , the Green function \hat{G} of the perturbed system $\hat{H} = \hat{H}_0 + \Delta V$ can be deduced by the solution of the Dyson equation

$$\hat{G}(z) = \hat{G}_0(z) + \hat{G}_0(z) \Delta V \hat{G}(z) \quad (3.2.8)$$

$$= \hat{G}_0(z) + \hat{G}_0(z) \hat{T} \hat{G}_0(z), \quad (3.2.9)$$

where the transition operator or *t*-matrix $\hat{T} = \Delta V + \Delta V \hat{G}_0 \hat{T}$ is motivated. This enables to solve the Dyson equation exactly. \hat{T} accounts for scattering properties of the entire system, which is composed of single-site scatterers represented by the single-site *t*-matrix t_n and multiple scattering coming from the scattering-path operator $\hat{\tau}_{nm}$ [112, 293]:

$$\hat{T} = \sum_{nm} \hat{\tau}_{nm} \quad \text{where} \quad \hat{\tau}_{nm} = \hat{t}_n \delta_{nm} + \sum_k \hat{t}_n \hat{G}_0 (1 - \delta_{nk}) \hat{\tau}_{km}. \quad (3.2.10)$$

The multiple-scattering contribution $\hat{\tau}_{nm}$ transfers a wave at site n to a wave at site m and takes into account all possible paths. This allows to express the density of states in terms of the scattering-path operator (Lloyd's formula [177, 295, 296]),

$$N(\varepsilon) = -\frac{1}{\pi} \Im \text{Tr} \ln(\hat{\tau}) \quad (3.2.11)$$

Due to the spherical representation of the wave function (3.2.2), the particle propagator \hat{G} as well as the scattering-path operator $\hat{\tau}$ can be written into angular momentum representation (structural Green function matrix)¹ [190, 293]

$$G_{nm}(r, r', \varepsilon) = \sum_L \mathcal{R}_n^L(r_{<}; \varepsilon) \left(\mathcal{I}_n^L(r_{>}; \varepsilon) \right)^\dagger \delta_{nm} + \sum_{LL'} \mathcal{R}_n^L(r_n; \varepsilon) \tau_{nm}^{LL'} \left(\mathcal{R}_m^{L'}(r'_m; \varepsilon) \right)^\dagger, \quad (3.2.12)$$

where $r_{<} = \min(r_n, r'_n)$, $r_{>} = \max(r_n, r'_n)$ and $r_n = r - R_n$. This transition allows the reduction of the original integral equation into a convenient matrix equation. $L = (l, m)$ is a combined quantum number: the angular momentum l and magnetic quantum number m (in the relativistic case: $L = (\kappa, \mu)$, where κ is the spin-orbit and μ the magnetic quantum number [293]). \mathcal{R} and \mathcal{I} are the regular and irregular solution of the radial Schrödinger (or Dirac) equation. $g_{nm}^{LL'}$, related to the structural form $\tau_{nm}^{LL'}$ via the Dyson equation [293]

$$\tau_{nm}^{LL'} = \delta_{nm} t_n^{LL'} + \sum_{k \neq n, L'', L'''} t_n^{LL''} g_{nk}^{L''L'''} \tau_{km}^{L''L'}, \quad (3.2.13)$$

is the *structure constant* established by Korringa and Rostoker. At the end, equation (3.2.12) reflects the fundamentals of multiple-scattering theory.

Via Fourier transformation, which transforms periodic systems into the reciprocal space, and in terms of the matrices in L -space, equation (3.2.13) turns into the *fundamental equation of multiple-scattering theory*

$$\boldsymbol{\tau}(\varepsilon, \mathbf{k}) = \left(\mathbf{t}^{-1}(\varepsilon, \mathbf{k}) - \mathbf{g}(\varepsilon, \mathbf{k}) \right)^{-1}. \quad (3.2.14)$$

The structural form $\mathbf{g}(\varepsilon, \mathbf{k})$ depends only on the geometry of the lattice [293] and not on the scattering properties. More precisely, \mathbf{t}^{-1} is only a function of the cell potential, whereas \mathbf{g} accounts for the structure of the lattice. This admits to solve equation (3.2.13) instantaneously [88]. To obtain the potential V for the system of choice, a self-consistent loop for the potential is established in DFT, calculating the electron density from the known Green function. The spherical symmetry of V truncates L at some relatively small numbers $L = 2, 3, 4, \dots$

In equation (3.2.13) the reference system G_0 for the free-space solution [74] can be applied. Its structural constant, however, decays weakly in space, which implies that a huge number of atoms has to be considered and numerical instabilities appear. Szunyogh, Zeller and Zahn [262, 284, 294, 297] developed the screened Korringa-Kohn-Rostoker method that starts, first, from the free electron gas G_0 and transfers, by using the Dyson equation, the solution to a reference system G' . In a second G' will be used to achieve the Green function G for the system of interest. Here, good results are obtainable only when the screened structure constants are calculated with ≥ 5 nearest-neighbor shells of repulsive scatterers [200]. This provides a faster decrease of the wave function in the realspace and improves convergence.

So far, neither spin nor coupling between the spin and the orbital degrees of freedom were tackled. The spin polarization in the Dirac equation and, therefore, in the fully relativistic KKR Green function method is considered in the potential via the Zeeman term, which accounts for the coupling between the magnetization density (3.1.3) and the magnetic field

¹The abbreviation $G^{nm}(\mathbf{r}, \mathbf{r}') = G(\mathbf{r} + \mathbf{R}_n, \mathbf{r}' + \mathbf{R}_m)$ is used here.

\mathbf{B} [116, 136, 293]

$$(c\hat{\alpha}\hat{\mathbf{p}} + \hat{\beta}mc^2 + v_{eff}(\mathbf{r}) - \hat{\beta}\boldsymbol{\sigma} \cdot \mathbf{B})\psi_i(\mathbf{r}) = \varepsilon_i\psi_i(\mathbf{r}). \quad (3.2.15)$$

In the non-relativistic case, two decoupled quantization axes of the spin ($\mathbf{B} = \pm B\mathbf{e}_z$) implying for the structure constant form

$$\mathbf{g}_{nm} = \begin{pmatrix} \mathbf{g}_{nm}^{\uparrow\uparrow} & 0 \\ 0 & \mathbf{g}_{nm}^{\downarrow\downarrow} \end{pmatrix}. \quad (3.2.16)$$

In general, this is also manifested within the spinor representation of the single-site scatterer \mathbf{t}_n^{-1} for an arbitrary quantization axis \mathbf{e}_n (here $\mathbf{e}_n = \mathbf{e}_z$) [293]

$$\mathbf{t}_n^{-1} = \frac{1}{2} (\mathbf{t}_{n;\uparrow}^{-1} + \mathbf{t}_{n;\downarrow}^{-1}) \mathbf{1} + \frac{1}{2} (\mathbf{t}_{n;\uparrow}^{-1} - \mathbf{t}_{n;\downarrow}^{-1}) (\mathbf{e}_n \cdot \boldsymbol{\sigma}). \quad (3.2.17)$$

\uparrow and \downarrow indicate the spin-up and the spin-down states, respectively. The coupling between the electron spin and the magnetic moment within a $s-d$ model illustrates a preferred alignment of the spin in the magnetic moment direction (figure 3.2.2).

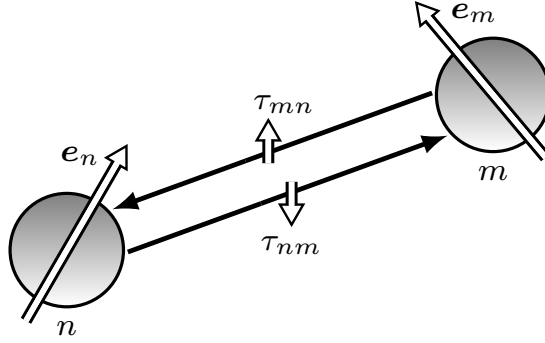


Figure 3.2.2.: Scattering process between two sites n and m (gray shaded spheres) with local magnetization density represented by \mathbf{e}_n and \mathbf{e}_m (white filled arrows). The scattering path operator $\boldsymbol{\tau}_{nm}$ refers to the direction \mathbf{e}_0 , shown by the small arrows. In the non-relativistic case only two directions in \mathbf{e}_n occur, parallel and antiparallel to \mathbf{e}_0 . In the relativistic case, however, the magnetization \mathbf{e}_n is a continuous quantity on the unit sphere and a spin-flip in back-scattering becomes probable.

In the relativistic case, the magnetization direction is a continuous quantity, projected on a unit sphere. A spin flip in the scattering process becomes probable, which consequences in non-zero off-diagonal elements in the structure constant

$$\mathbf{g}_{nm} = \begin{pmatrix} \mathbf{g}_{nm}^{\uparrow\uparrow} & \mathbf{g}_{nm}^{\uparrow\downarrow} \\ \mathbf{g}_{nm}^{\downarrow\uparrow} & \mathbf{g}_{nm}^{\downarrow\downarrow} \end{pmatrix}. \quad (3.2.18)$$

and $\mathbf{t}_{n;\sigma}^{-1}$ becomes itself a function of the magnetic moment orientation,

$$\mathbf{t}_n^{-1}(\mathbf{e}) = \mathbf{R}^\dagger(\mathbf{e}, \mathbf{e}_0) \mathbf{t}_n^{-1}(\mathbf{e}_0) \mathbf{R}(\mathbf{e}, \mathbf{e}_0). \quad (3.2.19)$$

This expression defines the scattering probability of a single-site scattering matrix with the magnetic moment direction \mathbf{e} referred to the ground state orientation \mathbf{e}_0 and considers the coupling between the spin and the electron reservoir via relativistic rotation matrices \mathbf{R} [293]. \mathbf{R} is a unitary representation of that $\mathcal{O}(3)$ transformation which rotates the \mathbf{e}_0 axis along \mathbf{e} .

For a deeper discussion of improvements in the Korringa-Kohn-Rostoker method, one should refer to [77, 82, 194, 219]

3.3 Magnetic properties within multiple-scattering theory

The magnetic exchange as well as the anisotropy in the Heisenberg model are derived from energy variation (energy variation principle). Therefore, the energy change ΔE in the interacting many-body electron system (3.1.3) is assumed to be the same energy variation δE_0 for the non-interacting electron system via the magnetic force theorem. Correlations, however, are always included through the correlation functional in the Kohn-Sham equation.

Magnetic force theorem Having the solution of the Kohn-Sham equation (3.1.7) at hand, the energy is expressed in terms of an kinetic and potential energy T and V of the non-interacting electrons $E_0 = T + V = \sum_i \varepsilon_i N_i$, as well as the Hartree and the exchange-correlation energy $E_1 = E_H + E_{xc}$. N_i is the occupation number of state i with the energy ε_i . The self-consistent iteration of the energy can be mapped in two steps [123, 174, 184, 195, 218, 279]: *i*) variation of the non-interacting electron problem with constant Hartree- and exchange-correlation energy E_1 ; *ii*) the potential relaxes into a new energy state by changing E_1 (change of the electron density $n \rightarrow n + \delta n$). If the effective potential is changed, also the energy E_0 will be perturbed

$$\Delta E = \delta E_0 + \delta_{pot} E_0 - \delta E_1. \quad (3.3.1)$$

If the occupation numbers are constant, the last two terms cancel each others, except for a volume contribution, where \mathcal{S} is the surface element and $\delta \mathcal{S}$ is the change of the surface [43, 218]

$$\Delta E = \delta E_0 - \int n^2 \frac{\delta \varepsilon_{xc}}{\delta n} \delta \mathcal{S} \cdot \mathbf{d}\mathcal{S} \quad (3.3.2)$$

This is the so called *magnetic force theorem* that predicts, in case of a constant volume, the relation between the energy change of the non-interacting and the interacting electron systems. This fundamental theorem can be used to determine, for example, the exchange integrals J_{ij} .

Lichtenstein formula The Heisenberg energy reads $E = -\sum_{ij} J_{ij} \mathbf{m}_i \cdot \mathbf{m}_j$. If a single magnetic moment is tilted out of the ferromagnetic order, given by the case $J_{ij} > 0 \forall i, j$, then the magnetic energy will increase by:

$$\delta E_i = -2 \sum_j J_{ij} \mathbf{m}_j \cdot \delta \mathbf{m}_i. \quad (3.3.3)$$

The same logic holds also for two magnetic moments, when the interaction between the moments among themselves as well as the exchange between the moments and the ferromagnetic host is considered. The energy grows in this case by about $\delta E = -J_{ij}\theta^2/2$, where θ is the small tilting angle out of the ferromagnetic equilibrium¹. Under conservation of the number of electrons, this variation is proportional to the energy perturbation determined in the magnetic force theorem (3.3.2)

$$\delta E = - \int^{E_F} \delta N(\varepsilon) d\varepsilon. \quad (3.3.4)$$

The integration runs up to the Fermi energy E_F . N is the integrated density of states, which can be substituted with Lloyd's formula [174]

$$\delta E = -\frac{1}{\pi} \int \Im \text{Tr} \ln \hat{\tau} \left(\mathbf{1} + \delta \hat{t}^{-1} \hat{\tau} \right) d\varepsilon. \quad (3.3.5)$$

The Fourier transform of the free energy and, thus, of the perturbed single-site scattering δt^{-1} allows to use the spinor representation (3.2.17). Finally, the Lichtenstein formula [173, 174] is expressed from comparison of the two energy variations from the Heisenberg model and from (3.3.5):

$$J_{ij} = -\frac{1}{\pi} \int^{E_F} \Im \text{Tr} \Delta \mathbf{t}_i \boldsymbol{\tau}_{ij} \Delta \mathbf{t}_j \boldsymbol{\tau}_{ji} d\varepsilon, \quad (3.3.6)$$

with $\Delta \mathbf{t}_i = \left(\mathbf{t}_{i,\uparrow}^{-1} - \mathbf{t}_{i,\downarrow}^{-1} \right)$. This features the magnetic exchange as the difference of the spin-up and spin-down potential on site i and j and its orbital overlap due to τ_{ij} that is essential for occurrence of magnetism (see section 2.1).

Magnetic anisotropy The free energy of the system, deduced from the magnetic-force theorem, is independent of the direction of the magnetization. Magnetization, however, favors some direction with respect to the crystal symmetry (see section 2.1): the realignment of the magnetic moment in a not symmetry-preferred direction costs the magnetic anisotropy energy

$$E_{\text{MCA}} = E(\mathbf{M}_1) - E(\mathbf{M}_0). \quad (3.3.7)$$

Since spin-orbit coupling in the Dirac equation breaks the symmetry with respect to the magnetization direction, the energy for magnetization \mathbf{M}_0 (quantization axis in the magnetic “soft” direction) differs from the energy for \mathbf{M}_1 (quantization axis in the “hard” direction). So, the magnetocrystalline anisotropy is obtainable within the fully relativistic multiple-scattering theory.

In a quasi-relativistic model, where the Pauli equation is used [220], Bruno [42] developed a simplified theory to observe the anisotropy

$$E_{\text{MCA}} \approx \langle \mathbf{L} \cdot \mathbf{S} \rangle_{\mathbf{M}_1} - \langle \mathbf{L} \cdot \mathbf{S} \rangle_{\mathbf{M}_0}. \quad (3.3.8)$$

Here, \mathbf{L} and \mathbf{S} are the orbital and the spin momenta of the electron. Selected systems, such as multiple-phase multiferroica Fe/BTO [27], proved good agreement between the anisotropy calculated with the Dirac and the Pauli equation.

¹The energy variation regards to a ferromagnetic host with the magnetization in z -direction. Thus, $\delta \mathbf{m}_i = (0, \sin(\theta), \cos(\theta))$, which can be Taylor-expanded to reach such results.

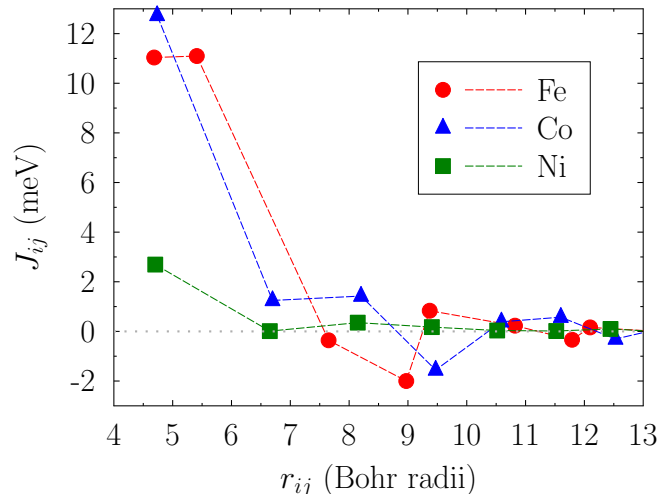


Figure 3.3.1.: Calculated magnetic exchange parameter versus distance r for bcc-Fe (red circles), fcc-Co (blue triangles) and fcc-Ni (green squares) bulk. In three-dimensional crystal structures the J_{ij} drop off proportional to $1/r^3$, which is the case for all three materials. Typical for Fe are equal nearest- and next-nearest-neighbor interactions. In first order for all three Stoner magnets, a simple mean field method predicts a smaller phase transition temperature compared to the experiment .

Having both characteristics — magnetic exchange and anisotropy — at hand, various magnetic properties are accessible and were studied during my PhD. For instance, the superparamagnetic state as well as the switching behavior of 2 ML thick triangular Co islands on Cu(111) can be studied, exhibiting nanodomain formations due to the shape anisotropy beyond the Stoner-Wohlfarth model [33]. Magnetic oxides, such as SrRuO₃ [84] or SrTcO₃ [28], are promising materials for multiferroic and exchange-bias applications only, if the magnetic order is stable up to room temperature. The Jahn-Teller distortion [138] indicates the sensitivity of the d -orbitals (‘magnetic orbitals’) to lattice distortions, strain and phonons. The minority spin-channel located just above the Fermi surface in the half-metallic perovskite La_{2/3}Sr_{1/3}MnO₃, e.g., gets occupied due to tetragonal distortion, leading to a strong decrease of the effective exchange coupling and, thus, a lowering of the Curie temperature [36]. Beside the manipulation of the magnetism via strain, an electrical manipulation of the magnetic order is offered by topological insulators, where magnetism can be varied by the Dirac cone of the surface state [210]. This state survives, e.g., in Sb₂Te₃ under weak doping with magnetic atoms, where the impurities form magnetic clusters [183].

3.4 Tight-binding model

The tight-binding (TB) model is an empirical scheme for construction of Hamiltonians by placing ‘atomic-like orbitals’ at atomic sites and allowing electrons to hop between these through the orbital overlap [66, 243].

Strong lattice periodic potentials with bound, localized electron states depict the tight-binding model as one of the two bounding cases: *i*) weak potentials and nearly free electrons (electron gas) and *ii*) strong and localized potentials. The second model acts between the

limits that the overlap is strong to manipulate the effective velocity in the dispersion relation, but still, weak enough to hold the description of an isolated atom at position \mathbf{R} . Consequently, the Schrödinger equation for the isolated atom reads:

$$\hat{H}_{\mathbf{R}}(\mathbf{r}) \phi_n(\mathbf{r}) = \varepsilon_n \phi_n(\mathbf{r}), \quad (3.4.1)$$

where ε_n and ϕ_n are the eigenvalues and the eigenstates of the isolated-atom Hamiltonian. Bringing together N such isolated atoms splits the N -times degenerated states due to the Coulomb interaction (figure 3.4.1) and one has to solve a many-body problem:

$$\hat{H}(\mathbf{r}) \psi_{\mathbf{k},n}(\mathbf{r}) = \varepsilon_{\mathbf{k},n} \psi_{\mathbf{k},n}(\mathbf{r}). \quad (3.4.2)$$

n characterizes the state with the energy $\varepsilon_{\mathbf{k},n}$. The wave function $\psi_{\mathbf{k},n}$ is composed those of correlated isolated atoms. The Hamilton operator with the attractive crystal potentials $V(\mathbf{r} - \mathbf{R})$

$$\hat{H} = -\frac{\nabla^2}{2m} + \sum_{\mathbf{R}'} V(\mathbf{r} - \mathbf{R}') = \hat{H}_{\mathbf{R}} + \underbrace{\sum_{\mathbf{R}' \neq \mathbf{R}} V(\mathbf{r} - \mathbf{R}')}_{\Delta V(\mathbf{r})} \quad (3.4.3)$$

can be separated into on-site energy contributions (atom at \mathbf{R}) and potentials ΔV coming from the other lattice sites \mathbf{R}' . The latter contribution is considered as weak in this treatment [7].

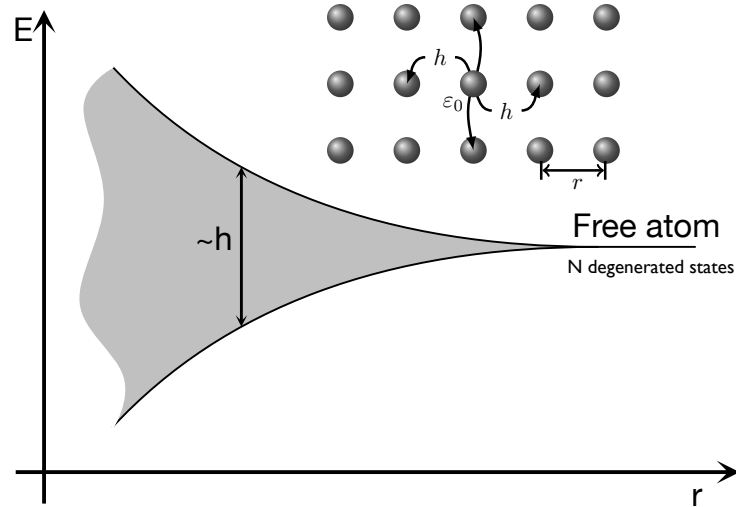


Figure 3.4.1.: Band splitting of N degenerate states, coming from N localized atoms, with respect to the atomic separation \mathbf{r} . Due to the large number of atoms N and the resulting dense-graded energy levels, the splitting results in a continuous region (marked by the shaded area). The width is proportional to the transition probability h between the nearest neighboring atoms.

Hence, the arrangement of homogeneous atoms in the crystal is treated as a perturbation in the atomic (isolated) problem and the states ψ_n of the Hamilton operator \hat{H} can be constructed from the wave function ϕ_n of the ‘isolated’ atomic Hamiltonian $\hat{H}_{\mathbf{R}}$. In process, the atomic states ϕ_n are also eigenstates of \hat{H} . The weak potential perturbation implies no

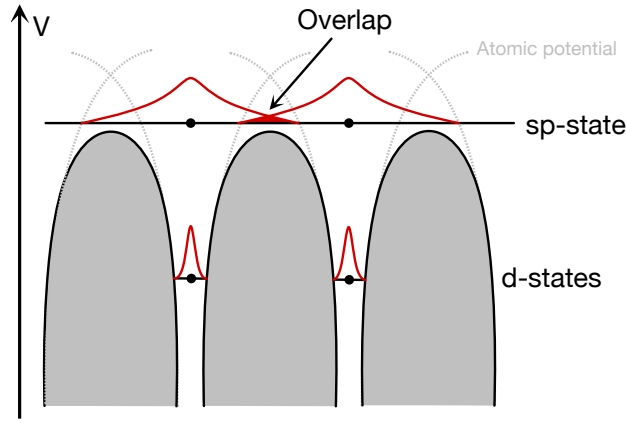


Figure 3.4.2.: Periodic crystal potential and the resulting overlap of the atomic wave-functions. Due to merged single atoms and the interaction of the nuclei, the potential landscape alters (dotted lines - potential of single atoms, gray area - potential landscape as closeness of single atom arrangement). Core states, e.g. d-states, are localized and lie lower in energy. sp-electrons (located above the shaded area) are long-ranged, delocalized states with high energy, moving almost free through the crystal. Orbital overlap appears, which has to be accounted as weak. Otherwise, the tight binding method becomes arguable for this state.

chemical bond, whereupon $\phi_n(\mathbf{r} - \mathbf{R})$ vanishes in the region of $\Delta V(\mathbf{r})$. Consequently, the eigenstates of \hat{H} are constructible as Bloch states

$$\psi_{\mathbf{k},n}(\mathbf{r}) = \frac{1}{\sqrt{N}} \sum_{\mathbf{R}} e^{i\mathbf{k}\cdot\mathbf{R}} \phi_n(\mathbf{r} - \mathbf{R}) \quad (3.4.4)$$

that obey the periodicity of the crystal lattice. The Bloch theorem [22] predicts equal probability of finding an electron in each Brillouin cell. Since in crystals or molecules a chemical bond must exist, the condition $\Delta V\phi_n = 0$ can be only valid for inner core states, but not for outer atomic levels. The Bloch states (3.4.4) are not anymore the exact eigenstates of the Hamiltonian \hat{H} ; they are not orthogonal [7]. In particular, the overlap integrals are smaller than 1. The non-orthonormal basis can be maintained using Wannier states $w_n(\mathbf{r} - \mathbf{R})$ [7]. These fulfill the orthonormal condition and are not necessarily extended in the atomic basis. In general, the Wannier functions are unknown and not unique.

Let the Bloch states (3.4.4) be the eigenstates of \hat{H} , then the eigenvalues can be obtained using the Ritz variational principle [234]

$$\varepsilon_{\mathbf{k},n} = \frac{\langle \psi_{\mathbf{k},n} | \hat{H} | \psi_{\mathbf{k},n} \rangle}{\langle \psi_{\mathbf{k},n} | \psi_{\mathbf{k},n} \rangle}. \quad (3.4.5)$$

If one neglects the three-center integrals (due to the small overlap between the wave functions) [243], the eigenstates $\varepsilon_{\mathbf{k},n}$ in the tight-binding approximation read

$$\varepsilon_{\mathbf{k},n} = \varepsilon_n + \frac{\beta(\mathbf{R}) + \sum_{\mathbf{R}' \neq \mathbf{R}} e^{-i\mathbf{k}\cdot\mathbf{R}'} h(\mathbf{R}')}{1 + \sum_{\mathbf{R}' \neq \mathbf{R}} e^{-i\mathbf{k}\cdot\mathbf{R}'} \alpha(\mathbf{R}')}, \quad (3.4.6)$$

where only the site at \mathbf{R} (central atom) is considered. The atomic energy shifts due to the potential of the neighboring atoms

$$\beta(\mathbf{R}) = \int \phi_n^*(\mathbf{r}) \sum_{\mathbf{R}' \neq \mathbf{R}} V(\mathbf{r} - \mathbf{R}') \phi_n(\mathbf{r}) \, d\mathbf{r}, \quad (3.4.7)$$

is, in most cases, small. α is the overlap integral resulting from the non-orthonormal basis (Bloch states)

$$\alpha(\mathbf{R}) = \int \phi_n^*(\mathbf{r} - \mathbf{R}) \phi_n(\mathbf{r}) \, d\mathbf{r}. \quad (3.4.8)$$

h 's are the transfer integrals (“hopping” integrals)

$$h(\mathbf{R}) = \int \phi_n^*(\mathbf{r} - \mathbf{R}) V(\mathbf{r} - \mathbf{R}) \phi_n(\mathbf{r}) \, d\mathbf{r}, \quad (3.4.9)$$

which indicate the transfer probability from one atom to the next one and represent also the bandwidth (figure 3.4.1); the inverse effective mass of the bottom tight-binding bands is direct proportional to the transfer integrals [66]. One way to determine the transition integrals is the interpolation scheme maintained by Slater and Koster parametrization [247], whereas the direction cosines can be taken from the Slater-Koster table.

If the wave function $\phi_n(\mathbf{r})$ is assumed to be a linear combination of atomic orbitals (LCAO) $\sum_{\nu} c_{n,\nu}(\mathbf{k}) \phi_{\nu}(\mathbf{r} - \mathbf{R}_n)$, then the solution of the TB model will become equivalent to an eigenvalue problem

$$\mathbf{H}(\mathbf{k}) \mathbf{c}_n(\mathbf{k}) = \varepsilon_{\mathbf{k},n} \mathbf{c}_n(\mathbf{k}). \quad (3.4.10)$$

The weights in the LCAO *ansatz* are eigenvectors $\mathbf{c}_n(\mathbf{k}) = \{c_{n,\nu}(\mathbf{k}) : \nu = 1, \dots, N_b\}$ of the tight-binding Hamilton matrix $\mathbf{H}(\mathbf{k}) = \{H_{\nu,\mu}(\mathbf{k}) = \langle \mathbf{k}, \nu | \hat{H} | \mathbf{k}, \mu \rangle : \nu, \mu = 1, \dots, N_b\}$, where N_b are the numbers of bands and $|\mathbf{k}, \mu\rangle$ is the Hilbert space representation of $\psi_{\mathbf{k},n}$.

The tight-binding method describes very well partially filled d -states of transition-metals as well as insulators [51, 62, 171]. In addition, the ability of considering spin-orbit coupling [140] and exchange interaction [12] make the tight-binding method even more attractive. The tight-binding Hamiltonian, present in this thesis, consists of three parts: the on-site energies and the hopping elements \hat{H}_0 , the spin-orbit coupling \hat{H}_{SOC} and the Zeeman term \hat{H}_{mag} . Equation (3.2.5) transfers the TB-Hamilton into Green function, to consider disorder and alloys [21, 70, 87, 168] as well as layer-resolved properties based on renormalization techniques [26, 129].

For some energy levels and their corresponding wave function with a larger spacial expansion than the lattice constant, however, the validity of the TB model becomes arguable due to the larger overlap (figure 3.4.3, $E - E_F > 5$ eV). Apart of that, the tight-binding model accounts for the electron-electron interaction only by an effective potential that becomes important for magnetic systems or conduction effects. Hence, it is indispensable to prove the validity of the tight-binding model with aforementioned *ab-initio* methods (figure 3.4.3).

But still, I used the tight-binding model with a $sp^3d^5f^7$ -orbital basis to characterize magnetic properties, especially the intrinsic dissipation α in the magnetization dynamics (section 3.7 and results in section 4.2) and the exchange splitting as a function of the spin temperature. A genetic algorithm fit on band structures coming from first principles was performed to

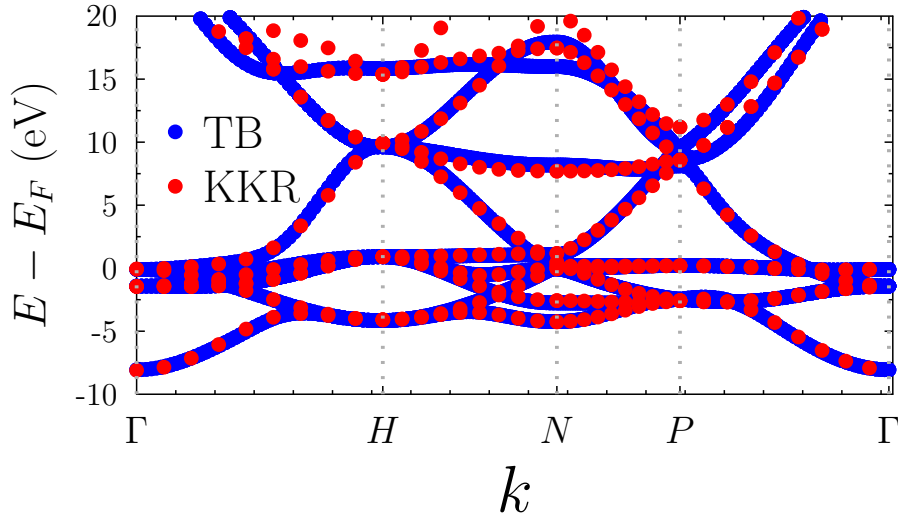


Figure 3.4.3.: Non-spinpolarized bandstructure for Fe-Bulk calculated with the tight-binding (blue symbols) and the KKR (red symbols) method. Up to the Fermi level E_F both methods agree well. For energies higher than $E_F + 5$ eV (valence and conducting states), the tight-binding method deviates, since the assumption of strong bonds fails for nearly free electrons. More precisely, the variance is an artifact of the finite orbital basis.

obtain the Slater-Koster parameter. Beside the magnetic properties, the tight-binding model was also used to characterize the surface state in topological insulators (not shown in this thesis).

3.5 Anisotropic magnetic exchange within crystals with low symmetry

Coherent and ordered magnetic materials are well understood within the Heisenberg model [60, 95, 96, 175, 261, 289], introduced in section 2.1. However, recent studies on thin films [14, 25], complex ferroelectric structures [290] and low-dimensional systems [192] reveal non-collinearity in spin textures. Such spin formations are discoverable on a nm-length scale using scanning tunneling microscopy (STM) [19, 20], magneto-optical Kerr effect measurements (MOKE) [231], X-ray magnetic circular dichroism (XMCD) [188] or spin-polarized electron-energy loss spectroscopy (SPEELS) [85, 229, 276]. The Heisenberg Hamiltonian (2.1.5) does not comprise non-collinearity, since it makes no statement about lattice symmetries. In contrast to the experimentally postulated spin spiral structures it couples two magnetic moments parallel to each other, if $J > 0$. Nevertheless, due to uniaxial anisotropy, domain wall formation—a special kind of non-collinearity—appears on a typical length $w = \sqrt{A/K} \sim 10$ nm, where A and K are the magnetic exchange density and the magnetocrystalline anisotropy, respectively [47]. The domain length of the non-collinear structures discussed in the earlier listed publications and in this thesis, however, are smaller than the typical magnetic domain wall length w , indicating a mechanism driven by non-uniaxial anisotropy. Hence, second-order anisotropy energy contributions have to prefer a canting between two sites i and j , forced by strong spin-orbit coupling and the

reduction of the spatial symmetry; the Heisenberg model must be generalized, passing the *ansatz*

$$\hat{H} = \sum_{ij} E_{ij} = - \sum_{ij} \mathbf{m}_i \mathbf{l}_{ij} \mathbf{m}_j. \quad (3.5.1)$$

The generalized Heisenberg exchange tensor \mathbf{l}_{ij} is not necessarily rotational invariant, but, due to energy conservation ($E_{ij} = -\mathbf{m}_i \mathbf{l}_{ij} \mathbf{m}_j \stackrel{!}{=} E_{ji} = -\mathbf{m}_j \mathbf{l}_{ji} \mathbf{m}_i$), satisfies $\mathbf{l}_{ij} = (\mathbf{l}_{ji})^T$. It is convenient to decompose the interaction matrix in order to obtain a relation between \mathbf{l}_{ij} and the scalar Heisenberg parameters J_{ij}

$$\mathbf{l}_{ij} \equiv \underbrace{\frac{1}{3} \text{Tr}(\mathbf{l}_{ij}) \mathbf{E}}_{J_{ij}} + \underbrace{\frac{1}{2} (\mathbf{l}_{ij} + (\mathbf{l}_{ij})^T) - \frac{1}{3} \text{Tr}(\mathbf{l}_{ij}) \mathbf{E}}_{\mathbf{S}_{ij}} + \underbrace{\frac{1}{2} (\mathbf{l}_{ij} - (\mathbf{l}_{ij})^T)}_{\mathbf{A}_{ij}}. \quad (3.5.2)$$

The homogeneous first part is related to the scalar exchange integrals J_{ij} of the Heisenberg model [47, 293]. The symmetric \mathbf{S}_{ij} and the antisymmetric anisotropic exchange \mathbf{A}_{ij} are trace-less. \mathbf{S}_{ij} enters as an additional uniaxial anisotropy, preferring selected orientation of the magnetic moments due to the crystal. The non-diagonal elements of \mathbf{S}_{ij} are in practice negligible and the symmetric anisotropic exchange reduces to $\tilde{\mathbf{S}}_i = \sum_j \mathbf{S}_{ij}$.

The vector

$$D_{ij}^\gamma \equiv \frac{1}{2} \sum_{\alpha\beta} \epsilon_{\gamma\alpha\beta} I_{ij}^{\alpha\beta}, \quad (3.5.3)$$

relates the Dzyaloshinskii-Moriya (DM) interaction with the antisymmetric part \mathbf{A}_{ij} [293]

$$E_{ij}^{\text{DM}} = \mathbf{D}_{ij} \cdot (\mathbf{m}_i \times \mathbf{m}_j). \quad (3.5.4)$$

This type of antisymmetric anisotropic exchange was first predicted by Dzyaloshinskii in 1958 [75, 76] due to symmetry arguments and describes instead of the uniaxial anisotropy (see section 2.1) a unidirectional anisotropy: the energy conservation related to equation 3.5.4 maintains that the DM vectors are antisymmetric in the site indices ($\mathbf{D}_{ij} = -\mathbf{D}_{ji}$). The antisymmetric exchange energy \mathbf{A}_{ij} favors parallel alignment of \mathbf{D}_{ij} in high-symmetry directions and magnetic order, where the magnetic moments are perpendicular to \mathbf{D}_{ij} . This kind of interaction characterizes the polar nature of the magnetization with respect to the crystal structure. Moreover, Moriya postulates symmetry rules [75, 76, 203] for the \mathbf{D} -vector between two coupled moments \mathbf{m}_i and \mathbf{m}_j located at \mathbf{r}_i and \mathbf{r}_j , respectively (\mathbf{R} fixes the point bisecting the line $\overline{\mathbf{r}_i \mathbf{r}_j}$):

- i)* If the inversion center is located in \mathbf{R} , then \mathbf{D} will be zero (figure 3.5.1 a).
- ii)* If the mirror plain is perpendicular to $\overline{\mathbf{r}_i \mathbf{r}_j}$ and passes through \mathbf{R} , then \mathbf{D} will be parallel to the mirror plane (figure 3.5.1 b).
- iii)* If the mirror plane includes the points \mathbf{r}_i and \mathbf{r}_j , then \mathbf{D} will be perpendicular to this mirror plane (figure 3.5.1 c).
- iv)* If a two-fold rotation axis is perpendicular to $\overline{\mathbf{r}_i \mathbf{r}_j}$ and passes through \mathbf{R} , then \mathbf{D} will be perpendicular to this two-fold axis (figure 3.5.1 d).
- v)* If there is an n -fold axis ($n > 2$) along $\overline{\mathbf{r}_i \mathbf{r}_j}$, \mathbf{D} will be parallel to $\overline{\mathbf{r}_i \mathbf{r}_j}$.

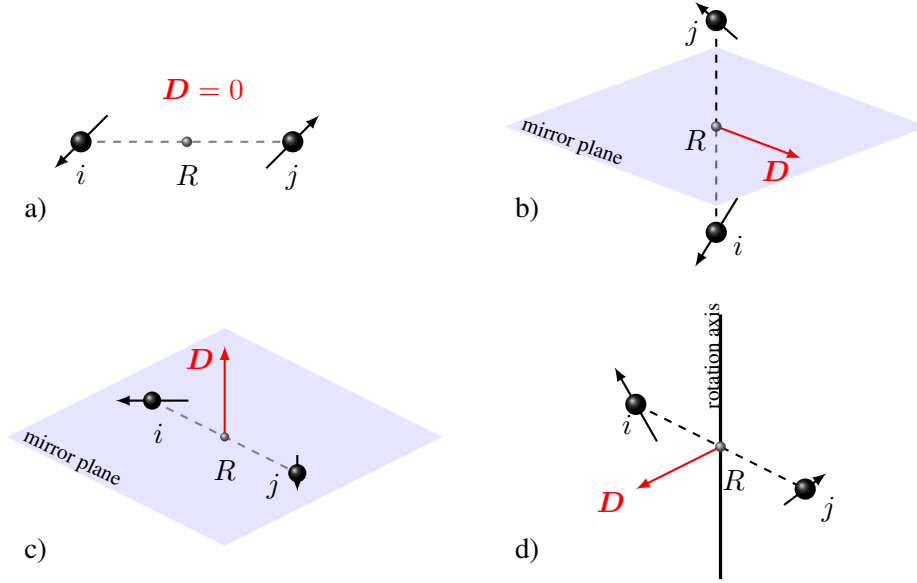


Figure 3.5.1.: Diagram of lattice symmetries that contribute to the Dzyaloshinskii-Moriya interaction: a) with inversion center (antiferromagnetic state), b) and c) if inversion symmetry is broken and mirror plane symmetry exists (blue plane), d) if inversion symmetry is broken and rotational symmetry exists (black line). The resulting DM-vector is illustrated by the red arrow. The dotted line denotes the vector connecting two sites i and j , added to guide the eye.

Moriya showed in addition, how to calculate the antisymmetric exchange interaction for localized magnetic systems (insulators) [203–205]. He postulates the dependence of \mathbf{D}_{ij} on the spin-orbit coupling, since it breaks both time reversal and space inversion symmetries, which is also important for superexchange and the RKKY interaction. In metals, however, the exchange mechanism is forced by band magnetism or double exchange [134] and even more factors affect unidirectional magnetic coupling, such as the character of the occupied orbitals, the crystal field and the number of d -electrons [65].

The antisymmetric exchange interaction dominates the coupling, e.g., in spin glasses, where a disordered magnet contains non-magnetic impurities with strong spin-orbit coupling [92, 248]. Since Moriya’s two-center approach applies only to systems with localized magnetic moments, Fert and Levy (1980) [97, 172] developed a three-center model, which is based on the s-d Heisenberg-Hamiltonian for itinerant systems, considering that local exchange exists between a conduction electron at \mathbf{r} with spin \mathbf{S} and two localized spins, \mathbf{m}_i and \mathbf{m}_j at sites \mathbf{R}_i and \mathbf{R}_j , as well as spin-orbit scattering with a non-magnetic impurity at site \mathbf{R}_n . In second-order perturbation theory, the RKKY model comprises correlations, where an electron is polarized by \mathbf{m}_i , scattered at the orbital momentum \mathbf{L} and finally polarizes \mathbf{m}_j . The effective exchange

$$V = -J_{sd} \delta(\mathbf{r} - \mathbf{R}_i) \mathbf{S} \cdot \mathbf{m}_i - J_{sd} \delta(\mathbf{r} - \mathbf{R}_j) \mathbf{S} \cdot \mathbf{m}_j + \lambda(\mathbf{r}) \mathbf{S} \cdot \mathbf{L} \quad (3.5.5)$$

generates the Dzyaloshinskii-Moriya interaction

$$\mathbf{D}_{ij} = D_0 \sum_n \frac{\sin(k_F (R_{ij} + R_{in} + R_{jn}) + \phi)}{1 + J_{sd} (R_{ij} + R_{in} + R_{jn})} \frac{(\mathbf{e}_{in} \cdot \mathbf{e}_{jn}) \mathbf{e}_{in} \times \mathbf{e}_{jn}}{R_{ij} R_{in} R_{jn}}. \quad (3.5.6)$$

Here, \mathbf{R}_{in} is the distance vector between the magnetic site i and the non-magnetic site n and $\mathbf{e}_{in} = \mathbf{R}_{in}/R_{in}$. D_0 , k_F and ϕ are the strength of the Dzyaloshinskii-Moriya interaction, the Fermi momentum and a phase shift, respectively. More precisely, $D_0 \propto \lambda J_{sd}^2 / E_F k_F^3$. Equation (3.5.6) reminds of a RKKY-type interaction, which is not invariant under rotation of the spin system. Furthermore, this type of antisymmetric exchange suggests significant DM contributions in materials with broken spatial inversion symmetry, where the magnetism originates from super- or direct exchange, e.g. in perovskites [80, 241] (inverse Dzyaloshinskii-Moriya effect, figure 3.5.2). Fert and Levy conclude that the s-d type coupling is only valid [172], if the local density of states at the Fermi edge weighted by the SOC constant is $\lambda n(E_F) \ll 1$ (Stoner-like criteria).

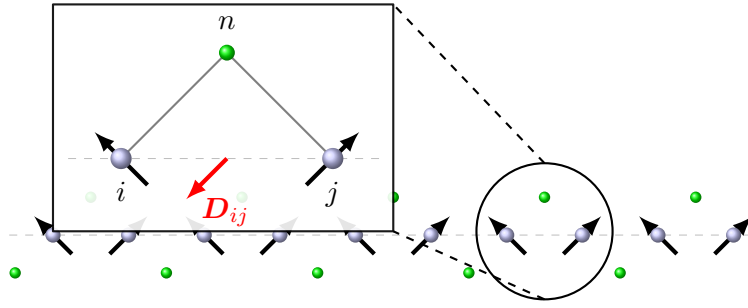


Figure 3.5.2.: Dzyaloshinskii-Moriya interaction in perovskites and spin glasses. Due to the displaced atom at site n , the symmetry is reduced and anisotropic exchange becomes important (red arrow). The direction of the Dzyaloshinskii-Moriya vector \mathbf{D}_{ij} is from equation (3.5.6).

An inversion center is not present at surfaces. Moriya's rules, however, regard only to DM vectors between a surface and a bulk site; but no predictions of DM contributions between two surface sites can be made [65]. In most cases, the antisymmetric anisotropic exchange is located in-plane and relate to the surface normal (figure 3.5.3) as well as to the invariant rotation operation of particular surfaces. On surfaces with a two-fold real- and spin-space rotation symmetry around the surface normal \mathbf{n} it becomes clear that $\mathbf{D} \cdot \mathbf{n} = 0$. Suppose \mathbf{q} is the propagation vector of a non-collinear structure, a mirror plane perpendicular to \mathbf{q} implies $\mathbf{D} \cdot \mathbf{q} = 0$, whereas a mirror plane parallel to \mathbf{q} prefers perpendicular arrangement of \mathbf{D} to the mirror plane [122]. The Dzyaloshinskii-Moriya torque is also not solvable analytically, but under some restrictions an analytical energy minimization can be studied [122]. For instance, when the DM vector is localized in the direction of the hard axis, a non-collinear periodic spin-configuration will be the ground state if and only if $|\mathbf{D}| > 4/\pi \sqrt{AK}$, where A and $K = K_y - K_x$ are again the exchange stiffness and the anisotropy, respectively. This shows that the effect of the DM interaction depends strongly on the relations between the anisotropy constants and the direction of the \mathbf{D} vector.

The interaction matrix \mathbf{I} in equation (3.5.1) is also observable using the KKR Green function method (section 3.2). More precisely, the derivation of \mathbf{I} from the total energy is similar to Lichtenstein's exchange integrals, accounting explicitly the orientation of the normalized magnetic moment $\mathbf{e}(\theta, \phi)$. Thus, the matrix elements $I_{ij}^{\mu\nu}$ correspond to the second-order

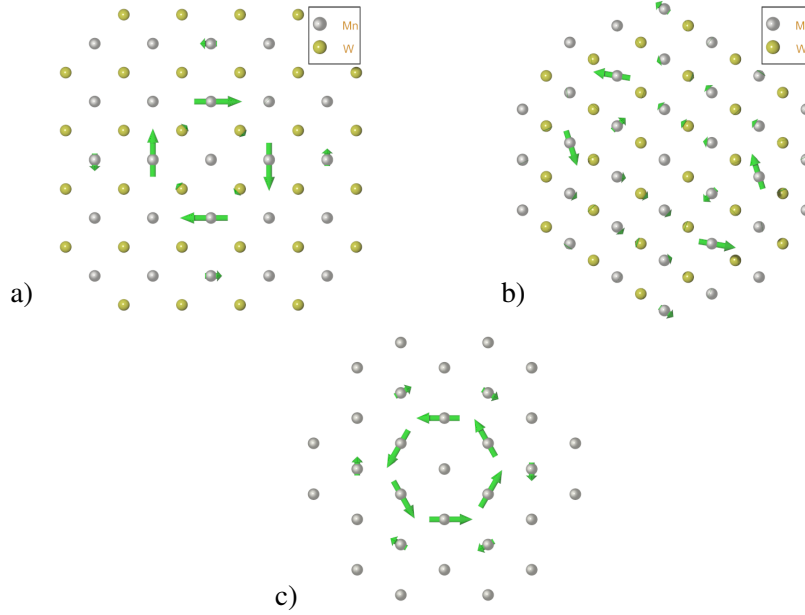


Figure 3.5.3.: Set of calculated Dzyaloshinskii-Moriya vectors for a) 1ML Mn/W(001), b) 1ML Mn/W(110) and c) 1ML Fe/Ir(111). The spheres indicate the atom positions in the xy plane. Different colors characterize the surface (gray spheres) and the subsurface layer (yellow spheres). The DM vectors (green arrows), regarded from the center atom, correlates to the symmetry of the surface and are located in the xy plane: Both Mn/W(001) and Mn/W(110) have a four-fold rotation axis in z direction, where Fe/Ir(111) offers a three-fold character. The DM-interaction is short-ranged (typically first and second nearest neighbors) and owns also contributions to the sub-surface layer (induced magnetic moment). The DM-vectors agreed with those observed experimentally [14, 25, 91, 270].

derivative of the free energy with respect to spherical coordinates θ , ϕ at sites i and j , as shown by Zabloudil et al. [293]. The free energy within the magnetic force theorem and Lloyd's formula (3.2.11) yield

$$F = -\frac{1}{\pi} \Im m \int^{E_F} \text{Tr} \ln \tau(\varepsilon) d\varepsilon. \quad (3.5.7)$$

The scattering path operator $\tau = \tau(\mathbf{e})$ and the scattering matrix $\mathbf{t} = \mathbf{t}(\mathbf{e})$ are functions of the normalized magnetic moment \mathbf{e} , represented by a rotation (3.2.19) out of the spin quantization axis \mathbf{e}_0 . Thus, the scattering path τ' for a slightly tilted magnetic moment at site i ,

$$\ln \tau' = \ln(\mathbf{m} + \Delta \mathbf{m}_i - \mathbf{g}_0)^{-1} = \ln \tau - \ln(\mathbf{1} + \tau \Delta \mathbf{m}_i), \quad (3.5.8)$$

is expressible in terms of the old reference state τ , where $\mathbf{m} = \mathbf{t}^{-1}$. Taking into account terms up to second order in $\Delta \mathbf{m}_i$ and using the Taylor expansion of the logarithmic function, the variation of the free energy with respect to the tilted magnetic moment

$\Delta F = F' - F = -\frac{1}{\pi} \Im \int^{E_F} \text{Tr} (\ln \boldsymbol{\tau}'(\varepsilon) - \ln \boldsymbol{\tau}(\varepsilon)) d\varepsilon$ gives [271]

$$\frac{\partial^2 F}{\partial \varphi_i \varphi_i} = -\frac{1}{\pi} \Im \int^{E_F} \text{Tr} \left[-\tau_{ii} \frac{\partial^2 \mathbf{m}_i}{\partial \varphi_i \varphi_i} + \tau_{ii} \frac{\partial \mathbf{m}_i}{\partial \varphi_i} \tau_{ii} \frac{\partial \mathbf{m}_i}{\partial \varphi_i} \right] d\varepsilon, \quad (3.5.9)$$

$$\frac{\partial^2 F}{\partial \varphi_i \vartheta_i} = -\frac{1}{\pi} \Im \int^{E_F} \text{Tr} \left[-\tau_{ii} \frac{\partial^2 \mathbf{m}_i}{\partial \varphi_i \vartheta_i} + \tau_{ii} \frac{\partial \mathbf{m}_i}{\partial \varphi_i} \tau_{ii} \frac{\partial \mathbf{m}_i}{\partial \vartheta_i} \right] d\varepsilon, \quad (3.5.10)$$

$$\frac{\partial^2 F}{\partial \vartheta_i \vartheta_i} = -\frac{1}{\pi} \Im \int^{E_F} \text{Tr} \left[-\tau_{ii} \frac{\partial^2 \mathbf{m}_i}{\partial \vartheta_i \vartheta_i} + \tau_{ii} \frac{\partial \mathbf{m}_i}{\partial \vartheta_i} \tau_{ii} \frac{\partial \mathbf{m}_i}{\partial \vartheta_i} \right] d\varepsilon. \quad (3.5.11)$$

This derivations link to the on-site exchange matrix \mathbf{l}_{ii} and account for the magnetocrystalline anisotropy in the generalized Heisenberg model.

The site-off-diagonal terms ($i \neq j$) rely on the rotation of two magnetic moments at site i and j , simultaneously. Consequently, the scattering matrix for the perturbed magnetic system $\boldsymbol{\tau}'$ is put as

$$\ln \boldsymbol{\tau}' = \ln(\mathbf{m} + \Delta \mathbf{m}^i + \Delta \mathbf{m}^j - \mathbf{g}_0)^{-1} = \ln \boldsymbol{\tau} - \ln \left[\mathbf{1} + \boldsymbol{\tau}(\Delta \mathbf{m}^i + \Delta \mathbf{m}^j) \right]. \quad (3.5.12)$$

Udvardi et al. [271] showed that this expression can be reduced to $\ln \boldsymbol{\tau}' - \ln \boldsymbol{\tau} \approx \boldsymbol{\tau} \Delta \mathbf{m}^i \boldsymbol{\tau} \Delta \mathbf{m}^j$, that agrees with the Lichtenstein formula. Thus,

$$\frac{\partial^2 F}{\partial \varphi_i \varphi_j} = -\frac{1}{\pi} \Im \int^{E_F} \text{Tr} \left[\tau_{ji} \frac{\partial \mathbf{m}_i}{\partial \varphi_i} \tau_{ij} \frac{\partial \mathbf{m}_j}{\partial \varphi_j} \right] d\varepsilon, \quad (3.5.13)$$

$$\frac{\partial^2 F}{\partial \varphi_i \vartheta_j} = -\frac{1}{\pi} \Im \int^{E_F} \text{Tr} \left[\tau_{ji} \frac{\partial \mathbf{m}_i}{\partial \varphi_i} \tau_{ij} \frac{\partial \mathbf{m}_j}{\partial \vartheta_j} \right] d\varepsilon, \quad (3.5.14)$$

$$\frac{\partial^2 F}{\partial \vartheta_i \vartheta_j} = -\frac{1}{\pi} \Im \int^{E_F} \text{Tr} \left[\tau_{ji} \frac{\partial \mathbf{m}_i}{\partial \vartheta_i} \tau_{ij} \frac{\partial \mathbf{m}_j}{\partial \vartheta_j} \right] d\varepsilon. \quad (3.5.15)$$

These formulas replace the Lichtenstein formula, which has been derived for systems without spin-orbit coupling (section 3.3). It considers the modification of scattering properties not only from flipping the magnetic moment between two states \uparrow, \downarrow (Δt , discrete spin states, Ising-type), but also from rotation of the moment (∂t^{-1} , continuous spin states, Heisenberg-type). The correspondence between the derivations in the free energy and the exchange matrix elements $I_{ij}^{\nu\mu}$ is listed in Appendix B.

Various applications of this multiple-scattering approach show good agreement with experiments: e.g Mn/W(001) and Mn/W(110) [91, 270], Cr trimer on Au(111) [255] or Fe/Pt(111) [34]. However, spin vortex formation, known as Skyrmion structures, observed in Fe/Ir(111)[14, 25] requires additional biquadratic terms in the exchange mechanism, which will not be discussed in this thesis. The latter example shows the major role of symmetry lack in nanoscopic magnetic structures.

In view of the surface bearing, especially in systems with strong spin-orbit coupling, I also account the anisotropic exchange of the above mentioned magnetic systems. Therefore, I extended an existing fully relativistic multiple-scattering Green function code (*omni* from PD Dr. rer. nat. habil. Jürgen Henk). This add-on reproduces the already found Dzyaloshinskii-Moriya vectors quite well (figure 3.5.3). Since the (111)-surfaces are known for special growing conditions, visible e.g. in Co on Cu(111), and predict high anisotropic exchange e.g. in case of Ir(111), my central research point relates to this surfaces covered with 1 ML Fe or Co (Fe on Pt(111) published in [34]). Here, calculations

show (not listed in this thesis) that the ratio between the nearest-neighbor anisotropic and isotropic exchange D/J in systems with strong spin-orbit coupling, such as Rh(111), Pd(111) or Pt(111), appears typically one or two orders smaller than in Ir(111), where $D/J \approx 1$.

3.6 Disordered local moment theory

In the previous section 3.5, the Heisenberg model was improved by using the interaction matrix \mathbf{l}_{ij} instead of a scalar J_{ij} . This accounts for orbital symmetry via anisotropic exchange interaction. However, these exchange integrals are defined for zero temperature, where a magnetic ordered state exists, but are used for finite temperature and magnetic disordered states, e.g. in Monte Carlo methods or in dynamic simulations. The resulting phase transition temperature is often underestimated with respect to the experiment (for Fe bulk the theory gives $T_C \approx 700$ K [260]; experiment $T_C = 1033$ K [108]). The mismatch between theory and experiment is attributed to the temperature independence of exchange parameter. In terms of the three temperature reservoir model, motivated in the introductory chapter, the electron temperature enhances formation of electron-hole pairs, the electron equilibrium population (Fermi-Dirac distribution, Sommerfeld approximation) changes and thus, it affects the exchange interaction. In magnetic materials, however, the influence of the spin temperature on the electron states gets more important, which is so far completely disregarded. Hence, there is need for a method that includes the spin temperature in the magnetic exchange constants $J_{ij}(T_s)$. The phonon temperature, however, is neglected but is important for magnetic exchange as well.

Coherent potential approximation Alloys offer a broad range of applications¹ and are featured by a host system with impurities, where the substitutional defects can either be ordered or disordered. Especially in the latter case, it is computationally demanding to calculate large clusters with randomly distributed dopants. When using the Green function techniques (see section 3.2) it is computationally effortless to obtain the scattering path operator for an impurity system. In this context, the model should go beyond the virtual crystal approximation (VCA), where only an effective potential was build by summing up the individual potentials weighted by their concentrations. In fact, the charge density of the dopant must be considered [89]. Additional scattering processes appear from the embedded impurities, which are represented by the on-site scattering matrix \mathbf{X} [293]. Within the coherent potential approximation (CPA) [250, 274] this defect will be treated by a mean-field theory for the electron structure of a substitutional binary alloy and is often used in the context of a tight-binding approach. The model assumes an impurity atom embedded in a periodic effective *medium* that behaves on the average like an alloy (figure 3.6.1). This medium should be calculated self-consistently.

An impurity of type ν injects an additional scattering event \mathbf{t}_ν at site i in the coherent effective medium. This effective medium has different scattering properties, represented by the \mathbf{t}_c -matrix and the scattering path operator $\boldsymbol{\tau}_c$ as the primary host system; thus

¹From www.globalspec.com/reference/46879/203279/industrial-application-of-alloys

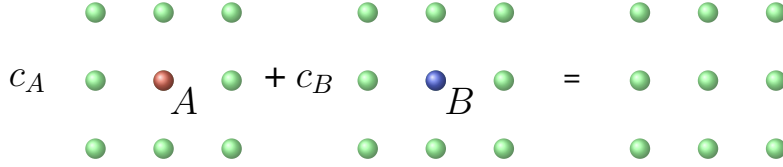


Figure 3.6.1.: Coherent potential approximation for a binary alloy $A_{1-x}B_x$. In a host system, represented by A (red spheres), impurities are embedded (B; blue spheres), which leads to an effective (CPA) medium (green spheres). This medium comprises additional scattering events in the host and the impurity system. Hence, loosely speaking, the resulting system is the average over both systems weighted by their concentrations.

[112]

$$\mathbf{X}_{i,\nu} = \left[\left(\mathbf{t}_{i,c}^{-1} - \mathbf{t}_{i,\nu}^{-1} \right)^{-1} - \tau_{ii,c} \right]^{-1}. \quad (3.6.1)$$

The condition to obtain a coherent medium is that, on average, the additional impurity scattering, which replace t_c , vanishes [112] (figure 3.6.1): $\sum_{\nu} c_{\nu} \mathbf{X}_{i,\nu} = 0$. In terms of a defect matrix

$$\mathbf{D}_{i,\nu} = \mathbf{1} + \mathbf{X}_{i,\nu} \tau_{ii,c}, \quad (3.6.2)$$

this criteria reads $\sum_{\nu} c_{\nu} \mathbf{D}_{i,\nu} = 1$. Consequently, the scattering event on site i occupied with an impurity atom of type ν can be obtained using a Dyson-like equation [112]

$$\tau_{ii,\nu} = \tau_{ii,c} + \tau_{ii,c} \mathbf{X}_{i,\nu} \tau_{ii,c}. \quad (3.6.3)$$

$\tau_{ii,c}$ has to be found self-consistently using a fix-point iteration scheme and the CPA condition. In spite of its wide application, the CPA is limited because it is a single-site mean-field theory. However, whenever there is either strong disordered fluctuation scattering or when local environment effects like short-range ordering, clustering and segregation, or local lattice distortion become important, the single-site CPA becomes inadequate. Especially for high concentrations of the dopant impurity clusters can be created and, thus, the single-site CPA approximation fails. Hence, other models like the cluster CPA [202], the embedded cluster [114] or the non-local CPA [157] were developed.

The misfit between experimentally measured and theoretically predicted phase transition temperatures T_C indicates a strong coupling between the electron system and the magnetic moments. To substantiate this, the density functional theory (see section 3.1), e.g., can be extended, which was first done by Mermin [193, 230]: the single-particle entropy Ω_{xc} was regarded in the effective one-electron field v_{xc} , expressed in terms of spin-dependent pair correlation functions. Thermal fluctuations create excitations of particle-hole pairs (Stoner excitation), that underestimate the thermally induced spin excitations and do not satisfy the fluctuation-dissipation theorem [52, 214]. Apart from Mermin's model, Györfy et al. postulate a method, involving thermal perturbation as fluctuating 'local moments' e_i at site i . This is the *disordered local moment theory*. [118, 178, 228, 252, 253].

Conduction electrons in metals move 'quasi-free' through the crystal [7]. The Heisenberg model fails due the non-local electron correlation on a very short time scale. But each lattice

site will be occupied by electrons with a certain spin direction. Incoming electrons change their orientation due to the interaction with the predominant spin on site i . Angular momentum conservation and the additional charges affect the local field at site i and, therefore, the local magnetic moment \mathbf{m}_i . In particular, the timescale of the spin fluctuation is large compared to the hopping time of the quasi-free electrons. This is the timescale separation *ansatz* (adiabatic limit), where, on the one hand, the magnetic moments in the electronic structure are used as constant and well-defined, as well as, on the other hand, the magnetic moment couples only to the thermal bath determined by the three-reservoir model. Consequently, the disordered local moment picture acts as a statistical model, where the temperature is mimicked by a probability distribution $P^{(n)}$, affecting the average magnetic moment $\mathbf{n} = M/M$,

$$\mathbf{n} = \langle \mathbf{e}_i \rangle = \int \dots \int \mathbf{e}_i P^{(n)}(\{\mathbf{e}\}) d\mathbf{e}_1 \dots d\mathbf{e}_N. \quad (3.6.4)$$

The magnetic configuration is represented by a set of unit vectors \mathbf{e}_i , $\{\mathbf{e}\} = \{\mathbf{e}_1, \mathbf{e}_2, \dots, \mathbf{e}_N\}$. This set of classical unit vectors qualifies the degrees of freedom and, thus, the phase space for the thermodynamic distribution reads

$$P^{(n)}(\{\mathbf{e}_i\}) = \frac{1}{Z} e^{-\beta \Omega^{(n)}(\{\mathbf{e}_i\})}. \quad (3.6.5)$$

Z is the partition function and $\Omega^{(n)}(\{\mathbf{e}\})$ is the grand canonical potential, which is equivalent to those of Mermin. Expressing measurable physical quantities in terms of an average requires ergodicity. In principle, a phase transition of second order, such as the magnetic phase transition, is not ergodic. However, due to the time separation *ansatz*, where now snapshots of the system with the resolution time τ will be taken, the quantities are ergodic and the long-time average can be replaced by the averages over the ensemble of the local moment configurations $\{\mathbf{e}_i\}$. As a result in the paramagnetic phase ($T \geq T_C$), where the set of magnetic moments $\{\mathbf{e}_i\}$ at site i is randomly distributed, $P^{(n)}$ will be equal in each space direction. In the ferromagnetic limit ($T = 0$ K), however, P is a δ -function; all moments are aligned parallel to the average magnetic moment \mathbf{n} .

The variation of a local magnetic moment \mathbf{e}_i is related to the modulation of the Kohn-Sham potential. Similar to alloys in the CPA, this variation is immersed like a magnetic impurity in an effective magnetic medium with the average direction \mathbf{n} . The defect matrix \mathbf{D}_i as well as the local scattering contribution \mathbf{t}_i of this impurity become functions of \mathbf{e}_i . Thus, the CPA criterium [47]

$$\int_{\mathcal{S}} P^{(n)}(\{\mathbf{e}_i\}) \mathbf{D}_{i,\mathbf{n}}(\mathbf{e}_i) d\mathbf{e}_i = 1 \quad (3.6.6)$$

holds. The integration runs over the spherical surface \mathcal{S} . The spin degrees of freedom d scores in two different models: *i*) a binary Ising-type alloy, where the spin degree of freedom is $d = 1$ (binary model) and the magnetic moments switch between two spin configurations $\mathbf{e}_i \in \{\uparrow, \downarrow\}$ or *ii*) a Heisenberg-type model, where the spin degree of freedom is $d = 3$ and the magnetic states is ‘continuous’ on a unit sphere.

In the first Ising-type model, the CPA condition (3.6.6) is replaced by the sum over discrete spin sets $\{\mathbf{e}\} = \{\uparrow, \downarrow\}$ weighted by the particular concentration c_\uparrow and $c_\downarrow = 1 - c_\uparrow$. Thus, thermally caused fluctuations are included by different concentration ratios and enter not directly into the model. A mapping $c_\uparrow(T)$ could be achieved by comparing the average magnetic moment $M(c_\uparrow)$ coming from first-principles calculations with the average magnetic

moment of, e.g., a Monte Carlo method $M^{MC}(c_{\uparrow}, T)$ [17, 18, 32, 35, 196]. Within the Monte Carlo method the classical Heisenberg model (2.1.5) can be solved with a set of exchange parameters $\{J_{ij}^{\uparrow}\}$ for a given concentration [35]. For details of the Monte Carlo method, one should refer to [17, 18, 32, 144, 208].

In the second model, the set $\{\mathbf{e}\}$ is continuous and the two thermal limits—paramagnetic and ferromagnetic state—end up in a Gaussian on a unit sphere (see appendix A), the von Mises-Fisher distribution [99]:

$$P^{(d)}(\mathbf{e}; \mathbf{n}, \kappa) = \frac{\kappa^{\frac{d}{2}-1}}{(2\pi)^{\frac{d}{2}} I_{\frac{d}{2}-1}(\kappa)} \exp(\kappa \mathbf{n}^T \mathbf{e}). \quad (3.6.7)$$

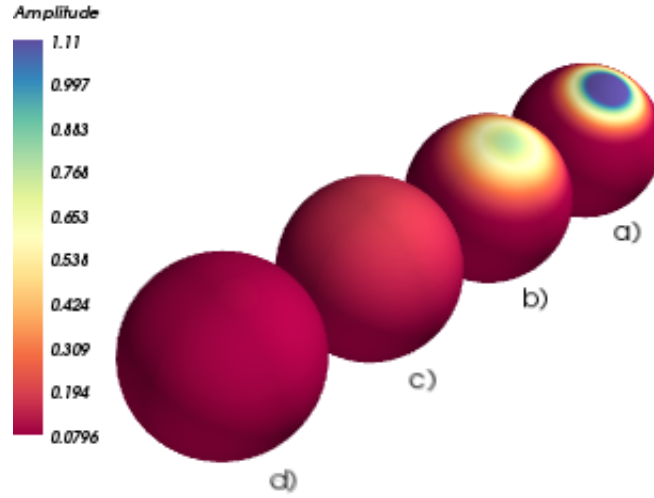


Figure 3.6.2.: Von Mises-Fisher distribution for different width κ : a) $\kappa = 10.0$, b) $\kappa = 5.0$, c) $\kappa = 1.0$, and d) $\kappa = 0.1$. The distribution demonstrates the average orientation of a set $\{\mathbf{e}\}$ of magnetic moments. The smaller κ , the broader is the distribution and the larger is the disorder in the magnetic system: a) mirrors an ordered ferromagnetic state in the direction \mathbf{n} (blue spot), where d) mimics the paramagnetic state.

The inverse distribution width κ correlates to the temperature: the larger the temperature, the smaller is κ (figure 3.6.2); d is the dimension of the problem (for the continuous spin system $d = 3$). $I_{\frac{d}{2}-1}(\kappa)$ are the modified Bessel functions [1]; κ and its mapping $\kappa(T)$ derive from the grand canonical potential $\Omega^{(n)}$. In a mean-field approximation [142, 281], the distribution width is directly proportional to the Weiss field h and, thus, the distribution function (3.6.5) becomes equivalent to the Boltzmann distribution $P^{(n)} \sim \exp(-h/k_B T)$. To construct the grand canonical potential as a function of the Weiss field, $\Omega^{(n)}$ is expressed in terms of the magnetic force theorem (section 3.3),

$$\Omega^{(n)}(\mathbf{e}) = - \int f(\varepsilon, \mu) N(\varepsilon, \mathbf{e}) d\varepsilon, \quad (3.6.8)$$

where f is the Fermi-Dirac distribution with the chemical potential μ and N is the integrated density of states. Buruzs et al. [47] establish the average grand canonical potential in second

order Taylor expansion and in terms of the CPA defect matrix \mathbf{D} ,

$$\begin{aligned} \langle \Omega^{(n)} \rangle_{e_i} &= \Omega_0 \\ &+ \frac{1}{\pi} \Im \int f(\varepsilon, \mu) \left(\ln \det \boldsymbol{\tau}_c^{(n)}(\varepsilon) - \ln \det \mathbf{D}_i^{(n)}(\varepsilon, \mathbf{e}_i) - \left\langle \sum_{j \neq i} \ln \det \mathbf{D}_j^{(n)}(\varepsilon, \mathbf{e}_j) \right\rangle \right) d\varepsilon. \end{aligned} \quad (3.6.9)$$

Here, Ω_0 and $\boldsymbol{\tau}_c$ are the grand canonical potential of the trial system G_0 and the CPA multiple scattering matrix, respectively. From the Peierls-Feynman inequality [93] it follows that the grand canonical potential in the distribution function (3.6.5) is approximated by an arbitrary trial grand canonical potential. This can be expanded as a sum of terms containing different orders of local-moment interaction. The first-order term is written as $\mathbf{h}_i^{(n)} \cdot \mathbf{e}_i$ [47], where $\mathbf{h}_i^{(n)}$ is the Weiss field

$$\mathbf{h}_i^{(n)} = \frac{3}{4\pi} \int_S \mathbf{e}_i \langle H^{(n)} \rangle_{e_i} d\mathbf{e}_i. \quad (3.6.10)$$

$\langle \dots \rangle_{e_i}$ notes the restricted statistical average with \mathbf{e}_i . The Weiss field at site i reads by comparing (3.6.10) with (3.6.9)

$$h_i(\kappa) = -\frac{3}{4\pi^2} \Im \int \int_S \mathbf{e}_i \cdot \mathbf{n} \ln \det \mathbf{D}(\mathbf{e}_i, \kappa, \varepsilon) d\varepsilon d\mathbf{e}_i. \quad (3.6.11)$$

\mathbf{D} is the aforementioned CPA defect matrix and \mathbf{e}_i the magnetization direction at site i in the effective medium. Since the defect matrix and, thus, the Weiss field are functions of κ ($T(\kappa) = \hbar(\kappa)/k_B \kappa$), the distribution width is governed by a fix-point method for the given temperature \tilde{T} .

The introduced magnetic temperature (in the Ising-type case by concentration mapping and in the Heisenberg case by a Gauss distribution on a unit sphere) affects various quantities $Q(T)$ of interests, e.g. the exchange splitting and the density of states (figure 3.6.3). To point out the qualitatively different interpretations of both methods, one can focus on the local and total density of states (DOS). Due to the exchange interaction in magnets, the DOS of different spin channels split up and electronic states near the Fermi energy become spin polarized (typically d -states; figure 3.6.3 a). However, a random set of magnetic moments $\{\mathbf{e}\}$ (paramagnetic state) populates the spin polarization uniformly, since both spin channels are scattered with equal probability in the consolidated s-d model. As a result, the exchange splitting vanishes (figure 3.6.3 b). In the Ising-type disordered local moment theory both moment orientations appear in an effective medium on each lattice site (figure 3.6.3 c) and result in equivalent scattering probabilities for spin-up and spin-down channels. The total as well as the local density of states will be the same. Moreover, the magnetization at site i is also zero, however, the moments of each orientation \uparrow, \downarrow ‘survive’ with reduced length. In the Heisenberg-type case, each site is ferromagnetically ordered, since reduction of the magnetic moment length due to longitudinal relaxations predicted in the Bloch equations [23] are not included. The net magnetization follows from a site average. Hence, the local density remains spin-polarized, but, in the total averaged DOS, the exchange splitting vanishes.

Not only the single electron behavior, but also the correlation between the electrons and, therefore, the exchange integral J will be influenced by the ‘local moment’ fluctuations. In the Ising-type binary alloy, the magnetic moment of an \uparrow -atom is along the z direction (\mathbf{e}_\uparrow)

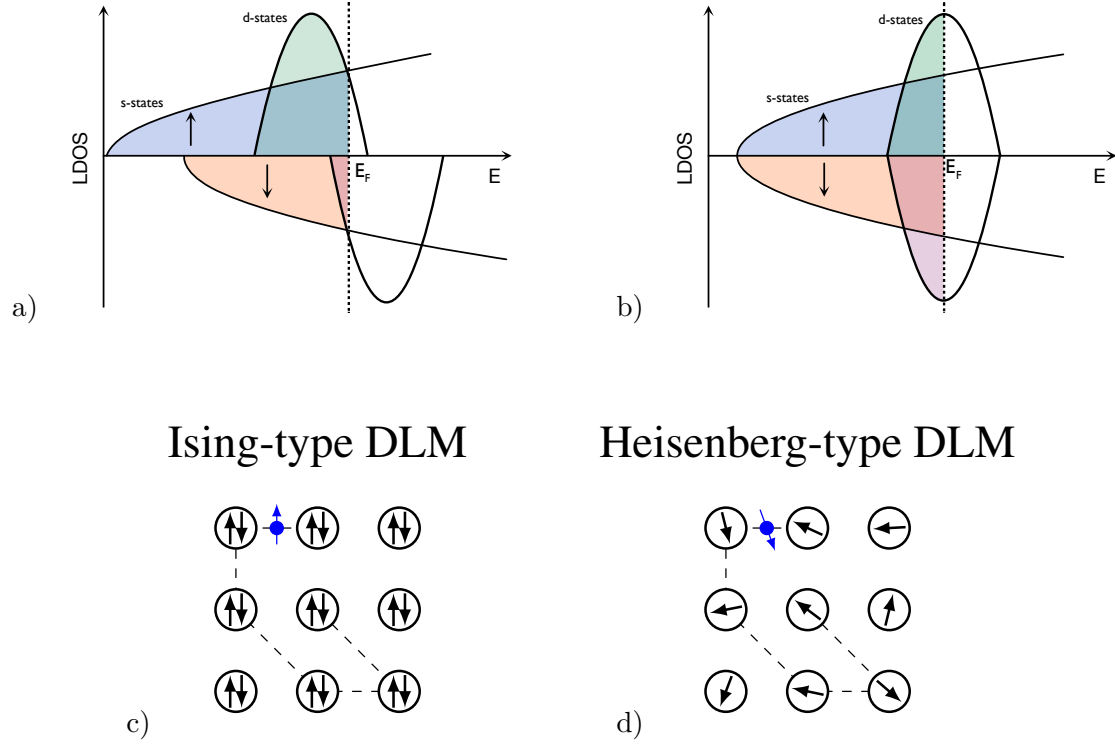


Figure 3.6.3.: Scheme of the local density of states in the disordered local moment theory a) in the ferromagnetic state and b) in the paramagnetic state (only for Ising type). Although the total density is equal to the local density of states due to the effective medium in the Ising-binary DLM, the total DOS in the Heisenberg-type DLM consists of an ensemble average of polarized local density of states; the exchange splitting in the total density vanishes. c) and d) illustrate the difference between both models: the electrons in the Ising model scatter on an effective potential containing opposite spin direction, whereas in the Heisenberg model the potential at site i is dominated only by one spin direction, but on site-average the magnetization is zero.

and that of an \downarrow -atom along the $-z$ direction ($\mathbf{e}_{\downarrow} = -\mathbf{e}_{\uparrow}$). This defines an effective exchange constant J^{eff}

$$J_{ij}^{\text{eff}} = \sum_{\mu, \nu = \uparrow, \downarrow} c_{\nu} c_{\mu} J_{i\nu, j\mu} \mathbf{e}_{\mu} \cdot \mathbf{e}_{\nu}. \quad (3.6.12)$$

The spin-dependent scattering processes $\tilde{\tau}_{i\nu, j\mu} = \mathbf{D}_{i\nu} \tau_{ij, c} \mathbf{D}_{j, \mu}$ in the Ising-binary alloy end up with

$$J_{i\nu, j\mu} = -\frac{1}{\pi} \int^{E_F} \Im \text{Tr} \Delta \mathbf{t}_{i\nu} \tilde{\tau}_{i\nu, j\mu} \Delta \mathbf{t}_{j\mu} \tilde{\tau}_{j\mu, i\nu} d\varepsilon, \quad (3.6.13)$$

in analogy to the Lichtenstein formula (section 3.3). In contrast to the scalar magnetic exchange in the one-dimensional spin case, the (relativistic) Heisenberg-type DLM calls for the matrix representation of the magnetic coupling (introduced in section 3.5),

$$\mathbf{I}_{ij}^{\text{eff}} = \int_{\mathcal{S}} \int_{\mathcal{S}} \mathbf{e}_i \mathbf{l}(\mathbf{e}_i, \mathbf{e}_j) \mathbf{e}_j d\mathbf{e}_i d\mathbf{e}_j. \quad (3.6.14)$$

Here,

$$\frac{\partial^2 E}{\partial \varphi_i \partial \varphi_j}(\mathbf{e}_i, \mathbf{e}_j, \mathbf{e}_0) = -\frac{1}{\pi} \Im \int \text{Tr} \left[\tilde{\boldsymbol{\tau}}_{ji} \boldsymbol{\Delta}_i^\varphi(\mathbf{e}_i, \mathbf{e}_0) \tilde{\boldsymbol{\tau}}_{ij} \boldsymbol{\Delta}_j^\varphi(\mathbf{e}_j, \mathbf{e}_0) \right] d\varepsilon, \quad (3.6.15)$$

$$\frac{\partial^2 E}{\partial \varphi_i \partial \vartheta_j}(\mathbf{e}_i, \mathbf{e}_j, \mathbf{e}_0) = -\frac{1}{\pi} \Im \int \text{Tr} \left[\tilde{\boldsymbol{\tau}}_{ji} \boldsymbol{\Delta}_i^\varphi(\mathbf{e}_i, \mathbf{e}_0) \tilde{\boldsymbol{\tau}}_{ij} \boldsymbol{\Delta}_j^\vartheta(\mathbf{e}_j, \mathbf{e}_0) \right] d\varepsilon, \quad (3.6.16)$$

$$\frac{\partial^2 E}{\partial \vartheta_i \partial \vartheta_j}(\mathbf{e}_i, \mathbf{e}_j, \mathbf{e}_0) = -\frac{1}{\pi} \Im \int \text{Tr} \left[\tilde{\boldsymbol{\tau}}_{ji} \boldsymbol{\Delta}_i^\vartheta(\mathbf{e}_i, \mathbf{e}_0) \tilde{\boldsymbol{\tau}}_{ij} \boldsymbol{\Delta}_j^\vartheta(\mathbf{e}_j, \mathbf{e}_0) \right] d\varepsilon, \quad (3.6.17)$$

where $\tilde{\boldsymbol{\tau}}_{i,j} = \mathbf{D}_i(\mathbf{e}_j) \boldsymbol{\tau}_{ij,c} \mathbf{D}_j(\mathbf{e}_j)$ is the scattering path of the perturbed system and

$$\begin{aligned} \hat{\Delta}_i^\nu(\mathbf{e}_i, \mathbf{e}_0) &= \left(\frac{d\mathbf{R}}{d\nu_i} \Big|_{\mathbf{e}_0} \right) \hat{t}_i^{-1}(\mathbf{e}^0) \mathbf{R}^\dagger(\mathbf{e}_i, \mathbf{e}^0) \\ &+ \mathbf{R}(\mathbf{e}_i, \mathbf{e}^0) \hat{t}_i^{-1}(\mathbf{e}^0) \left(\frac{d\mathbf{R}}{d\nu_i} \Big|_{\mathbf{e}_0} \right)^\dagger \end{aligned} \quad (3.6.18)$$

is the angle derivative of equation (3.2.19) with the reference magnetization \mathbf{e}_0 .

Both disordered local moment models can be applied to calculate the spin temperature dependence of other quantities of interest. For instance Buruzs et al. [47] deal with the layer-resolved uniaxial anisotropy K in Co thin films on Cu(001) and found a reduction of $|K|$ with the temperature. In particular, some layers exhibit a rotation of the easy axis from an in-plane to an out-of-plane direction. Moreover, he looked at the spin-disorder in electric resistivity by means of disordered local moment theory and discovered an increase of the resistivity with temperature, which becomes significant for magnetic nanocontacts [9], especially for a domain wall in such contacts. Applications of the DLM model in magnetization dynamics, e.g, can improve theoretical predictions of the magnon lifetimes. Hence, it has been argued that this model should be suitable for every ground state study of magnetic materials at finite temperatures.

In contrast to Buruzs et al. [47], my studies related to the question on the spin-temperature dependence of the density of states, the exchange splitting and the magnetic exchange parameters J , especially near the magnetic phase transition. Hereby, this model should clarified the influence of the spin to the electron reservoir. In a first step, an Ising-type disordered local moment picture was applied to bulk Stoner magnets [35]. In accordance to the dissipation-fluctuation theorem, I observed an increase of the exchange coupling with the temperature and, thus, an improvement of the critical exponents in the Monte Carlo simulation. However, the disadvantage in the Ising-type DLM model is the mapping to the Monte Carlo method. Since the MC method did not reproduce the magnetization behavior at surfaces quite well, a layer and surface resolved phase transition behavior was not obtainable. Hence, I developed the Heisenberg-type disordered local moment model for exchange parameters \mathbf{l}_{ij} in the fully-relativistic KKR code *omni*. Due to the mean-field picture, however, this model allowed only simulating spin temperature around $T_s = 0$ K. For instance several monolayer (1-6 ML) Fe on Cu(001) exhibits antiferromagnetic or ferromagnetic coupling between the layers, depending on the film thickness. I found (not shown in this thesis) that in the critical case of 3 ML Fe on Cu(001) a transition between different layer-resolved spin configurations can appear at a certain temperature. In according to the reduced lattice degrees of freedom at the surface, the top-most layer couples stronger to the thermal bath than the other layers.

3.7 Gilbert damping tensor

Designing magnetic devices requires a detailed characterization of dynamical magnetic properties. One distinct property is the magnetic relaxation time, that is mostly affected by the magnetic damping in the equation of motion (2.2.11). So far, in almost all dynamic simulations the Gilbert damping α is assumed as a phenomenological parameter [13, 15, 83]. Observing damping from first principles appears still to be an unresolved puzzle in magnetization dynamics simulations. Experimentally, α is measurable from the width of the ferromagnetic-resonance peak (FMR) (section 2.2). The width of the resonance peak is usually caused by intrinsic and extrinsic relaxation effects. The sample defects or impurities cause spatially fluctuating magnetic properties and control the extrinsic damping mechanism. The intrinsic damping, however, is the damping of the system itself and is focused on the following. In metallic ferromagnets, highlighted in this thesis, the damping is often caused by electron-magnon and electron-phonon scattering and can be influenced by eddy currents¹ [63], interface/surface relaxations or spin-flip scattering processes (Elliot-Yafet type) [94, 286]. The latter is used e.g. to tune spin-pumping mechanisms. There exist two approaches — the torque-torque correlation model [77] and the Fermi-surface breathing model — to study Gilbert damping α [145, 165]; these will be introduced in the following.

Torque-Torque correlation model The classical equation of motion for normalized atomic magnetic moments $\mathbf{e} = \mathbf{m}/m_s$ (LLG) can be generalized by Gilbert's *ansatz* of a damping tensor [109]:

$$\frac{d\mathbf{e}}{dt} = \mathbf{e} \times \left(-\gamma \mathbf{B} + \boldsymbol{\alpha} \frac{d\mathbf{e}}{dt} \right). \quad (3.7.1)$$

The precession around and the damping towards the effective field \mathbf{B} implicate a perturbation of the magnetic energy $E_{\text{mag}} = \mathbf{B} \cdot \mathbf{e}$ [245]:

$$\frac{dE_{\text{mag}}}{dt} = - \left[\boldsymbol{\alpha} \frac{d\mathbf{e}}{dt} \right] \cdot \mathbf{e} \times \mathbf{B} = \frac{1}{\gamma} \frac{d\mathbf{e}}{dt} \cdot \left[\boldsymbol{\alpha} \frac{d\mathbf{e}}{dt} \right], \quad (3.7.2)$$

where the field \mathbf{B} is assumed constant in time (adiabatic limit). The loss of angular momentum and energy (dissipation) is determined by [78, 185] $dE_{\text{dis}}/dt = \langle d\hat{H}/dt \rangle$. Due to the spin-orbit coupling, the many-body Hamilton operator \hat{H} does not commute with the spin operator, since \hat{H} depends on the magnetic moment $\hat{H}(t) = \hat{H}(\mathbf{e}(t))$. Lets assume an equilibrium state with the magnetization \mathbf{e}_0 . The evolution out of equilibrium is represented by $\mathbf{e}(t) = \mathbf{e}_0 + \mathbf{u}(t)$. Supposing $\mathbf{u}(t)$ is small, the many-body Hamiltonian

$$\hat{H}(t) = \hat{H}(\mathbf{e}_0) + \mathbf{u}(t) \cdot \left. \frac{\partial \hat{H}}{\partial \mathbf{u}} \right|_{\mathbf{e}_0} + \mathcal{O}(\mathbf{u}^2) \quad (3.7.3)$$

within the linear response formalism [46, 164] yields

$$\frac{dE_{\text{dis}}}{dt} = -\pi\hbar \sum_{\mu\nu} \sum_{ij} \frac{du^\mu}{dt} \frac{du^\nu}{dt} \left\langle \psi_i \left| \frac{\partial \hat{H}}{\partial u^\mu} \right| \psi_j \right\rangle \left\langle \psi_j \left| \frac{\partial \hat{H}}{\partial u^\nu} \right| \psi_i \right\rangle \delta(\epsilon_F - \epsilon_i) \delta(\epsilon_F - \epsilon_j). \quad (3.7.4)$$

¹<http://www.physlink.com/education/askexperts/ae527.cfm>

If the dissipation is solely within the magnetic subsystem, then $E_{\text{mag}} = E_{\text{dis}}$. Contrasting the linear-response formula (3.7.4) with magnetic energy modulation (3.7.2) yields the Gilbert damping tensor

$$\alpha^{\mu\nu} = -\frac{\hbar\gamma}{\pi m_s} \text{Tr} \left(\frac{\partial \hat{H}}{\partial u^\mu} \Im G(\epsilon_F^+) \frac{\partial \hat{H}}{\partial u^\nu} \Im G(\epsilon_F^+) \right). \quad (3.7.5)$$

$\mu, \nu = x, y, z$ are the tensor components. $\boldsymbol{\alpha}$ is thus given by a torque-torque correlation function if

$$T^\mu \equiv \frac{\partial \hat{H}}{\partial u^\mu} \quad (3.7.6)$$

is identified as the magnetic torque. Here, the Kubo-Greenwood equation for the damping is similar to that for the electrical conductivity $\sigma^{\mu\nu}$ [49]:

$$\sigma^{\mu\nu} = -\frac{\hbar\gamma}{\pi V} \text{Tr} \left(\hat{j}^\mu \Im G(\epsilon_F^+) \hat{j}^\nu \Im G(\epsilon_F^+) \right), \quad (3.7.7)$$

where \hat{j} is the current operator [30]. The Kubo-Greenwood formalism, however, gives no assumptions to the time scale on which the magnetic moments fluctuate. Thus, it fails dealing with ultrafast magnetization dynamics (adiabatic theory).

The side limit of the KKR Green function maybe expressed in matrix notation (3.2.12). Since the single-site part is real in this choice of boundary conditions, it does not contribute to the damping. Inserting the Green function expression (3.2.12) into (3.7.5), the damping tensor reads

$$\alpha_{nm}^{\mu\nu} = -\frac{\hbar\gamma}{\pi m_s} \text{Tr} \left[\mathbf{T}_n^\mu (\Im \boldsymbol{\tau}_{nm}) \mathbf{T}_m^\nu (\Im \boldsymbol{\tau}_{mn}) \right], \quad (3.7.8)$$

evaluated at E_F^+ . The torque matrices are then given by

$$T_n^{LL'\mu} = \int \left(\mathcal{R}_n^L \right)^\dagger T^\mu \mathcal{R}_n^L d\mathbf{r}. = \int \left(\mathcal{R}_n^L \right)^\dagger [\beta \sigma^\mu B(\mathbf{r})] \mathcal{R}_n^{L'} d\mathbf{r}. \quad (3.7.9)$$

\mathcal{R} is the regular solution of the Dirac-Kohn-Sham equation (see section 3.2). Here, only the Zeeman term depends on the change of the magnetic moment. The Gilbert equation is related to the action of the magnetization on the electronic system and, thus, driven by the spin-orbit coupling included in the Dirac equation (3.2.15). In the rigid-spin approximation [150] (no longitudinal magnetization fluctuations), a modification of the potential at site n is given by rotating the magnetization with respect to the equilibrium direction \mathbf{e}_0 . The single-site scattering matrix $t_n^{LL'}(\mathbf{e})$, which depends on the new magnetic orientation \mathbf{e} via the unitary transformation (3.2.19) and which is associated to the potential $V(\mathbf{e})$, can be finally derived as

$$\Delta \mathbf{t}_n = \mathbf{t}_n(\mathbf{e}) - \mathbf{t}_n(\mathbf{e}_0) = \sum_\mu \mathbf{T}_n^\mu u_\mu \quad \text{and} \quad \frac{d\mathbf{t}_n}{d\mu} = \mathbf{T}_n^\mu. \quad (3.7.10)$$

Definition (3.7.8) illustrates the non-local and anisotropic character of the energy transfer.

Ebert et al. [77] determine furthermore the phonon temperature by displacing an atom n about the value \mathbf{s}_ν^n and applying a transformation matrix $U_{LL'}^n(\mathbf{s}_\nu, \varepsilon)$ to the equilibrium KKR single-site t-matrix t_0 . The thermal root mean square displacement is approximated

by the Drude model. These lattice vibrations are discussed as the major contribution to the damping α and without calculating the electron-phonon self-energy. In principle, the spin and electron temperatures can also be added using the disordered local moment theory and Fermi-Dirac statistics, respectively.

To obtain a fully *ab-initio* magnetization dynamics study, I develop an add-on for the fully-relativistic KKR code *omni*. Here, the calculated damping constants (not shown in this thesis) are in accordance with the extrapolated one from Ebert et al. [78] for bulk Stoner magnets. Since Ebert et al. study bulk damping, my analysis is related rather to magnetic surfaces and nanostructures (not shown in this thesis) without the effect of phonon-temperature. Applications on surfaces, especially for those with high spin-orbit coupling, predict high damping e.g. in the size of $\alpha \approx 0.5$ for 1ML Fe on Pt(111). Applications on nanoparticles will be future work.

Breathing Fermi-surface model Beside the Kubo-Greenwood *ansatz* for itinerant damping α [78], there exists another model introduced by Kamberský et al. [145, 146, 165], which takes into account the shape of the Fermi surface. Most of the properties in metals (electrical, optical or magnetic) are influenced by the form of the Fermi surface: e.g. the electric current depends on the occupation number variation of states near the Fermi edge [7]. The Kamberský model is based on an effective single-electron theory. It models the transfer of energy and angular momentum from the electrons to the nuclei via electron scattering processes due to spin-orbit coupling. Consequently, the energies of the Bloch states $\varepsilon_{\mathbf{k},n}$, characterized by the band index n and the wave vector \mathbf{k} , depend also on the direction of the magnetic moment $\mathbf{e} = m/m_s$. Small variations in $\mathbf{e} \rightarrow \mathbf{e}' = \mathbf{e} + \delta\mathbf{e}$ affect the shape of the Fermi surface (the surface ‘breathing’, figure 3.7.1) as well as the population number of states near the Fermi level.

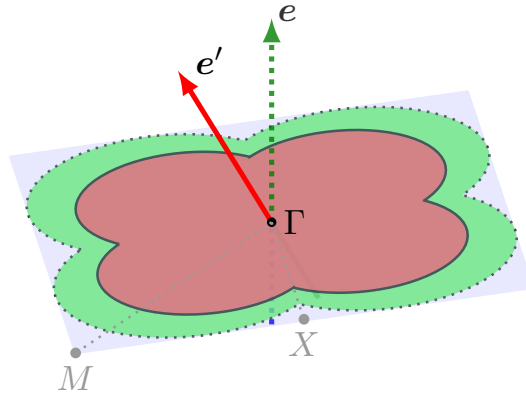


Figure 3.7.1.: Principle scheme of the breathing Fermi-surface model: Due to the spin-orbit coupling, the rotation of the magnetic moment $\mathbf{e} \rightarrow \mathbf{e}'$ (green and red arrow) manipulates the occupation statistics in the Brillouin zone (light blue plane), which runs out-of-equilibrium. The Fermi-surface shape changes (green and red plane).

The equilibration back into the ground state is influenced by the relaxation time $\tau_{\mathbf{k},n}$ (relaxation time approximation) [7], indicating how fast the electron population relaxes into the ground state. The model holds only if the magnetization dynamics is slow enough, so that the electron system is at any instant in its ground state with respect to the momentary

magnetic configuration (adiabatic approximation). Within this ‘sliding window’, there exists only precession without damping in the equation of motion. Moreover, the relaxation time approach is phenomenologically introduced, since there is no model to identify the detailed microscopic mechanisms of energy and angular momentum transfer. This back-transitions appear typically close to the Fermi level E_F and depend strongly on the scattering of the electrons at impurities or lattice vibrations. The damping of the magnetic precession then results from the phase lag between the change of \mathbf{e} and the electron population response, known as Clogston valence-exchange mechanism [59].

Damping contributes as an additional field in the Landau-Lifshitz-Gilbert equation, characterized by the derivation of the total energy E with respect to the variation of the magnetization $\delta \mathbf{e}$

$$\mathbf{B}^{diss} = -m_s^{-1} \frac{\partial E}{\partial \delta \mathbf{e}} = -\frac{1}{m_s \Omega} \sum_{\mathbf{k}, n} \frac{\partial \varepsilon_{\mathbf{k}, n}}{\partial \delta \mathbf{e}} \eta_{\mathbf{k}, n}, \quad (3.7.11)$$

where $\eta_{\mathbf{k}, n}$ is the population number. The evolution $d\eta_{\mathbf{k}, n}/dt = -1/\tau_{\mathbf{k}, n} (\eta_{\mathbf{k}, n} - f_{\mathbf{k}, n})$ [165]—from the out-of-equilibrium population back into the ground state—simplifies using Taylor expansion to: $\eta_{\mathbf{k}, n} = f_{\mathbf{k}, n} - \tau_{\mathbf{k}, n} df_{\mathbf{k}, n}/dt$. Here, $f_{\mathbf{k}, n} = f(\varepsilon_{\mathbf{k}, n})$ is the Fermi function. $\tau_{\mathbf{k}, n}$ is the lifetime of the state $|\mathbf{k}, n\rangle$ and includes the whole scattering processes information of the states $|\mathbf{k}, n\rangle$, where different n will result in different relaxation times. This *ansatz*, however, is valid only for intraband but not for interband scattering processes. When comparing the dissipation field \mathbf{B}^{diss} with the LLG equation (see section 2.2) in the adiabatic limit, the Gilbert damping tensor reads [145, 165]

$$\alpha^{\nu\mu} = \frac{g\pi}{m_s} \frac{1}{(2\pi)^3} \sum_n \int \frac{\partial f_{\mathbf{k}, n}}{\partial \varepsilon_{\mathbf{k}, n}} \frac{\partial \varepsilon_{\mathbf{k}, n}}{\partial \delta e_\nu} \frac{\partial \varepsilon_{\mathbf{k}, n}}{\partial \delta e_\mu} \frac{\tau_{\mathbf{k}, n}}{\hbar} d\mathbf{k}, \quad (3.7.12)$$

where a uniform relaxation time $\tau_{\mathbf{k}, n} \rightarrow \tau$ is used. Towards Gilbert’s general assumption [109] (see section 2.2), the damping parameter is a tensor [86, 254], where $\nu, \mu = x, y, z$, and increases with decreasing scattering frequency τ^{-1} . The latter can be approximated by the Drude model for itinerant electrons and claims a T^2 temperature behavior for the electron-electron interaction and a T temperature behavior for the electron-phonon interaction. The relaxation time τ depends on the mean free path of the electrons in the electromagnetic skin depth. So the model does not consider anomalous skin effect conditions.

Here, the spin-orbit coupling is the only contribution that forces the ‘breathing’ of the Fermi surface. Thus, Gilmore et al. [110] show

$$\alpha^{\mu\nu} = \frac{g\pi}{m_s} \frac{1}{(2\pi)^3} \sum_{n, m} \int \Gamma_{nm}^\mu(k) \Gamma_{nm}^\nu(k) W_{nm}(\mathbf{k}) d\mathbf{k}, \quad (3.7.13)$$

which corresponds to Fermi’s golden rule. The matrix element $\Gamma_{nm}(l) = \langle n, \mathbf{k} | \hat{\mathbf{T}} | m, \mathbf{k} \rangle$ of the torque operator $\hat{\mathbf{T}} = [\boldsymbol{\sigma}, \hat{H}_{so}]$ quantifies transitions between states in band n and m induced by the spin-orbit torque, where $\boldsymbol{\sigma}$ are the Pauli matrices and $|\mathbf{k}, n\rangle$ are eigenstates of the many-body electron Hamiltonian \hat{H} . The transitions can have an intra- and inter-band character (figure 3.7.2), where, however, the first account for the major contribution. These ‘hoppings’ of the electrons are weighted by the spectral overlap $W_{nm}(\mathbf{k}) = \int \eta(\varepsilon) A_{\mathbf{k}, n}(\varepsilon, \Gamma) A_{\mathbf{k}, m}(\varepsilon, \Gamma) d\varepsilon$. The spectral functions $A_{\mathbf{k}, n}$ are Lorentzians centered around the band energy $\varepsilon_{\mathbf{k}, n}$ and broadened by the scattering rate with lattice defects (electron-phonon coupling; width of the spectral function $\Gamma = \hbar/\tau$, where \hbar is the Planck constant):

larger scattering rates increase the transition rate. $\eta(\varepsilon)$ is the derivative of the Fermi-Dirac distribution with respect to the energy. In Gilmore's work [110], however, expression (3.7.13) regards only to an ordered magnetic state in reference direction \mathbf{e}_z . Since $\delta\mathbf{e}$ is always perpendicular to \mathbf{e} , the magnetization change has only x - and y -components and, thus, the tensor elements α_{xx} and α_{yy} are non-zero. Furthermore, Gilmore addresses the damping constant as the sum over the diagonal elements, since the off-diagonal ones are e.g. zero in cubic bulk systems. The full tensor, however, can be extracted by using different reference directions.

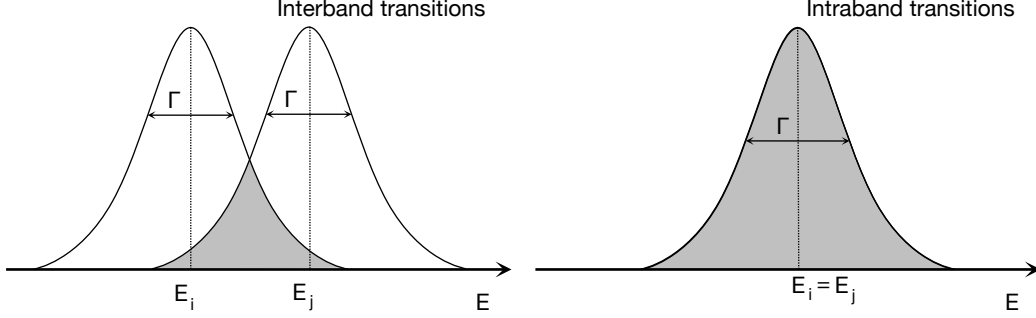


Figure 3.7.2.: Inter- and intra-band transition driven by the band broadening. The larger the overlap (gray shaded area) between the two Lorentzians, the larger is the transition probability. The width of the distribution is driven by the electron-phonon interaction.

The band broadening, represented by the Lorentzians, can be better approached by the Green function $\Im m G(\mathbf{k}, \varepsilon \pm i\Gamma) = \mp \sum_n |n\rangle \langle n| A_\Gamma(\varepsilon - \varepsilon_{\mathbf{k},n})$, since it broadens and shifts maxima in the spectral function, especially electronic states at energies close to the Fermi level. In the Green function approach, Γ is taken as the imaginary part of the energy, at which the Green function is evaluated. This offset from the real energy axis provides a more accurate description with respect to the *ab initio* results [110] than the Lorentzian approach. In addition, the Green function technique allows observing disorder based on the CPA (section 3.6). Consequently, the Kamberský formula is directly proportional to the torque-torque correlation model of Ebert et al. [78]

$$\alpha^{\mu\nu} = \frac{g}{\pi m_s} \frac{1}{(2\pi)^3} \int \int \eta(\varepsilon) \hat{T}^\mu \Im m G(\varepsilon \pm i\Gamma, \mathbf{k}) \hat{T}^{\nu\dagger} \Im m G(\varepsilon \pm i\Gamma, \mathbf{k}) d\varepsilon d\mathbf{k}. \quad (3.7.14)$$

In contrast to the computational heavy KKR Green function method by Ebert et al. [78], this can be numerically evaluate by a tight-binding method, where the Slater-Koster parameter can be obtained by fitting DFT band structures. This allows a simplified modeling of the damping tensor at the surface. Here, a layer-resolved real-space representation is achievable via renormalization techniques in the tight-binding model, introduced by Henk et al. [26, 129, 179], and the Fourier transformed Green function, that accounts for the Bloch phase factor. Defining a double index $I = (i, n)$ for a atom in layer n at site i represents the Gilbert damping in real-space

$$\alpha_{I,J}^{\mu\nu} = \frac{g}{\pi m_s} \int \eta(\varepsilon) \hat{T}_n^\mu \Im m G_{IJ}(\varepsilon + i\Gamma) \hat{T}_m^{\nu\dagger} \Im m G_{JI}(\varepsilon + i\Gamma) d\varepsilon \text{ where } I \neq J. \quad (3.7.15)$$

Similar to the correlation equation for the magnetic exchange (Lichtenstein formula), only off-site terms occur in the equation (3.7.15), motivating the energy dissipation α as a non-local quantity. In contrast to the Kubo-Greenwood equation, the Kamberský model considers also the electron temperature via the Fermi statistics. However Fähnle et al. [86, 254]

show the incompleteness of this model: they predict a strong dependence due to non-collinear spin structure, which comes from an additional exchange interaction term in the Hamiltonian and results in a site-resolved, magnetic moment dependent character $\alpha_{r,r'}(\{\mathbf{e}\})$. The Kamberský model, however, implies the dependence of α on magnetic moment through the torque operator $\hat{\mathbf{T}}(\mathbf{e})$. “This means that at least for systems, for which the degree of relative canting of magnetic moments is different for different parts of the system (e.g., very high in the core of a magnetic vortex and much smaller outside), it does not make sense to use just one damping matrix” (Fähnle [86]). They also point out that for nanostructures like atomic monolayers or islands, the damping is zero for some orientations of magnetic moment \mathbf{e} .

Kamberský’s non-local damping model [38, 272] transfers the equation of motion into space retarded dynamics as it was proposed by Bose [31]

$$\frac{d\mathbf{m}}{dt} = \mathbf{m} \times \left(-\gamma \mathbf{B} + \frac{1}{m_s} \sum_{ij} \alpha_{ij}[\mathbf{m}, T_s, T_e, T_l] \frac{d\mathbf{m}_j}{dt} \right), \quad (3.7.16)$$

where the damping part is, in addition, a function of the electron, spin and phonon temperature, clarifying once more the strong correlation between the reservoirs on ultra short scale. The retardation in space still occurs, when the magnetic system is in a non-coherent state, like in nutation or in systems with strong spin-orbit coupling, that forces also anisotropic angular momentum transfer (Dzyaloshinskii-Moriya interaction).

A second access to obtain the Gilbert damping constant is provided by the Kamberský model, which I implemented in the framework of tight-binding model. Compared to the KKR method, this has the advantage of computational efficient calculations with simplified model extensions. Here, the main focus lay on the correlation of the Gilbert damping to the various microscopic reservoirs as well as on the layer-resolved non-locality of the damping, predicting energy transfer to neighboring sites [266]. I applied this model to the Stoner magnets, just to compare with already existing theoretical and experimental values.

Selected Results

As the present work is a cumulative thesis, selected results will be covered below. A common aspect of the present work is to extend the atomistic magnetization dynamic simulations so that, first, the model is fully *ab initio*, second, it includes a deeper understanding of the correlation between the electron, the magnetic and the phonon system as well as the role of symmetry and, third, it covers physical effects on a femtosecond time- and nanometer lengthscale. Therefore, each hereinafter publications focus on selected parts of the extended model of dynamics and ground state properties.

In particular, they highlight a better description of the Curie temperature, when the temperature dependence of the exchange coupling constants is taken into account (► 1, in section 4.1). For this purpose, the model of disordered local moment is applied to bulk Stoner magnets.

The next publication (► 2, in section 4.2) deals with ultrathin magnetic films with strong spin-orbit coupling. It examines the non-collinear structure in Fe/Pt(111), which resolves a discrepancy between experiment and theory.

The role of Gilbert damping in bulk and various surface states of Stoner magnets is present in the next publication (► 3, in section 4.3). The applied model reveals strong dependences on the three thermal reservoirs, the surface normal and the electron-phonon coupling. More precisely, spatial retardation originates from a non-local character of the damping. The results support Fähnle's claims of anisotropic and non-local damping and give good agreement with experiment.

The question about magnetic mass and its impact in the dynamics, will be answered in the last publication (► 4, in section 4.4) about magnetic nutation. The extended Landau-Lifshitz-Gilbert equation predicts nutation on the timescale of the magnetic interaction formation (femtosecond timescale).

- ▶ 1 Böttcher, D. and Henk, J.: *Temperature-dependent Heisenberg exchange coupling constants from linking electronic-structure calculations and Monte Carlo simulations*, Journal of Magnetism and Magnetic Materials **324**, (4),pp 610-615 (2012)
- ▶ 2 Böttcher, D., Ernst, A. and Henk, J.: *Non-collinear magnetism in ultrathin films with strong spin-orbit coupling from ab initio first principles*, Journal of Nanoscience and Nanotechnology **12**, (9),pp 7516-7519 (2012)
- ▶ 3 Thonig, D. and Henk, J.: *Gilbert damping tensor within the breathing Fermi surface model: anisotropy and non-locality*, New Journal of Physics **16**, (1),pp 013032/1-14 (2014)
- ▶ 4 Böttcher, D. and Henk, J.: *Significance of nutation in magnetization dynamics of nanostructures*, Physical Review B **86**, (2),pp 020404(R)/1-4 (2012)

In front of each article a short introduction to the topic and a brief summary of the main results are presented.

Nevertheless, a brief overview over the other important publications should also be covered. In a first study, the magnetization dynamics of Co nanoislands on Cu(111) is investigated on the atomic scale by means of the Landau-Lifshitz-Gilbert equation. The exchange and anisotropy constants of the spin Hamiltonian are computed from first principles. I focused on hysteresis loops and magnetic switching in dependence on temperature, island size, and strength of an external magnetic field. The magnetic switching of nanoislands whose magnetization is reversed on the sub-nanosecond time scale is found consistent with the Stoner-Wohlfarth theory. I separate the superparamagnetic from the ferromagnetic regime and provide evidence that nanodomains can exist at least on a sub-picosecond time scale. Since the results of this paper are mostly from my diploma thesis, I would refer to [32, 33].

Next, I was interested in the control of the critical temperature T_C of ferromagnetic $\text{La}_x\text{Sr}_{1-x}\text{MnO}_3$ (LSMO) by distorting the crystal structure, as was reported by Thiele et al (2007 Phys. Rev. B 75 054408). To confirm these findings theoretically, I investigate the electronic as well as the magnetic ground state properties of $\text{La}_{2/3}\text{Sr}_{1/3}\text{MnO}_3$ as a function of tetragonal lattice distortions, using a multiple-scattering Green function method. Within this approach, I calculate exchange coupling constants as well as the phase transition temperature from first principles. Comparing my findings with those for $\text{La}_{2/3}\text{Sr}_{1/3}\text{CoO}_3$ (LSCO), I find that the decrease of T_C is much stronger in LSMO than in LSCO. My findings can be explained by the electronic structures and are also in accordance with the experiment. The computed decrease of T_C with distortion is smaller than observed experimentally, a result that corroborates the importance of phonon contributions.

However, due to the extensive subject of oxidic material and its required theoretical basics, I did not attached the related publication to this thesis. For more details I recommend my publication [36].

In another numerical study [267], I reported on a theoretical investigation of artificial spin-ice dipolar arrays, using a geometry adopted from recent experiments [A. Farhan et al., Nature Phys. 9 (2013) 375]. The number of thermal magnetic string excitations in the square lattice is drastically increased by a vertical displacement of rows and columns. I find large increments especially for low temperatures and for string excitations with quasi-monopoles of charges ± 4 . By kinetic Monte Carlo simulations I address the thermal stability of such excitations, thereby providing time scales for their experimental observation. For more details I would like to refer to [267].

Even more magnetic materials and magnetic effects were investigated, which are presented in a concept map (appendix C). The different topics were studied using my own developed computer code, called *CaHmd* (classical atomistic Heisenberg magnetization dynamics)¹. Here, e.g. the atomistic Landau-Lifshitz-Gilbert equation, the Landau-Lifshitz-Miyazaki-Seki equation, the Landau-Lifshitz-Bloch equation, as well as a Monte Carlo method and a kinetic Monte-Carlo method were implemented. The code is able to consider the spin-transfer torque as well as to solve the three-temperature model. An extension with a tight-binding method allows a computational efficient calculation of important magnetic parameters, such as the Gilbert damping tensor. Here, the tight-binding parameters were fitted using a genetic algorithm. Thus, my simulation package opens a broad ‘window’ into simulating nanomagnets.

¹The computer code *CaHmd* is available via writing a mail to danny.thonig@gmail.com

4.1 Magnetic systems at elevated temperatures by non-relativistic disordered local moment theory

The phase transition is determined by the interaction strength J between two magnetic moments. With the Lichtenstein formula at hand, a theoretical prediction of exchange parameter sets $\{J_{ij}\}$ is available. In particular, this multiple-scattering expression is derived assuming an ordered magnetic state. However, the magnetic order will transfer into a high-symmetry state (paramagnetic state), if the temperature is increased. The sharp transition at T_C dedicated by exchange sets for the ordered magnetic state, however, often underestimates T_C as compared to the experiment. In order to overcome this problem, the disordered local moment theory provides a method for describing the paramagnetic state and offering enhanced effective Heisenberg exchange parameters in the disordered configuration. This indicates a strong correlation between the magnetism and the electron ground state as well as the temperature dependence of J .

The paper proposes a new method based on the disordered local moment theory that reveals the temperature-dependent coupling constants $J_{ij}(T)$ for the range $T \in [0, T_C]$. First-principles calculations for Ising-type binary alloy were performed, where in a magnetically ordered host, e.g. in z direction, impurities of concentration $c_{\downarrow} = 1 - c_{\uparrow}$ with the opposite moment direction, say in $-z$, were embedded. More precise, $c_{\downarrow} = 0$ relates to the ferromagnetic and $c_{\downarrow} = 0.5$ to the paramagnetic state. Let us assume the first-principles average magnetization $M(c)$ for a given concentration is equal to the average magnetization $M^{\text{MC}}(c, T)$ for a given c and T in Monte Carlo calculations, a mapping of concentration versus temperature $c(T)$ was obtained, and thus, temperature-dependent Heisenberg exchange parameters $J_{ij}(T)$.

The method was applied to typical Stoner magnets like Fe and Co, where a zero average magnetization was observed in the paramagnetic state, but the individual magnetic moments m_{\downarrow} and m_{\uparrow} stay finite. Furthermore, the exchange interactions for the subsystem $J_{i\mu, j\nu}$, where $\mu, \nu \in \{\uparrow, \downarrow\}$, decrease for the ordered states $\uparrow\uparrow$ and $\downarrow\downarrow$, but increases for the disordered states $\uparrow\downarrow$ and $\downarrow\uparrow$. Thus, the effective J^{eff} , defined by the weighted sum over all subsystems, increases with temperature. Considering both magnetic moment and exchange coupling in Monte Carlo simulations improves critical exponents by about 10% and pushes the phase transition temperature towards the experimental value.

The refined exchange parameters J_{ij} should be considered in many applications, e.g. describing demagnetization effects within the Landau-Lifshitz-Gilbert equation. The $c(T)$ mapping is also adaptive for characterizing the temperature dependence of other quantities of interest, such as the magnetocrystalline anisotropy, the Dzyaloshinskii-Moriya interaction, the magnetic Gilbert damping or the density of states. Both the reduced spin dimension and the mapping to statistical methods like Monte Carlo are limiting factors of the Ising-type model. Using Heisenberg-type DLM, these limitations are eliminated, which allows the determination of temperature- and layer-resolved magnetic properties, which was studied for Stoner magnets and 1-6 ML Fe on Cu(001) (not shown in this thesis). But, the Weiss field (mean field) approach permits studies only in the temperature range around $T = 0$ K.



Temperature-dependent Heisenberg exchange coupling constants from linking electronic-structure calculations and Monte Carlo simulations

D. Böttcher^{a,b}, A. Ernst^a, J. Henk^{a,*}

^a Max-Planck-Institut für Mikrostrukturphysik, Weinberg 2, D-06120 Halle (Saale), Germany

^b Institut für Physik, Martin-Luther-Universität Halle-Wittenberg, Von-Seckendorff-Platz 1, D-06120 Halle (Saale), Germany

ARTICLE INFO

Article history:

Received 12 July 2011

Received in revised form

19 August 2011

Available online 8 September 2011

Keywords:

Classical spin models

Exchange coupling

Numerical simulations

Electronic-structure calculations

ABSTRACT

We propose a method to calculate the temperature dependence of Heisenberg exchange coupling constants J_{ij} . Within the formalism of disordered local moments (DLM), the magnetization and the J_{ij} are computed from first principles for any concentration c of the magnetic constituents. The exchange coupling constants are then used in Monte Carlo (MC) simulations to compute the temperature dependence of the magnetization for the given c . By comparing the magnetization from DLM calculations and from MC simulations we obtain a mapping of temperature versus concentration and eventually temperature-dependent J_{ij} . The approach which is applied to bulk Fe and Co can for example improve critical exponents.

© 2011 Elsevier B.V. All rights reserved.

1. Motivation

The classical Heisenberg model is widely used to describe ground-state properties and phase transitions in magnetic systems. In particular critical temperatures T_c , critical exponents, and magnetization curves $\langle m \rangle(T)$ can be calculated. It is also part of atomistic magnetization dynamics simulations within the framework of the Landau–Lifshitz–Gilbert equation (e.g. Refs. [1,2]).

An exchange coupling constant J_{ij} in the classical Heisenberg model, whose Hamiltonian reads

$$H = - \sum_{ij} J_{ij} \hat{m}_i \cdot \hat{m}_j, \quad (1)$$

quantifies the energy change upon rotating the local magnetic moments (unit vectors) \hat{m}_i at site i and \hat{m}_j at site j . The J_{ij} are taken either as adjustable parameters or are computed from first principles.

First-principles electronic-structure calculations are usually performed for zero temperature. The set $\{J_{ij}\}$ of exchange coupling constants is obtained from the energy change of tilting local magnetic moments or from a Kubo–Greenwood-type expression of Green functions [3]. From these J_{ij} , critical temperatures can be calculated within the mean-field approximation or the random-phase approximation; or they are used in simulations, for example in Monte Carlo simulations. In any case, the J_{ij} are computed for $T = 0$ K but are taken to describe systems at finite temperatures.

In contrast to the preceding, the disordered local moment (DLM) picture [4–6] describes paramagnetic systems, that is at temperatures $T \geq T_c$. Within the DLM approach, nonzero local magnetic moments are maintained but the directions of these fluctuate so strongly that the average magnetization vanishes. In their simplest form, the thermal fluctuations are modeled by a substitutional Ising-type alloy whose constituents \uparrow and \downarrow are oppositely magnetized atoms (local moment orientations $\hat{m}_\uparrow = -\hat{m}_\downarrow$). At alloy concentration $c_\uparrow = 1 - c_\downarrow = 0.5$, that is at T_c , the two local moments cancel although m_\uparrow and m_\downarrow are nonzero; this in contrast to the Stoner model in which the magnetization vanishes everywhere in space at T_c (i.e. $m_\uparrow = m_\downarrow = 0$). In first-principles calculations, the DLM approach can be treated within the coherent potential approximation (CPA) [7] from which the set $\{J_{ij}\}$ can be computed as well.

With respect to the preceding, we are concerned with two different sets of exchange constants: $\{J_{ij}(0)\}$ and $\{J_{ij}(T_c)\}$. This suggests the problem whether one can obtain sets $\{J_{ij}(T)\}$ for every temperature between 0 K and T_c . Since in the CPA modeling of the DLM approach $c_\uparrow = 1$ would be equivalent to $T = 0$ K and $c_\uparrow = 0.5$ to $T = T_c$, the task is to map the entire concentration range [0.5, 1.0] onto the temperature range [0 K, T_c]. However, there is no direct relation $c_\uparrow \leftrightarrow T$ within the DLM approach itself; consequently the mapping $T(c_\uparrow)$ requires an additional ingredient which in this work is the classical Heisenberg model.

In this paper, we propose a simple way to obtain sets $\{J_{ij}(T)\}$ as follows. The exchange parameters are computed from first principles within the DLM approach at a concentration c_\uparrow . This set $\{J_{ij}(c_\uparrow)\}$ is then used in Monte Carlo (MC) simulations of the classical Heisenberg model at a temperature T . The requirement

* Corresponding author.

E-mail address: henk@mpi-halle.de (J. Henk).

that the average magnetization $\langle m \rangle(c_\uparrow)$ in the DLM calculations and $\langle m \rangle(T; c_\uparrow)$ in the MC simulations are equal yields the mapping $T(c_\uparrow)$. We apply this approach to bulk Fe and Co. Problems and improvements are discussed as well.

Before introducing the approach a few notes on other first-principles approaches to the temperature dependence of magnetism are in order. Pindor et al. [7] used the DLM formalism as well but the temperature dependence was restricted to the self-consistent electronic-structure calculation, in the spirit of the finite-temperature version of spin-density functional theory. The magnetic fluctuations were modeled by a paramagnetic Ising-type alloy (with concentration 50%, treated within the CPA). A two-step approach to the temperature dependence was introduced by Ruban et al. [8]. There, the exchange interaction constants were determined from constrained local spin-density approximation calculations and subsequently used in a model Hamiltonian to investigate finite-temperature magnetic properties. Drchal et al. investigated the joint effect of temperature and disorder on the interlayer exchange coupling [9]. There, the temperature entered the exchange coupling energy via the Fermi–Dirac distribution; magnetic fluctuations were not considered.

Using a relativistic DLM approach, Buruzs [10] studied temperature-dependent properties of thin films. This approach is computationally demanding because it involves both rotational averaging over the magnetic-moment directions and the computation of Weiss fields. Since each local Weiss field is aligned along the average magnetization, the magnetization curve is given by a Langevin function. Although not done in Ref. [10], this formalism allows to calculate the temperature dependencies of both Heisenberg exchange-coupling constants and Dzyaloshinskii–Moriya vectors. In the present approach which uses the computationally less demanding Ising-type averaging, the temperature-concentration mapping is lost but is reintroduced by comparison with Heisenberg Monte Carlo simulations. In the latter, the local Weiss fields are determined by the local magnetic moments within the finite range of exchange interactions. As a consequence, the magnetization curve is no longer a Langevin function and critical exponents can be improved.

The paper is organized as follows. Computational aspects of the proposed approach are given in Section 2. Its applications to Fe (3.1) and Co (3.2) are presented and discussed in Section 3. Conclusions and a brief outlook are given in Section 4.

2. Computational aspects

The Heisenberg exchange coupling constants J_{ij} of bulk bcc Fe and hcp Co are calculated from first principles using a scalar-relativistic multiple-scattering approach (KKR, Korringa–Kohn–Rostoker method [11]), with the exchange-correlation functional taken from Ref. [12].

For sites $i \neq j$, the exchange coupling constants are given by [3]

$$J_{ij} = \frac{1}{4\pi} \text{tr} \int^{E_F} \Delta t_i \tau_{ij}^\dagger \Delta t_j \tau_{ji}^\dagger dE, \quad (2)$$

with $\Delta t_i \equiv t_i^\uparrow - t_i^\downarrow$, t_i^σ and τ_{ij}^σ are the spin-resolved KKR single-site scattering matrices and the scattering-path matrices in spin-angular-momentum representation ($\sigma = \uparrow, \downarrow$) [11]. τ_{ij} describes the propagation of an electron from site j to site i . The energy integral runs up to the Fermi energy E_F .

The ferromagnet at temperature T is described as a substitutional binary alloy within the coherent potential approximation (CPA) [13–16]. Each site is occupied by an atom magnetized along the z direction (\uparrow) with concentration c_\uparrow and an atom magnetized along the $-z$ direction (\downarrow) with concentration $c_\downarrow = 1 - c_\uparrow$; local moment orientations are denoted by \uparrow and \downarrow while spin orientations are denoted by \uparrow and \downarrow . At $c_\uparrow = 1$ the sample is perfectly

magnetically ordered, which corresponds to $T = 0$ K. At $c_\uparrow = 0.5$ it is paramagnetic, which corresponds to $T = T_c$. Within the KKR-CPA approach used in this paper, short-range order is neglected.

The \uparrow and \downarrow atoms are created at site i in the effective CPA medium by defect matrices $D_{i\mu}$ ($\mu = \uparrow, \downarrow$) [11]. The effective CPA medium is described by scattering-path matrices τ_{ij}^{CPA} . More precisely, a defect of type μ at site i and a defect of type ν at site j are introduced by replacing τ_{ij} by $\tilde{\tau}_{i\mu, j\nu} \equiv D_{i\mu} \tau_{ij}^{\text{CPA}} D_{j\nu}$. Without vertex corrections, that is by approximating the configurational average of the product of scattering-path matrices in Eq. (2) by a product of the individual configurational averages, we have

$$J_{i\mu, j\nu} = \frac{c_\mu c_\nu}{4\pi} \text{tr} \int^{E_F} \Delta t_{i\mu} \tilde{\tau}_{i\mu, j\nu}^\dagger \Delta t_{j\nu} \tilde{\tau}_{j\nu, i\mu}^\dagger dE, \quad \mu, \nu = \uparrow, \downarrow. \quad (3)$$

Since the CPA equations are solved self-consistently at each energy E , this approach is beyond a rigid-band model.

We define effective exchange coupling constants

$$J_{ij}^{\text{eff}} \equiv J_{i\uparrow, j\uparrow} - J_{i\uparrow, j\downarrow} - J_{i\downarrow, j\uparrow} + J_{i\downarrow, j\downarrow}. \quad (4)$$

A positive (negative) $J_{i\mu, j\nu}$ favors parallel (antiparallel) alignment of the local moments ($J_{i\uparrow, j\downarrow} = J_{i\downarrow, j\uparrow}$). As a result, $J_{i\uparrow, j\downarrow}$ and $J_{i\downarrow, j\uparrow}$ appear with a minus sign in Eq. (4). The set of $\{J_{ij}^{\text{eff}}\}$ enters the classical Heisenberg model, Eq. (1), which is solved by Monte Carlo simulations [17,18].

The mapping $T(c_\uparrow)$ of the concentration c_\uparrow on the temperature T is obtained via the average magnetization $\langle m \rangle$ which can be computed from the Heisenberg MC simulations and the first-principles DLM calculations. First, we choose a concentration $c_\uparrow = 1 - c_\downarrow$ and compute within the DLM picture $\langle m \rangle(c_\uparrow)$ and the set $\{J_{ij}(c_\uparrow)\}$. This set is then used in the Heisenberg MC simulations in which the temperature T is scanned, yielding the magnetization curve $\langle m \rangle(T; c_\uparrow)$. The requirement $\langle m \rangle(T; c_\uparrow) = \langle m \rangle(c_\uparrow)$ fixes T for the chosen c_\uparrow , which yields eventually the mapping $T(c_\uparrow)$.

3. Results and discussion

3.1. Fe

3.1.1. Electronic structure and magnetization

The concentration dependence of the exchange coupling constants is completely determined by those of the scattering-path matrices $\tilde{\tau}_{j\nu, i\mu}^\sigma$ and of the single-site scattering matrices $\Delta t_{i\mu}$ in Eq. (3). Hence, we first address the electronic structure by means of the density of states (DOS; Fig. 1).

The d -majority states for ferromagnetic Fe are almost completely occupied [cf. the shoulder at E_F for $c_\uparrow = 1$ in Fig. 1(a)]. These states become depopulated with decreasing c_\uparrow so that at $c_\uparrow = 0.5$ the sample is nonmagnetic. For $c_\uparrow = 1$ the DOS is strongly textured, which indicates an ordered configuration; for smaller concentrations, the DOS is smeared out, as is typical for a disordered configuration. Similar densities of states were found by averaging over random local-moment configurations with mean-field distribution [19].

The trends in the total DOS show also up in the impurity DOS [Fig. 1(b) and (c)]. Note that for $c_\uparrow = 1$ the \uparrow -DOS is identical to the total DOS in (a). Further for $c_\uparrow = 0.5$ the host is nonmagnetic and consequently the spin- \uparrow DOS of an \uparrow impurity is the same as spin- \downarrow DOS of a \downarrow impurity. An analogous relation holds for the opposite spin projection.

In the Stoner picture, the magnetization vanishes for a paramagnetic sample everywhere in space. In the DLM picture, however, the host magnetization $\langle m \rangle = c_\uparrow m_\uparrow + c_\downarrow m_\downarrow$ vanishes but the impurity magnetizations m_\uparrow and m_\downarrow themselves remain finite [Fig. 2(a)]. More precisely, $m_\uparrow = -m_\downarrow$ for $c_\uparrow = 0.5$; they are, in absolute value, as large as the magnetization of ferromagnetic

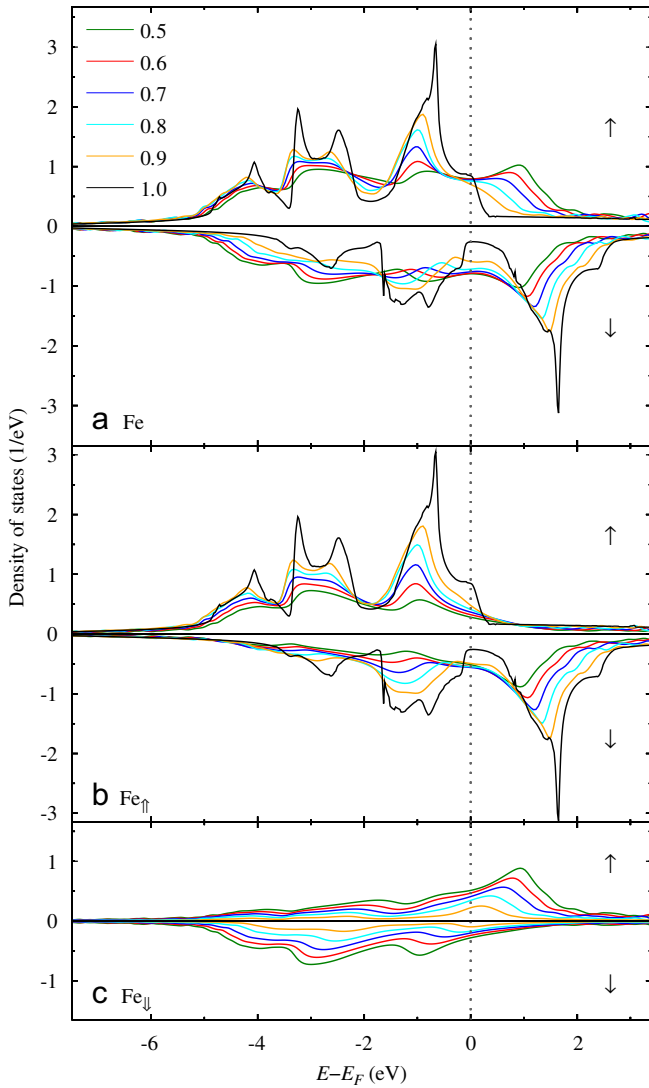


Fig. 1. Spin-resolved electronic structure of bulk Fe. (a) The total density of states (DOS) is shown for different concentrations c_\uparrow , as indicated (majority spin \uparrow , minority spin \downarrow). (b) Density of states for an \uparrow impurity in the effective CPA medium, weighted by the concentration c_\uparrow . (c) As (b) but for a \downarrow impurity. The Fermi energy is E_F .

bcc-Fe ($2.26 \mu_B$ at $T=0$ K) so that the concentration-weighted moments $c_\uparrow m_\uparrow$ and $c_\downarrow m_\downarrow$ depend almost linearly on their concentration. Consequently, $\langle m \rangle$ depends to a very good approximation linearly on c_\uparrow as well.

3.1.2. Heisenberg exchange coupling constants

As an example, we address the concentration dependence of the nearest-neighbor exchange coupling constants [Fig. 2(b)]. For $c_\uparrow = 0.5$ the host is nonmagnetic, that is $(\tau_{ij}^{\text{cpa}})^\uparrow = (\tau_{ij}^{\text{cpa}})^\downarrow$ in Eq. (3); therefore $J_{\uparrow\uparrow} = J_{\downarrow\downarrow} = -J_{\uparrow\downarrow} = -J_{\downarrow\uparrow}$. As a consequence of the decreasing (in absolute value) $J_{\downarrow\downarrow}$, $J_{\uparrow\downarrow}$, and $J_{\downarrow\uparrow}$ with c_\uparrow , the effective exchange coupling constant J_{eff} decreases monotonously, which implies a smaller critical temperature T_c for $c_\uparrow = 1$ than for 0.5.

J_{eff} shows a rapid drop close to $c_\uparrow = 1$ which is due to the contribution of $J_{\uparrow\uparrow}$. This decay may be related to the spin-resolved DOS of an \uparrow impurity in the energy range close to E_F [Fig. 1(b)]. The energies around E_F are important because the electronic structure at these energies determine essentially the electron

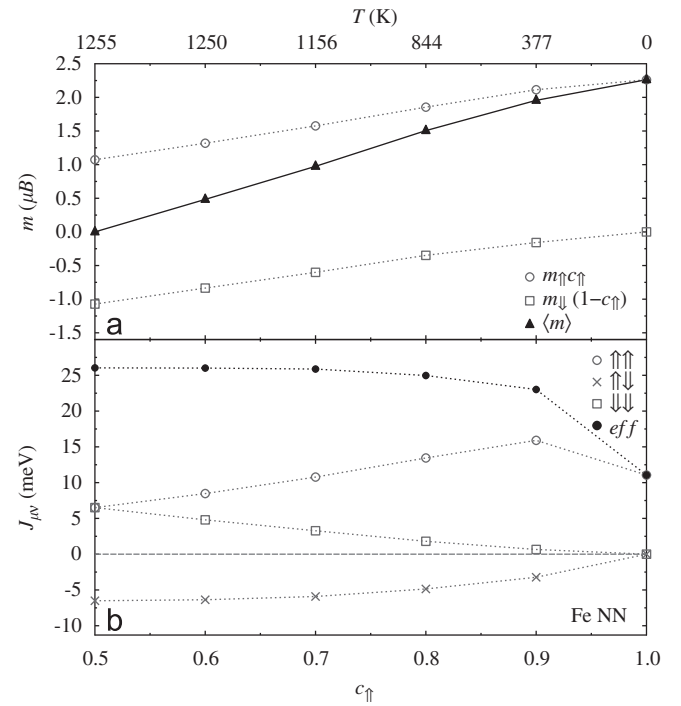


Fig. 2. Magnetization and exchange coupling in bulk Fe. (a) The concentration-weighted impurity magnetizations $c_\uparrow m_\uparrow$ (circles) and $c_\downarrow m_\downarrow$ (squares) are displayed versus concentration $c_\uparrow = 1 - c_\downarrow$. The average magnetization $\langle m \rangle = c_\uparrow m_\uparrow + c_\downarrow m_\downarrow$ (triangles) is shown in addition. (b) Nearest-neighbor exchange coupling constants $J_{\uparrow\uparrow}$ (empty circles), $J_{\uparrow\downarrow}$ (crosses), $J_{\downarrow\downarrow}$ (empty squares) are depicted versus concentration c_\uparrow . The effective constant J_{eff} (filled circles) decreases with c_\uparrow . The temperature scale at the top axis refers to the $T \leftrightarrow c_\uparrow$ mapping shown in Fig. 5. Lines serve as guides to the eye.

propagation. The densities of states of both spin projections are almost constant for small c_\uparrow . But both show ‘jumps’ from $c_\uparrow = 0.9$ to 1.0. These ‘jumps’ may be the reason for the fast decrease of $J_{\uparrow\uparrow}$ in that concentration range. Please be aware that this argument is by no means strict but handwaving.

The nearest-neighbor exchange constant for $c_\uparrow = 1$ compares well with data from the literature; cf. for example Refs. [20–22]. While the $J_{i\uparrow,j\uparrow}$ oscillate with distance $d_{ij} \equiv |\vec{r}_i - \vec{r}_j|$ [Fig. 3(a)], in particular for $c_\uparrow = 1$ (asterisks), the exchange constants $J_{i\uparrow,j\downarrow}$ (b) and $J_{i\downarrow,j\downarrow}$ (c) are sizable only for nearest neighbors ($d_{ij} = 4.69$ Bohr). This implies that at small c_\uparrow , or close to T_c , the local Weiss fields in the Heisenberg model are given mainly by the average magnetization of the nearest-neighbor shells. At c_\uparrow close to 1, or at low temperatures, the Weiss fields are determined in a larger interaction range. As a consequence, the magnetization curves $\langle m \rangle(T; c_\uparrow)$ show different critical exponents, as we will discuss in Section 3.1.3.

3.1.3. Critical temperature and temperature-concentration mapping

As motivated in the preceding subsection, the critical temperature T_c decreases with concentration, as is fully confirmed by the Monte Carlo simulations (Fig. 4). The nonzero magnetizations $\langle m \rangle(T; c_\uparrow)$ for $T > T_c$ that are typical for finite systems do not allow a precise determination of T_c . Hence, the T_c 's were obtained from MC simulations with various system sizes using Binder's fourth cumulant U_4 (Refs. [18,23]; 3180 sites were used for Fig. 4).

For concentrations c_\uparrow up to 0.7, T_c is almost constant and then decays smoothly [filled circles in Fig. 5(a)]. This finding is in line with the concentration dependence of the nearest-neighbor

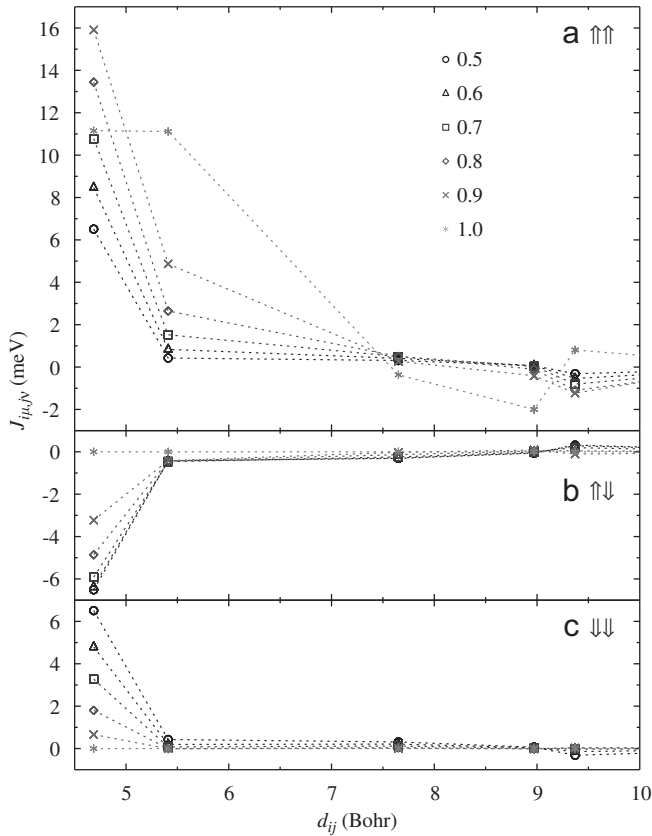


Fig. 3. Distance dependence of the exchange coupling constants in bulk Fe. The exchange constants $J_{ij\nu}$, defined in Eq. (3), are shown versus distance $d_{ij} \equiv |\vec{r}_i - \vec{r}_j|$ for (a) $\mu = \nu = \uparrow$, (b) $\mu = \uparrow$, $\nu = \downarrow$, and (c) $\mu = \nu = \downarrow$. The symbols represent different concentrations $c_{\uparrow} = 1 - c_{\downarrow}$, as indicated in (a). Lines serve as guides to the eye.

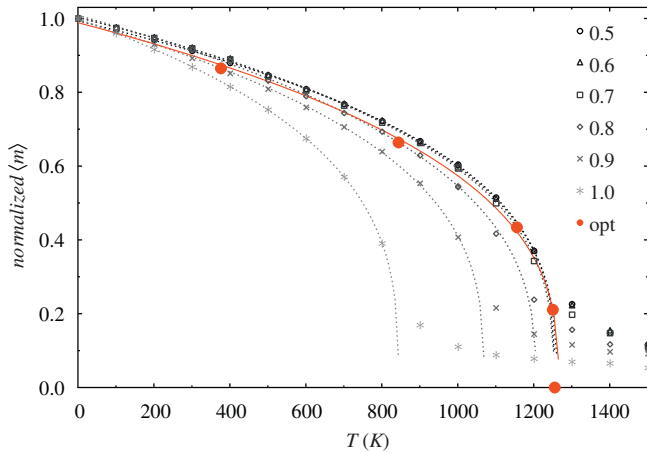


Fig. 4. Magnetization-temperature curves $\langle m \rangle(T; c_{\uparrow})$ for bulk Fe, as obtained from Monte Carlo simulations and normalized to $\langle m \rangle$ for $T = 0$ K. Curves for different concentrations c_{\uparrow} are distinguished by symbols, as indicated. The magnetization curve using the temperature-concentration mapping from Fig. 5 is shown in addition ('opt', large filled circles). Each magnetization curve has been approximated by $\langle m \rangle \propto (T_c - T)^{\beta}$, with fixed T_c (dotted lines).

exchange coupling constants [Fig. 2(b)]. For $c_{\uparrow} = 1$, the T_c of 844 K is smaller than the experimental value (1045 K) while for $c_{\uparrow} = 0.5$ it is larger (1255 K; a similar mismatch was found by Buruzs [10]). The same holds for T_c from the mean-field approximation (1002 K and 1731 K, respectively) but the covered temperature range is much larger than that in the MC calculations.

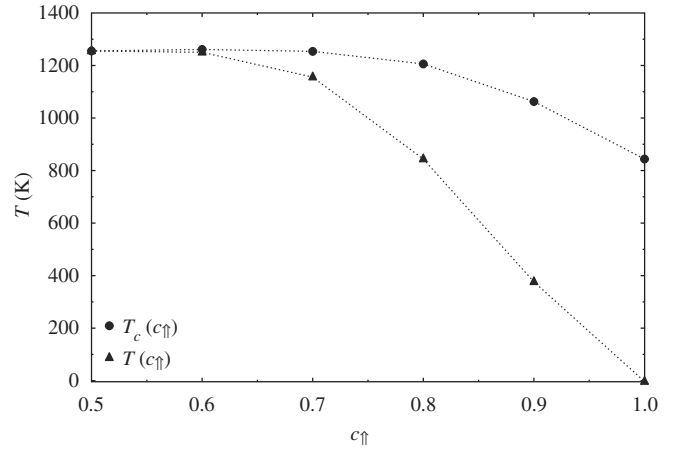


Fig. 5. Critical temperature and temperature-concentration mapping of bulk Fe. T_c is displayed versus concentration c_{\uparrow} (filled circles), while the temperature-concentration mapping $T(c_{\uparrow})$ is displayed by filled triangles. $\partial T / \partial c_{\uparrow} = \partial T_c / \partial c_{\uparrow} = 0$ at $c_{\uparrow} = 0.5$. Lines serve as guides to the eye.

The mismatch of the T_c obtained from the MC simulations and the experimental values may be explained as follows. While the DLM calculation for $c_{\uparrow} = 0.5$ mimics a random configuration and the calculation for $c_{\uparrow} = 1$ mimics the perfectly ordered configuration, it is conceivable that the best description is obtained by a disordered configuration with short-range order [24,25]. Short-range order can be accounted for within the non-local CPA, the embedded-cluster CPA [26] or the locally self-consistent Green function method [27]. Other reasons might be that the present DLM calculations use an Ising-type alloy [5,7] instead of a rotationally averaged alloy. In the latter case, the configuration average has to be performed over *all directions* of the local magnetic moments rather than by averaging over the *two orientations* \uparrow and \downarrow .

Eventually, we obtain the mapping $T(c_{\uparrow})$ by equating $\langle m \rangle(c_{\uparrow})$ from the DLM calculations [Fig. 2(a)] and $\langle m \rangle(T; c_{\uparrow})$ from the MC simulations (Fig. 4), which is shown as filled triangles in Fig. 5 and also displayed as top axis in Fig. 2. The mapping is monotonous but nonlinear.

As an application we show the $\langle m \rangle(T)$ curve for the 'optimal' (temperature-dependent) set of $\{J_{ij}(T)\}$ in Fig. 4 ('opt', large filled circles). It interpolates smoothly between the curve for $c_{\uparrow} = 1.0$ at low temperatures and the curve for $c_{\uparrow} = 0.5$ close to T_c . As a consequence, the critical exponent β is about 10% larger than that for $c_{\uparrow} = 0.5$. The 'optimal' MC value of 0.349 is closer to the literature value of 0.365 [28] than those for $c_{\uparrow} = 0.5$ (0.314) and $c_{\uparrow} = 1.0$ (0.315). β was obtained by approximating $\langle m \rangle(T)$ by $(T_c - T)^{\beta}$ (dotted lines in Fig. 4), in which T_c has been fixed by the U_4 analysis [18,23].

3.2. Co

While the DLM approach works well for Fe, it fails for Ni. For example, the local magnetic moments vanish for paramagnetic Ni. Co has with one d electron more than Fe and one d electron less than Ni. Hence, it falls in-between Fe and Ni, which shows up as significantly reduced local moment for paramagnetic Co (about $0.80 \mu_B$) as compared to that of ferromagnetic Co ($1.60 \mu_B$). These findings call for an improved DLM approach that, for example, takes into account short-range order.

Regardless of these shortcomings we present in Fig. 6 the major outcomes of our computations for hcp Co. In contrast to Fe (Fig. 5), T_c increases with c_{\uparrow} [filled circles in Fig. 6(b)] which is in line with the reduced local magnetic moments and the slightly

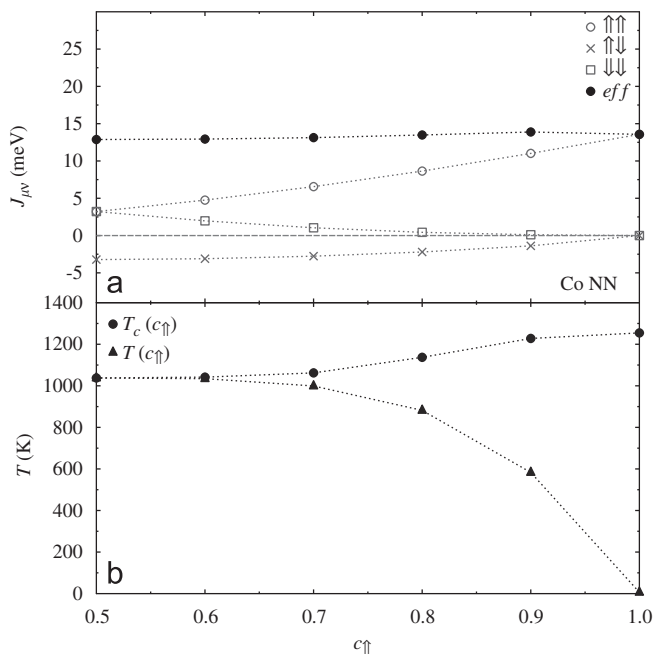


Fig. 6. Temperature-dependent exchange coupling in bulk Co. (a) Nearest-neighbor exchange coupling constants $J_{\uparrow\uparrow}$ (empty circles), $J_{\uparrow\downarrow}$ (crosses), $J_{\downarrow\downarrow}$ (empty squares) are depicted versus concentration c_{\uparrow} . The effective constant J_{eff} (filled circles) increases slightly with c_{\uparrow} . (b) Critical temperature and temperature mapping. T_c is displayed versus concentration c_{\uparrow} (filled circles), while the temperature mapping $T(c_{\uparrow})$ is represented by filled triangles. Lines serve as guides to the eye.

increasing effective exchange coupling constant [Fig. 6(a)]. Consequently, T_c is closest to the experimental value of 1388 K for $c_{\uparrow} = 1$ (1255 K).

The general shape of the temperature-concentration mapping for Co [filled triangles in Fig. 6(b)] agrees with that for Fe (Fig. 5). But while the curve for Fe is almost linear for $c_{\uparrow} > 0.7$, the Co mapping is bent downward. We attribute this observation to the almost constant J_{eff} of Co [filled circles in Fig. 6(a)] in contrast to the decreasing ones of Fe [filled circles in Fig. 2(b)].

4. Concluding remarks

In this paper, we propose a procedure to improve on the first-principles basis of Heisenberg exchange coupling constants. Since (i) the computation of Heisenberg exchange coupling constants within the DLM formalism is straightforward in any electronic-structure computer code that is based on Green functions and (ii) Monte Carlo simulations of the classical Heisenberg model can be regarded as standard as well, we see many applications for refined J_{ij} , in particular in magnetization dynamics calculations based on the Landau–Lifshitz–Gilbert equation. There, the Gilbert damping constant depends on temperature [29]; further, thermal fluctuations are modeled as random magnetic fields [1,2]. Hence, it is obvious to use temperature-dependent exchange coupling constants in the spin Hamiltonian as well. To complement the Heisenberg model, one could also include the temperature dependence of the magnetocrystalline anisotropy [30].

The purpose of the present study is to introduce the basic idea of the approach and to present a few applications. It also suggests paths for improvement: we expect that taking into account short-range order in the DLM calculations could result in better critical

temperatures, which would also amend the temperature-concentration mapping. Rotational averaging rather than Ising-type averaging could improve the results as well; note that rotational averaging is a necessary ingredient if spin-orbit coupling should be accounted for, e.g. the Dzyaloshinskii–Moriya interaction [10,31–33].

The Dzyaloshinskii–Moriya interaction can lead to noncollinear magnetism in non-centrosymmetric systems, for example in ultrathin films on a substrate (e.g. Fe/Ir(111) [34]). The noncollinear magnetic structure gives rise to a ‘magnetic lattice’ constant which is determined by the ratios of Heisenberg exchange, magnetocrystalline anisotropy, and strength of the Dzyaloshinskii–Moriya interaction. Both may differ in their distance dependence and in their temperature dependence. Thus, one might speculate that a noncollinear structure, and hence its magnetic lattice constant, can vary significantly with temperature.

Acknowledgments

This work is supported by the *Sonderforschungsbereich*762 ‘Functional Oxide Interfaces’. DB is a member of the International Max Planck Research School on Science and Technology of Nanostructures, Halle, Germany. We appreciate helpful discussions with A. Marmodoro.

References

- [1] B. Skubic, J. Hellsvik, L. Nordström, O. Eriksson, A method for atomistic spin dynamics simulations: implementation and examples, *Journal of Physics: Condensed Matter* 20 (2008) 315203.
- [2] D. Böttcher, A. Ernst, J. Henk, Atomistic magnetization dynamics in nanostructures based on first principles calculations: application to Co nanoislands on Cu(111), *Journal of Physics: Condensed Matter* 23 (2011) 296003.
- [3] A.I. Liechtenstein, M.I. Katsnelson, V.P. Antropov, V.A. Gubanov, Local spin density functional approach to the theory of exchange interactions in ferromagnetic metals and alloys, *Journal of Magnetism and Magnetic* 67 (1987) 65.
- [4] J. Staunton, B.L. Gyorffy, A.J. Pindor, G.M. Stocks, H. Winter, The “Disordered local moment” picture of itinerant magnetism at finite temperatures, *Journal of Magnetism and Magnetic* 45 (1984) 15–22.
- [5] B.L. Gyorffy, A.J. Pindor, J. Staunton, G.M. Stocks, H. Winter, A first-principles theory of ferromagnetic phase transitions in metals, *Journal of Physics F: Metal Physics* 15 (6) (1985) 1337–1386.
- [6] S.S.A. Razeef, J.B. Staunton, L. Szunyogh, B.L. Györfy, Local moments and magnetic correlations above the Curie temperature in thin films on and embedded in nonmagnetic substrates: Fe/Cu(100), Co/Cu(100), and Fe/W(100), *Physical Review B* 66 (2002) 094415.
- [7] A.J. Pindor, J. Staunton, G.M. Stocks, H. Winter, Disordered local moment state of magnetic transition metals: a self-consistent KKR CPA calculation, *Journal of Physics F: Metal Physics* 13 (1983) 979.
- [8] A.V. Ruban, S. Khmelevskiy, P. Mohn, B. Johansson, Temperature-induced longitudinal spin fluctuations in Fe and Ni, *Physical Review B* 75 (2007) 054402.
- [9] V. Drchal, J. Kudrnovský, P. Bruno, P.H. Dederichs, P. Weinberger, The combined effect of temperature and disorder on interlayer exchange coupling in magnetic multilayers, *Philosophical Magazine* B 78 (1998) 571.
- [10] A. Buruzs, Temperature Dependent Magnetic Properties of Thin Films and Bulk Ferromagnets: An Implementation of the Disordered Local Moment Scheme, PhD Thesis, Fakultät für Physik, Technische Universität Wien, Vienna, 2008.
- [11] J. Zabloudil, R. Hammerling, L. Szunyogh, P. Weinberger (Eds.), *Electron Scattering in Solid Matter*, Springer, Berlin, 2005.
- [12] J.P. Perdew, Y. Wang, Accurate and simple analytic representation of the electron-gas correlation energy, *Physical Review B* 45 (1992) 13244.
- [13] P. Soven, Coherent-potential model of substitutional disordered alloys, *Physical Review* 156 (1967) 809.
- [14] B.L. Gyorffy, Coherent-potential approximation for a nonoverlapping-muffin-tin-potential model of random substitutional alloys, *Physical Review B* 5 (1972) 2382.
- [15] J.S. Faulkner, G.M. Stocks, Calculating properties with the coherent-potential approximation, *Physical Review B* 21 (1980) 3222.
- [16] P.J. Durham, B.L. Gyorffy, A.J. Pindor, On the fundamental equations of the Korringa-Kohn-Rostoker (KKR) version of the coherent potential approximation (CPA), *Journal of Physics F: Metal Physics* 10 (1980) 661.

- [17] N. Metropolis, A.W. Rosenbluth, M.N. Rosenbluth, E. Teller, Equation of state calculations by fast computing machines, *Journal of Chemical Physics* 21 (1953) 1087.
- [18] K. Binder, Applications of Monte Carlo methods to statistical physics, *Reports on Progress in Physics* 60 (1997) 487.
- [19] A.L. Wysocki, R.F. Sabirianov, M. van Schilfgaarde, K.D. Belashchenko, First-principles analysis of spin-disorder resistivity of Fe and Ni, *Physical Review B* 80 (2009) 224423.
- [20] A. Sakuma, First principles study on the exchange constants of the 3d transition metals, *Journal of Physical Society of Japan* 68 (1998) 620.
- [21] M. van Schilfgaarde, V.P. Antropov, First-principles exchange interactions in Fe, Ni, and Co, *Journal of Applied Physics* 85 (1999) 4827.
- [22] I. Turek, J. Kudrnovský, V. Drchal, P. Bruno, Exchange interactions, spin waves, and transition temperatures in itinerant magnets, *Philosophical Magazine* 86 (2006) 1713.
- [23] K. Binder, D.W. Heermann, *Monte Carlo Simulation in Statistical Physics: An Introduction*, third ed, Springer, Berlin, 1997.
- [24] K.S. Chana, J.H. Samson, M.U. Luchini, V. Heine, Magnetic short-range order in iron above T_c ? Statistical mechanics with many-atom interactions, *Journal of Physics: Condensed Matter* 3 (1991) 6455.
- [25] D. Reiser, J. Henk, H. Gollisch, R. Feder, Theory of temperature-dependent electronic structure and photoemission of ultrathin ferromagnetic films, *Solid State Communications* 93 (1995) 231.
- [26] P. Weinberger, R. Dirl, A.M. Boring, A. Gonis, A.J. Freeman, Fully relativistic Korringa-Kohn-Rostoker coherent-potential-approximation embedded-cluster-method evaluation of short-range-order effects in substitutional alloys containing heavy elements, *Physical Review B* 37 (1988) 1383.
- [27] I.A. Abrikosov, A.M.N. Niklasson, S.I. Simak, B. Johansson, A.V. Ruban, H.L. Skriver, Order-N Green's function technique for local environment effects in alloys, *Physical Review Letters* 76 (1996) 4203.
- [28] M. Getzlaff, *Fundamentals of Magnetism*, Springer, Berlin, 2008.
- [29] H. Ebert, S. Mankovsky, D. Ködderitzsch, P.J. Kelly, Ab-initio calculation of the Gilbert damping parameter via linear response formalism, arxiv:1102.4551v1 [cond-mat.mtrl-sci] (2011).
- [30] A. Buruzs, P. Weinberger, L. Szunyogh, L. Udvardi, P.I. Chleboun, A.M. Fischer, J.B. Staunton, Ab initio theory of temperature dependence of magnetic anisotropy in layered systems: applications to thin Co films on Cu(100), *Physical Review B* 76 (6) (2007) 064417.
- [31] I. Dzyaloshinsky, A thermodynamic theory of "weak" ferromagnetism of antiferromagnetics, *Journal of Physics and Chemistry of Solids* 4 (4) (1958) 241. doi:10.1016/0022-3697(58)90076-3.
- [32] T. Moriya, Anisotropic superexchange interaction and weak ferromagnetism, *Physical Review* 120 (1960) 1.
- [33] L. Udvardi, L. Szunyogh, K. Palotás, P. Weinberger, First-principles relativistic study of spin waves in thin magnetic films, *Physical Review B* 68 (2003) 104436.
- [34] K. von Bergmann, S. Heinze, M. Bode, G. Bihlmayer, S. Blügel, R. Wiesendanger, Complex magnetism of Fe monolayer on Ir(111), *New Journal of Physics* 9 (2007) 396.

4.2 Non-collinear spin structures in ultrathin (111)-films

Ultrathin (1ML-thick) Fe films on Ir(111) reveal a complex non-collinear Skyrmion-type spin structure. The mechanism is incited by strong spin-orbit coupling effects appearing also in other (111) substrates like Pt, Rh, and Pd. Skyrmion formation shows a net magnetization, an evidence that was also found by Moulas et. al [206] in ultrathin Fe on Pt(111). The hybridization between Fe and Pt as well as the strong spin-orbit coupling hints to a non-collinear magnetic structure. The paper considers the Heisenberg model that consists of the full magnetic interaction matrix \mathbf{I}_{ij} , which was computed from first principles. A domain wall-like structure was found, originating the in-plane-oriented three-fold symmetric Dzyaloshinskii-Moriya interaction. This formation is similar to these observed in Mn/W(110) as well as Fe/W(110). The wave length and the direction of the occurring spin-spiral results from the competition between the isotropic and the anisotropic exchange, where in the Fe/Pt(111) the fraction of both coupling mechanisms is by an order of magnitude smaller than in Fe/Ir(111). Hence, no low-temperature Skyrmions without a magnetic field do not exist in Fe/Pt(111).

To mimic the experimental findings, an external magnetic field perpendicular to the surface was applied, lifting the non-collinear field structure into a parallel orientation of the magnetic moments to the external magnetic field.

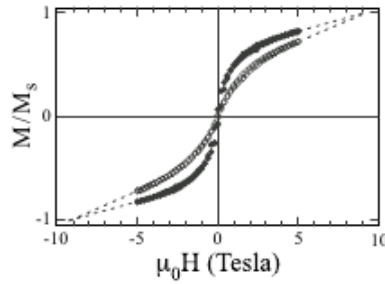


Figure 4.2.1.: Magnetization curve for 1 ML Fe on Pt(111), taken from Ref. [206]. The hysteresis is measured at $T = 10$ K for the external field in z -direction (solid circles) and 70° (open circles) out of the direction perpendicular to the surface.

Theoretically a net magnetization of $0.813M_S$ at 5 T was obtained. At 10 T, the local magnetic moments are still not completely rotated out-of-plane and towards the magnetic field, indicating incomplete saturation. This agrees with the experiment (figure 4.2.1, $M(5\text{ T}) = 0.85M_S$) and concludes that the non-collinear spin structure explains and removes the disagreement between experiment and theory in [206]. Beside the experimental results, theory predicts a decrease of the phase transition temperature due to spin-orbit coupling: without DM interaction $T_C = 670$ K, with DM-interaction $T_C = 590$ K. This confirms the phase transition temperature postulations by Rausch and Nolting [232] for low-dimensional magnets. Hence, the findings indicate also a strong impact of the spin-orbit interaction on the time-dependent phenomena based on the Landau-Lifshitz-Gilbert equation. Magnetic excitations by a external magnetic field pulse can show long-term magnons, which is a task for a future studies.



Noncollinear Magnetism in Ultrathin Films with Strong Spin-Orbit Coupling from *Ab Initio*

D. Böttcher^{1,2,*}, A. Ernst¹, and J. Henk¹

¹Max-Planck-Institut für Mikrostrukturphysik, Weinberg 2, D-06120 Halle, Saale, Germany

²Institut für Physik, Martin-Luther-Universität Halle-Wittenberg, D-06120 Halle, Saale, Germany

Fe and Pt are paradigms for ferromagnetism and strong spin-orbit coupling, respectively. Their combination—in an ultrathin Fe film on a Pt(111) substrate—is thus expected to modify the magnetic structures. We report on a theoretical investigation of a monolayer of Fe on Pt(111), using a generalized Heisenberg model that includes the complete spin interaction matrices I_{ij} computed from first principles. We find a noncollinear periodic configuration that is strongly determined by the Dzyaloshinskii-Moriya interaction. Taking into account a magnetic field to mimic recent experiments, this noncollinear structure solves the disagreement between the experimental magnetization and the average magnetization for a ferromagnetic system. The critical temperature decreases from 670 K to 590 K due to spin-orbit coupling.

Keywords: Dzyaloshinskii-Moriya Interaction, Ultrathin Films, Magnetic Ground State Properties.

1. MOTIVATION

The properties of ultrathin magnetic films depend strongly on the substrate,¹ as has been shown experimentally by spin-polarized scanning tunneling microscopy and magneto-optical Kerr spectroscopy. In particular spin-orbit coupling (SOC) induces a symmetry breaking in magnetic systems, which e.g., shows up as magneto-crystalline anisotropy. Together with the exchange interaction, the magnetic anisotropy manifests itself in the formation of domain walls. In non-centrosymmetric systems, the Dzyaloshinskii-Moriya (DM) interaction results in noncollinear magnetic structures, preferably at surfaces and in ultrathin films.² The magnetic properties of a monolayer Fe on Pt(111) are still not understood completely. On one hand, Moulas et al.³ showed that by applying an external magnetic field of 5 T the magnetization is barely $1.2 \mu_B$; the saturation field is roughly estimated to 10 T. On the other hand, first-principles electronic-structure calculations using a Korringa-Kohn-Rostoker Green's function method³ or the Vienna *Ab-Initio* Simulation Package⁴ support ferromagnetic order, an Fe magnetic moment of about $3.0 \mu_B$ and an induced Pt moment of $0.25 \mu_B$. We regard these contradictory results as an indication for a noncollinear magnetic structure in Fe/Pt(111) which may be driven by the strong SOC in Pt. Noncollinear magnetism due to SOC has been shown for FePt-alloy clusters

deposited on Pt(111).^{5,6} In this paper we report on a first-principles investigation of a monolayer Fe on Pt(111) that includes SOC. Using a generalized Heisenberg model, we focus on the question on how spin-orbit coupling manifests itself in the magnetic ground-state properties and the magnetic structure of Fe/Pt(111).

2. OUTLINE OF THE THEORETICAL APPROACH

2.1. First-Principles Calculations

To investigate the magnetic properties of a monolayer Fe on Pt(111), we performed first-principles electronic-structure calculations using a relativistic Korringa-Kohn-Rostoker Green's function method.^{7,8} Solving the Dirac equation for a spin-polarized system, spin-orbit coupling and magnetism are treated on equal footing. Wavefunctions and scattering matrices have been calculated up to an orbital momentum of $l_{\max} = 3$. The site-dependent potentials are described in the atomic sphere approximation. The film-substrate system is taken as translationally invariant parallel to the layers but semi-infinite perpendicular to the layers. We adopt the interlayer spacing derived by Hardrat et al.¹ who found an inward relaxation of the monolayer fcc Fe by 12.7% of the Pt bulk interlayer distance (lattice constant $a = 2.81 \text{ \AA}$; Fig. 1).

From the *ab initio* calculations, we derived the complete spin interaction matrix of a generalized Heisenberg

*Author to whom correspondence should be addressed.

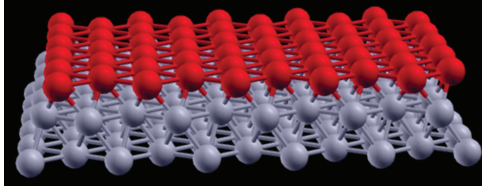


Fig. 1. Schematic view of a monolayer Fe on Pt(111). Only the first two layers of Pt (gray spheres) are important for the spin structure in the Fe film (red spheres).

model,⁷ within the framework of the magnetic force theorem.^{9–14}

2.2. Spin Hamiltonian and Interaction Matrix

The Heisenberg model

$$H = - \sum_{i \neq j} J_{ij} \mathbf{m}_i \cdot \mathbf{m}_j \quad (1)$$

where \mathbf{m}_i and \mathbf{m}_j are classical normalized magnetic moments and J_{ij} is their exchange constant, is a standard model for magnetic materials. Since the J_{ij} are isotropic and symmetric, it does not account for spin-orbit coupling effects. A straightforward generalization is given by

$$H = - \sum_{ij} \mathbf{m}_i I_{ij} \mathbf{m}_j \quad (2)$$

where I_{ij} is the full 3×3 interaction matrix ($I_{ij} = I_{ij}^T$). Decomposing I_{ij} as

$$I_{ij} \equiv J_{ij} \mathbf{1} + S_{ij} + A_{ij} \quad (3)$$

one recovers the Heisenberg exchange $J_{ij} = (1/3) \text{tr} I_{ij}$. The anisotropic and traceless parts S_{ij} and A_{ij} split into a symmetric and an antisymmetric contribution, $S_{ij} = (1/2) \cdot (I_{ij} + I_{ij}^T) - J_{ij} \mathbf{1}$ and $A_{ij} = (1/2)(I_{ij} - I_{ij}^T)$. This implies that only the J_{ij} force the system into a collinear state. The anisotropic antisymmetric components include the Dzyaloshinskii-Moriya vectors

$$D_{ij}^\alpha \equiv \frac{1}{2} \sum_{\beta\gamma} \varepsilon_{\alpha\beta\gamma} I_{ij}^{\beta\gamma}, \quad \alpha, \beta, \gamma = x, y, z \quad (4)$$

that describe the noncollinearity between two magnetic moments;¹⁵ they are closely linked to the symmetry of the system.

The complete Hamiltonian then reads

$$H = - \sum_{i \neq j} [J_{ij} \mathbf{m}_i \cdot \mathbf{m}_j + \vec{D}_{ij} \cdot (\mathbf{m}_i \times \mathbf{m}_j) + \mathbf{m}_i S_{ij} \mathbf{m}_j] - \sum_i \mathbf{m}_i I_{ij} \mathbf{m}_i - \sum_{ij} \mathbf{m}_i Q_{ij} \mathbf{m}_j + H_{\text{ext}} \quad (5)$$

The fourth term correlates to the uniaxial anisotropy of the system, whereas the fifth term accounts for the

dipole–dipole interaction (shape anisotropy). The dipolar matrix Q_{ij} is given by

$$Q_{ij}^{\mu\nu} = \frac{\mu_0}{8\pi} \frac{3r_{ij}^\mu r_{ij}^\nu - r_{ij}^2 \delta^{\mu\nu}}{r_{ij}^5}, \quad r_{ij} = r_i - r_j; \quad \mu, \nu = x, y, z \quad (6)$$

where r_i is the location of the atom i . Eventually, an external magnetic field is described by the Zeeman term in H_{ext} . The magnetic properties of the systems in thermal equilibrium are obtained by a standard Monte-Carlo method^{16,17} using the Metropolis algorithm.

3. RESULTS AND DISCUSSION

3.1. Spin-Resolved Electronic Properties

The electronic-structure calculations yield that the majority bands in the Fe layer are almost completely filled, unlike the minority bands that show a sharp maximum at the Fermi level (Fig. 2). As a consequence of the reduced dimensionality of the film, the Fe magnetic moment ($3.03 \mu_B$) is increased with respect to Fe bulk ($2.26 \mu_B$) and agrees with that given by Hardrat et al.¹ ($3.10 \mu_B$). Hybridization of Fe and Pt electronic states results in induced Pt magnetic moments that decrease rapidly toward the bulk (first Pt-layer $0.26 \mu_B$; second Pt-layer $0.01 \mu_B$; Fig. 2). This is a first hint on that the Pt substrate, with its large spin-orbit coupling, can indeed have a profound influence on the magnetic structure in the Fe adlayer.

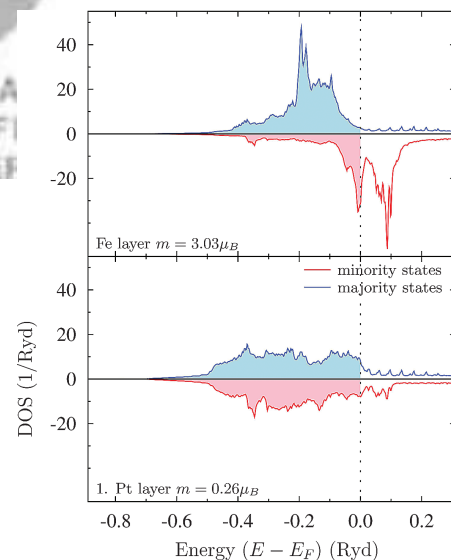


Fig. 2. Spin-resolved electronic structure of a monolayer Fe on Pt(111). The density of states (DOS) is given for the Fe layer (top) and the first Pt layer (bottom). The strong exchange splitting in Fe ($3.03 \mu_B$) and the hybridization of Fe with Pt electronic states leads to a sizable induced moment in the first Pt layer ($0.26 \mu_B$).

3.2. Magnetic Configuration of a Monolayer Fe on Pt(111)

In the Monte Carlo simulations for the magnetic ground state we consider the first three layers (Fe layer and the two subsequent Pt layers) because only these show relevant magnetic moments and spin interactions.

First, we discuss the effects of the individual contributions in the spin Hamiltonian on the magnetic configurations. The nearest-neighbor Heisenberg exchange constant exhibits ferromagnetic behavior ($J_{\text{INN}} > 0$); the magnetocrystalline anisotropy is in-plane (parallel to the surface). Hence, without the DM contribution, we obtain an in-plane collinear ground state with an average atomic moment of $1.59 \mu_{\text{B}}$, in clear contrast to experiment ($1.0 \mu_{\text{B}}$ from Ref. [3]).

Inclusion of the symmetric anisotropic part S_{ij} in the Hamiltonian maintains this spin configuration in general. In contrast to the DM part, this term tends to tilt pairs of magnetic moments in the same direction. Hence it can be interpreted as an additional contribution to the magnetocrystalline anisotropy that slightly changes the easy axis for each pair of moments. As a consequence, the local magnetic moments deviate more strongly from the general easy axis than without S_{ij} , even at very low temperatures. These fluctuations of the easy axes can be viewed as a broadening of the global energy minimum that also gives rise to fluctuations of the transition region width w .

The Dzyaloshinskii-Moriya contribution turns out to be significant only for nearest neighbor sites, as was deduced by successively reducing the interaction range in the MC calculations; it tends to tilt magnetic moments mutually and is strongly linked to the symmetry of the system (Fig. 3). It produces as an outcome of our calculations a periodic noncollinear configuration which shows up in both the Fe layer and the subsurface Pt layers (Fig. 4; not shown for Pt); this corroborates the significant coupling of Fe and Pt found in the density of states (Fig. 2). Since the magnetic structure contains in-plane and perpendicular components, it reminds at a combination of (very narrow) Bloch and Néel walls.

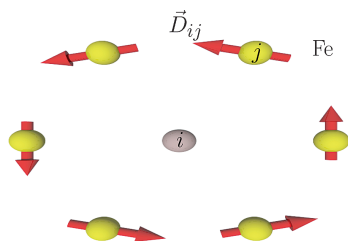


Fig. 3. Dzyaloshinskii-Moriya interaction in a monolayer Fe on Pt(111). Arrows depict the DM vectors D_{ij} between two magnetic moments i (central site, fixed) and j in the Fe adlayer. Because of the three-fold symmetry, DM contributions from an in-plane ring structure, with antisymmetric interactions with respect to site i .

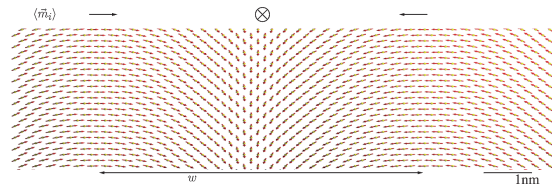


Fig. 4. Noncollinear magnetism in a monolayer Fe on Pt(111). Because of strong spin-orbit coupling effects, the local magnetic moments (arrows) form a periodic noncollinear magnetic structure. The moment averaged over one magnetic unit cell vanishes, but the moment averaged over the length w of the transition range is about $1.0 \mu_{\text{B}}$.

An impression of the interplay of the individual contributions to the Hamiltonian is provided by ratios $J:K:S:D$. We obtain for the Fe-Fe interaction 75:1:9:16, in contrast to the Fe-Pt interaction 8:1:1:2. While in both cases the Heisenberg exchange dominates, the ratio $J:D$ is almost identical for Fe-Fe and Fe-Pt (about 8:1), giving further support to the importance of the SOC and hybridization. The magnetic lattice constant can be estimated from domain-wall theory within a continuum model. Without DM interaction, the width w of the transition region is given by

$$w = \sqrt{\frac{A}{K}} \quad (7)$$

where A and K are the exchange density and the average anisotropy, respectively. With DM contribution, an analytical solution for w has been achieved only for DM vectors aligned along the z -direction, enlarging the transition region w . From the calculated parameters we obtain $w = 3.8 \text{ nm}$, which is slightly smaller than half of the magnetic lattice constant (Fig. 4). Taking into account the DM contribution, w is increased to 6.7 nm . A closer analysis of the MC simulations yields that this increase can indeed be attributed to the DM contributions.

Averaging over the magnetic unit cell gives a vanishing net magnetization. Restricting the average to the transition region, as indicated by the double arrow in Figure 4, produces a net moment of about $1.0 \mu_{\text{B}}$.

The perpendicular components of the local moments are very well described by an arithmetic function. Further, the symmetric anisotropic interaction leads to tiny fluctuations of the magnetic lattice constant; these are attributed to the anisotropic symmetric contributions to the exchange matrices.

We now focus on the magnetic phase transition. Since a noncollinear configuration is not well characterized by its average magnetization, we deduce the critical temperature from the nearest-neighbor spin correlation function

$$S = \frac{1}{N} \sum_i \frac{1}{N_i} \sum_j |\mathbf{m}_i \cdot \mathbf{m}_j| \quad (8)$$

Here, N is the number of sites in the sample and N_i the number of nearest neighbor atoms of site i . An alternative

measure is the spin–spin correlation function (SSCF)

$$s(dr) = \langle \mathbf{m}_r \cdot \mathbf{m}_{r+dr} \rangle_r \quad (9)$$

of magnetic moments at a distance dr . The SSCF of Fe/Pt(111) behaves like $\cos(\pi dr/w)$ at very low temperatures. For increasing thermal fluctuations, its amplitude decreases and eventually vanishes at the Curie temperature T_C . From this general behavior we derive Curie temperatures of 670 K without DM interaction. With DM interaction, the Curie temperature is reduced to 590 K which is in good agreement with 0.6 of T_C for bulk Fe (1043 K), as found by Rausch and Nolting.¹⁸

Eventually, we consider the dependency of the average magnetization on an external magnetic field perpendicular to the surface. We recall that a magnetization of $1.2 \mu_B$ has been found experimentally at 5 T; even at 10 T the sample was not driven into saturation.³ To mimic these experiments we performed MC simulations with the magnetic-field term (up to 10 T). As consequence of the strong SOC, the local magnetic moments maintain sizable in-plane components (cf. Fig. 4 for zero field) but are tilted out-of-plane with increasing field strength. For a field of 5 T we obtain a net magnetization of $1.3 \mu_B$. Also at 10 T, the local magnetic moments are not completely rotated out-of-plane, indicating incomplete saturation. Since these findings agree nicely with experiment,³ we conclude that the theoretically predicted noncollinear structure solves the aforementioned puzzle.

4. CONCLUSION

Ultrathin films with strong spin-orbit coupling show noncollinear spin structures, as is demonstrated for a monolayer Fe on Pt(111). Using Monte-Carlo calculations for a generalized Heisenberg model, in which spin-orbit contributions are taken into account and whose parameters are obtained from first-principles calculations, we find a periodic arrangement of toroidal structures. This noncollinear structure solves the discrepancy of the experimental magnetization and the theoretical magnetization for a ferromagnetic configuration. Our findings call for new experiments in order to verify the predicted magnetic structure.

We expect a strong impact of the spin-orbit interaction on time-dependent phenomena, as is currently investigated within an atomistic approach based on the stochastic Landau–Lifshitz–Gilbert equation. First calculations for systems perturbed by a magnetic field pulse show long-term excitations which may excite magnons.

Acknowledgments: D. Böttcher is member of the International Max Planck School for Science and Technology of Nanostructures. This work is supported by the *Sonderforschungsbereich 762* ‘Functionality of Oxide Interfaces.’

References and Notes

1. B. Hardrat, A. Al-Zubi, P. Ferriani, S. Blügel, G. Bihlmayer, and S. Heinze, *Phys. Rev. B* **79**, 094411 (2009).
2. K. von Bergmann, S. Heinze, M. Bode, G. Bihlmayer, S. Blügel, and R. Wiesendanger, *New J. Phys.* **9**, 396 (2007).
3. G. Moulas, A. Lehnert, S. Rusponi, J. Zabloudil, C. Etz, S. Ouazi, M. Etzkorn, P. Bencok, P. Gambardella, P. Weinberger, and H. Brune, *Phys. Rev. B* **78**, 214424 (2008).
4. A. Lehnert, S. Dennler, P. Blonski, S. Rusponi, M. Etzkorn, G. Moulas, P. Bencok, P. Gambardella, H. Brune, and J. Hafner, *Phys. Rev. B* **82**, 094409 (2010).
5. A. Enders, R. Skomski, and J. Honolka, *J. Phys.: Condens. Matt.* **22**, 433001 (2010).
6. S. Mankovsky, S. Bornemann, J. Minár, S. Polesya, H. Ebert, J. B. Staunton, and A. I. Lichtenstein, *Phys. Rev. B* **80**, 014422 (2009).
7. J. Zabloudil, R. Hammerling, L. Szunyogh, and P. Weinberger (eds.), *Electron Scattering in Solid Matter*, Springer, Berlin (2005).
8. D. Böttcher, A. Ernst, and J. Henk, *J. Phys.: Condens. Matt.* **23**, 29 (2011).
9. A. I. Lichtenstein, M. I. Katsnelson, V. P. Antropov, and V. A. Gubanov, *J. Magn. Magn. Mater.* **67**, 65 (1987).
10. P. Strange, H. Ebert, J. B. Staunton, and B. L. Gyorffy, *J. Phys.: Condens. Matt.* **1**, 3947 (1989).
11. G. H. O. Daalderop, P. J. Kelly, and M. F. H. Schuurmans, *Phys. Rev. B* **41**, 11919 (1990).
12. X. Wang, D.-S. Wang, R. Wu, and A. J. Freeman, *J. Magn. Magn. Mater.* **159**, 337 (1996).
13. M. D. Stiles, S. V. Halilov, R. A. Hyman, and A. Zangwill, *Phys. Rev. B* **64**, 104430 (2001).
14. S. S. Dhesi, G. van der Laan, E. Dudzik, and A. B. Shick, *Phys. Rev. Lett.* **87**, 067201 (2001).
15. T. Moriya, *Phys. Rev.* **120**, 1 (1960).
16. N. Metropolis, A. W. Rosenbluth, M. N. Rosenbluth, and E. Teller, *J. Chem. Phys.* **21**, 1087 (1953).
17. K. Binder (ed.), *Monte Carlo Methods in Statistical Physics*, Springer, Berlin (1979).
18. R. Rausch and W. Nolting, *J. Phys.: Condens. Matt.* **21**, 376002 (2009).

Received: 29 March 2011. Accepted: 29 October 2011.

4.3 Gilbert damping tensor within the breathing Fermi surface model: anisotropy and non-locality

Developing and optimizing new magnetic devices for spintronic applications calls for detailed studies on magnetization dynamics. A distinctive property is the relaxation rate, which in nanoscopic magnetic simulations is introduced as Gilbert's phenomenological damping parameter α . The larger α , the faster is the magnetic equilibration. This parameter is often assumed local and isotropic, in agreement with ferromagnetic resonance spectroscopy. But experiments and theoretical observations on the atomic scale [83], in particular in low-dimensional systems, suggest an anisotropic spin-orbit contribution and, thus, an anisotropic damping.

In the framework of the Kamberský model and based on first-principles calculations, the Gilbert damping was detected as a non-local quantity. Using tight-binding Green function techniques, both magnetic disorder as well as layer-resolution, based on renormalization methods, were obtained. The Slater-Koster parametrization was fitted via a genetic algorithm to band structures obtained with a multiple-scattering KKR code.

The role of different contributions is analyzed in detail: the damping is guided from the equilibration of the excited population state back into the ground state. If there is no equilibrating-force (coupling to other reservoirs), the relaxation time is enlarged and transitions within degenerate electronic states (intra-band transition) become important. Contrary, if the electron reservoir correlates to other reservoirs, this equilibration will be accelerated by occupying bands of different energy (inter-band transition) and thus, the damping becomes larger. This indicates e.g. strong electron-phonon coupling Γ : for small Γ , the dissipation was found large and decreasing with stronger coupling up to a minimum, where the inter-band transitions become important. This trend was observed in both Fe and Co and verified by other first-principles methods [110], ensuring a correct modeling by the tight-binding theory. Using disordered local moment theory, a significant electron-spin coupling was also revealed that increases the damping with temperature. This agrees with the fluctuation-dissipation theorem: the stronger the fluctuations, the higher is the dissipation. The electron temperature, however, determines a large spectral overlap and, therefore, also faster relaxation.

Anisotropies occur always at surfaces and depend on the surface orientation. Renormalization allows to study layer-resolved dissipation, e.g. on various Co surfaces. Only small changes in the coordination number of the (100), (110) and (111)-surface indicate low energy dissipation variations. The anisotropy in dissipation accounts for an oscillating increase of the damping towards the surface. The highest damping on the topmost layer agrees again with the dissipation-fluctuation theorem and is due to a higher electron density at the Fermi surface than in the other layers. Moreover, a monotonic decrease of the damping parameter α_{0J} with the distance r_J was found, demonstrating a strong spatial retardation in the magnetization dynamics. More precisely, nutation will appear as a complex superposition of inertia and non-local energy dissipation.

Gilbert damping tensor within the breathing Fermi surface model: anisotropy and non-locality

D. Thonig^{1,2} and J. Henk²

¹ Max-Planck-Institut für Mikrostrukturphysik, Weinberg 2, D-06120 Halle (Saale), Germany

² Institut für Physik, Martin-Luther-Universität Halle-Wittenberg, D-06120 Halle (Saale), Germany

E-mail: dboettch@mpi-halle.de

Abstract. In magnetization dynamics, the Gilbert damping α is often taken as a parameter. We report on a theoretical investigation of α , taking into account crystal symmetries, spin-orbit coupling, and thermal reservoirs. The tensor α is calculated within the Kamberský breathing Fermi-surface model. The computations are performed within a tight-binding electronic structure approach for bulk and semi-infinite systems. Slater-Koster parameters are obtained by fitting the electronic structure to first-principles results obtained within multiple-scattering theory. We address the damping tensor for bulk and surfaces of the transition metals Fe and Co. The role of various contributions are investigated: intra- and interband transitions, electron and magnetic temperature as well as surface orientation. Our results reveal a complicated non-local, anisotropic damping that depends on all three thermal reservoirs.

PACS numbers: 75.10.Hk, 75.30.-m, 75.40.Mg

1. Introduction

Magnetic devices and magnetic reversal effects are strongly affected by their rate of energy transfer (dissipation): the larger this transfer, the faster is the magnetic equilibration. Regarding spintronics applications, there is an ongoing search for materials with preferably small damping [1]. The magnetization dynamics on a nanometer length scale and on a femtosecond time scale can be described by the Landau-Lifshitz-Gilbert equation [2]. Here, the dissipation is introduced by Gilbert's phenomenological parameter α [3] that includes all possible damping mechanisms. The damping parameter is taken as local and isotropic, in agreement with ferromagnetic resonance spectroscopy [4, 5].

The coupling of the magnetization to the electronic degrees of freedom is mediated by the spin-orbit coupling. Detailed measurements on the atomic scale as well as theoretical models for nanostructures reveal a non-uniform spin-orbit coupling [6] which is responsible for local magnetic anisotropies. Hence, the Gilbert damping should also be anisotropic and site-dependent, in particular in low-dimensional systems.

To calculate the damping constant from first principles Ebert et al. [7] suggest a model that shows good agreement with experiments. Based on linear response theory, their torque-torque correlation model was applied to an $\text{Fe}_{1-x}\text{Co}_x$ alloy and to various 5d transition metals. Thermal effects are included by phonon scattering in an alloy-analogy model.

Besides linear response theory, there exists also the breathing Fermi surface model of Kamberský [8, 9]. This model considers the non-equilibrium population of electronic states that is forced by the change of the magnetic moments. The coupling of the electronic spin to the electronic eigenstates is of spin-orbit nature. The model predicts a significant damping in metals with strong spin-orbit coupling, e.g. 4f metals. Also ultrathin films are predicted to exhibit strong damping [10].

The energy change near the Fermi surface of the Stoner magnets Fe and Co has been investigated by Gilmore et al. [11], using the Kamberský model in a projector augmented wave method. Although in good agreement with experimental findings, their results do not comply with those by Fähnle et al.: in [12] a dependence of the damping α on the magnetic moment's direction [13] as well as on temperature is established. The latter has been observed experimentally [14, 15] and confirmed theoretically [7, 10]. Furthermore, the damping can become anisotropic and non-local [16–18], leading to a damping tensor α_{ij} . The anisotropic and non-local character of the magnetic damping is also achievable within the Kamberský model.

In this paper we report on a theoretical investigation of the anisotropic and non-local Gilbert damping in the framework of the Kamberský model. To calculate the damping tensor, we use a tight-binding (TB) model. The tight-binding parameters have been obtained by fitting the electronic structures to those of a first-principles fully relativistic multiple scattering Korringa-Kohn-Rostoker (KKR) method using a genetic algorithm. Semi-infinite systems are treated by a renormalization scheme for the Green

function. These together with the generalized Kamberský equation allow to calculate the damping tensor layer- as well as temperature-resolved. We compare our results to published data for Fe and Co. The role of various contributions are analyzed in detail: electronic intra- and interband transitions, electron and magnetic temperature as well as surface orientation. Our results reveal a complicated non-local, anisotropic damping that depends on all three thermal reservoirs.

The paper is organized as follows. Computational details and theoretical basics are given in section 2. The damping properties of bulk magnets are discussed in section 3.1, for surfaces in section 3.2.

2. Theoretical and computational aspects

We consider a ferromagnetic system whose Bloch states, characterized by the band index n at wavevector \mathbf{k} , have energies $\varepsilon_{\mathbf{k},n}$. Due to the spin-orbit coupling, the magnetization \mathbf{m} with direction \mathbf{e} affects the eigenstates: Tilting \mathbf{m} by a small change $\delta\mathbf{e}$ generates a non-equilibrium population state which can be viewed as a deviation — or breathing — of the Fermi surface. The non-equilibrium distribution relaxes toward the equilibrium distribution within a time $\tau_{\mathbf{k},n}$ (relaxation time approximation). This relaxation is driven by the coupling Λ of the electron reservoir to the lattice reservoir, that is via electron-phonon coupling. Following Gilmore et al. [11], this breathing Fermi surface model of Kamberský [8,9] in a generalized form and within the isotropic relaxation time approximation ($\tau_{\mathbf{k},n} \rightarrow \tau$) results in the damping tensor α with elements

$$\alpha^{\nu\mu} = \frac{g\pi}{m} \sum_{n,m} \int \eta(\varepsilon_{\mathbf{k},n}) \left(\frac{\partial \varepsilon_{\mathbf{k},n}}{\partial \delta \mathbf{e}} \right)_{\nu} \left(\frac{\partial \varepsilon_{\mathbf{k},m}}{\partial \delta \mathbf{e}} \right)_{\mu} \frac{\tau}{\hbar} \frac{d\mathbf{k}}{(2\pi)^3} \quad \nu, \mu = x, y, z. \quad (1)$$

$\eta(\varepsilon_{\mathbf{k},n}) = \left. \frac{\partial f(\varepsilon)}{\partial \varepsilon} \right|_{\varepsilon_{\mathbf{k},n}}$ is the derivative of the Fermi-Dirac distribution $f(\varepsilon)$ with respect to the energy; n and m are band indices.

The spin-orbit coupling \hat{H}_{so} correlates the magnetization with the electronic ground state, giving rise to the magnetocrystalline anisotropy. Hence, the torque matrix elements $\left(\frac{\partial \varepsilon_{\mathbf{k},n}}{\partial \delta \mathbf{e}} \right)_{\nu}$ can be obtained from $\varepsilon(\delta\mathbf{e}) = \langle n, \mathbf{k} | e^{i\boldsymbol{\sigma} \cdot \delta\mathbf{e}} \hat{H}_{\text{so}}(\mathbf{e}) e^{-i\boldsymbol{\sigma} \cdot \delta\mathbf{e}} | m, \mathbf{k} \rangle$, where $|n, \mathbf{k}\rangle$ are the eigenstates of the Hamiltonian \hat{H} and $\boldsymbol{\sigma}$ is the vector of Pauli matrices. With $\Gamma_{nm} \equiv \langle n, \mathbf{k} | [\boldsymbol{\sigma}, \hat{H}_{\text{so}}] | m, \mathbf{k} \rangle$, which accounts for the transitions between the states in band n and m , the damping tensor $\alpha^{\mu\nu}$ reads

$$\alpha^{\nu\mu} = \frac{g\pi}{m} \sum_{n,m} \int \Gamma_{nm}^{\nu} \Gamma_{nm}^{\mu} W_{nm}(\mathbf{k}) \frac{d\mathbf{k}}{(2\pi)^3}. \quad (2)$$

The scattering events depend on the overlap $W_{nm}(\mathbf{k}) \equiv \int d\varepsilon \eta(\varepsilon) A_{\Lambda}^{\mathbf{k},n}(\varepsilon) A_{\Lambda}^{\mathbf{k},m}(\varepsilon)$ of the spectral function $A_{\Lambda}^{\mathbf{k},n}$, which is a Lorentzian centered at $\varepsilon_{\mathbf{k},n}$. Its width is determined by the coupling strength Λ to the lattice. Replacing the Bloch states by the Green function, the spectral function can be written as $\text{Im} \hat{G}(\mathbf{k}, \varepsilon \pm i\Lambda) = \mp \sum_n |n\rangle \langle n| A_{\Lambda}(\varepsilon - \varepsilon_{\mathbf{k},n})$. Hence, we end up with a result similar to the torque-torque-correlation model [7],

$$\alpha^{\nu\mu} = \frac{g}{m\pi} \int \int \eta(\varepsilon) \text{Tr} \left(\hat{T}^{\nu} \text{Im} \hat{G} \hat{T}^{\mu} \text{Im} \hat{G} \right) \frac{d\mathbf{k}}{(2\pi)^3} d\varepsilon, \quad (3)$$

	Fe	Co		Fe	Co
ε_s	6.006	5.322	$(ss\sigma)$	-1.494	-1.144
ε_p	12.658	14.000	$(sp\sigma)$	-2.035	-1.708
ε_{t2g}	-0.853	-1.389	$(sd\sigma)$	0.769	0.435
ε_{eg}	-0.955	-1.402	$(pp\sigma)$	2.901	3.113
λ_p	0.200	0.100	$(pp\pi)$	-0.112	-0.204
λ_d	0.080	0.070	$(pd\sigma)$	-0.903	-0.233
B_s	0.436	-0.329	$(pd\pi)$	0.303	0.510
B_p	0.793	-1.237	$(dd\sigma)$	-0.623	-0.515
B_{t2g}	2.069	1.572	$(dd\pi)$	0.412	0.387
B_{eg}	2.034	1.526	$(dd\delta)$	-0.066	0.093

Table 1. Tight-binding parameters for bulk bcc Fe and fcc Co, obtained from a genetic algorithm. The notation follows that of Slater and Koster [20] for the on-site energies ε (left) and hopping parameters (right). λ and B stand for orbital-dependent spin-orbit coupling strength and exchange splitting, respectively.

where $\hat{\mathbf{T}} \equiv [\boldsymbol{\sigma}, \hat{H}_{so}]$.

To obtain the Green function, we use a tight-binding model [19] based on the Slater-Koster parameterization [20,21]. The tight-binding parameters, including the spin-orbit coupling strength, are obtained by fitting the tight-binding band structures to *ab initio* band structures, using a genetic algorithm [22] (table 1). The fitness function is taken from [23], with an accuracy better than 10^{-4} eV. The parameters are in good agreement with those reported in Refs. [24–26]. The first-principles band structures were calculated within a fully relativistic multiple-scattering Green function approach (Korringa-Kohn-Rostoker method [KKR]) [27].

Having a reliable tight-binding description of the bulk electronic structure at hand, we proceed by computing the electronic structure of a semi-infinite system, using a renormalization scheme [28,29]. The result is the layer- and site-resolved Green function, with site i in layer n indexed as $I \equiv (n, i)$. This allows to define the layer- and site-resolved damping tensor by:

$$\alpha_{IJ}^{\nu\mu} = \frac{g}{m\pi} \int \eta(\varepsilon) \text{Tr} \left(\hat{T}_n^\nu \text{Im} \hat{G}_{IJ} \hat{T}_m^\mu \text{Im} \hat{G}_{JI} \right) d\varepsilon, \quad I \neq J. \quad (4)$$

We perform a fifth-order Keast quadrature method in the first Brillouin zone \mathbf{k} integration with up to 10^5 mesh points for bulk and 10^6 mesh points for surface calculations. For small Λ (less than about $5 \cdot 10^{-3}$ eV), these dense meshes are necessary to suppress spurious non-zero off-diagonal elements of the damping tensor which in principle should vanish to the cubic symmetry in bulk systems. The energy integration is approximated by a Gauss-Legendre quadrature with 32 supporting points in a small energy range around the Fermi level.

Various components of the entire system contribute to α due to different relaxation processes. This is qualitatively described by three separate but coupled reservoirs:

the magnetic moments, the lattice, and the electrons [30, 31], assuming the adiabatic limit. The electron temperature T_e is modeled by the width of the Fermi distribution, whereas the temperature of the magnetic system, the spin temperature T_s , is mimicked within the disordered local moment theory which is based on the coherent potential approximation (CPA) [32, 33]. For the time being, the electron-phonon coupling is set constant. The above tensorial representation yields furthermore the dependence of the Gilbert damping on the magnetization direction, $\boldsymbol{\alpha}_{IJ} = \boldsymbol{\alpha}_{IJ}(\mathbf{e})$, which is mediated by the spin-orbit coupling.

The calculated Gilbert damping is used in an atomistic formulation of the Landau-Lifshitz-Gilbert equation [2, 3, 34]. The temporal evolution of the magnetic moment \mathbf{m}_i at site i reads [16, 17]

$$\frac{\partial \mathbf{m}_i}{\partial t} = \mathbf{m}_i \times \left(-\gamma \mathbf{B}_i + \sum_j \frac{1}{|\mathbf{m}_j|} \alpha_{i,j} \frac{\partial \mathbf{m}_j}{\partial t} \right) \quad (5)$$

The effective field $\mathbf{B}_i = \partial \hat{H}_{\text{mag}} / \partial \mathbf{m}_i$ is fixed by the Hamiltonian \hat{H}_{mag} which comprises the Heisenberg exchange interaction, the dipole-dipole energy, the magnetocrystalline anisotropy and a Zeemann term. Explicitly,

$$\hat{H}_{\text{mag}} = - \sum_{ij} \mathbf{m}_i \mathbf{l}_{ij} \mathbf{m}_j + \sum_i \mathbf{B}_{\text{ext}} \cdot \mathbf{m}_i. \quad (6)$$

$\mathbf{l}_{ij} = J_{ij} \mathbf{E} + \mathbf{Q}_{ij}$ for $i \neq j$ contains the Heisenberg exchange parameter J_{ij} and the dipolar interaction matrix $Q_{ij}^{\nu\mu} = \frac{1}{2} \frac{\mu_0}{4\pi} \frac{3r_{ij}^\nu r_{ij}^\mu - r_{ij}^2 \delta^{\nu\mu}}{r_{ij}^5}$ between to sites i and j with distance $\mathbf{r}_{ij} = \mathbf{r}_i - \mathbf{r}_j$. \mathbf{E} is the unit matrix. \mathbf{l}_{ii} determines the magnetocrystalline anisotropy. The Heisenberg exchange interactions J_{ij} as well as the anisotropies \mathbf{l}_{ii} have been calculated from first principles within the KKR framework, using the Lichtenstein formula [35] and the magnetic force theorem [27]; for details see [36].

3. Results and discussion

3.1. Damping constant of bulk materials

In this section, we first address the two approaches to α , (1) and (3), and compare our tight-binding data to the *ab initio* results reported in [11]. We assume a ferromagnetically ordered system with magnetic moments in \mathbf{e}_z direction. Tilting a magnetic moment toward \mathbf{e}_x or \mathbf{e}_y yields an effective torque matrix element $T^- \equiv \langle n, \mathbf{k} | [\sigma^-, \hat{H}_{\text{so}}] | m, \mathbf{k} \rangle$, where $\sigma^- \equiv \sigma^x - i\sigma^y$. The cubic symmetry in bulk bcc Fe and fcc Co dictates that the damping tensor is diagonal, in agreement with our calculations. The damping constant α is given then by the trace of the damping tensor $\boldsymbol{\alpha}$ for the reference magnetization direction \mathbf{e}_z ($\alpha = \alpha^{xx} + \alpha^{yy}$) [11].

The reliability of our tight-binding parameterization is proven by the agreement of the damping constant α with those reported in [11] (figure 1). For comparison, the tight-binding damping constants have to be scaled by a factor of $1/4\pi^2$, which we attribute to a different definition of the Lorentzian in [11].

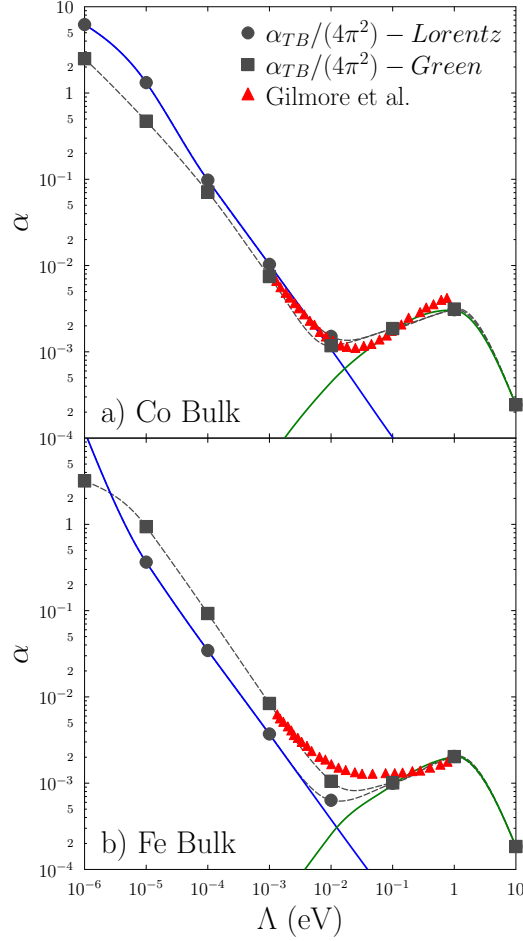


Figure 1. Calculated bulk Gilbert damping constant α versus phonon coupling strength Λ for Co (a, top) and Fe (b, bottom), in logarithmic scale. The results obtained by our tight-binding method base on Lorentz broadening (black circles) or on Green functions (black triangles). The curvature close to the minima is a superposition of inter- (green line) and intraband (blue line) transitions; the latter vanish for large Λ . Data reproduced from [11] (‘Gilmore et al.’) are presented as red triangles. The dotted lines are guides to the eye.

For large electron-phonon coupling Λ , α decreases, which is interpreted as follows. α comprises both intraband transitions ($n = m$ in (2); blue line in figure 1) and interband transitions ($n \neq m$; green line in figure 1) [11]. For small Λ , the intraband transitions play a major role and $\alpha^{\text{intra}}(\Lambda)$ can be approximated linear. For large Λ , the broad Lorentzians lead to an increase of the interband contribution which eventually dominates the intraband contribution. For even larger Λ , the Gilbert damping drops again, resulting in the maximum at $\Lambda \approx 1$. However, this is an artifact of the finite orbital basis in the tight-binding approach which does not describe well electronic states far off the Fermi level (at ≈ 10 eV). Nevertheless, the approach reproduces the *ab initio* results of [11] in the range $\Lambda \in [0.001, 1]$ well.

In the ‘Lorentz’ approach (2), the coupling Λ defines the width of the energy window in which transitions Γ_{nm} are accounted for; the electronic structure itself is unaffected. In the Green function approach, Λ is taken as the imaginary part of the energy at which the Green functions is evaluated. This offset from the real energy axis provides a more accurate description with respect to the *ab initio* results [11] than the Lorentzian approach, in particular for Fe. This may be understood from the fact that a finite Λ broadens and shifts maxima in the spectral function; hence, electronic states at energies around the Fermi level that are weakly weighted by $\eta(\varepsilon)$ contribute to the damping. Furthermore, their contribution depends on their orbital composition and on the strength of the spin-orbit coupling.

We now discuss the dependence of α on the reservoir temperatures and focus first on the spin temperature T_s . The dependence of α on the magnetic moment direction \mathbf{e} , on the electron-phonon coupling Λ as well as on transitions involving energetically lower states suggests a correlation between the spin-, the lattice-, and the electron temperature [37]. The spin temperature T_s is modeled within the disordered local moment (DLM) theory [38, 39]. This approach is based on a substitutional binary alloy that is described within the coherent potential approximation (CPA) [32, 33, 40]; the host material comprises sites with magnetization along the reference direction \mathbf{e} , with concentration c_\uparrow , and sites with magnetization along $-\mathbf{e}$, with concentration $c_\downarrow = 1 - c_\uparrow$ [41] (figure 2). Zero spin temperature is obtained for $c_\uparrow = 1.0$ (ferromagnetic case), whereas the critical temperature is given for $c_\uparrow = 0.5$ (paramagnetic case). The mapping of the impurity concentration on the spin temperature can be obtained by comparing magnetizations derived from DLM electronic-structure calculations and from temperature-dependent Monte Carlo calculations [41, 42].

The dependence of α on the spin temperature (figure 2) is in agreement with the dissipation-fluctuation theorem which states, roughly speaking, that the dissipative reaction of the system is proportional to the fluctuation. Here, the electron system tries to stabilize the magnetic order with increasing T_s (that is increasing magnetic fluctuations or decreasing concentration) by increasing the Gilbert damping which models the dissipation. The sizable change of α with concentration suggests that a constant α may be inappropriate for modeling magnetic systems at elevated temperatures, for example using the Landau-Lifshitz-Gilbert equation.

We now turn to the dependence of α on the electron temperature T_e . The electron temperature is included via η in (1) and accounts for transitions between states in a narrow energy window above the Fermi level. An electron-hole pair relaxes faster from the non-equilibrium population (which is induced by the spin-orbit coupling) towards the equilibrium than in the zero temperature case; thus, α decreases with decreasing relaxation time τ . This mechanism is contrasted by the fact that more electronic states around the Fermi level are involved in the relaxation process, leading to an increase of α . Hence, the Kamberský model postulates a competition between these two mechanisms (figure 3).

We limit the dependence of α on the electron temperature by the energy window

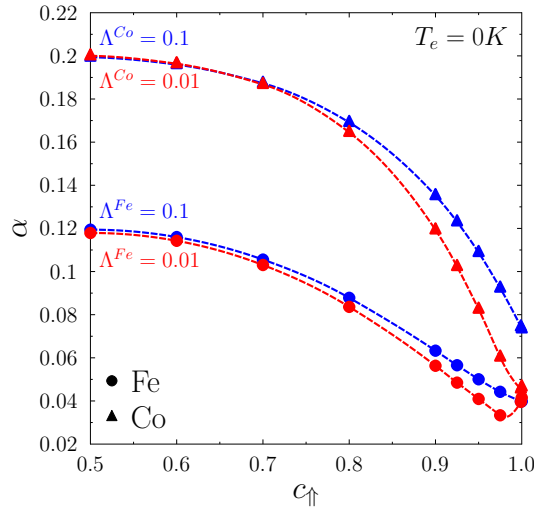


Figure 2. Damping constant α versus spin temperature T_s for bulk Co (triangles) and Fe (circles), as modeled by the concentration c_{\uparrow} in the disordered local moment theory (see text). The concentration is inversely proportional to the temperature [41]. Data for electron-phonon coupling $\Lambda = 0.1$ eV (0.01 eV) are displayed in blue (red). The electron temperature T_e is zero. Lines serve as guides to the eye.

around the Fermi level ε_F to $\varepsilon_{\text{cut}} = 0.01$ eV, 0.1 eV, and 1.0 eV (figure 3). For a large energy window of $\varepsilon_{\text{cut}} = 1$ eV, $\alpha(T_e)$ increases non-linearly with electron temperature; a similar trend is found for the magnetic temperature T_s . This finding is explained by the large spectral overlap W_{nm} (figure 3a): W_{nm} is constrained by the derivative η of the Fermi-Dirac distribution. The higher the temperature, the larger is the spectral overlap (color shaded areas in figure 3a) and therefore, α increases. If ε_{cut} is smaller than the underlying range of the Fermi-Dirac distribution, α decreases with temperature.

The electron-phonon coupling is, at present, roughly modeled by a constant Λ . Phonons can be included via the spatial dependence of the tight-binding parameters, for example using Harrison's law [21] or by a polynomial representation [43]. In particular the latter reproduces well phonon dispersions. The atomic displacements change the electronic structure around the Fermi level and remove degeneracies in the band structure; thus, the accompanying decrease of contributions from intraband transitions will reduce α [7]. In addition, electron-magnon scattering or the Elliott-Yafet-type spin scattering mechanism could be included [44].

The damping tensor (1) motivated in [12, 13] accounts for transitions between states with different reference spin direction and, thus, also for spin-flip transitions. For cubic symmetry, the damping tensor is diagonal. In contrast to bulk system, off-diagonal elements could be nonzero in systems with reduced symmetry, for example at surfaces.

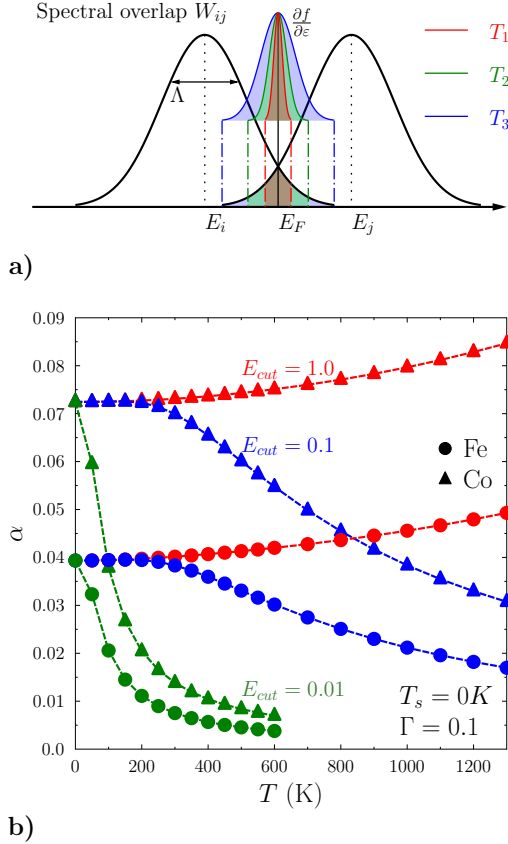


Figure 3. a) Illustration of the spectral overlap contribution between electronic state i and j for temperatures $T_1 < T_2 < T_3$. With increasing temperature the relevant energy window around the Fermi energy E_F becomes larger, leading to an increased Gilbert damping α . b) α versus electron temperature T_e for a fixed electron-phonon coupling $\Lambda = 0.1$ for Co (triangles) and Fe (circles). Energy cut-offs are distinguished by colors: $\varepsilon_{\text{cut}} = 0.01$ eV green, 0.1 eV blue, and 1.0 eV red. The spin temperature T_s is zero. Lines serve as guides to the eye.

3.2. Damping tensor at surfaces

In the following, we address the electronic contribution to the damping tensor α at surfaces. As examples, we focus on (001), (110) and (111) surfaces of fcc-Co with Cu lattice constant 3.54 \AA , addressing thus thick Co films on Cu surfaces.

The Rayleigh dissipation functional predicts energy transfer between neighboring sites $I \neq J$ [45,46]. Hence, the energy transfer rate has to be considered as a non-local, rather than as a local (on-site) quantity [3]. In contrast, on-site contributions account for a local coupling to the lattice reservoir (phonons). To simplify the discussion, we define a shell-averaged damping tensor $\alpha(r)$ by considering a reference site i_0 in layer n_0 ($I_0 = (n_0, i_0)$) and summing up contributions from all sites j in layer m ($m \neq n_0$ and $j \neq i_0$) that are located on a sphere with radius r (figure 4).

For all three surfaces, the energy transfer is short-ranged, as is evident from the

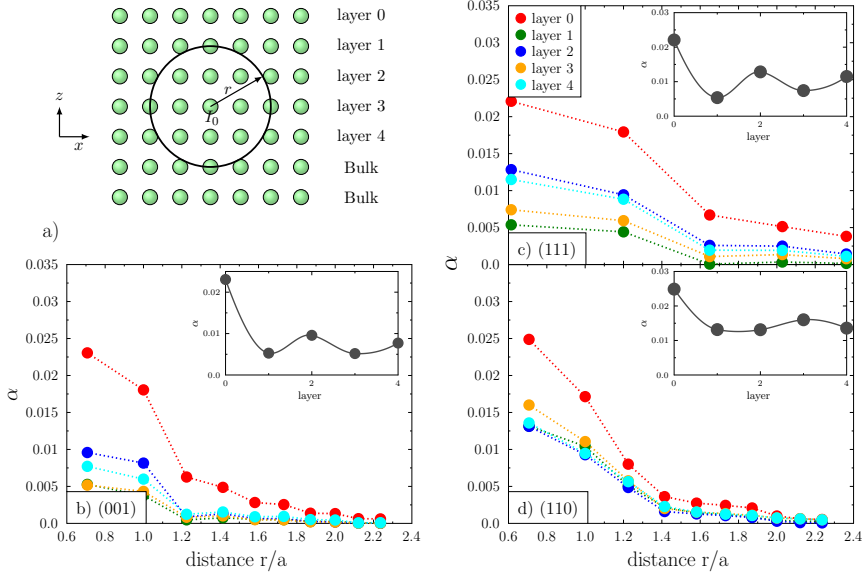


Figure 4. a) Schematic view of the summation method in a cubic lattice to obtain $\alpha(r)$. For a given r all atoms are account for that are located on the circle. b) — d) Layer-resolved non-local damping constant for different Co surfaces: b) (001), c) (110) and d) (111). The electron-phonon coupling Λ is 0.01 eV. The non-local character of the damping within the layers disappears within few nanometer distance; in contrast, a non-monotonic decrease of the damping constant with respect to the layer index is observed (layers are distinguished by colors). The damping does not depend significantly on the surface orientation.

decrease of α with distance r (figure 4). The damping depends also on the surface orientation: the nearest-neighbor α 's differ slightly ($\alpha_{NN,I_0}^{(001)} = 0.023$, $\alpha_{NN,I_0}^{(110)} = 0.025$, and $\alpha_{NN,I_0}^{(111)} = 0.022$), as can be explained qualitatively by the coordination numbers of site I_0 (8, 7, and 9 for (001), (110), and (111), respectively). If only nearest-neighbor hopping would be considered, a reduced coordination yields a small electron hopping probability (small band width), resulting in both a minute energy transfer and damping constant.

α decreases with layer index (inset in figure 4). The topmost layer shows the largest dissipation for all three surfaces, which is in accordance with the fluctuation-dissipation theorem. NB: in the Landau-Lifshitz-Gilbert equation, the fluctuation amplitude (that is the width of the Gaussian distribution of the random magnetic field [2]) reads $\alpha \cdot k_B T / \gamma m$; hence, the response at a temperature T is stronger at the surface than in the bulk. The dependence of α on the layer index is non-monotonous and exhibits oscillations; this finding is at variance with results reported in [47] but agrees with those in [16,17]. The oscillations can be explained by the density of states of the d states which ‘carry’ the magnetic moment of Co.

The density of states of d orbitals at the Fermi level is largest for the surface layer (figure 5). It oscillates similarly to α ; this coincidence has been already noticed

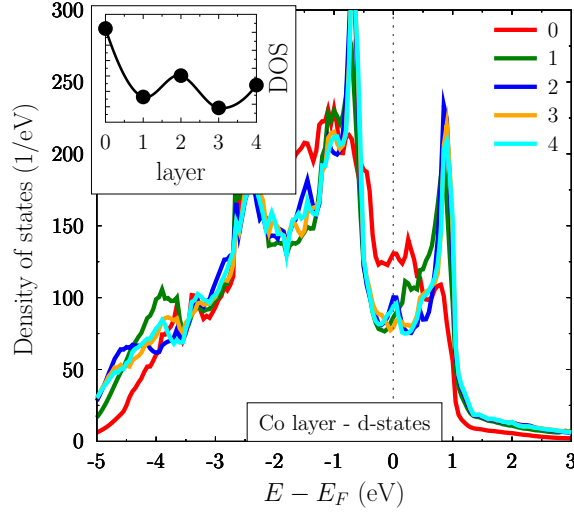


Figure 5. Layer-resolved density of states (DOS) of d states in fcc Co(001). Layers are marked by different colors; the topmost layer is 0. The Fermi level is depicted as dotted line. The inset shows the DOS at the Fermi level versus layer index (top surface layer $n = 0$).

in [7] and [48]. The oscillations are explained by the behavior of t_{2g} and e_g states: the DOS $n_{t_{2g}}(\varepsilon_F)$ decreases monotonically with layer index but $n_{e_g}(\varepsilon_F)$ shows an oscillatory behavior.

Eventually, we address how the non-locality of the Gilbert damping α_{ij} affects the magnetization dynamics in different layers, using (5). The non-locality is relevant in an incoherent magnetic configuration, e.g. in demagnetization processes [48] or in nutation [49]; in case of a coherent precession of the magnetic moments, the sum in (5) can be replaced by an effective constant $\alpha_i^{\text{eff}} = \sum_j \alpha_{ij}$ [10]. We discuss its effect for the nutation in a 2-layer thick Co film on Cu(111) [49]. Here, we include $\alpha(r)$ from Co(111) up to third-nearest neighbors (figure 6).

An initial incoherent state is prepared by perturbing randomly the coherent precession around the anisotropy field at time $t = 0$. Then, an external magnetic field with a strength of $B = 5$ T is abruptly switched on. We study three cases: accounting for (i) the non-local α_{ij} , (ii) an effective α by summing over the distances r , and (iii) an effective α by summing over distance r but weighted with the respective coordination numbers.

Both the nutation lifetime and the amplitude are reduced with higher damping, which supports the proportionality of the moment of inertia and the damping [50]. Case (ii) exhibits the smallest damping and, thus, a larger duration of the nutation. For case (i) the energy transfer to the neighboring sites accelerates the relaxation process compared to the other two cases.

A coherent precession of all magnetic moments (figure 6a) gives a small phase shift (up to 10 fs), which is due to the direct coupling to the inert motion of site j . In an incoherent state, the evolution of j appears as a superimposed ‘noisy signal’ (red

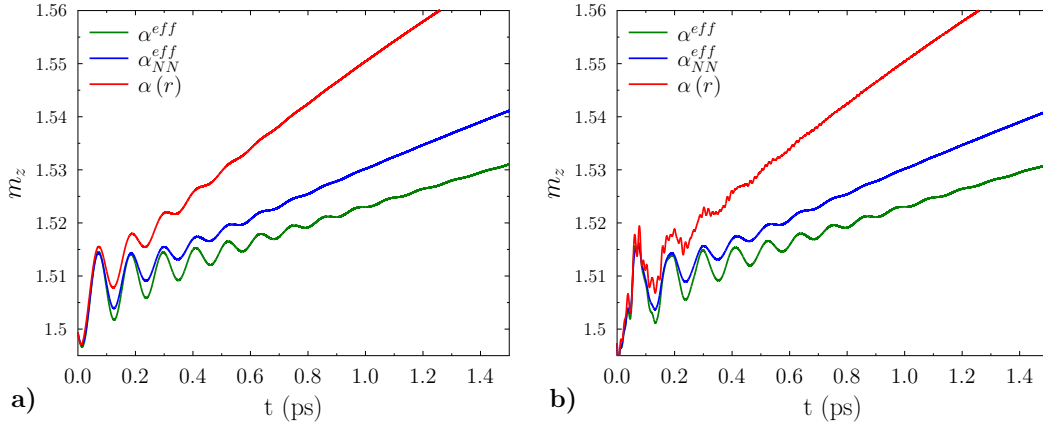


Figure 6. Nutation of a surface magnetic moment in a two layer thick Co film on Cu(111) of a) a coherent and b) a non-coherent spin state. m_z is shown versus time for different damping scenarios: considering the non-local α_{ij} (red); effective α integrated over the distance r (green, 0.083 for the surface and 0.021 for the subsurface layer), and effective α integrated over r and weighted by the coordination number (blue, 0.12 for the surface and 0.028 for the subsurface layer).

in figure 6b). According to the angular-momentum transfer present in the Heisenberg model, the energy transfer depends to the coordination: the higher the coordination number, the faster is the relaxation. We conclude that anisotropic dissipation is advantageous in relaxation and switching processes in magnetic nanostructures.

4. Conclusion

We present a calculational method to obtain the Gilbert damping tensor based on the breathing Fermi-surface model. Within a tight-binding approach the layer-dependence of the damping has been obtained. The non-local dissipation rate depends mildly on the surface orientation but strongly on the layer and on the distance to neighboring sites. In the tensor representation, the correlation to the reference magnetization results in a non-homogeneous dissipation, which suggests to consider the dependence of the Gilbert damping on the direction of the magnetic moments in future magnetization dynamics simulations.

We also studied the dependence of the Gilbert damping constant on the electron and spin temperatures. The damping increases with temperatures, in contrast to experimental observations; this finding supports that the phonon temperature is the major thermal contribution. The present comparably simple approximation of the electron-phonon coupling has to be improved in a future implementation. Nevertheless, also the spin- as well as the electron temperature should be considered in incoherent magnetization effects.

5. Acknowledgments

This work is supported by the *Sonderforschungsbereich* 762 ‘Functionality of Oxide Interfaces’. DT is a member of the International Max Planck Research School on Science and Technology of Nanostructures, Halle, Germany.

References

- [1] C. Liu, C. Mewes, M. Chshiev, T. Mewes, and W. H. Butler. Origin of low Gilbert damping in half metals. *Appl. Phys. Lett.*, 95:022509, 2009.
- [2] B. Skubic, J. Hellsvik, L. Nordström, and O. Eriksson. A method for atomistic spin dynamics simulations: Implementation and examples. *J. Phys.: Condens. Matt.*, 20:315203, 2008.
- [3] T. L. Gilbert. A phenomenological theory of damping in ferromagnetic materials. *IEEE Transact. Magn.*, 40:6, 2004.
- [4] G. D. Fuchs, J. C. Sankey, V.S. Pribiag, L. Qian, P. M. Braganca, A. G. F. Garcia, E. M. Ryan, Zhi-Pan Li, O. Ozatay, D. C. Ralph, and R. A. Buhrman. Spin-torque ferromagnetic resonance measurements of damping in nanomagnets. *Appl. Phys. Lett.*, 91:062507, 2007.
- [5] M. Oogane, T. Wakitani, S. Yakata, R. Yilgin, Y. Ando, A. Sakuma, and T. Miyazaki. Magnetic damping in ferromagnetic thin films. *Jap. J. Appl. Phys.*, 45:3889–3891, 2006.
- [6] C. Etz, M. Costa, O. Eriksson, and A. Bergman. Accelerating the switching of magnetic nanoclusters by anisotropy-driven magnetization dynamics. *Phys. Rev. B*, 86:224401, 2012.
- [7] H. Ebert, S. Mankovsky, D. Ködderitzsch, and J. P. Kelly. Ab-initio calculation of the Gilbert damping parameter via linear response formalism. *Phys. Rev. Lett.*, 107:066603, 2011.
- [8] J. Kuneš and V. Kamborský. First-principles investigation of the damping of fast magnetization precession in ferromagnetic 3d metals. *Phys. Rev. B*, 65:212411, 2002.
- [9] V. Kamborský. *Czechoslovak Journal of Physics, Section B*, 34:1111, 1984.
- [10] S. Mankovsky, D. Ködderitzsch, G. Woltersdorf, and H. Ebert. First-principles calculation of the Gilbert damping parameter via the linear response formalism with application to magnetic transition-metals and alloys. *arXiv:1301.2114v1 [cond-mat.other]*, 2013.
- [11] K. Gilmore, Y. U. Idzerda, and M. D. Stiles. Identification of the dominant precession-damping mechanism in Fe, Co, and Ni by first-principles calculations. *Phys. Rev. Lett.*, 99(2):027204, Jul 2007.
- [12] M. Fähnle and D. Steiauf. Breathing Fermi surface model for noncollinear magnetization: A generalization of the Gilbert equation. *Phys. Rev. B*, 73:184427, 2006.
- [13] D. Steiauf and M. Fähnle. Damping of spin dynamics in nanostructures: An *ab initio* study. *Phys. Rev. B*, 72:064450, 2005.
- [14] S. M. Bhagat and P. Lubitz. Temperature variation of ferromagnetic relaxation in the 3d transition metals. *Phys. Rev. B*, 10:179–185, 1974.
- [15] B. Heinrich and Z. Frait. Temperature dependence of the FMR linewidth of iron single crystal platelets. *Phys. Stat. Sol.*, 23:26–27, 1966.
- [16] N. Umetsu, D. Miura, and A. Sakuma. Theoretical study on Gilbert damping of nonuniform magnetization precession in ferromagnetic metals. *Journal of the Physical Society of Japan*, 81:114716, 2012.
- [17] Y. Brataas, A. Tserkovnyak and G. Bauer. Magnetization dissipation in ferromagnets from scattering theory. *Phys. Rev. B*, 84:054416, 2011.
- [18] C. Vittoria, S. D. Yoon, and A. Widom. Relaxation mechanism for ordered magnetic materials. *Phys. Rev. B*, 81:014412, 2010.
- [19] A. T. Paxton, J. Grotendorst, N. Attig, S. Blügel, and D. Marx. An introduction to the tight binding approximation - implementation by diagonalization. *Multiscale Simulation Methods in Molecular Science*, 42:145–176, 2009.

- [20] J. C. Slater and G. F. Koster. Simplified LCAO method for the periodic potential problem. *Phys. Rev.*, 94:1498–1524, 1954.
- [21] W. A. Harrison. *Electronic Structure and the Properties of Solids*. W. H. Freeman, San Francisco, 1980.
- [22] D. E. Goldberg. *Genetic Algorithms in Search, Optimization, and Machine Learning*. Addison-Wesley, 1989.
- [23] F. Starrost, S. Bornholdt, C. Solterbeck, and W. Schattke. Band-structure parameters by genetic algorithm. *Phys. Rev. B*, 53:12549, 1996.
- [24] W. Zhong, G. Overney, and D. Tománek. Structural properties of Fe crystal. *Phys. Rev. B*, 47:1, 1993.
- [25] G. Liu, D. Nguyen-Manh, B. G. Liu, and D. G. Pettifor. Magnetic properties of point defects in iron within the tight-binding-bond stoner model. *Phys. Rev. B*, 71:174115, 2005.
- [26] M. Okutani and T. Jo. Orbital magnetic moment in superlattices of transition metals. *Journal of the Physical Society of Japan*, 69:598–606, 2000.
- [27] J. Zabludil, R. Hammerling, L. Szunyogh, and P. Weinberger. *Electron Scattering in Solid Matter*. Springer, Berlin, 2005.
- [28] J. Henk and W. Schattke. A subroutine package for computing Green’s functions of relaxed surfaces by the renormalization method. *Comp. Phys. Commun.*, 77:69, 1993.
- [29] A. Bödicker, W. Schattke, J. Henk, and R. Feder. Interface electronic structure by the renormalization method: Theory and application to Sb/GaAs. *J. Phys.: Condens. Matter.*, 6:1927, 1994.
- [30] M. B. Agranat, S. I. Ashitkov, and A. B. Granovskii. Interaction of picosecond laser pulse with the electron, spin, phonon subsystems of nickel. *Zh. Eksp. Teor. Fiz.*, 86:1376–1379, 1984.
- [31] A. Kirilyuk, A. V. Kimel, and T. Rasing. Ultrafast optical manipulation of magnetic order. *Rev. Mod. Phys.*, 82:2731, 2010.
- [32] P.M. Laufer and D. A. Papaconstantopoulos. Tight-binding coherent-potential-approximation study of the electronic states of palladium-noble-metal alloys. *Phys. Rev. B*, 35:17, 1987.
- [33] J. A. Blackman and D. M. Esterling. Generalized locator-coherent-potential approach to binary alloys. *Phys. Rev. B*, 4:8, 1971.
- [34] L. D. Landau and E. M. Lifshitz. Theory of dispersion of magnetic permeability in ferromagnetic bodies. *Phys. Z. Sowjetunion*, 8:153, 1935.
- [35] A. I. Liechtenstein, M. I. Katsnelson, V. P. Antropov, and V. A. Gubanov. Local spin density functional approach to the theory of exchange interactions in ferromagnetic metals and alloys. *J. Magn. Magn. Mater.*, 67:65, 1987.
- [36] D. Böttcher. Theoretische Beschreibung der Magnetisierungsdynamik von Nanostrukturen. Master’s thesis, Martin-Luther-University Halle-Wittenberg, 2010.
- [37] A. Kirilyuk, A. V. Kimel, and T. Rasing. Laser-induced magnetization dynamics and reversal in ferrimagnetic alloy. *Rep. Prog. Phys.*, 76:026501, 2013.
- [38] J. Staunton, B. L. Gyorffy, A. J. Pindor, G. M. Stocks, and H. Winter. The “Disordered Local Moment” Picture of Itinerant Magnetism at Finite Temperatures. *J. Magn. Magn. Mater.*, 45:15–22, 1984.
- [39] B L Gyorffy, A J Pindor, J Staunton, G M Stocks, and H Winter. A first-principles theory of ferromagnetic phase transitions in metals. *J. Phys. F: Met. Phys.*, 15(6):1337–1386, 1985.
- [40] J. S. Faulkner. Scattering theory and cluster calculations. *J. Phys. C: Sol. State Phys.*, 10:4661, 1977.
- [41] D. Böttcher, A. Ernst, and J. Henk. Temperature-dependent Heisenberg exchange coupling constants from linking electronic-structure calculations and Monte Carlo simulations. *J. Magn. Magn. Mater.*, 324:610, 2012.
- [42] K. Binder, editor. *Monte Carlo Methods in Statistical Physics*. Springer, Berlin, 1979.
- [43] D. A. Papaconstantopoulos and M. J. Mehl. The Slater-Koster tight-binding method: A computationally efficient and accurate approach. *J. Phys.: Condens. Matter.*, 15:R413, 2003.

- [44] V. Kamberský. Spin-orbital Gilbert damping in common magnetic metals. *Phys. Rev. B*, 76:134416, 2007.
- [45] B. Torby. *Energy method: Advanced Dynamics for Engineers*. HRW Series in Mechanical Engineering. United States of America: CBS College Publishing, 1984.
- [46] L. Meirovitch. *Methods of Analytical Dynamics*. MacGraw-Hill Book Company, New York, 1970.
- [47] E. Barati, M. Cinal, D. M. Edwards, and A. Umerski. Calculation of gilbert damping in ferromagnetic films. *EPJ Web of Conferences*, 40:18003, 2013.
- [48] A. Mann, J. Walowski, M. Münzenberg, S. Maat, M. J. Carey, J. R. Childress, C. Mewes, D. Ebke, V. Drewello, G. Reiss, and A. Thomas. Insights into ultrafast demagnetization in pseudogap half-metals. *Phys. Rev. X*, 2:041008, 2012.
- [49] D. Böttcher and J. Henk. Significance of nutation in magnetization dynamics of nanostructures. *Phys. Rev. B*, 86:020404, 2012.
- [50] M.-C. Ciornei, J.M. Rubi, and J.-E. Wegrowe. Magnetization dynamics in the inertial regime: Nutation predicted at short time scales. *Phys. Rev. B*, 83:020410, 2011.

4.4 Nutation in magnetic nanostructures

Below the adiabatic limit, where the timescale of magnetic precession is of the same order as the electron equilibration, the magnetization reacts inert to perturbations. The time scale, where this phenomenon appears, is of the order of the magnetic exchange (from $E = \hbar/\tau$ follows $10 \text{ eV} \approx 65 \text{ fs}$). The dynamics of the magnetic moment becomes similar to that of a gyroscope that introduces the moment of inertia in its equation of motion. The resulting nutation, however, has not been proved experimentally. Hence, the question about the conditions of appearing magnetic nutation arises. In this paper, the extended Landau-Lifshitz-Gilbert equation is applied. The extension results from the mesoscopic non-equilibrium thermodynamics and postulates the inertia as the second time-derivative of the magnetic moment.

The significance of nutation in magnetization dynamics of nanostructures was studied for a single magnetic moment, an Fe chain, and 2ML thick Co islands on Cu(111). In process, a single magnetic moment still shows nutation under unphysical conditions, such as strong external magnetic fields. The main impact of nutation is the emergence of angular momentum transfer, described by the Heisenberg model, as it is demonstrated for Fe chains and nanoislands. Due to the reduced coordination, the cycloid (nutation) amplitude at rim sites is larger than in the center of the nanostructures, but due to angular momentum conservation law the inertia signal does not have any influence to the average magnetic moment. Gilbert damping α , in addition, reduces the magnitude and, thus, the nutation life time, which is estimated to be $100 - 500 \text{ fs}$. Nutation owed to temperature is describable as a time retardation effect, replacing the commonly used white noise by a colored thermal noise modeled with the Landau-Lifshitz-Miyazaki-Seki equation (studied in a post processing - figure 2.3.3; not shown in the following paper). This postulates the existence of nutation still present at small finite temperatures ($T \leq 1 \text{ K}$).

Significance of nutation in magnetization dynamics of nanostructures

D. Böttcher^{1,2,*} and J. Henk²

¹Max-Planck-Institut für Mikrostrukturphysik, Weinberg 2, D-06120 Halle (Saale), Germany

²Institut für Physik, Martin-Luther-Universität Halle-Wittenberg, D-06120 Halle (Saale), Germany

(Received 10 February 2012; revised manuscript received 4 May 2012; published 18 July 2012)

The dynamics of magnetic moments in nanostructures is closely linked to that of gyroscopes. The Landau-Lifshitz-Gilbert equation describes precession and relaxation but does not include nutation. Both precession and relaxation have been observed in experiments, in contrast to nutation. The extension of the atomistic Landau-Lifshitz-Gilbert equation by a nutation term allows us to study the significance of nutation in magnetization dynamics of nanostructures: for a single magnetic moment, a chain of Fe atoms, and Co islands on Cu(111). We find that nutation is significant at low-coordination sites and on the time scale of about 100 fs; its observation challenges strongly today's experimental techniques.

DOI: 10.1103/PhysRevB.86.020404

PACS number(s): 75.70.Ak, 75.78.Jp, 75.10.Hk

Investigations of the magnetization dynamics in nanoscale systems have become very important in the recent past. Hot topics comprise, for example, current-induced domain-wall motion¹ and demagnetization effects upon femtosecond laser pulses.^{2,3} On time scales from microseconds down to femtoseconds, the dynamics of magnetic systems is well characterized by the Landau-Lifshitz-Gilbert (LLG) equation

$$\frac{\partial \mathbf{M}}{\partial t} = \mathbf{M} \times \left(-\gamma \mathbf{B}^{\text{eff}} + \frac{\alpha}{M_s} \frac{\partial \mathbf{M}}{\partial t} \right) \quad (1)$$

for the average magnetic moment \mathbf{M} (Ref. 4). It describes the precession of \mathbf{M} around and its relaxation towards the effective field \mathbf{B}^{eff} (Ref. 5).

Precession is well known from the classical mechanics of a gyroscope. If an external force tilts the rotation axis of the gyroscope off the direction of the gravity field, then the gyroscope starts to precess around the gravitational field with a tilt angle ψ (Fig. 1, large circle). Because of the inertia, the rotation axis shifts to larger angles than ψ . Thus, the rotation axis does not coincide with the angular-momentum direction, which results in an additional precession of the gyroscope around the angular-momentum axis (Fig. 1, small circle), called nutation. The trajectory is a cycloid with the tilt angle $\phi(t) = \bar{\phi}[1 - \cos(\omega_n t)]$ and the azimuthal angle $\theta(t) = \bar{\phi}[\omega_n t - \sin(\omega_n t)]$. In most cases, nutation is small compared to precession ($\bar{\phi} < \psi$).

Given the similarity of gyroscope dynamics and magnetization dynamics, Döring introduced the concepts of mass and inertia in macrospin systems,⁶ especially for domain walls. De Leeuw and Robertson proved the existence of a domain-wall mass experimentally.⁷ Spin nutation was first predicted in Josephson junctions.⁸⁻¹² It was shown that in a magnetic tunnel junction, a local spin inserted into the junction can be electrically controlled, using short bias voltage pulses. Ciornei *et al.*^{13,14} studied the role of inertia in damped dynamics using a macrospin approach, thereby neglecting the magnetic exchange interaction within the sample, and concluded that nutation will have a lifetime of picoseconds.

Up to now, nutation has not been observed in magnetization dynamics, possibly because the effect is too small and appears on the time scale of the magnetic exchange interaction. However, with respect to the recent enormous progress in ultrafast

spectroscopies (e. g., Ref. 15), experimental techniques will access the femtosecond time scale soon. This raises the question under what circumstances nutation can be observed in magnetic nanostructures.

In this paper, we give an answer to the above question for selected nanostructures by means of the atomistic Landau-Lifshitz-Gilbert equation. The spin Hamiltonian comprises the exchange interactions, the magnetocrystalline anisotropy, as well as an external magnetic field. The Heisenberg exchange and the anisotropy constants are calculated from first principles. Starting from an almost collinear magnetic state, an external magnetic field \mathbf{B} is switched on abruptly, resulting in nutation of the local magnetic moments. We consider model systems such as a single moment (atom), Fe chains of various lengths, and Co islands on Cu(111).

The magnetization dynamics is described by an atomistic Landau-Lifshitz-Gilbert equation^{16,17}

$$\frac{\partial \mathbf{m}_i}{\partial t} = \mathbf{m}_i \times \left(-\gamma \mathbf{B}_i^{\text{eff}} + \frac{\alpha}{m_i} \frac{\partial \mathbf{m}_i}{\partial t} + \frac{\gamma \iota}{m_i} \frac{\partial^2 \mathbf{m}_i}{\partial t^2} \right), \quad (2)$$

which is extended by a nutation term. \mathbf{m}_i is the local atomic moment ($|\mathbf{m}_i| = m_i$) at site i . γ and $\alpha \ll 1$ are the gyromagnetic ratio and the Gilbert damping, respectively. The magnetic moment of inertia ι is expressed as $\iota = \frac{\alpha \tau}{\gamma}$ (taken from Ref. 13), with the relaxation time τ that enlarges or reduces the period of the nutation cycloid. The nutation part (usually not considered in magnetization dynamics) is treated as in Refs. 13 and 18, following Döring's concept of magnetic-moment mass.⁶ Temperature effects are neglected.

The first term in Eq. (2) accounts for the precession of \mathbf{m}_i around the local effective field $\mathbf{B}_i^{\text{eff}}$, whereas the second term describes the relaxation of \mathbf{m}_i toward $\mathbf{B}_i^{\text{eff}}$ due to inelastic processes. The third term models the nutation due to a change in $\mathbf{B}_i^{\text{eff}}$. The local effective field $\mathbf{B}_i^{\text{eff}} = -\partial \hat{H} / \partial \mathbf{m}_i$ is obtained from the Hamiltonian

$$\hat{H} = \hat{H}_{\text{ex}} + \hat{H}_{\text{mca}} + \hat{H}_{\text{dd}} + \hat{H}_{\text{ext}}. \quad (3)$$

\hat{H}_{ex} is the Heisenberg exchange interaction

$$\hat{H}_{\text{ex}} = - \sum_{ij} J_{ij} \mathbf{m}_i \cdot \mathbf{m}_j, \quad (4)$$

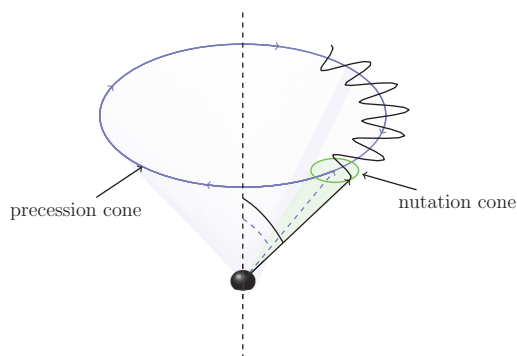


FIG. 1. (Color online) Precession and nutation of a gyroscope or a magnetization vector. The large circle sketches the precession cone around the effective magnetic field (marked as blue (dark gray) line). The inertia leads to the nutation, i. e., an additional precession [green (gray) small circle]. The trajectory is thus a cycloid (black wavy line).

where J_{ij} are the Heisenberg exchange constants. The magnetocrystalline anisotropy

$$\hat{H}_{\text{mca}} = \sum_i K_i (\mathbf{m}_i \cdot \mathbf{e}_{\text{mca}})^2 \quad (5)$$

is assumed uniaxial, with “easy axis” \mathbf{e}_{mca} and anisotropy constants K_i . The demagnetization field yields the shape anisotropy

$$\hat{H}_{\text{dd}} = -\frac{1}{2} \frac{\mu_0}{4\pi} \sum_{ij} \frac{3(\mathbf{m}_i \cdot \mathbf{r}_{ij})(\mathbf{m}_j \cdot \mathbf{r}_{ij}) - (\mathbf{m}_i \cdot \mathbf{m}_j) r_{ij}^2}{r_{ij}^5}. \quad (6)$$

$\mathbf{r}_{ij} \equiv \mathbf{r}_i - \mathbf{r}_j$ is the distance between sites i and j (μ_0 vacuum permeability). Eventually, the Zeeman term

$$\hat{H}_{\text{ext}} = -\mu_B \mathbf{B} \cdot \sum_i \mathbf{m}_i \quad (7)$$

accounts for an external field \mathbf{B} .

Prior to the magnetization-dynamics calculations, we computed the electronic and magnetic structures of bulk Fe and a 2-monolayer-thick Co film on Cu(111) from first principles, using a multiple-scattering approach.¹⁹ Our relativistic Korringa-Kohn-Rostoker method²⁰ relies on the local spin-density approximation to density-functional theory, with Perdew-Wang exchange-correlation potential.²¹ Based on the *ab initio* calculations, both the exchange constants J_{ij} and the anisotropy constants K_i were computed from the magnetic-force theorem (e. g., Ref. 22).

The nutation term in the LLG equation (2) can be interpreted as follows: The Heisenberg model describes the transfer of angular momentum \mathbf{L} between two atomic moments, where the total angular momentum is conserved within the entire system. This results in precession because $\frac{\partial \mathbf{L}}{\partial t} = \mathbf{M}$. An external field \mathbf{B} can also transfer angular momentum and tilts the moment off the angular-momentum axis, analogous to the classical gyroscope. However, the moments respond inert and start to nutate on a femtosecond time scale because they are coupled by the Heisenberg exchange interaction. The cycloid period of the nutation is affected by the relaxation time τ . An increased Gilbert damping leads on one hand to a decrease of

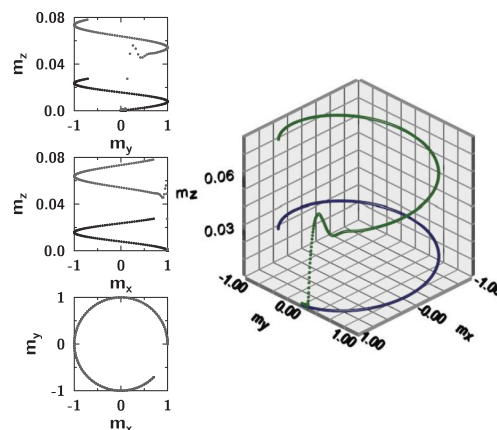


FIG. 2. (Color online) Nutation of a single magnetic moment. The external magnetic field \mathbf{B} along z is abruptly increased from 1 to 51 T. Blue (green) line: trajectory without (with) the nutation term in the LLG equation (2). The panels on the left-hand side show the vector components [dark gray (gray): without (with) nutation term]; note the different scales of the Cartesian axes. Relaxation time $\tau = 1$ ps, Gilbert damping $\alpha = 0.005$, total duration 600 fs.

the nutation effect and on the other hand increases the inertia. Nutation becomes important if the time scale of the change of \mathbf{B} is smaller than the angular-momentum relaxation time. The latter can be estimated from the Heisenberg exchange parameters ($J \approx 12$ meV for nearest neighbors in bulk Fe) and the relaxation time to be in the order of tens of femtoseconds.

Application 1: Single magnetic moment. It suggests itself that a single moment should have the strongest nutation.¹³ If an external magnetic field \mathbf{B} is applied, e. g., in z direction, the magnetic moment precesses around the external field with the Larmor frequency $\omega = \gamma B$. An abrupt increase of \mathbf{B} changes the angular velocity of the precession: Without the nutation term in Eq. (2), the precession becomes only faster (blue line in Fig. 2). However, with the nutation term in Eq. (2), nutation shows up as a cycloid with a small lifetime (green line): the abrupt increase of the z component of the magnetic moment is due to the huge external magnetic field which is, admittedly unphysically, suddenly increased.

Despite the unphysical parameters (given in Fig. 2), the nutation amplitude is very weak. We attribute this finding to a change of the *strength* of \mathbf{B} , rather than a change of its *direction* (cf. Ref. 13 in which a pronounced nutation is found for the latter case).

Our finding supports that nutation is hard to observe in a macrospin system under realistic physical conditions. It suggests that nutation is more significant when changing the external-field direction or by taking into account the effective field coming from nearby magnetic moments [Eq. (4); the single magnetic moment of this model system is apparently not affected by other magnetic moments]. This supposition is proved in the next examples.

Application 2: Chain of Fe atoms. The role of angular-momentum transfer due to Heisenberg exchange is investigated by means of Fe chains of finite lengths. The exchange constants J_{ij} are deliberately taken from bulk Fe ($J = 12.6$ meV for nearest neighbors and $J = 11.3$ meV for next-nearest neighbors); since the exchange parameters

depend on the dimensionality ($\approx \frac{1}{r_{\text{dim}}}$), this is an approximation, the anisotropies K_i are set to zero. The system is initially prepared in a slightly noncollinear state to which the external field is applied after 1 ps; because of the typical relaxation time of about 5 ps, this intermediate state is still not perfectly

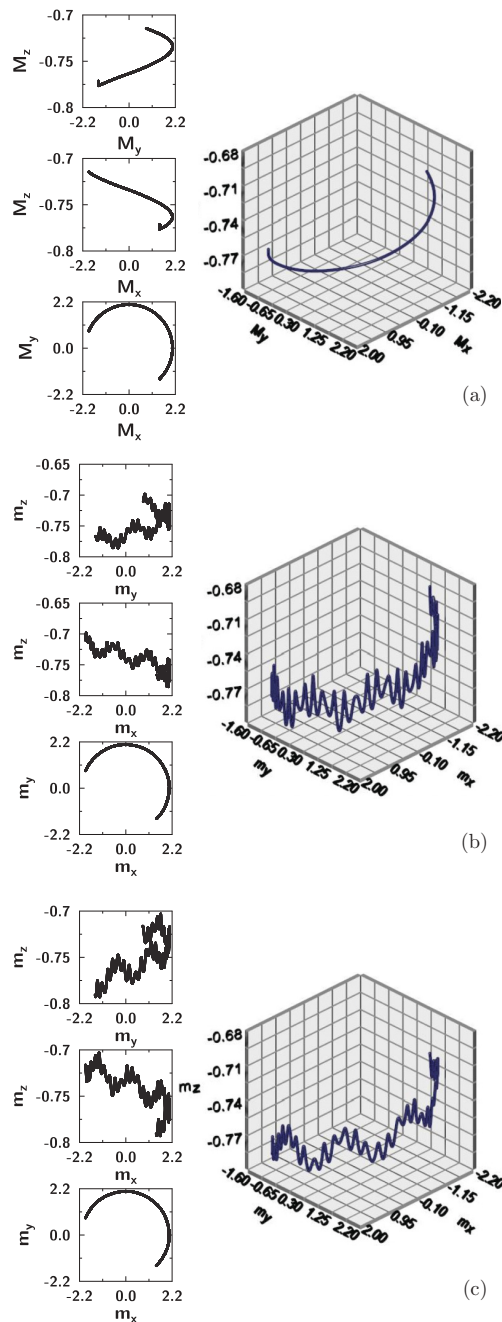


FIG. 3. (Color online) Nutation in an Fe chain with five atoms. A magnetic field of 10 T in the z direction is applied abruptly to the collinear ground state. (a)–(c) Trajectories of the average magnetization (a), the central moment (b), and an edge moment (c). The panels on the left-hand side show the vector components; note the different scales of the Cartesian axes. Relaxation time $\tau = 1$ fs, Gilbert damping $\alpha = 0.004$, atomic distance 2.863 Å, total duration 2 ps.

collinear. As in the first example, we apply a sudden increase of the external field.

We exemplify our findings for a chain of five atoms. The nutation is small compared to the precession: the typical amplitude is about $0.2\mu_B$ – $0.4\mu_B$ for a single moment. The average magnetization \mathbf{M} shows no considerable effect [Fig. 3(a)], similar to the single magnetic moment in the first application. In the present case, however, the reason is a phase shift between single magnetic moments due to the noncollinear initial state, the magnetic coupling, and the inertia that leads to cancellation [Figs. 3(b) and 3(c)].

The amplitude of the nutation depends also on the number of interacting neighbors in the ensemble: smaller for the central moment [Fig. 3(b)], larger for an edge moment [Fig. 3(c)]. The correlation between the magnetic moments increases with the coordination number, which results on one hand in a larger effective field and on the other hand in a reduced nutation lifetime and amplitude.

With increasing damping α , both magnitude and lifetime of the nutation decrease. A high damping speeds up the relaxation towards the collinear configuration. Depending on the ratio of exchange field and magnetic field, different forms of cycloids occur (not shown here): an elongated or an abbreviated cycloid.

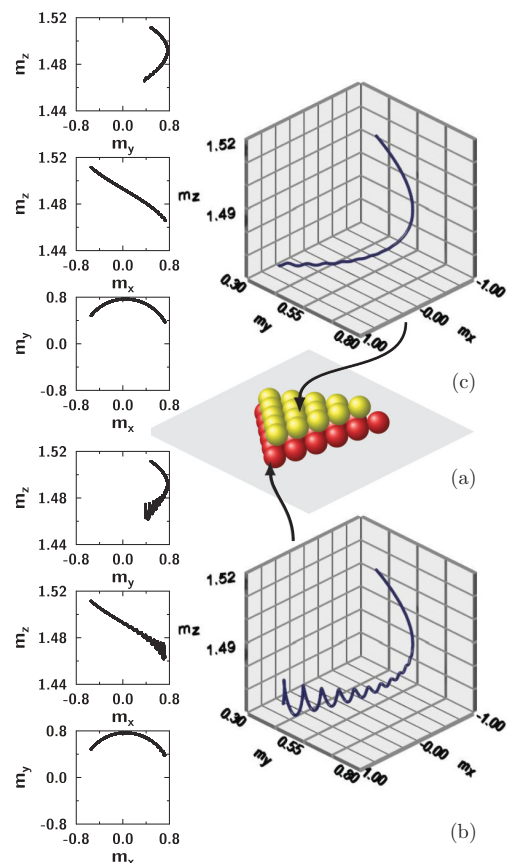


FIG. 4. (Color online) Nutation in 2-monolayer-thick Co island on Cu(111) with 36 atoms. (a) Schematic illustration of the triangular-shaped Co island. The Cu substrate is not shown. (b) and (c) Trajectory of a corner atom (b) and a center atom (c), respectively. The panels on the left-hand side show the vector components; note the different scales of the Cartesian axes. $\tau = 1$ fs, $\alpha = 0.02$, total duration 2 ps.

Especially, the first form is due to collective excitations (e. g., from excitations of magnons perpendicular to the magnetic field).

Application 3: Co nanoislands on Cu(111). As seen before, the nutation strength of a local moment depends on the coordination number of the respective atom. This effect becomes even stronger in a nanoisland as compared to a chain. To support this observation further, we address a 2-monolayer-thick Co island on Cu(111) with 36 atoms in total. Here, the effective field incorporates the magnetocrystalline anisotropy, calculated from *ab initio* (for details see Ref. 23). The chosen Gilbert damping α of 0.02 is typical for nanostructures (Refs. 16 and 23). The abrupt magnetic-field increase of 5 T perpendicular to the island results in a stronger nutation at a corner atom [Fig. 4(b)] as compared to that for a center atom [Fig. 4(c)]. For even larger islands (not shown here), the nutation at a center atom can vanish completely, but that at a corner atom remains. Because of the angular-momentum conservation, the average magnetic moment exhibits no nutation (not shown here).

We estimate the range of nutation lifetimes to about 100 fs up to 500 fs (a lifetime of a few ps was found in Ref. 13). This rather short time scale corroborates why nutation has not been measured so far. The dependence on the coordination number suggests that nutation is negligible in bulk materials. An increase of the relaxation time τ enlarges the cycloid period because the system reacts more inert; increasing the damping constant reduces the cycloid amplitude and the nutation decays much faster.

Temperature effects are usually incorporated in the LLG equation by a white-noise ansatz, i. e., $\mathbf{B}_i^{\text{eff}}$ is replaced by

$\mathbf{B}_i^{\text{eff}} + \mathbf{b}_i(t)$ where $\mathbf{b}_i(t)$ is an uncorrelated random field.¹⁶ However, this approach does not hold in the presence of the nutation term: the process is no longer a Markov process due to the second derivative in the LLG equation. The occurring temporal correlations can be included by a color-noise approach.²⁴ Using nevertheless white noise, the random fields result in a broadening of the trajectories because both the nutation as well as the precession axes are varied randomly. Hence, the nutation effects reported are significantly reduced (not shown here).

Concluding remarks. Nutation is significant on the femtosecond time scale since a typical damping constant of 0.01 . . . 0.1 reduces the nutation lifetime to about 100 fs. It shows up preferably in low-dimensional systems, e. g., at edges and corners but with a small amplitude with respect to the precession. These findings lead to the conclusion that the observation of nutation effects is a strong challenge for experimental investigations.

Since the inertia of moment and the dissipation depend on the environments of the local magnetic moments, one could improve the theory by replacing the damping constant and the moment-of-inertia constant by respective tensors, both of which could be computed from first principles.^{18,25,26} Further, there is, to our knowledge, no theoretical foundation for a Langevin dynamics including nutation at finite temperatures.

Acknowledgements. This work is supported by the *Sonderforschungsbereich 762* “Functional Oxide Interfaces.” D.B. is a member of the International Max Planck Research School on Science and Technology of Nanostructures, Halle, Germany.

*Corresponding author: dboettch@mpi-halle.de

¹I. M. Miron, T. Moore, H. Szambolics, L. D. Buda-Prejbeanu, S. Auffret, B. Rodmacq, S. Pizzini, J. Vogel, M. Bonfim, A. Schuhl, and G. Gaudin, *Nat. Mater.* **10**, 419423 (2011).

²B. Koopmans, G. Malinowski, F. Dalla Longa, D. Steiauf, M. Fähnle, T. Roth, M. Cinchetti, and M. Aeschlimann, *Nat. Mater.* **9**, 259 (2010).

³G. Malinowski, F. Dalla Longa, J. H. H. Rietjens, P. V. Paluskar, R. Huijink, H. J. M. Swagten, and B. Koopmans, *Nat. Phys.* **4**, 855 (2008).

⁴R. Skomski, *J. Phys.: Condens. Matter* **15**, R841 (2003).

⁵M. C. Hickey and J. S. Moodera, *Phys. Rev. Lett.* **102**, 137601 (2009).

⁶W. Döring, *Z. Naturforsch. A* **3**, 373 (1948).

⁷F. De Leeuw and J. M. Robertson, *J. Appl. Phys.* **46**, 3182 (1975).

⁸J.-X. Zhu and J. Fransson, *J. Phys.: Condens. Matter* **18**, 9929 (2006).

⁹J. Fransson, *Nanotechnology* **19**, 285714 (2008).

¹⁰J. Fransson and J.-X. Zhu, *New J. Phys.* **10**, 013017 (2008).

¹¹Z. Nussinov, A. Shnirman, D. P. Arovas, A. V. Balatsky, and J. X. Zhu, *Phys. Rev. B* **71**, 214520 (2005).

¹²J.-X. Zhu, Z. Nussinov, A. Shnirman, and A. V. Balatsky, *Phys. Rev. Lett.* **92**, 107001 (2004).

¹³M.-C. Ciornei, J. M. Rubi, and J.-E. Wegrowe, *Phys. Rev. B* **83**, 020410 (2011).

¹⁴M.-C. Ciornei, Ph.D. thesis, Ecole Polytechnique, Universidad de Barcelona, 2010.

¹⁵E. G. Gamaly, *Phys. Rep.* **508**, 91 (2011).

¹⁶B. Skubic, Ph.D. thesis, Uppsala Universitet, Uppsala, 2007.

¹⁷B. Skubic, J. Hellsvik, L. Nordström, and O. Eriksson, *J. Phys.: Condens. Matter* **20**, 315203 (2008).

¹⁸S. Bhattacharjee, L. Nordström, and J. Fransson, *Phys. Rev. Lett.* **108**, 057204 (2012).

¹⁹*Electron Scattering in Solid Matter*, edited by J. Zabloudil, R. Hammerling, L. Szunyogh, and P. Weinberger (Springer, Berlin, 2005).

²⁰J. Henk, in *Handbook of Thin Film Materials*, Vol. 2, edited by H. S. Nalwa (Academic, San Diego, 2002), Chap. 10, p. 479.

²¹J. P. Perdew and Y. Wang, *Phys. Rev. B* **45**, 13 244 (1992).

²²A. I. Liechtenstein, M. I. Katsnelson, V. P. Antropov, and V. A. Gubanov, *J. Magn. Magn. Mater.* **67**, 65 (1987).

²³D. Böttcher, A. Ernst, and J. Henk, *J. Phys.: Condens. Matter* **23**, 296003 (2011).

²⁴U. Atxitia, O. Chubykalo-Fesenko, R. W. Chantrell, U. Nowak, and A. Rebei, *Phys. Rev. Lett.* **102**, 057203 (2009).

²⁵A. Brataas, Y. Tserkovnyak, and G. E. W. Bauer, *Phys. Rev. Lett.* **101**, 037207 (2008).

²⁶H. Ebert, S. Mankovsky, D. Ködderitzsch, and P. J. Kelly, *Phys. Rev. Lett.* **107**, 066603 (2011).

Conclusion and Outlook

The main scope of this thesis was to go beyond the obvious transition of a mesoscopic continuous picture into an atomistic discrete description, to account for the non-statistical impact of microscopic degrees of freedom, and to characterize magnetic properties on a nm-length- and a fs-time-scale, which is a fundamental question for applications in technology and basic research. Contrary to past dynamics and ground-state studies, the thesis considers strong correlations between the spin, electron and lattice reservoirs in the magnetic equilibration. As an important new aspect, the temperature dependence of the magnetic exchange coupling as well as the magnetic damping was pointed out. Especially for the latter, a link to all three reservoirs was found, but neglected in previous microscopic magnetic simulations. Both quantities were revealed as anisotropic, especially in materials with reduced symmetry or at surfaces. Furthermore, my results address the fundamental question of retardation in nanostructures close to the adiabatic and quantum-mechanical limit, which is known from the mechanics as nutation and which calls for experimental proofs. To treat all this requests, existing theoretical models were extended and applied to basic magnetic materials. In process, the thesis deals with applications on layered magnetic systems, systems with reduced symmetry as well as nanostructures. *Ab initio* calculations using the full-relativistic multiple-scattering Green function method (Korringa-Kohn-Rostoker method) and the tight-binding model were carried out to obtain the electronic ground state and the resulting magnetic properties. The magnetic ground state and magnetic evolution were studied with Monte Carlo methods and the Landau-Lifshitz-Gilbert equation, respectively. Both methods were developed further by the kinetic Monte Carlo method and the Landau-Lifshitz-Miyazaki-Seki equation. This allows a wide analysis of various static or dynamic magnetic properties.

In particular, the thesis treats various topics of atomistic magnetic properties, especially those exhibiting misfits with experimental predictions. For example, the theoretical corroboration of experimentally measured phase transition temperature T_C predicts often too small values. Taking into account the local magnetic fluctuations via the disorder local moment theory, however, solves the obstacle. It expedites the fundamental understanding of the correlation between electron and spin reservoir as well as the physics of magnetic phase transition.

The discrepancy between experiment and theory in ultra-thin magnetic films states for imperfection of the magnetic exchange model. Introducing the exchange tensor accounts for

additional mechanism preferring spiraled magnetic structures. This is especially important in case of inversion symmetry breaking and materials with strong spin-orbit coupling, which makes the orbital degree of freedom important for magnetic properties. Zero average magnetic moment in 1 ML Fe on Pt(111) is the consequence of the anisotropic exchange, whereas applying an external magnetic field induces an additional symmetry breaking that annihilates the spiral structure. The same is also observable by using other ‘heavy’ substrates such as Ir(111), Pd(111) and Rh(111).

The spin-orbit coupling manifests itself also in the energy dissipation, regarding magnetic damping. Hence, the aforementioned surfaces are also promising for spintronic application due to their high damping. The breathing Fermi-surface model accounts for the electronic part of the magnetic damping. Beyond Gilbert’s assumption a non-local energy transfer was depicted in the Landau-Lifshitz-Gilbert equation, calling for retardation on the atomistic length scale. Various dependences are pointed out: tensor character, the coupling to the spin and phonon reservoir, weak dependence on the surface normal, as well as energy transfer to neighboring sites (non-locality).

The non-local damping, however, plays a crucial role only in non-coherent states. Such states appear on the timescale of magnetism formation estimated from the Nyquist theorem, which lets the magnetic moments react inert and calls for retardation in time. The moment precession around the angular momentum axis, in addition to the motion coming from the effective magnetic field, is due to the occurred moment of inertia. This results in a cycloidal trajectory. Studies on single magnetic moment, magnetic chains and nanoislands conclude the relevance of nutation on a time scale of 100 – 500 fs and on low-coordinated sites in the magnetic lattice.

The Landau-Lifshitz-Gilbert equation together with Monte Carlo methods offers a fundamental possibility for simulating magnetism on the atomistic scale without considering quantum mechanics. It has the potential for large conceptual as well as methodological developments. With the importance of complex magnetic structures due to shrinking length scale in technology, such as magnetic sensors or magnetic storage devices, the question about magnetic reversal or control of magnetism becomes important; it can be addressed by atomic magnetization dynamics. On time and length scales, where quantum mechanical effects appear, strong correlations and couplings to other nanoscopic degrees of freedom occur, approximated in the first order via an additional random field. However, in order to improve the methodology and getting the correct physics, this assumption of a random field is no longer valid. The correlation between the three reservoirs (electron, spin and phonon) must be ‘weaved’ within the magnetization dynamics: the exchange coupling as well as the anisotropy field become explicitly temperature-dependent; the lack in orbital symmetry leads to anisotropic exchange, and strain weakens magnets. Vice versa, the magnetic noise reduces the exchange splitting in the density of states, affects the relaxation of an excited electron system or reduces the bonding length. In particular, the degrees of freedoms, ‘living’ on a shorter time scale than magnetism (ultrashort time scale physics), demonstrate retardation in time and space. Both will result in dephasing of the magnetic moments and, thus, lead to an increase of damping and faster magnetic reversal. Consequently, the presented theory offers a way to design and simulate magnetic materials for fundamental technology applications, such as MRAM or racetrack memory devices. It may pave access for novel technological applications like magnetic diodes, magnetic transistors or other magnetic logical elements, which can have significant impact to computer technologies.

On the methodological side, much can be done in terms of improving accuracy of the sim-

ulations: the Heisenberg-type disorder local moment theory, e.g, can be used to study the layer-resolved phase transitions, which is impossible in the Ising-type case. The formation of spin spirals and Skyrmions in low-dimensional systems requires a magnetic model that includes the biquadratic exchange term. Furthermore, a study of the inverse Dzyaloshinskii-Moriya effect in type *I* multiferroics gives a closer look inside the role of crystal symmetry. Such atomistic displacements arise also as phonons that dominate the thermal dependency of magnetic damping. Apart from damping, inertia of magnetic moments becomes important on fs-second timescale and requires an *ab initio* theory as well as experimental verification. Although calculations of spin-electron correlation within the model presented in this thesis give a good agreement with experiment, calculating this correlation with self-consistent methods based on time-dependent density functional theory still presents a serious challenge for theory.

Heisenberg-type disordered local moment theory: Distribution function

In section 3.6 the von Mises-Fisher distribution was motivated as the statistical distribution function, describing an ensemble of magnetic moments $\{\mathbf{e}\}$. In the paramagnetic state (temperature $T \geq T_C$), the moments fluctuate so that each orientation is equally probable. The distribution of orientations $P(\mathbf{e})$ is thus constant,

$$P(\mathbf{e}) = \frac{1}{4\pi}. \quad (\text{A.1})$$

In the ferromagnetic state (temperature $T = 0$), however, the magnetization does not fluctuate at all, giving

$$P(\mathbf{e}) = \delta(\mathbf{e} - \mathbf{n}). \quad (\text{A.2})$$

It is strictly aligned along \mathbf{n} . With the two limits—ferromagnetic and paramagnetic state—in mind, one can construct a state at an intermediate temperature T , $0 \leq T \leq T_C$. For this, one needs to find an intermediate distribution function. The distribution function has to fulfill the normalization condition

$$1 = \int_0^{2\pi} \int_0^\pi P(\theta, \phi) \sin \theta \, d\phi \, d\theta = \int_0^{2\pi} P_\phi \, d\phi \int_0^\pi P_\theta \sin \theta \, d\theta. \quad (\text{A.3})$$

In the paramagnetic state, both P_θ and P_ϕ are constant. Hence, it follows

$$\int_0^\pi P_\theta(\theta) \sin \theta \, d\theta = 2c_\theta \equiv 1 \quad \text{and} \quad \int_0^{2\pi} P_\phi \, d\phi = 2\pi c_\phi \equiv 1. \quad (\text{A.4})$$

c_θ and c_ϕ are some constants. Thus, $P(\theta, \phi) = \frac{1}{4\pi}$.

In the ferromagnetic state, the magnetization is oriented along $\mathbf{n} = (\theta_n, \phi_n)$. Hence, one uses the *ansatz*

$$P(\theta, \phi) = c \delta(\theta - \theta_n) \delta(\phi - \phi_n). \quad (\text{A.5})$$

The normalization then gives $\frac{1}{c} = \sin \theta_n$. Both limits are fulfilled by considering a multi-dimensional Gauss function $P_d = \frac{1}{\sqrt{(2\pi)^d |\boldsymbol{\Sigma}|}} \exp\left(-1/2 (\mathbf{e} - \mathbf{n})^T \boldsymbol{\Sigma} (\mathbf{e} - \mathbf{n})\right)$, where d is the

dimension (here $d = 3$) and $\mathbf{\Sigma}$ is a symmetric covariant matrix. Von Mises and Fisher consider $\mathbf{\Sigma}$ so that P reads

$$P_3(\mathbf{e}; \mathbf{n}, \kappa) = C_3(\kappa) \exp\left(\kappa \mathbf{n}^T \mathbf{e}\right), \quad (\text{A.6})$$

and

$$C_3(\kappa) = \frac{\kappa}{4\pi \sinh \kappa} = \frac{\kappa}{2\pi(e^\kappa - e^{-\kappa})}.$$

C_3 is mainly the modified Bessel function of order $1/2$, $(\sinh z)/z$; cf. Ref. [1, 10.2.13]). Hence, for intermediate temperatures, the δ -distributions of the ferromagnetic order are represented by the von Mises-Fisher distribution $P_3(\mathbf{e}; \mathbf{n}, \kappa)$. This accounts for any (transversal) fluctuation¹ expressed as a finite offset from this direction with a weight $P_3(\mathbf{e}; \mathbf{n}, \kappa)$.

¹Longitudinal fluctuations of the magnetization are neglected in this theory. This is why the von Mises-Fisher distribution is used: it gives a distribution on the unit sphere.

Anisotropic exchange and free-energy derivatives

In section 3.5 the Lichtenstein formula for the generalized interaction model was presented. Due to the continuous change of the magnetic moments, various derivatives of the free energy with respect to the spherical representation of the magnetic moment were introduced. This appendix chapter will show how this second order derivatives correlate to the tensor elements $I_{ij}^{\mu\nu}$ of the Heisenberg model.

The energy variation with respect to polar and azimuthal angles of the spins is determined from $\hat{H} = -\sum_{ij} \mathbf{m}_i \mathbf{l}_{ij} \mathbf{m}_j$:

$$\frac{\partial^2 \hat{H}}{\partial \mu_i \partial \nu_j} = \frac{1}{2} \left(\sum_{s \neq j} \frac{\partial^2 \mathbf{m}_j}{\partial \mu_s \partial \nu_j} \mathbf{l}_{js} \mathbf{m}_s \delta_{ij} + \frac{\partial \mathbf{m}_j}{\partial \nu_j} \mathbf{l}_{ji} \frac{\partial \mathbf{m}_i}{\partial \mu_i} (1 - \delta_{ij}) \right. \quad (\text{B.1})$$

$$\left. + \frac{\partial \mathbf{m}_i}{\partial \mu_i} \mathbf{l}_{ij} \frac{\partial \mathbf{m}_j}{\partial \nu_j} (1 - \delta_{ij}) + \sum_{r \neq j} \mathbf{m}_r \mathbf{l}_{rj} \frac{\partial^2 \mathbf{m}_j}{\partial \mu_j \partial \nu_j} \delta_{ij} \right). \quad (\text{B.2})$$

μ and ν denote the polar and the azimuthal angles, respectively. Since $\partial^2 \hat{H} / \partial \mu_i \partial \nu_j = \partial^2 \hat{H} / \partial \nu_j \partial \mu_i$, a direct link between both derivatives can be made [293]. Thus, the site-diagonal terms for the x reference orientation are given by

$$\frac{\partial^2 \hat{H}}{\partial \varphi_i \partial \varphi_i} = -\sum_{s \neq i} I_{is}^{xx}, \quad (\text{B.3})$$

$$\frac{\partial^2 \hat{H}}{\partial \vartheta_i \partial \vartheta_i} = -2K_i - \sum_{s \neq i} I_{is}^{xx}, \quad (\text{B.4})$$

$$\frac{\partial^2 \hat{H}}{\partial \varphi_i \partial \vartheta_i} = 0, \quad (\text{B.5})$$

$$\frac{\partial^2 \hat{H}}{\partial \vartheta_i \partial \varphi_i} = 0, \quad (\text{B.6})$$

while the off-diagonal terms read

$$\frac{\partial^2 \hat{H}}{\partial \varphi_i \partial \varphi_j} = I_{ij}^{yy}, \quad (\text{B.7})$$

$$\frac{\partial^2 \hat{H}}{\partial \vartheta_i \partial \vartheta_j} = I_{ij}^{zz}, \quad (\text{B.8})$$

$$\frac{\partial^2 \hat{H}}{\partial \varphi_i \partial \vartheta_j} = -I_{ij}^{yz}, \quad (\text{B.9})$$

$$\frac{\partial^2 \hat{H}}{\partial \vartheta_i \partial \varphi_j} = -I_{ij}^{zy}. \quad (\text{B.10})$$

The site-diagonal terms for the y reference orientation are given by

$$\frac{\partial^2 \hat{H}}{\partial \varphi_i \partial \varphi_i} = - \sum_{s \neq i} I_{is}^{yy} \quad (\text{B.11}) \quad \frac{\partial^2 \hat{H}}{\partial \varphi_i \partial \vartheta_i} = 0, \quad (\text{B.13})$$

$$\frac{\partial^2 \hat{H}}{\partial \vartheta_i \partial \vartheta_i} = -2K_i - \sum_{s \neq i} I_{is}^{yy} \quad (\text{B.12}) \quad \frac{\partial^2 \hat{H}}{\partial \vartheta_i \partial \varphi_i} = 0, \quad (\text{B.14})$$

while the off-diagonal terms read

$$\frac{\partial^2 \hat{H}}{\partial \varphi_i \partial \varphi_j} = I_{ij}^{xx}. \quad (\text{B.15}) \quad \frac{\partial^2 \hat{H}}{\partial \varphi_i \partial \vartheta_j} = I_{ij}^{xz}. \quad (\text{B.17})$$

$$\frac{\partial^2 \hat{H}}{\partial \vartheta_i \partial \vartheta_j} = I_{ij}^{zz}. \quad (\text{B.16}) \quad \frac{\partial^2 \hat{H}}{\partial \vartheta_i \partial \varphi_j} = I_{ij}^{zx}. \quad (\text{B.18})$$

The site-diagonal terms for the z reference orientation are given by

$$\frac{\partial^2 \hat{H}}{\partial \varphi_i \partial \varphi_i} = - \sum_{s \neq i} I_{is}^{zz}, \quad (\text{B.19}) \quad \frac{\partial^2 \hat{H}}{\partial \varphi_i \partial \vartheta_i} = 0, \quad (\text{B.21})$$

$$\frac{\partial^2 \hat{H}}{\partial \vartheta_i \partial \vartheta_i} = -2K_i - \sum_{s \neq i} I_{is}^{zz}, \quad (\text{B.20}) \quad \frac{\partial^2 \hat{H}}{\partial \vartheta_i \partial \varphi_i} = 0, \quad (\text{B.22})$$

while the off-diagonal terms read

$$\frac{\partial^2 \hat{H}}{\partial \varphi_i \partial \varphi_j} = I_{ij}^{yy}, \quad (\text{B.23}) \quad \frac{\partial^2 \hat{H}}{\partial \varphi_i \partial \vartheta_j} = -I_{ij}^{yx}, \quad (\text{B.25})$$

$$\frac{\partial^2 \hat{H}}{\partial \vartheta_i \partial \vartheta_j} = I_{ij}^{xx}, \quad (\text{B.24}) \quad \frac{\partial^2 \hat{H}}{\partial \vartheta_i \partial \varphi_j} = -I_{ij}^{xy}. \quad (\text{B.26})$$

Overview of treated models

Since this dissertation gives only a small insight into the research topics of my graduation, an overview of all considered topics and applied methods is shown in figure C.1.

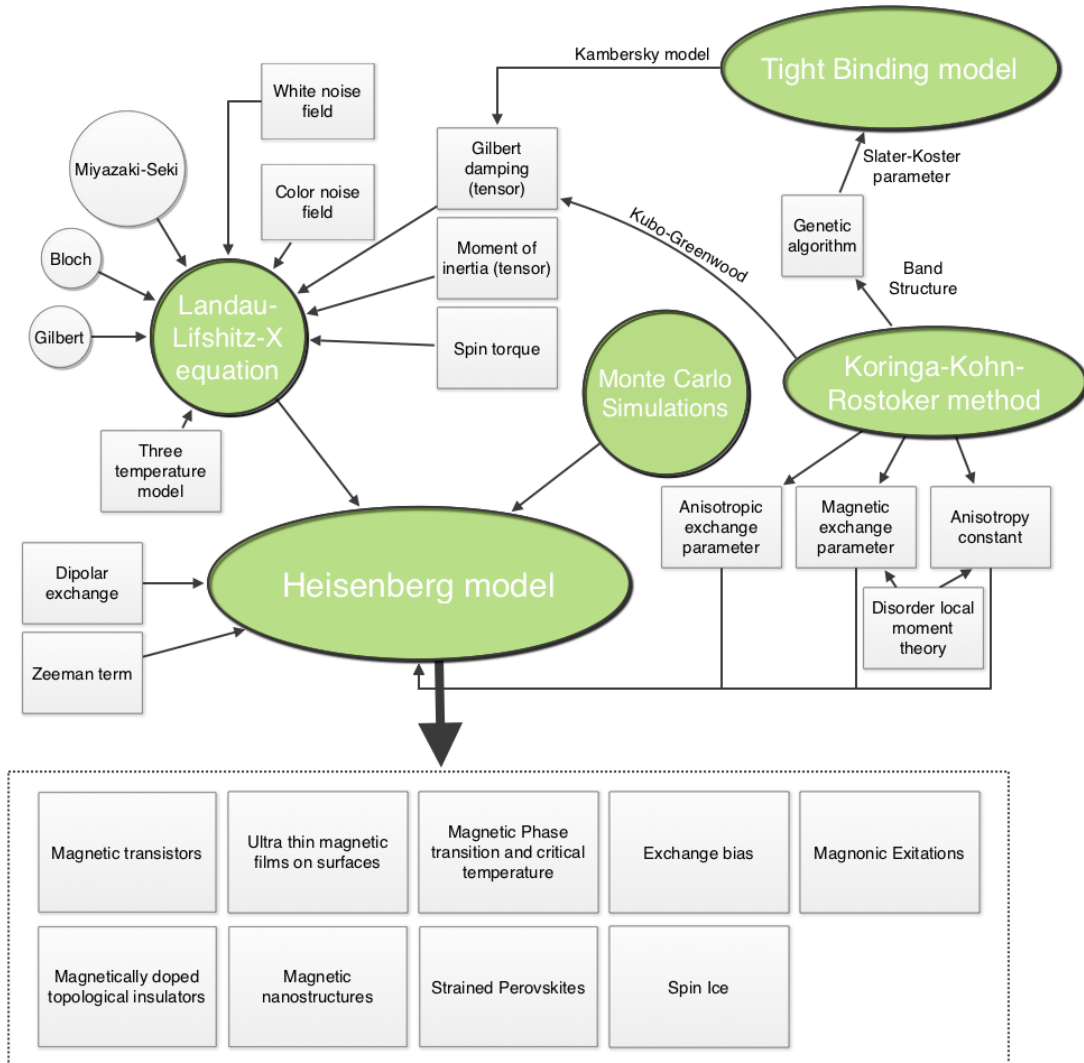


Figure C.1.: Overview of all considered topics (bottom dotted box) and applied methods (green and gray boxes). The concept map shows also the strong correlation between the method that simulates the electron properties and those that consider magnetic states.

Bibliography

- [1] *Handbook of Mathematical Functions*, edited by M. Abramowitz and I. A. Stegun (Dover Publications, New York, 1970).
- [2] Agranat, M. B., Ashitkov, S. I., and Granovskii, A. B., *Zh. Eksp. Teor. Fiz.* **86**, 1376 (1984).
- [3] Anderson, P., *Physical Review* **79**, 350 (1950).
- [4] Anisimov, A. N., Platow, W., Pouloupoulos, P., Wisny, W., Farle, M., Baberschke, K., Isberg, P., Hjörvarsson, B., and Wäppling, R., *Journal of Physics: Condensed Matter* **9**, 10581 (1997).
- [5] Anisimov, V. I., Aryasetiawan, F., and Lichtenstein, A. I., *Journal of Physics: Condensed Matter* **9**, 767 (1997).
- [6] Anisimov, V. I., Korotin, M. A., and Kumaev, E. Z., *Journal of Physics: Condensed Matter* **2**, 3973 (1990).
- [7] Ashcroft, N. W. and Mermin, N. D., *Solid State Physics* (Holt-Saunders International Editions, London, 1976).
- [8] Atxitia, U., Chubyakalo-Fesenko, O., Kazantseva, N., Hinzke, D., Nowak, U., and Chantreil, R. W., *Applied Physics Letters* **91**, 232507 (2007).
- [9] Balogh, L., Palotás, K., Udvardi, L., Szunyogh, L., and Nowak, U., *Physical Review B* **86**, 024406 (2012).
- [10] Barman, A., Wang, S., Hellwig, O., Berger, A., Fullerton, E. E., and Schmidt, H., *Journal of Applied Physics* **101**, 09D102 (2007).
- [11] Barth, U. V. and Holm, B., *Physical Review B* **54**, 8411 (1996).
- [12] Barthel, S., Czycholl, G., and Bouzerar, G., *European Physics Journal B* **86**, 11 (2013).
- [13] Bergman, A., Skubic, B., Hellsvik, J., Nordström, L., Delin, A., and Eriksson, O., *Physical Review B* **83**, 224429 (2011).
- [14] von Bergmann, K., Heinze, S., Bode, M., Bihlmayer, G., Blügel, S., and Wiesendanger, R., *New Journal of Physics* **9**, 396 (2007).
- [15] Bergqvist, L., Taroni, A., Bergman, A., Etz, C., and Eriksson, O., *Physical Review B* **87**, 144401 (2013).
- [16] *Hysteresis in magnetism*, edited by G. Bertotti (Academic Press Elsevier, 1998).
- [17] *Monte Carlo Methods in Statistical Physics*, edited by K. Binder (Springer, Berlin, 1979).
- [18] Binder, K. and Heermann, D. W., *Monte Carlo Simulation in Statistical Physics: An Introduction*, 3rd ed. (Springer, Berlin, 1997).
- [19] Binnig, G. and Rohrer, H., *Reviews of Modern Physics* **59**, 615 (1987).

- [20] Binnig, G. and Rohrer, H., *Reviews of Modern Physics* **71**, S324 (1999).
- [21] Blackman, J. A. and Esterling, D. M., *Physical Review B* **4**, 8 (1971).
- [22] Bloch, F., *Zeitschrift für Physik* **52**, 555 (1928).
- [23] Bloch, F., *Physical Review* **70**, 460 (1946).
- [24] Blombergen, N., *Physical Review* **78**, 572 (1950).
- [25] Bode, M., Heide, K., von Bergmann, K., Ferriani, P., Heinze, S., Bihlmayer, G., Kubetzka, A., Pietzsch, O., Blügel, S., and R., W., *Nature* **447**, 190 (2007).
- [26] Bödicker, A., Schattke, W., Henk, J., and Feder, R., *Journal of Physics: Condensed Matter* **6**, 1927 (1994).
- [27] Borek, S., *Magnetooptische und magnetische Eigenschaften zweikomponentiger Multiferroica*, Ph.D. thesis, Martin Luther University Halle-Wittenberg (2013).
- [28] Borisov, V. S., Maznichenko, I. V., Böttcher, D., Ostanin, S., Ernst, A., Henk, J., and Mertig, I., *Physical Review B* **85**, 134410/1 (2012).
- [29] Born, M. and Oppenheimer, R., *Annalen der Physik* **84**, 457 (1927).
- [30] Bose, P., *Influence of the interface structure on the electronic transport in planar tunnel junctions: a first-principle investigation*, Ph.D. thesis, Marthin-Luther-Universität Halle-Wittenberg (2010).
- [31] Bose, T., *Mesoskopische Beschreibung stochastischer und retardierter Magnetisierungsdynamik*, Ph.D. thesis, Martin Luther university Halle/Wittenberg (2013).
- [32] Böttcher, D., *Theoretische Beschreibung der Magnetisierungsdynamik von Nanostrukturen*, Master's thesis, Martin-Luther-University Halle-Wittenberg (2010).
- [33] Böttcher, D., Ernst, A., and Henk, J., *Journal of Physics: Condensed Matter* **23**, 29 (2011).
- [34] Böttcher, D., Ernst, A., and Henk, J., *J. Nanosci. Nanotech.* **12**, 7516 (2012).
- [35] Böttcher, D., Ernst, A., and Henk, J., *Journal of Magnetism and Magnetic Materials* **324**, 610 (2012).
- [36] Böttcher, D. and Henk, J., *Journal of Physics: Condensed Matter* **25**, 136005/1 (2013).
- [37] Box, G. E. P. and Müller, M. E., *Annals of Mathematical Statistics* **29**, 610 (1958).
- [38] Brataas, A., Tserkovnyak, Y., and Bauer, G., *Physical Review B* **84**, 054416 (2011).
- [39] Brown, R., *Phil. Mag.* **4**, 161 (1828).
- [40] Brown, W. F., *Physical Review* **130**, 5 (1963).
- [41] Brown, W. F., *Micromagnetics* (Robert E. Krieger Publishing, Huntington, 1978).
- [42] Bruno, P., *Physical Review B* **39**, 865(R) (1989).
- [43] Bruno, P., *Physical Review Letters* **90**, 8 (2003).
- [44] Buczek, P., Ernst, A., and Sandratskii, L. M., *Physical Review Letters* **105**, 097205 (2010).
- [45] Buczek, P., Ernst, A., Sandratskii, L. M., and Bruno, P., *Journal of Magnetism and Magnetic Materials* **322**, 1396 (2010).
- [46] Buczek, P. A., *Spindynamik komplexer itineranter Magnete*, Ph.D. thesis, Martin-Luther-Universität Halle-Wittenberg (2009).

-
- [47] Buruzs, A., *Temperature dependent magnetic properties of thin films and bulk ferromagnets: An implementation of the Disordered Local Moment Scheme*, Ph.D. thesis, Technische Universität Wien (2008).
- [48] *Encyclopedia of Materials: Science and Technology*, edited by K. H. J. Buschow, R. W. Cahn, M. C. Flemings, B. Ilschner, E. J. Kramer, S. Mahajan, and P. Veyssi re (Pergamon, 2001).
- [49] Butler, W. H., *Physical Review B* **31**, 3260 (1985).
- [50] Callen, H., *Journal of the Physics and Chemistry of Solids* **4**, 256 (1958).
- [51] Chadi, D. J. and Cohen, M., *physica status solidi (b)* **68**, 405 (1975).
- [52] *Introduction to Modern Statistical Mechanics*, edited by D. Chandler (Oxford University Press, 1987).
- [53] *The mathematical theory of non-uniform gas, chapter 3 - The equation of Boltzmann and Maxwell*, edited by S. Chapman and T. Cowling (Cambridge University Press, 1970).
- [54] Chen, F., Zhang, Q. F., Li, J. H., Qi, Y. J., Lu, C. J., Chen, X. B., Ren, X. M., and Zhao, Y., *Applied Physics Letters* **89**, 092910 (2006).
- [55] Chicharro, J. M., Bay n, A., and Salazar, F., *Journal of Magnetism and Magnetic Materials* **268**, 348 (2004).
- [56] Chico, J., Etz, C., Bergqvist, L., Eriksson, O., Fransson, J., Delin, A., and Bergman, A., arXiv:1308.0986v1 [cond-mat.mtrl-sci](2013).
- [57] Ciornei, M.-C., *Role of magnetic inertia in damped macrospin dynamics*, Ph.D. thesis, Ecole Polytechnique, Universidad de Barcelona (2010).
- [58] Ciornei, M.-C., Rubi, J., and Wegrowe, J.-E., *Physical Review B* **83**, 020410 (2011).
- [59] Clogston, A. M., *Bell Syst. Tech. J.* **34**, 739 (1955).
- [60] *Magnetism and Magnetic Materials*, edited by J. M. D. Coey (Cambridge University Press, 2009).
- [61] Coffey, W. T., Kalmykov, Y. P., and Waldron, J. T., *The Langevin Equation* (World Scientific, New Jersey, 2004).
- [62] Cohen, R. E., Mehl, M. J., and Papaconstantopoulos, D. A., *Physical Review B* **50**, 19 (1994).
- [63] Colaioni, F., Durin, G., and Zapperi, S., *Physical Review B* **76**, 224416 (2007).
- [64] Cole, L. A. and Perdew, J. P., *Physical Review A* **25**, 1265 (1982).
- [65] Cr pieux, A. and Lacroix, C., *Journal of Magnetism and Magnetic Materials* **182**, 341 (1998).
- [66] *Theoretische Festk rperphysik*, edited by G. Czycholl (Springer-Verlag Berlin Heidelberg, 2008).
- [67] Dai, W. and Niu, T., *Nonlinear Analysis: Hybrid Systems* **2**, 121 (2008).
- [68] D ne, M., *Beschreibung der elektronischen Struktur korrelierter Systeme mittels lokaler Selbstwechselwirkungskorrekturen im Rahmen der Vielfachstreuungstheorie*, Ph.D. thesis, Martin-Luther-Universit t Halle-Wittenberg (2008).
- [69] *Non-Equilibrium Thermodynamic*, edited by S. R. DeGroot and P. Mazur (Dover Publications Inc. New York, second edition, 1984).
- [70] DeWeert, M. J., Papaconstantopoulos, D. A., and Pickett, W. E., *Physical Review B* **39**, 7 (1989).

- [71] Dirac, P. A., Proc. Roy. Soc. London Ser. A. **112**, 661 (1926).
- [72] Dirac, P. A., Proc. Roy. Soc. London Ser. A. **133**, 60 (1931).
- [73] Döring, W., Zeit. Naturforsch **3a**, 373 (1948).
- [74] *Green's functions with applications*, edited by D. G. Duffy (Chapman & Hall, 2001).
- [75] Dzyaloshinskii, I. E., Sov. Phys. JETP **5**, 1259 (1957).
- [76] Dzyaloshinskii, I. E., Journal of the Physics and Chemistry of Solids **4**, 241 (1958).
- [77] Ebert, H., Ködderitzsch, D., and Minár, J., Reports on Progress in Physics **74**, 096501 (2011).
- [78] Ebert, H., Mankovsky, S., Ködderitzsch, D., and Kelly, J. P., Physical Review Letters **107**, 066603 (2011).
- [79] Economou, E. N., *Green's Functions in Quantum Physics* (Springer, Springer, 1983).
- [80] Ederer, C. and Fennie, C. J., Journal of Physics: Condensed Matter **20**, 434219 (2008).
- [81] *Investigations on the Theory of Brownian Movement*, edited by A. Einstein (New York: Dover, 1956).
- [82] Ernst, A., *Multiple-scattering theory: new developments and applications*, Ph.D. thesis, Martin-Luther-Universität Halle-Wittenberg (2007).
- [83] Etz, C., Costa, M., Eriksson, O., and Bergman, A., Physical Review B **86**, 224401 (2012).
- [84] Etz, C., Maznichenko, I. V., Böttcher, D., Henk, J., Yaresko, A. N., Hergert, W., Mazin, I. I., Mertig, I., and Ernst, A., Physical Review B **86**, 064441/1 (2012).
- [85] Etzkorn, M., Anil Kumar, P. S., Vollmer, R., Ibach, H., and Kirschner, J., Surface Science **566–568**, 241 (2004).
- [86] Fähnle, M. and Steiauf, D., Physical Review B **73**, 184427 (2006).
- [87] Faulkner, J. S., Physical Review B **13**, 2391 (1976).
- [88] Faulkner, J. S., Journal of Physics C: Solid State Physics **10**, 4661 (1977).
- [89] Faulkner, J. S., Ujfalussy, B., Moghadam, N., Stocks, G. M., and Wang, Y., in *Properties of complex inorganic solids 2* (Kluwer Academic/ Plenum Publishers New York, 2000).
- [90] Fermi, E., Zeitschrift für Physik **48**, 73 (1928).
- [91] Ferriani, P., von Bergmann, K., Vedmedenko, E. Y., Heinze, S., Bode, M., Heide, M., Bihlmayer, G., Blügel, S., and Wiesendanger, R., Physical Review Letters **101**, 027201 (2008).
- [92] Fert, A. and Levy, P., Physical Review Letters **44**, 23 (1980).
- [93] Feynman, R. P., Physical Review **97**, 660 (1955).
- [94] Filip, A., *Spin Polarized Electron Transport in Mesoscopic Hybrid Devices*, Ph.D. thesis, Rijksuniversiteit Groningen (2002).
- [95] Fischer, G., Däne, M., Ernst, A., Lüders, M., Szotek, Z., and Temmerman, W. M., Physical Review B **80**, 014408 (2009).
- [96] Fischer, G., Sanchez, N., Adeagbo, W., Lüders, M., Szotek, Z., Temmerman, W. M., Ernst, A., Hergert, W., and Munoz, M. C., Physical Review B **84**, 205306 (2011).
- [97] *Spin Glass*, edited by K. Fischer and J. Hertz (Press Syndicate of University of Cambridge, 1991).

-
- [98] Fischer, O., Kugler, M., Maggio-Aprile, I., and Berthod, C., *Reviews of Modern Physics* **79**, 353 (2007).
- [99] Fisher, R. A., *Proc. Roy. Soc. London Ser. A.* **217**, 295 (1953).
- [100] Fokker, A. D., *Annalen der Physik* **348**, 810 (1914).
- [101] Fransson, J., *Journal of Physics: Condensed Matter* **19**, 285714 (2008).
- [102] Fransson, J. and Zhu, J.-X., *New Journal of Physics* **10**, 013017 (2008).
- [103] Fuchs, G. D., Sankey, J. C., Pribiag, V., Qian, L., Braganca, P. M., Garcia, A. G. F., Ryan, E. M., Li, Z.-P., Ozatay, O., Ralph, D. C., and Buhrman, R. A., *Applied Physics Letters* **91**, 062507 (2007).
- [104] Garanin, D. A., *Physical Review B* **55**, 3050 (1997).
- [105] Garanin, D. A., Ishchenko, V. V., and Panina, L. V., *Theo. Math. Phys.* **82**, 169 (1990).
- [106] Garcia-González, P. and Godby, R. W., *Physical Review B* **63**, 075112 (2001).
- [107] de Gennes, P.-G., *Physical Review* **118**, 141 (1960).
- [108] Getzlaff, M., *Fundamentals of Magnetism* (Springer, Berlin, 2008).
- [109] Gilbert, T. L., *IEEE Transactions on Magnetics* **40**, 6 (2004).
- [110] Gilmore, K., Idzerda, Y. U., and Stiles, M. D., *Physical Review Letters* **99**, 027204 (2007).
- [111] Ginzburg, V. L. and Pitaevskii, L. P., *Sov. Phys. Usp.* **30**, 168 (1987).
- [112] *Green Functions for Ordered and Disordered Systems*, edited by A. Gonis, *Studies in Mathematical Physics*, Vol. 4 (North-Holland, Amsterdam, 1992).
- [113] *Electron Correlations and Materials Properties 2*, edited by A. Gonis, N. Kioussis, and M. Cifitan (Kluwer Academic/Plenum, New York, 2003).
- [114] Gonis, A., Stocks, G. M., Butler, W. H., and Winter, H., *Physical Review B* **29**, 555 (1984).
- [115] Goodenough, J. B., *Physical Review* **100**, 564 (1955).
- [116] Gradhand, M., Czerner, M., Fedorov, D. V., Zahn, P., Yavorsky, B. Y., Szunyogh, L., and Mertig, I., *Physical Review B* **80**, 224413 (2009).
- [117] Gross, E. K. U. and Kohn, W., *Physical Review Letters* **55**, 2850 (1985).
- [118] Gyorffy, B. L., Pindor, A. J., Staunton, J., Stocks, G. M., and Winter, H., *Journal of Physics F: Metal Physics* **15**, 1337 (1985), <http://stacks.iop.org/0305-4608/15/1337>.
- [119] Hedin, L., *Ark. Fys.* **30**, 231 (1965).
- [120] Hedin, L., *Physical Review* **139**, A796 (1965).
- [121] Hedin, L., *Journal of Physics: Condensed Matter* **11**, R489 (1999).
- [122] Heide, M., *Magnetic domain walls in ultrathin films: Contribution of the Dzyaloshinskii-Moriya interaction*, Ph.D. thesis, Rheinisch-Westfälische technische Hochschule Aachen (2006).
- [123] Heine, V., *Solid State Physics* **35**, 1 (1980).
- [124] Heinrich, A. and Loth, S., *Science* **332**, 1039 (2011).
- [125] Heinrich, B. and Cochran, J. F., *Advances in Physics* **42**, 523 (1993).
- [126] Heisenberg, W., *Zeitschrift für Physik* **38**, 411 (1926).
- [127] Heisenberg, W., *Zeitschrift für Physik* **49**, 619 (1928).

- [128] Hellsvik, J., *Atomistic Spin Dynamics, Theory and Applications*, Ph.D. thesis, Uppsala University (2010).
- [129] Henk, J. and Schattke, W., *Computer Physics Communications* **77**, 69 (1993).
- [130] Hertel, R., *Journal of Magnetism and Magnetic Materials* **249**, 251 (2002).
- [131] *Giant Magneto-Resistance Devices*, edited by E. Hirota, H. Sakakima, and K. Inomata (Springer-Verlag Berlin Heidelberg, 2002).
- [132] Hjortstam, O., Baberschke, K., Wills, J. M., Johansson, B., and Eriksson, O., *Physical Review B* **55**, 15 026 (1997).
- [133] Hohenberg, P. and Kohn, W., *Physical Review B* **136**, 864 (1964).
- [134] Hu, C. D., *Journal of Physics: Condensed Matter* **24**, 086001 (2012).
- [135] Hubbard, J., *Proc. Roy. Soc. London Ser. A.* **276**, 238 (1963).
- [136] Huhne, T., Zecha, C., Ebert, H., Dederichs, P. H., and Zeller, R., *Physical Review B* **58**, 10 236 (1998).
- [137] Izyumov, Y. A., *AIP Conf. Proc.* **678**, 181 (2003).
- [138] Jahn, H. and Teller, E., *Proceedings of the Royal Society of London. Series A, Mathematical and Physical Sciences (1934-1990)* **161**, 220 (1937).
- [139] Jaubert, L. D. C. and Holdsworth, P. C. W., *Nature Phys.* **5**, 258 (2009).
- [140] Jones, M. D. and Albers, R. C., *Physical Review B* **79**, 045107 (2009).
- [141] *Theoretical Solid State Physics*, edited by W. Jones (Wiley and Sons, 1973).
- [142] Kadanoff, L. P., *Journal of Statistical Physics* **137**, 777 (2009).
- [143] Källén, G., *Helvetica Physica Acta* **25**, 417 (1952).
- [144] Kalos, M. H. and Whitlock, P. A., *Monte Carlo methods I.: Basics* (Wiley, New York, 1986).
- [145] Kamberský, V., *Can. J. Phys.* **48**, 2906 (1970).
- [146] Kamberský, V., *Czechoslovak Journal of Physics, Section B* **34**, 1111 (1984).
- [147] Kanamori, J., *Journal of the Physics and Chemistry of Solids* **10**, 87 (1959).
- [148] Kasuya, T., *Progress of Theoretical Physics* **16**, 45 (1956).
- [149] Kato, T., Matsumoto, Y., Okamoto, S., Kikuchi, N., Kitakami, O., Nishizawa, N., Tsunashima, S., and Iwata, S., *IEEE Transactions on Magnetics* **47**, 3036 (2011).
- [150] Ke, L., *First principles study of atomic-scale nanowires and dynamical transverse spin susceptibility*, Ph.D. thesis, Arizona State University (2009).
- [151] Khajetoorians, A. A., Wiebe, J., Chillian, B., and R., W., *Science* **332**, 1062 (2011).
- [152] Kilmontovich, Y. L., *Nonlinear Phenomena in Complex Systems* **5**, 372 (2002).
- [153] Kimel, A. V., *Physica* **3**, 20 (2010).
- [154] Kirilyuk, A., Kimel, A. V., and Rasing, T., *Reviews of Modern Physics* **82**, 2731 (2010).
- [155] Kirilyuk, A., Kimel, A. V., and Rasing, T., *Reports on Progress in Physics* **76**, 026501 (2013).
- [156] Kittel, C., *Einführung in die Festkörperphysik*, 6th ed. (R. Oldenburg, München, 1983).
- [157] Ködderitzsch, D., Ebert, H., Rowlands, D. A., and Ernst, A., *New Journal of Physics* **9**, 81 (2007).

- [158] Kohn, W., *Reviews of Modern Physics* **71**, 1253 (1999).
- [159] Kohn, W. and Rostoker, N., *Physical Review* **94**, 1111 (1954).
- [160] Kohn, W. and Sham, L. J., *Physical Review* **140**, A1133 (1965).
- [161] *Modern Thermodynamics, From Heat Engines to Dissipative Structures*, edited by D. Kondepudi and I. Prigogine (John Wiley & Sons, 1998).
- [162] Koralek, J. D., Meier, D., Hinton, J. P., Bauer, A., Parameswaran, S. A., Vishwanath, A., Ramesh, R., Schoenlein, R. W., Pfeleiderer, C., and Orenstein, J., *Physical Review Letters* **109**, 247204 (2012).
- [163] Korrying, J., *Physica* **13**, 392 (1947).
- [164] Kubo, R., *Journal of The Physical Society of Japan* **12**, 570 (1957).
- [165] Kuneš, J. and Kamberský, V., *Physical Review B* **65**, 212411 (2002).
- [166] Landau, L. D. and Lifshitz, E. M., *Phys. Z. Sowietunion* **8**, 153 (1935).
- [167] Langevin, P., *C. R. Acad. Sci.* **146**, 530 (1908).
- [168] Laufer, P. and Papaconstantopoulos, D. A., *Physical Review B* **35**, 17 (1987).
- [169] Lee, H. G., Huh, S. H., Jeong, J. W., Choi, B. J., Kim, S. H., and Ri, H. C., *J. Am. Chem. Soc.* **124**, 12094 (2002).
- [170] Lehmann, H., *Nuovo Cimento* **11**, 342 (1954).
- [171] Lent, C. S., Browen, M. A., Dow, J. D., Allgier, R. S., Sankey, O. F., and Ho, E. S., *Superlattices and Microstructures* **2**, 5 (1986).
- [172] Levy, P. M. and Fert, A., *Physical Review B* **23**, 4667 (1981).
- [173] Liechtenstein, A. I., Katsnelson, M. I., Antropov, V. P., and Gubanov, V. A., *Journal of Magnetism and Magnetic Materials* **67**, 65 (1987).
- [174] Liechtenstein, A. I., Katsnelson, M. I., and Gubanov, V. A., *Journal of Physics F: Metal Physics* **14**, 7 (1984).
- [175] Lima, A. B. and Costa, B. V., *Journal of Magnetism and Magnetic Materials* **263**, 324 (2003).
- [176] Liu, Y. W. and Zhang, Z. Z., *Science China Physics, Mechanics and Astronomy* **56**, 184 (2013).
- [177] Lloyd, P., *Proceedings of the Physical Society* **90**, 207 (1967).
- [178] Lombardo, P. and Avignon, M., *Physica B* **337**, 186 (2003).
- [179] Lopéz Sancho, M. P., Sancho, J. M. L., and Rubio, J., *Journal of Physics F: Metal Physics* **15**, 851 (1985).
- [180] Loth, S., Baumann, S., Lutz, C. P., Eigler, D. M., and Heinrich, A., *Science* **335**, 196 (2012).
- [181] Lovitch, L. and Tomozawa, Y., *II Nuovo Cimento Series 10* **24**, 1147 (1962).
- [182] Lüders, M., Ernst, A., Däne, M., Szotek, Z., Svane, A., Ködderitzsch, D., Hergert, W., Györfly, B. L., and Temmerman, W. M., *Physical Review B* **71**, 205109 (2005).
- [183] M. G. Vergniory, M. G., Thonig, D., Hoffmann, M., Maznichenko, I. V., Geilhufe, M., Otrokov, M. M., Zubizarreta, X., Ostanin, S., Marmodoro, A., Henk, J., Hergert, W., Mertig, I., Chulkov, E. V., and Ernst, A., arXiv:1306.6590 [cond-mat.mtrl-sci](2013).
- [184] *Electrons at the Fermi Surface*, edited by A. R. Mackintosh and O. K. Andersen (Cambridge

- University Press, 1980).
- [185] Mankovsky, S., Ködderitzsch, D., Woltersdorf, G., and Ebert, H., arXiv:1301.2114v1 [cond-mat.other](2013).
- [186] Mann, A., Walowski, J., Münzenberg, M., Maat, S., Carey, M. J., Childress, J. R., Mewes, C., Ebke, D., Drewello, V., Reiss, G., and Thomas, A., *Phys. Rev. X* **2**, 041008 (2012).
- [187] *Time-Dependent Density Functional Theory*, edited by M. A. L. Marques, U. C. A., F. Nogueira, A. Rubio, K. Burke, and E. K. U. Gross (Springer-Verlag Berlin Heidelberg, 2006).
- [188] *A Practical Guide to Magnetic Circular Dichroism and Spectroscopy*, edited by W. R. Mason (John Wiley & Sons, 2006).
- [189] *Pauli's Exclusion Principle*, edited by M. Massimi (Cambridge University Press, 2005).
- [190] Mavropoulos, P., Papanikolaou, N., Grotendorst, J., Blügel, S., and Marx, D., *Computational Nanoscience: Do It Yourself!* **31**, 131 (2006).
- [191] *Methods of Analytical Dynamics*, edited by L. Meirovitch (MacGraw-Hill Book Company, New York, 1970).
- [192] Menzel, M., Mokrousov, Y., Wieser, R., Bickel, J. E., Vedmedenko, E. Y. Blügel, S., Heinze, S., von Bergmann, K., Kubetzka, A., and Wiesendanger, R., *Physical Review Letters* **108**, 197204 (2012).
- [193] Mermin, N. D., *Physical Review* **137**, A1441 (1965).
- [194] Mertig, I., Mrosan, E., and Ziesche, P., *Multiple Scattering Theory of Point Defects in Metals: Electronic Properties* (B. G. Teubner, Leipzig, 1987).
- [195] Methfessel, M. and Kubler, J., *Journal of Physics F: Metal Physics* **12**, 141 (1982).
- [196] Metropolis, N., *Los Alamos Science Special*, 125(1987).
- [197] Miyazaki, K. and Seki, K., *The Journal of Chemical Physics* **108**, 7052 (1998).
- [198] Mizukami, S., Ando, K., and Miyazaki, T., *Japanese Journal of Applied Physics* **40**, 580 (2001).
- [199] *Introduction to the Theory of Metals*, edited by U. Mizutani (Cambridge University Press, 2001).
- [200] Moghadam, N. Y., Stocks, G. M., Újfalussy, B., Shelton, W. A., Gonis, A., and Faulkner, J. S., *Journal of Physics: Condensed Matter* **11**, 5505 (1999).
- [201] *The Hubbard Model—A Reprint Volume*, edited by A. Montorsi (World Scientific, Singapore, 1992).
- [202] Mookerjee, A., *Journal of Physics F: Metal Physics* **17**, 1511 (1987).
- [203] Moriya, T., *Physical Review* **120**, 1 (1960).
- [204] Moriya, T., *Physical Review Letters* **4**, 228 (1960).
- [205] Moriya, T., in *Metallic Magnetism*, edited by H. Capellmann (Springer-Verlag, Berlin, 1987) pp. 15–56.
- [206] Moulas, G., Lehnert, A., Rusponi, S., Zabloudil, J., Etz, C., Ouazi, S., Etzkorn, M., Bencok, P., Gambardella, P., Weinberger, P., and Brune, H., *Physical Review B* **78**, 214424 (2008).
- [207] *Variational Principles and Methods in Theoretical Physics and Chemistry*, edited by R. K.

- Nesbet (Cambridge University Press, 2002).
- [208] *Monte Carlo methods in statistical physics*, edited by M. E. J. Newman and G. T. Barkema (Oxford University Press, 1999).
- [209] Nishizaki, T. and Kobayashi, N., J. Phys. Conf. Ser. **150**, 012031 (2009).
- [210] Niu, C., Dai, Y., Zhu, Y., Ma, Y., Yu, L., Han, S., and Huang, B., Science Reports **2**, 976 (2012).
- [211] Niu, T. and Dai, J., 2009 **48**, 34 (International Journal of Thermal Sciences).
- [212] *Quantum Theory of Magnetism*, edited by W. Nolting and A. Ramakanth (Springer-Verlag Berlin, 2009).
- [213] *Markov Chains*, edited by J. Norris (Cambridge University Press, 1998).
- [214] Nyquist, H., Physical Review **32**, 110 (1928).
- [215] Obaidat, I., Kouvel, J. S., Huang, Y., and Friedman, G., Journal of Magnetism and Magnetic Materials **223**, 88 (2001).
- [216] *Stochastic differential equations: an introduction with applications*, edited by B. K. Øksendal (Springer Berlin, 2003).
- [217] Oogane, M., Wakitani, T., Yakata, S., Yilgin, R., Ando, Y., Sakuma, A., and Miyazaki, T., Japanese Journal of Applied Physics **45**, 3889 (2006).
- [218] Oswald, A., Zeller, R., Braspenning, P. J., and Dederichs, P. H., Journal of Physics F: Metal Physics **15**, 193 (1985).
- [219] Papanikolaou, N., Zeller, R., and Dederichs, P. H., Journal of Physics: Condensed Matter **14**, 2799 (2002).
- [220] Pauli, W., Zeitschrift der Physik **43**, 601 (1927).
- [221] Perdew, J., International Journal of Quantum Chemistry: Quantum Chemistry Symposium **19**, 497 (1986).
- [222] Perdew, J. P., Burke, K., and Ernzerhof, M., Physical Review Letters **77**, 3865 (1996).
- [223] Perdew, J. P., Chevary, S., Vosko, S. H., Jackson, K., Pederson, M., Singh, D. J., and Fiolhais, C., Physical Review B **46**, 6671 (1992).
- [224] Perdew, J. P., Chevary, S., Vosko, S. H., Jackson, K., Pederson, M., Singh, D. J., and Fiolhais, C., Physical Review B **48**, 4978(E) (1993).
- [225] Perdew, J. P. and Wang, Y., Physical Review B **45**, 13 244 (1992).
- [226] Perdew, J. P. and Zunger, A., Physical Review B **23**, 5048 (1981).
- [227] Pfliederer, C. and Rosch, A., Nature **465**, 880 (2010).
- [228] Pindor, A. J., Staunton, J., Stocks, G. M., and Winter, H., Journal of Physics F: Metal Physics **13**, 979 (1983).
- [229] Plihal, M., Mills, D. L., and Kirschner, J., Physical Review Letters **82**, 2579 (1999).
- [230] Prodan, E., Physica **3**, 99 (2010).
- [231] Qiu, Z. and Bader, S. D., Rev. Sci. Instrum. **71**, 1243 (2000).
- [232] Rausch, R. and Nolting, W., Journal of Physics: Condensed Matter **21**, 376002 (2009).

- [233] *Quantum Physics of Atoms, Molecules, Solids, Nuclei and Particles (2nd Edition)*, edited by R. Resnick and R. Eisberg (John Wiley & Sons, 1985).
- [234] Ritz, W., *Journal für die reine und angewandte Mathematik* **135**, 1 (1908).
- [235] Romaniello, P., *Time-Dependent Current-Density-Functional Theory for Metals*, Ph.D. thesis, Rijksuniversiteit Groningen (2006).
- [236] Ruderman, M. A. and Kittel, C., *Physical Review* **96**, 99 (1954).
- [237] Runge, E. and Gross, E. K. U., *Physical Review Letters* **52**, 997 (1984).
- [238] Sablik, M. J. and Jiles, D. C., *Journal of Physics D: Applied Physics* **32**, 1971 (1999).
- [239] Sandratskii, L. M., *Physical Review B* **76**, 045203 (2006).
- [240] Sandratskii, L. M., Singer, R., and Şaşıoğlu, E., *Physical Review B* **76**, 184406 (2007).
- [241] Sergienko, I. A. and Dagotto, E., *Physical Review B* **73**, 094434 (2006).
- [242] *Impurity Scattering in Metal Alloys*, edited by J. Singh Galsin (Springer-Verlag Berlin Heidelberg, 2001).
- [243] Singleton, D., *American Journal of Physics* **66**, 697 (1998).
- [244] Singleton, J., *Band Theory and Electronic Properties of Solids*, Oxford Master Series in Condensed Matter Physics (Oxford University Press, Oxford, 2001).
- [245] Skubic, B., *Spin Dynamics and Magnetic Multilayers*, Ph.D. thesis, Uppsala Universitet, Uppsala (2007).
- [246] Slater, J. C., *Physical Review* **51**, 846 (1937).
- [247] Slater, J. C. and Koster, G. F., *Physical Review* **94**, 1498 (1954).
- [248] Smith, D., *Journal of Magnetism and Magnetic Materials* **1**, 214 (1976).
- [249] Song, H.-S., Lee, K.-D., Sohn, J.-W., Yang, S.-H., Parkin, S. S. P., You, C.-Y., and Shin, S.-C., *Applied Physics Letters* **102**, 102401 (2013).
- [250] Soven, P., *Physical Review* **156**, 809 (1967).
- [251] Spaldin, N. and Fiebig, M., *Science* **309**, 5733 (2005).
- [252] Staunton, J., “Relativistic effects and disordered local moments in magnetism,” http://www.psi-k.org/newsletters/News_82/Highlight_82.pdf.
- [253] Staunton, J., Gyorffy, B. L., Pindor, A. J., Stocks, G. M., and Winter, H., *Journal of Magnetism and Magnetic Materials* **45**, 15 (1984).
- [254] Steiauf, D. and Fähnle, M., *Physical Review B* **72**, 064450 (2005).
- [255] Stocks, G. M., Eisenbach, M., Újfalussy, B., Lazarovits, B., Szunyogh, L., and Weinberger, P., *Progress in Material Science* **52**, 371 (2007).
- [256] *Magnetism: From Fundamentals to Nanoscale Dynamics*, edited by J. Stöhr and H. C. Siegmann (Springer-Verlag, Berlin, 2006).
- [257] Stoner, E. C., *Proceedings of the Royal Society A* **154**, 656 (1936).
- [258] Stoner, E. C., *Proceedings of the Royal Society A* **165**, 372 (1938).
- [259] Stoner, E. C. and Wohlfarth, E. P., *Philosophical Transactions of the Royal Society of London. Series A, Mathematical and Physical Sciences* **240**, 599 (1948).

-
- [260] Stuart, R. and Marshall, W., *Physical Review* **120**, 353 (1960).
- [261] Szunyogh, L. and Udvardi, L., *Journal of Magnetism and Magnetic Materials* **198-199**, 537 (1999).
- [262] Szunyogh, L., Újfalussy, B., Weinberger, P., and Kollár, J., *Physical Review B* **49**, 2721 (1994).
- [263] Tannous, C. and Gieraltowski, J., *European Journal of Physics* **29**, 475 (2008).
- [264] Tao, J., Perdew, J., Staroverov, V., and Scuseria, G. E., *Physical Review Letters* **91**, 146401 (2003).
- [265] Thomas, L. H., *Proceedings of the Cambridge Philosophical Society* **23**, 542 (1927).
- [266] Thonig, D. and Henk, J., *New Journal of Physics* **16**, 013032 (2014).
- [267] Thonig, D., Reissaus, S., Mertig, I., and Henk, J., arXiv:1310.6902 [cond-mat.mes-hall](2013).
- [268] *Energy method: Advanced Dynamics for Engineers*, edited by B. Torby (HRW Series in Mechanical Engineering. United States of America: CBS College Publishing, 1984).
- [269] *Giant Magnetoresistance: New Research*, edited by A. D. Torres and D. A. Perez (Nova Science Publishers, 2008).
- [270] Udvardi, L., Antal, A., Szunyogh, L., Buruzs, A., and Weinberger, P., *Physica B* **403**, 402 (2008).
- [271] Udvardi, L., Szunyogh, L., Palotás, K., and Weinberger, P., *Physical Review B* **68**, 104436 (2003).
- [272] Umetsu, N., Miura, D., and Sakuma, A., *Journal of the Physical Society of Japan* **81**, 114716 (2012).
- [273] Van Vleck, J. H., *Physical Review* **41**, 208 (1932).
- [274] Velický, B., *Physical Review* **184**, 614 (1969).
- [275] *Computational Quantum Mechanics for Materials Engineers - The EMTO Method and Applications*, edited by L. Vitos (Springer-Verlag Berlin Heidelberg, 2007).
- [276] Vollmer, R., Etzkorn, M., Anil Kumar, P. S., Ibach, H., and Kirschner, J., *Physical Review Letters* **91**, 147201 (2003).
- [277] Vosko, S. H., Wilk, L., and Nusair, M., *Canadian Journal of Physics* **58**, 1200 (1980).
- [278] Wangsness, R. K., *Physical Review* **98**, 927 (1955).
- [279] Weinert, M., Watson, R. E., and Davenport, J. W., *Physical Review B* **32**, 2115 (1985).
- [280] Weiss, P., *Comptes Rendus* **143**, 1136 (1906).
- [281] Weiss, P., *J. Phys. Theor. Appl.* **1**, 661 (1907).
- [282] Wieser, R., *Physical Review B* **84**, 054411 (2011).
- [283] Wieser, R., *Physical Review Letters* **110**, 147201 (2013).
- [284] Wildberger, K., Zeller, R., and Dederichs, P. H., *Physical Review B* **55**, 10074 (1997).
- [285] *The thermodynamics of fluid systems, chapter XIII - Kinetic processes*, edited by L. C. Woods (Calendron Press, 1975).
- [286] Wu, M. W., Jiang, J. H., and Weng, M. Q., *Physics Reports* **493**, 61 (2010).
- [287] Wu, R., in *Band-Ferromagnetism: Ground-State and Finite-Temperature Phenomena*, Lecture

- Notes in Physics, Vol. 580, edited by K. Baberschke, W. Nolting, and M. Donath (Springer, Berlin, 2001) p. 60.
- [288] Wu, R., Chen, L., and Freeman, A. J., *Journal of Magnetism and Magnetic Materials* **170**, 103 (1997).
- [289] Wysocki, A. L., *Finite temperature effects in magnetic materials: model and ab initio studies*, Ph.D. thesis, University Nebraska (2009).
- [290] Yang, J., Li, Z., Whangbo, M.-H., Wei, S.-H., Gong, X., and Xiang, H., *Physical Review Letters* **109**, 107203 (2012).
- [291] Yosida, K., *Physical Review* **106**, 893 (1957).
- [292] *Theory of Magnetism*, edited by K. Yosida (Springer-Verlag, Berlin, 1998).
- [293] *Electron Scattering in Solid Matter*, edited by J. Zabloudil, R. Hammerling, L. Szunyogh, and P. Weinberger (Springer, Berlin, 2005).
- [294] Zahn, P., *Screened Korringa-Kohn-Rostoker-Methode für Vielfachschichten*, Ph.D. thesis, Technische Universität Dresden, Dresden (1998).
- [295] Zeller, R., *Journal of Physics: Condensed Matter* **16**, 6453 (2004).
- [296] Zeller, R., *Journal of Physics: Condensed Matter* **17**, 5367 (2005).
- [297] Zeller, R., Dederichs, P. H., Újfalussy, B., Szunyogh, L., and Weinberger, P., *Physical Review B* **52**, 8807 (1995).
- [298] Zener, C., *Physical Review* **82**, 403 (1951).
- [299] *Electrons and phonons: the theory of transport phenomena in solids*, edited by J. Ziman (Clarendon Press, Oxford, 1960).

List of Publications

- i) Böttcher, D., Henk, J. and Ernst, A.: *Atomistic magnetization dynamics in nanostructures based on first principles calculations: application to Co nanoislands on Cu(111)*, Journal of Physics: Condensed Matter **23**, (29),pp 296003/1-8 (2011)
- ii) Böttcher, D. and Henk, J.: *Temperature-dependent Heisenberg exchange coupling constants from linking electronic-structure calculations and Monte Carlo simulations*, Journal of Magnetism and Magnetic Materials **324**, (4),pp 610-615 (2012)
- iii) Borisov, V. S., Maznichenko, I. V., Böttcher, D., Ostanin, S., Ernst, A., Henk, J., Mertig, I.: *Magnetic exchange interactions and antiferromagnetism of ATcO₃ (A = Ca, Sr, Ba) studied from first principles*, Physical Review B **85**, (13),pp 134410/1-8 (2012)
- iv) Böttcher, D., Ernst, A. and Henk, J.: *Noncollinear magnetism in ultrathin films with strong spin-orbit coupling from ab initio first principles*, Journal of Nanoscience and Nanotechnology **12**, (9),pp 7516-7519 (2012)
- v) Böttcher, D. and Henk, J.: *Significance of nutation in magnetization dynamics of nanostructures*, Physical Review B **86**, (2),pp 020404(R)/1-4 (2012)
- vi) Etz, C., Maznichenko, I. V., Böttcher, D., Henk, J., Yaresko, A. N., Hergert, W., Mazin, I. I., Mertig, I., Ernst, A.: *Indications of weak electronic correlations in SrRuO₃ from first-principles calculations*, Physical Review B **86**, (6),pp 064441/1-5 (2012)
- vii) Böttcher, D. and Henk, J.: *Magnetic properties of strained La_{2/3}Sr_{1/3}MnO₃ perovskites from first principles*, Journal of Physics: Condensed Matter **25**, (13),pp 136005/1-8 (2013)
- viii) M. G. Vergniory, M. M. Otrokov, D. Thonig, M. Hoffmann, I. V. Maznichenko, M. Geilhufe, X. Zubizarreta, S. Ostanin, A. Marmodoro, J. Henk, W. Hergert, I. Mertig, E. V. Chulkov, A. Ernst: *Exchange interaction and its tuning in magnetic binary chalcogenides*, Physical Review B **89**, (16),pp 165202/1-7 (2014)
- ix) Thonig, D. and Henk, J.: *Gilbert damping tensor within the breathing Fermi surface model: anisotropy and non-locality* New Journal of Physics **16**, (1),pp 013032/1-14 (2014)
- x) Thonig, D., Reißaus, S., Henk, J., Mertig, I.: *Thermal string excitations in artificial spin-ice dipolar arrays* arXiv:1310.6902 [cond-mat.mes-hall] (2013) (*submitted*)

Curriculum Vitae

Personal data:

name	Danny Thonig
address	Wolfstraße 2, 06110 Halle(Saale)
date of birth and place	06.05.1986, Bad Frankenhausen (Germany)
birth name	Böttcher

Education:

1992-1996	Primary school: “Am Tischplatt”
1996-1997	Secondary school: Jurie-Gagarin school Bad Frankenhausen
1997-2004	Grammar school: Kyffhäuser Gymnasium Bad Frankenhausen
2004-2005	Alternative civilian service at Maniske hospital Bad Frankenhausen
2005-2010	Studies of physics at Martin Luther University Halle-Wittenberg completed as graduate physicist (degree: Diplom-Physiker) Diploma title: “Theoretische Beschreibung der Magnetisierungsdynamik von Nanostrukturen” (“Magnetization dynamic theory in nanostructures“)
since 2010	PhD Studentship at Max Planck Institute of Microstructure Physics
since 2011	Member of the International Max Planck Research School for Science and Technology of Nanostructures

Danksagung

An dieser Stelle möchte ich mich bei allen Menschen herzlich bedanken, die zum Gelingen dieser Arbeit beigetragen haben. Meinen größten Dank gilt PD Dr. Jürgen Henk für die ausgezeichnete Betreuung. Ich möchte mich bedanken für seine unermüdliche Geduld bei zahlreichen und konstruktiven Diskussionen, ohne die ein gutes Gelingen der vorliegenden Arbeit kaum denkbar gewesen wäre. Sehr möchte ich mich auch für seine Zusammenarbeit in mehreren Projekten und der Möglichkeit, meine Erfahrungen im wissenschaftlichen Alltag zu erweitern, bedanken. In unseren Gesprächen schätzte ich stets seine fachliche Kompetenz und seine freundschaftliche und offene Art.

Einen besonderen Dank gilt auch Dr. Arthur Ernst für viele konstruktive Diskussionen und das Vertrauen in meine wissenschaftliche Arbeit. Sehr schätze ich seine offene Art und wissenschaftliche Kompetenz. Gern möchte ich ihm auch meinen Dank für seine verwaltende Arbeit in der Max-Planck-Research School zukommen lassen, in der er sich für wissenschaftlich hochwertige Vorlesungen und eine erstklassige Ausbildung stark machte. Weiter danke ich Frau Prof. Dr. I. Mertig, die mir die Anfertigung der Doktorarbeit in ihrer Fachgruppe ermöglichte, und Prof. Dr. E. Gross, der mir ein angenehmes Arbeitsumfeld und einen Arbeitsplatz am Max-Planck-Institut für Mikrostrukturphysik zur Verfügung gestellt hat. Sehr genossen habe ich die wissenschaftliche Fortbildung und die Diskussionen in den jeweiligen Fachgruppenseminaren.

Ich danke auch allen Mitgliedern der Fachgruppe Theoretische Physik und insbesondere der Arbeitsgruppe rund um Prof. Mertig für viele Diskussionen und die warmherzige Aufnahme in die Gruppe. Auch möchte ich meinen Dank Prof. Steffen Trimper als meinen Mentor in der international Max-Planck-Research School aussprechen. Ohne den unermüdlichen Einsatz des Clusteradministratorenteams bestehend aus Udo Schmidt, Dr. Frank Müller, Gabrielle Träger und Jens Böttger wären die sehr umfangreichen Berechnungen dieser Arbeit nicht möglich gewesen. Vielen Dank dafür. Bedanken möchte ich mich auch bei Ina Goffin, die mir bei Fragen zur Verwaltung und Organisation immer sehr geholfen hat. Meinen Dank gilt auch allen weiteren Wegbegleitern, die mir jederzeit mit Rat und viel Geduld zur Seite standen, wie z.B. meinem Bürokollegen Martin Hölzer, Dr. Maia Garcia Vergniory, Dr. Alberto Marmodoro, Dr. Thomas Bose, Dr. Hossein Mirhosseini, Dr. Nicki Hinsche, Vladislav Borisov und Safa Golrokh Bahoosh.

Am Ende gebührt meinen Freunden und meiner Familie ein großer Dank, da sie mir in allen Situationen halt gaben und mich zum Durchhalten auf dem Weg zum Abschluss dieser Arbeit ermuntert haben. Insbesondere bedanke ich mich bei meiner Frau Antje, die mir in den schwierigsten Stunden aufmunternd beigestanden und unbeschreiblich viel Rückhalt gegeben hat.

Eidstattliche Erklärung

Hiermit versichere ich, dass ich die von mir vorgelegte Arbeit

**Magnetization dynamics and magnetic ground
state properties from first principles**

selbstständig verfasst habe, dass ich die verwendeten Quellen und Hilfsmittel vollständig angegeben habe und dass ich die Stellen der Arbeit - einschließlich Tabellen, Karten und Abbildungen -, die anderen Werken oder dem Internet im Wortlaut oder dem Sinn nach entnommen sind, unter Angabe der Quelle als Entlehnung kenntlich gemacht habe.

Halle (Saale), den 05. November 2013

(Unterschrift)
Danny Thonig